Investigation on the contribution of the human TRPV3 channel to the transport of NH_4^+ in keratinocytes of human skin

Inaugural-Dissertation
to obtain the academic degree
Doctor rerum naturalium (Dr. rer. nat.)

submitted to the Department of Biology, Chemistry, Pharmacy
of Freie Universität Berlin

by

Hendrik Liebe

Berlin, 2024

Start of work: 1st November 2016
Submission: 2nd April 2024
Institute: Institute of Veterinary Physiology (WE02) – FU Berlin
Supervision: Prof. Dr. med. habil. Friederike Stumpff

Dean: Prof. Dr. Beate Paulus
Primary Reviewer: Prof. Dr. med. habil. Friederike Stumpff
Secondary Reviewer: Prof. Dr. Burkhard Kleuser

Disputation: 3rd July 2024

Descriptoren (nach CAB Thesaurus):

TRPV3
Ammonia
NH_4^+
Olmsted syndrome
Colon
Skin
Epithelial transport

Acknowledgement

I would like to express my deepest gratitude to my supervisor, Prof. Dr. med. habil. Friederike Stumpff**,** for her unwavering support, patience, and guidance throughout this research journey. Her expertise and insights have been invaluable in shaping this thesis. Thank you for giving me the chance to do research alongside you in the exciting field of cell physiology. Our collaboration has shown the potential when various branches of science complement each other to unravel complex problems.

I am also thankful to my committee members, Prof. Dr. med. vet. Jörg R. Aschenbach and Prof. Dr. rer. nat. Salah Amasheh, for their valuable feedback and constructive criticism especially concerning *Xenopus laevis* oocytes.

I would like to express heartfelt gratitude to my wife, Franziska Liebe, PhD, who not only supported me tirelessly throughout this journey but also served as my co-worker and co-author on all of our papers. Her zeal, dedication, and endless encouragement have been the cornerstone of my success. Thank you for being my partner in both life and research. Our sleepless nights in the laboratory investigating *Xenopus laevis* oocytes with microelectrodes and patch-clamp side by side will always have a special place in my heart.

I extend special thanks to the following individuals for their crucial contributions to this project:

- Dr. Gerhard Sponder, for his expertise in molecular and cell biology, which was essential to our success.
- Gisela Manz, for her support in the laboratory.
- Susanne Trappe, for fostering a familiar work environment and providing expertise in cell culture and microscopy.
- Manfred Sommerer, for his IT support.
- Katharina Söllig, for her support in the laboratory and for always being willing to lend an open ear.

Your contributions have been instrumental in the completion of this project, and I am deeply grateful for your support.

I am indebted to my family for their endless love, especially to my parents, Heike and Ronald Becker, for their help during the COVID-19 lockdown. Furthermore, I extend my sincere appreciation to Julie for her unwavering belief in me particularly during the final stages of this thesis. Her steadfast presence and light have provided clarity and inspiration, propelling me forward with renewed determination. Moreover, I am profoundly grateful to my son, Tristan, who has been my main priority during these challenging times. His revitalizing laughter,

courage, and boundless curiosity have been a constant source of ingenuity, reminding me to keep striving forward with open eyes and an open mind. Through his perspective, I have relearned to appreciate the small and big wonders that the world has to offer. Tristan, your presence in my life has been my greatest blessing, and I am forever grateful and proud to be your *Papa*.

Finally, I acknowledge the financial support provided by Sonnenfeld Stiftung and the DFG (DFG STU 258/7-1) which enabled me to pursue this research project.

Thank you to everyone who has been a part of this journey; your support has meant the world to me.

“Every mystery ever solved had been a puzzle from the dawn of the human species right up until someone solved it.”

— Eliezer Yudkowsky, Harry Potter and the Methods of Rationality

Statement of authorship

Name: Liebe

Surname: Hendrik

I herewith assure that I wrote the present thesis independently, that the thesis has not been partially or fully submitted as graded academic work and that I have used no other means than the ones indicated. I have indicated all parts of the work in which sources are used according to their wording or to their meaning. I am aware of the fact that violations of copyright can lead to injunctive relief and claims for damages of the author as well as a penalty by the law enforcement agency.

Berlin, 02.04.2024

Table of contents

List of figures

List of tables

Index of abbreviations

[ ]	concentration
$[Ca^{2+}]_i$	intracellular Ca^{2+} concentration
2-APB	2-aminoethoxydiphenyl borate
AKAP-5	a-kinase anchor protein 5
AQP	aquaporin
bTRPV3	bovine homologue of TRPV3
C	coulomb, unit of electric charge equivalent to $6.24 \cdot 10^{18}$ e
CaM	Calmodulin
cDNA	complementary DNA
CE	cornified envelope
cRNA	complementary RNA
doi	digital object identifier
EC_{50}	half maximal effective concentration
EDC	epidermal differentiation complex
EGFR	epidermal growth factor receptor
ER	endoplasmic reticulum
et al.	*et alia* (and others)
G	conductance
GWP	global warming potential
$G_x(y)$	conductance of the ion y measured in cells overexpressing x with H: hTRPV3 B: bTRPV3 C: controls
G573S	point mutation of the TRPV3 channel: glycine 573 serine
GFP	green fluorescent protein
hTRPV3	human TRPV3
$hTRPV3_{wt}$	wild-type human TRPV3
IFAP	Ichthyosis follicularis - atrichia – photophobia
IR	infrared
LBs	lamellar bodies
MBTPS2	membrane-bound transcription factor protease, site 2
MIM®	online Mendelian Inheritance in Man®
mTRPV3	mouse TRPV3
n.s.	not significant
NSCLC	non-small cell lung cancer
ORPHA	Orphanet
OS	Olmsted syndrome

PERP	p53 apoptosis effector related to PMP-22
PPK	palmoplantar keratoderma
Rh	rhesus-associated
RR	ruthenium red
TGF-α	transforming growth factor-α
TRP	transient light-induced receptor potentials
TRPV	vanilloid family of transient receptor potential
TRPV3	transient receptor potential cation channel, subfamily V, member 3
VSEPR	valence shell electron pair repulsion
WT	wild-type
X	*Xenopus laevis*

Abstract

Involvement of TRPV3 mutants in Olmsted syndrome is well-documented, yet the precise mechanisms underlying their pathogenicity remain elusive, particularly concerning trafficking and functionality within the cell membrane with controversial hypotheses in literature. Furthermore, and despite reports suggesting a role in NH_4^+ uptake in ruminant species, the permeability of the TRPV3 channel to this ion remained uncertain.

This study aims to elucidate the NH_4^+ permeability of human and bovine TRPV3 channels using *Xenopus laevis* oocytes and HEK-293 cells, with a primary focus on the human channel. Immunoblotting and immunostaining confirm the expression and trafficking of TRPV3 channels in both models as well as in native tissue. Notably, human skin equivalents and bovine rumen both showed distinct staining of the apical membrane of the top layer of keratinocytes with weaker cytosolic staining in the middle layers, suggesting potential roles in epithelial function. Functional assays, including single-channel patch clamp experiments and whole-cell studies with agonists, demonstrate the channels' responsiveness and permeability to NH_4^+ showing larger conductances in TRPV3 overexpressing cells. Furthermore, pH-sensitive microelectrodes were used to measure acidification by NH_4^+ in *Xenopus laevis* oocytes showing endogenous channels capable of NH_4^+ transport while also demonstrating significantly greater effects in TRPV3 expressing cells. These observations challenge conventional dogmas regarding membrane transport primarily via NH_3 diffusion. Expression of the TRPV3 mutant G573S in HEK-293 cells elucidates its impact on cell viability, with significant cell death observed and partial rescue via treatment with the established blocker ruthenium red. Crucially, immunofluorescence validated cytosolic expression, with membrane staining detected in a minority of cells. These observations argue for the hypothesis of a functional expression in the membrane where the gain-of-function mutation triggers the cascade ending in increased cell death.

Our study highlights the versatility of TRPV3 channels not only in Ca^{2+} signaling as extensively described in the literature, but also more generally as a cation transporter including for NH_4^+, with implications for various biological processes including skin physiology, ion homeostasis, pH regulation, and nitrogen utilization. These insights contribute to our evolving understanding of the biological role of TRPV3 and hold potential for informing future research and clinical interventions.

Zusammenfassung

Die Beteiligung von TRPV3-Mutanten am Olmsted-Syndrom ist gut dokumentiert. Dennoch bleiben die genauen Mechanismen ihrer Pathogenität unklar. Insbesondere der Einbau und die Funktionalität innerhalb der Zellmembran werden in der Literatur kontrovers diskutiert. Trotz Berichten über eine Rolle beim NH_4^+-Transport beim Wiederkäuer bleibt ferner die Durchlässigkeit des TRPV3 Kanals für dieses Ion ungewiss.

Diese Arbeit zielt darauf ab, die NH_4^+-Permeabilität von menschlichen und bovinen TRPV3-Kanälen zu klären. Dabei wurden *Xenopus laevis* Oozyten und HEK-293-Zellen als Modelsystem verwendet und der Schwerpunkt lag auf dem menschlichen Kanal. Immunoblotting und Immunfärbungen bestätigen die Expression und den Einbau von TRPV3-Kanälen in beiden Modellen sowie in nativem Gewebe. Menschliche Hautäquivalente und boviner Pansen zeigten eine deutliche Färbung der apikalen Membran der obersten Schicht der Keratinozyten mit schwächerer zytoplasmatischer Färbung in den mittleren Schichten. Dies weist darauf hin, dass der TRPV3 Kanal eine wichtige Rolle im Epithel spielen könnte. Funktionelle Untersuchungen mit *Patch-clamp-* und *Whole-cell* Experimenten zeigen eindeutig die Permeabilität der Kanäle für NH_4^+ mit größerer Leitfähigkeit in überexprimierenden Zellen. Darüber hinaus wurden pH-sensible Mikroelektroden verwendet, um die Ansäuerung durch NH_4^+ in *Xenopus laevis* Oozyten zu messen. Dabei konnten endogene Kanäle beobachtet werden, die eindeutig NH_4^+ transportierten. Dies stellt traditionelle Dogmen bezüglich des Membrantransportes in Frage, welche hauptsächlich in Form von NH_3-Diffusion erfolgen soll. Zusätzlich konnten signifikant größere Effekte in überexprimierenden Zellen beobachtet werden, was die NH_4^+-Leitfähigkeit von TRPV3 erneut aufzeigt. Eine Expression der TRPV3-Mutante G573S in HEK-293-Zellen verdeutlichte die toxischen Auswirkungen der *gain-of-function*-Mutante auf die Überlebensrate der Zellen, wobei nach Behandlung mit dem etablierten Blocker Ruthenium Rot eine Erhöhung der Zellvitalität beobachtet werden konnte. Zusätzlich konnte mittels Immunfluoreszenz die zytoplasmatische Expression und bei einer geringen Zahl an Zellen sogar eine Färbung der Mutante in der Membran dokumentiert werden. Diese Beobachtungen unterstützen somit eher die Hypothese einer funktionellen Expression in der Membran, in der die *gain-of-function*-Mutation den Kettenprozess auslöst, der zu vermehrtem Zelltod führt.

Während der TRPV3-Kanals bisher in der Literatur hauptsächlich im Rahmen seiner Rolle bei der Ca^{2+}-abhängigen Signaltransduktion untersucht wurde, beleuchtet unsere Studie seine Vielseitigkeit. Demnach könnte der TRPV3 ganz allgemein eine Rolle als Kationentransporter spielen, darunter auch für das NH_4^+-Ion, mit Auswirkungen auf verschiedene biologische Prozesse in der Hautphysiologie, des Ionenhaushalts, der pH-Regulierung und der

Stickstoffnutzung. Diese Erkenntnisse tragen zu unserem sich stetig entwickelnden Verständnis der biologischen Rolle des TRPV3 bei und bieten Potenzial für zukünftige Forschung und klinische Interventionen.

1

Introduction

1. Introduction

The transient receptor potential (TRP) channel family, comprising 28 mammalian members with divers functions such as thermoregulation [135,249], nociception [162,208], and transport [295] has garnered increasing interest [172] in recent years. This heightened attention was underscored by the joint Nobel Prize in Physiology and Medicine awarded in 2021 to David Julius and Ardem Patapoutian [177] but still multiple functions remain elusive. This study specifically delves into the non-selective transient receptor potential cation channel, subfamily V, member 3 (TRPV3). *Inter alia*, this channel is recognized for its involvement in thermoregulation [165], hair morphogenesis [43], and its association with the rare hereditary disease Olmsted syndrome (OS) [140]. Despite progress, it remains uncertain why the gain of function mutation of TRPV3 leads to OS which requires a deeper understanding of the role of TRPV3 and its properties. Conflicting hypotheses have been published [140,286], prompting a need for additional insights into the role of mutant TRPV3 in OS. TRPV3 is also gaining recognition for its growing significance in cattle as a potential candidate for ammonium uptake in rumen [137]. This is particularly relevant due to the high demand for strategies aimed at reducing the substantial amounts of nitrogen excreted into the environment [109], which can have disastrous consequences [229].

This study aimed to provide data for solving a part of this intriguing puzzle by investigating the permeability of human TRPV3 (hTRPV3) and bovine TRPV3 (bTRPV3) to NH_4^+ using *Xenopus laevis* (*X.*) oocytes and HEK-293 cells as expression systems and a TRPV3 vector co-expressing GFP, to localize TRPV3 in human skin and bovine rumen, and to explore the trafficking of the OS mutant G573S. Immunoblotting and immunostaining were used to verify the successful expression and trafficking of TRPV3 to the membranes in the models. Single-channel patch clamp was used to determine the permeability to NH_4^+ and Na^+. PH-sensitive microelectrodes were used to measure acidification by NH_4^+ in *X.* oocytes. Whole-cell experiments of HEK-293 cells expressing hTRPV3 were used to investigate the influx of NH_4^+ stimulated by the enantiomers of menthol. Cell viability was investigated in HEK-293 cells expressing the OS mutant G573S utilizing the known TRPV3 inhibitor ruthenium red (RR). The findings suggest TRPV3's role extends beyond Ca^{2+} signaling, potentially impacting nitrogen metabolism and epithelial functions such as skin cornification and intestinal NH_4^+ transport.

To elucidate these questions, this thesis will give a literature review in chapter 2 on the rare hereditary disease OS, the non-selective cation channel family TRP with a focus on TRPV3, the functions and structure of the human skin especially in regard to the role of TRPV3, and the importance of the TRPV3 in cattle related to the environmental footprint and NH_4^+

metabolism and transport. Afterwards, my publication Liebe *et al.* [139] investigating the human TRPV3 is attached which forms the heart of my research and of this dissertation. Then, Liebe *et al.* [137] investigating the bovine TRPV3 is attached. Both have been elaborated in shared co-authorship with Franziska Liebe who used the data on bTRPV3 to write her PhD thesis "*Funktionelle und molekularbiologische Untersuchungen zur Beteiligung von zwei TRP Kanälen an der Leitfähigkeit des Pansenepithels für Ammonium, Natrium, Kalium und Calcium"*. Furthermore, I contributed to the publications of Liebe *et al.* [138] on the effects of $butyrate^-$ on ruminal Ca^{2+} transport and to Schrapers *et al.* [220] exploring bovine TRPV3 as pathway for the uptake of divers cations. These publications do not form the backbone of my thesis but are appended. In chapter 5, my main research questions are discussed in detail followed by a conclusion in chapter 6, the bibliography, and the appendices ([138] and [220]).

2

Literature review

2. Literature review

2.1. Olmsted syndrome

The following exposition is mainly based upon the review on the Olmsted syndrome from Duchatelet *et al.* [63] and the publications from Wilson *et al.* and [280] Lin *et al.* [140].

General

The Olmsted syndrome (OS) is a rare hereditary congenital disease that was first described in 1927 by Olmsted [182]. Classically, this genodermatosis is characterized by the combination of bilateral mutilating transgredient palmoplantar keratoderma (PPK) and periorificial keratotic plaques. However, the 106 cases that have been reported worldwide until June 2019 [82] exhibited considerable clinical heterogeneity (see **Figure 1**). Typically, the symptoms develop in early childhood or are already observable at birth and worsen over time with a slow but progressive course. Although male cases are more frequent, OS is observed in both sexes.

Figure 1. Clinical features of OS

Exemplary symptoms from two patients from different families. The patient from the top featured severe calluses on the weight-bearing areas of the soles (A) and thin nail plates with koilonychias (B) at the age of 9. Three years later, she additionally showed perioral keratoderma and fine hair (C). The seven year old Brazilian patient featured milder calluses on the soles of the feet (D), blisters and peeling of skin on the fingertips (E), and lack of perioral hyperkeratosis (F). The figure was published by Wilson *et al*. [280]

Symptoms

The most abundant symptom PKK is initially focal and distributed on pressure points, gradually extending to most of the surface and becoming diffuse, massive, and thicker with time with deep painful fissures. The keratotic lesions are pruritic and may inflict pressure induced pain. Additionally, cases are known with focal or punctuate keratoderma [103,178]. Pain and itching with variable intensity is a frequent feature of OS [148,161,178,195,204,247] and painful PKK is reported in approximately half of reported cases. The pain and itch represent major causes of morbidity resulting in insomnia and interfering with grasping and walking. The vast majority of patients show abnormalities in hair growth including alopecia (diffuse, universal, or patchy), hypotrichosis, as well as sparse, thinning, curly, woolly, coarse, dry, or easily broken hair [60,161,246-248]. OS patients also show abnormalities in nails [60,73,130,161,178,180,247], oral cavity [17,75,85,161,195,214,250], sweating [193,202], eye lesions [121,287], growth [161,180,268], recurrent infections [24,75,85,121,128,133], immunity [55,85], predisposition to malignancies [16,57,100,180,292], teeth [6,114,195], hearing [69,85,195,203], bones [124,133,180,195,214,246], and other rare symptoms [5,9,85,133,182,195,250]. The thermosensation is not affected in OS patients even on affected areas [140].

Diagnosis and diagnostic methods

Initially, the diagnostic hallmarks of OS are the association of bilateral transgredient mutilating PPK and periorificial keratotic plaques. Due to the non-specific symptoms, OS has to be differentiated from other severe forms of PPK that are enlisted in **Table 1.**

Diesease	**Gene**	**Mode of inheritance**	**MIM®**	**Orphanet**
Vohwinkel syndrome [212]	GJB2, LOR	Autosomal dominant	MIM#124500 MIM#604117	ORPHA494 ORPHA79395
Mal de Meleda [12]	SLURP1	Autosomal recessive	MIM#248300	ORPHA87503
Papillon-Lefèvre syndrome [92]	CTSC	Autosomal recessive	MIM#245000	ORPHA678
Clouston syndrome [159]	GJB6	Autosomal dominant	MIM#129500	ORPHA189
Pachyonychia congenita [232]	KRT6A, KRT6B, KRT16, and KRT17	Autosomal dominant	MIM#167200 MIM#167210	ORPHA2309
Tyrosinemia type II [151]	TAT	Autosomal recessive	MIM#276600	ORPHA28378
Haim-Munk syndrome [187]	CTSC	Autosomal recessive	MIM#245010	ORPHA2342
Acrodermatitis enteropathica [118]	SLC39A4	Autosomal recessive	MIM#201100	ORPHA37

Table 1. Severe forms of PKK

The periorificial involvement is the unique characteristic of OS that allows exclusion of the above mentioned syndromes except for acrodermatitis enteropathica which can be excluded by measurement of zinc levels. In contrast to OS, patients suffering from acrodermatitis enteropathica show improvement after oral zinc therapy to treat the diagnostic low zinc concentrations in plasma. In conclusion, the distinctive symptoms of OS lead to the correct diagnosis. However, full-blown OS is not always observed. This makes the diagnosis challenging for patients with partial cutaneous expression of OS. In the absence of specific biologic markers, molecular genetics is the most powerful approach to establish the diagnosis when the clinical presentation is unusual.

Genetics

Although familial cases with different modes of inheritance are known, the vast majority of OS cases are sporadic. The genetic basis has been partially elucidated by the identification of mutations in TRPV3 in 16 OS patients with Chinese, Indian, Iranian, Arabic, and Caucasian genetic background [55,62,64,71,103,122,132,140,178]. Detailed information about this channel and its family are summarized in Chapter 0. According to Duchatelet *et al.* [63], 7 dominant point mutations of TRPV3 (G573S in 5 unrelated OS patients, Gly573Ala, Gln580Pro, Leu673Phe, Trp692Gly, and Trp692Cys each in a unique case) have been reported as illustrated in **Figure 2**. Several dominant mutations were demonstrated to be gain-of-function mutations as described in detail below under *Pathogenesis*. Based on protein-level amino acid sequences, three recessive point mutations (Trp521Ser, p.Gly568Cys and p.Gln216-Gly262del) were also reported. This shows that the amino acids Gly573 and Trp692 seem to be recurrently mutated. Recurrent mutations are defined as more frequently observed mutations than expected by chance. Recently, the novel mutations p.Ala675Thr [44] and p.Met672Ile [146] have been identified with others likely to follow. The vast majority of mutations are located in the S4-S5 linker or in the C-terminal part of the protein. It is currently unclear why OS caused by *TRPV3* mutations show clinical heterogeneity with either typical OS hallmarks or an incomplete phenotype with atypical features.

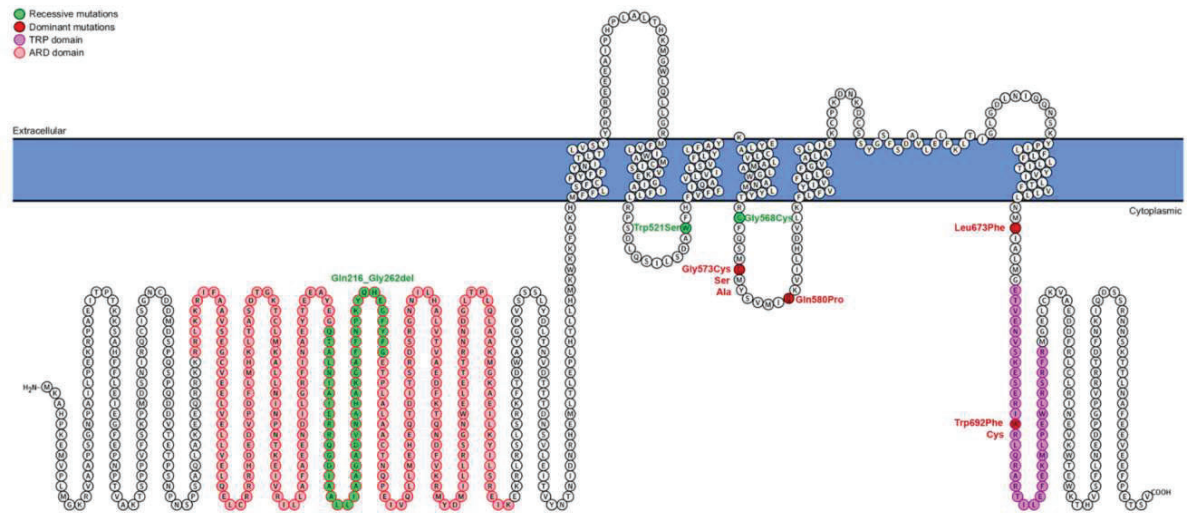

Figure 2. Schematic structure of TRPV3 and localization of reported OS mutations. Dominant mutations are indicated in red and recessive mutations in green. Amino acids localized in the ankyrin repeats domains and TRP domains are indicated in pink and purple, respectively [63].

Recently, Zhong *et al.* proposed a genotype-phenotype correlation of TRPV3-related OS [299]. They expressed seven variants in HEK-293 cells and characterized their channel behaviour

electrophysiologically. Their findings indicated that variations in the S4-S5 linker and TRP domain of TRPV3 significantly enhanced channel function which correlated with a severe phenotype whereas other variations appeared to exert milder effects on both channel function and phenotype. Still, genotype-phenotype correlations remain difficult to establish due to the rarity of OS.

Additionally, mutations in *MBTPS2* (membrane-bound transcription factor protease, site 2) gene (p.Phe464Ser and c.671-9 T>G, identified via protein-level aminoacid and coding DNA reference sequences, respectively [181]), have also been reported in recessive X-linked OS [94,268]. This gene encodes a zinc metalloprotease essential for endoplasmic reticulum stress responses and cholesterol homeostasis. Mutations in this gene are also known to cause a rare syndrome known as Ichthyosis follicularis - atrichia - photophobia (abbreviated as IFAP) [158] with 60 worldwide known cases until 2019 [119]. It can manifest with or without the BRESEK syndrome (MIM #308205, ORPHA2273), which is the acronym for the symptoms Brain anomalies, severe mental Retardation, Ectodermal dysplasia, Skeletal deformities (such as vertebral anomalies, scoliosis, polydactyly), Ear/eye anomalies (maldevelopment, small optic nerves, low set and large ears with hearing loss) and Kidney dysplasia/hypoplasia. The OS patient with the c.671-9 T>G mutation also presented with classical IFAP syndrome [268]. Previously reported patients with the same mutation in *MBTPS2* exhibited no OS-attributed features. The mechanisms are still unclear by which mutations of the *MBTPS2* gene lead to either OS or IFAP. However, Nemer *et al.* reported two cases with a recurrent mutation in *MBTPS2* and observed that WT *MBTPS2* regulates TRPV3 by inducing its activation which suggested an inter-relation between these two proteins [169].

Also, mutations of the *PERP* gene, which encodes the plasma membrane protein p53 apoptosis effector related to PMP-22, have also been reported to result in severe OS which shows the complexity and heterogeneity of the genetics leading to OS [53,61,236].

Considering the symptoms of the reported cases, there is no obvious clinical difference between OS patients exhibiting mutations of the *TRPV3*, *MBTPS2*, or *PERP* gene. It is highly likely that other factors like modifier genes, epigenetics and/or the environment have to play a major role for OS since clinical heterogeneity can be observed in patients with the same mutation and even in patients from the same family.

Pathogenesis

Although the pathogenesis of OS remains poorly understood, a defect in the expression of mature epidermal keratins (1 and 10) and persistence of basal keratins (5 and 14) [75,128,178,199] as well as increased expression of the mitotic marker ki-67 have been reported [69,203,247]. This leads to an improper proliferation of the involved immature areas which results in hyperkeratosis. It remains elusive by which mechanism the TRPV3 mutations lead to the OS pathogenesis which presents a major focus for research. Functional studies of four TRPV3 point mutations (Gly573Ser (from now on abbreviated as G573S), Gly573Cys, Trp692Gly and Gln580Pro) associated with OS [103] using patch clamp analysis on transfected HEK-293 cells clearly showed larger inward currents which the authors contributed to a highly increased open probability of the mutant channels as seen in **Figure 3** by Lin *et al.* [140].

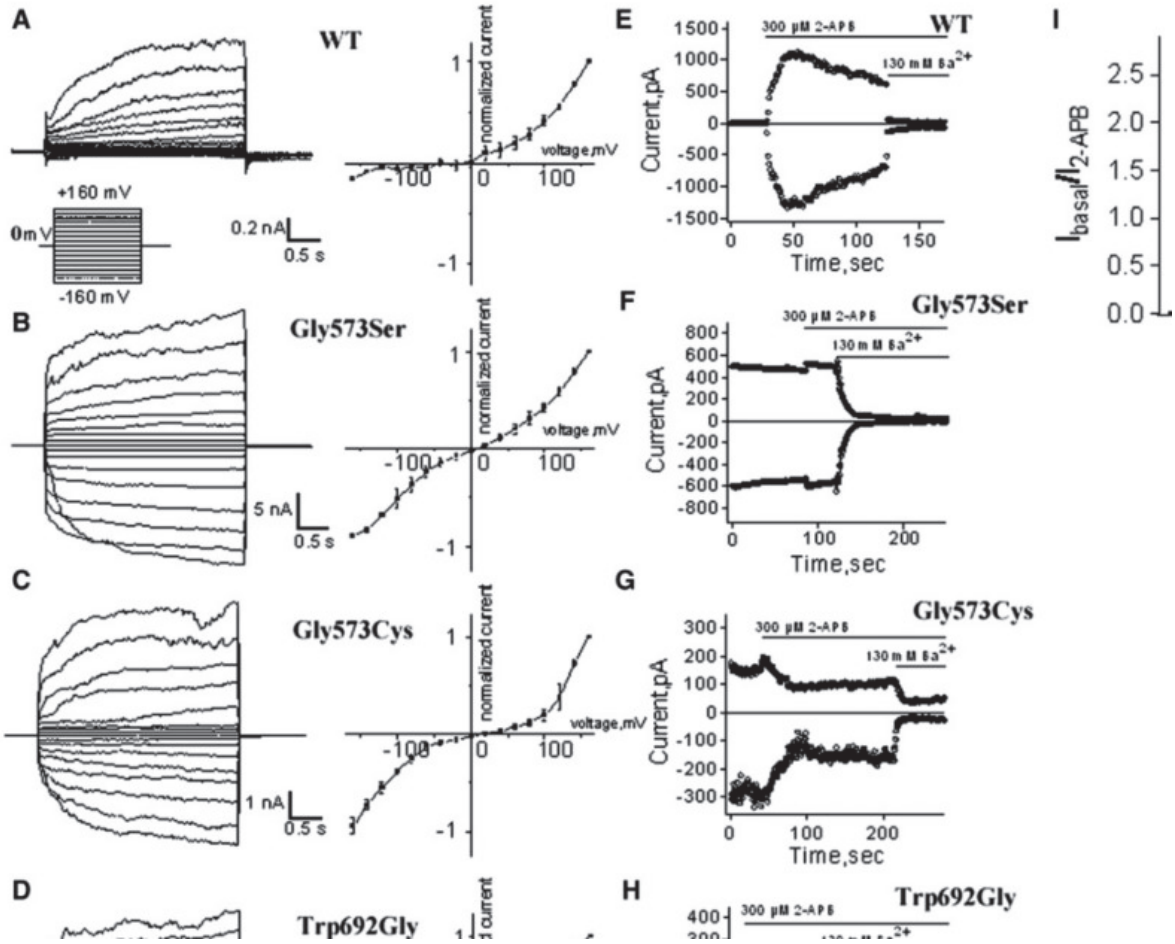

Figure 3. Whole-cell and inside-out recordings of TRPV3 currents from transfected HEK-293 cells

A–D) Representative whole-cell current traces in HEK-293 cells expressing TRPV3 or mutant channels in response to the voltage step protocol (left panels), and respective current-voltage plots from the steady-state currents (right panels).
E–H) Representative currents from inside-out patches in HEK-293 cells expressing TRPV3 or mutant channels in response to stimulation by 300 mM 2-APB (known TRPV3 agonist; see Figure 16C) or inhibition by 130 mM Ba^{2+} to assess the level of leak currents, at -80 mV and +80 mV. WT TRPV3 current is activated by 2-APB and followed by a characteristic decay. Note that the mutants Gly573Ser, Gly573Cys, and Trp692Gly show little activation, then inhibition in the presence of 2-APB, and a robust block by Ba^{2+}.
I) Comparison of ratios of currents evoked by 2-APB (300 mM) over basal currents between the WT and mutant channels. (t test, n = 3–7; p = 0.00001). Error bars represent SEM.
The figure and the description were published by Lin *et al.* [140].

Lin *et al.* [140] also observed a significantly increased apoptosis rate of overexpressing cells that could be partially rescued via incubation with the unspecific TRP blocker ruthenium red (RR; Figure 16A) as seen in **Figure 4**.

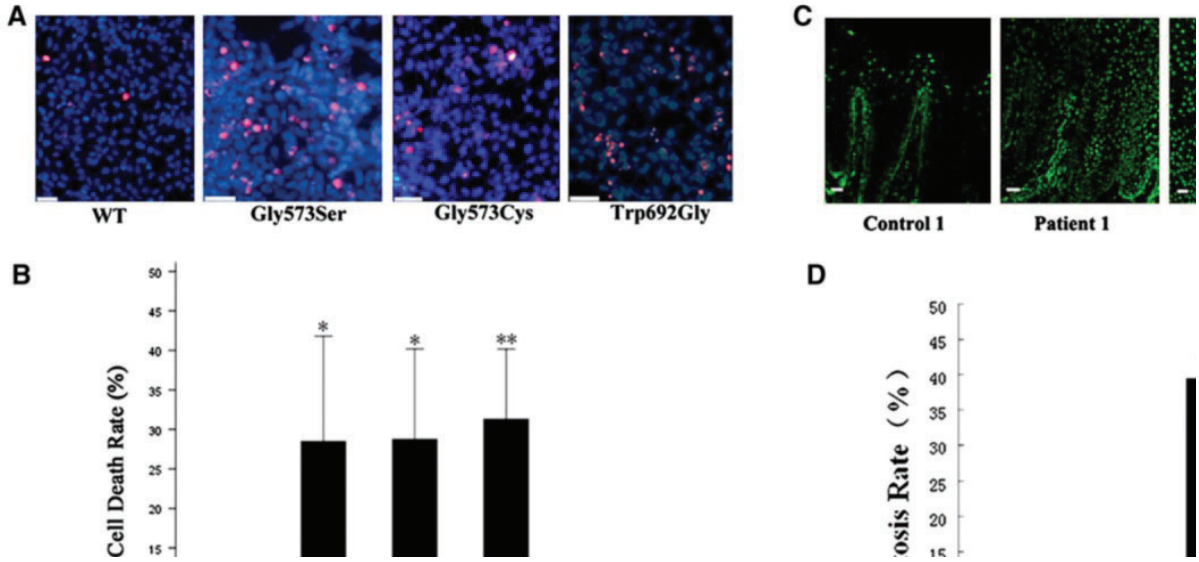

Figure 4. Cell death of transfected HEK-293 cells and apoptosis of keratinocytes of OS patients.

A) Merged images of transfected HEK-293 cells stained with propidiumiodid (red, Figure 16B) and Hoechst 33342 (blue). Mutants show significantly more propidiumiodid-positive cells compared to wild-type TRPV3.

B) Quantification of cell death rates in transfected HEK-293 cells (red nuclei/blue nuclei · 100 %). Data were averaged from three independent experiments. *p < 0.05, **p < 0.01.

C) Fluorescence microscope images (TUNEL method) of palm skin biopsy sections from an unrelated control and three patients. Large amount of apoptotic cells (with fluorescent nuclei) are seen in individuals with OS. The scale bars represent 50 mm.
D) Quantification of apoptotic keratinocytes in the skin sections. The mean proportion of apoptotic cells are significantly higher in the group of OS patients than in the group of normal controls (t test, n = 3, p = 0.000005). Error bars represent SEM.
The figure and the description were published by Lin *et al.* [140].

It was proposed that the gain-of-function mutations resulted in elevated intracellular Ca^{2+} concentrations (abbreviated as $[Ca^{2+}]_i$) inducing increased apoptosis. This hypothesis argues that enhanced cell death and increased $[Ca^{2+}]_i$ may drive OS. However, the mechanism by which an increased $[Ca^{2+}]_i$ with increased levels of apoptosis lead to the characteristic PKK with hyperkeratosis remains elusive.

Another group around Yadav [286] has explored the role of OS-causing TRPV3 mutants in keratinocytes using HaCaT cells and the GFP-tagged mutants Gly573Ser, Gly573Cys, Gly573Ala, and Trp692Gly. They demonstrated that these GFP-mutants have impaired trafficking, reduced surface expression, impaired cell adhesion, and abnormal lysosomal functions in comparison to the WT. Yadav proposed the hypothesis that TRPV3 is a lysosomal protein and that OS might be a lysosomal disorder. As seen in the confocal images in **Figure 5**, Yadav localized the WT in the plasma membrane and observed an enrichment in the cell-to-cell contact sites. However, the GFP-tagged mutants were localized in the perinuclear regions and were mainly restricted to the ER and in the nuclear envelope. Additionally, Yadav used an antibody (Alomone Labs, recognizes AA 464–478) specific for the extracellular loop region of TRPV3. Thus this antibody is able to detect TRPV3 present in the plasma membrane without permeabilizing the cells. As seen in **Figure 5d**, this antibody stained the plasma membrane of the WT but not of the OS mutants. Yadav also quantified the morphological parameters such as cell periphery and area of the HaCaT cells and observed smaller cell size, smaller cell periphery, and a rounder shape in mutants in comparison to the WT as visualized in **Figure 5e-g**.

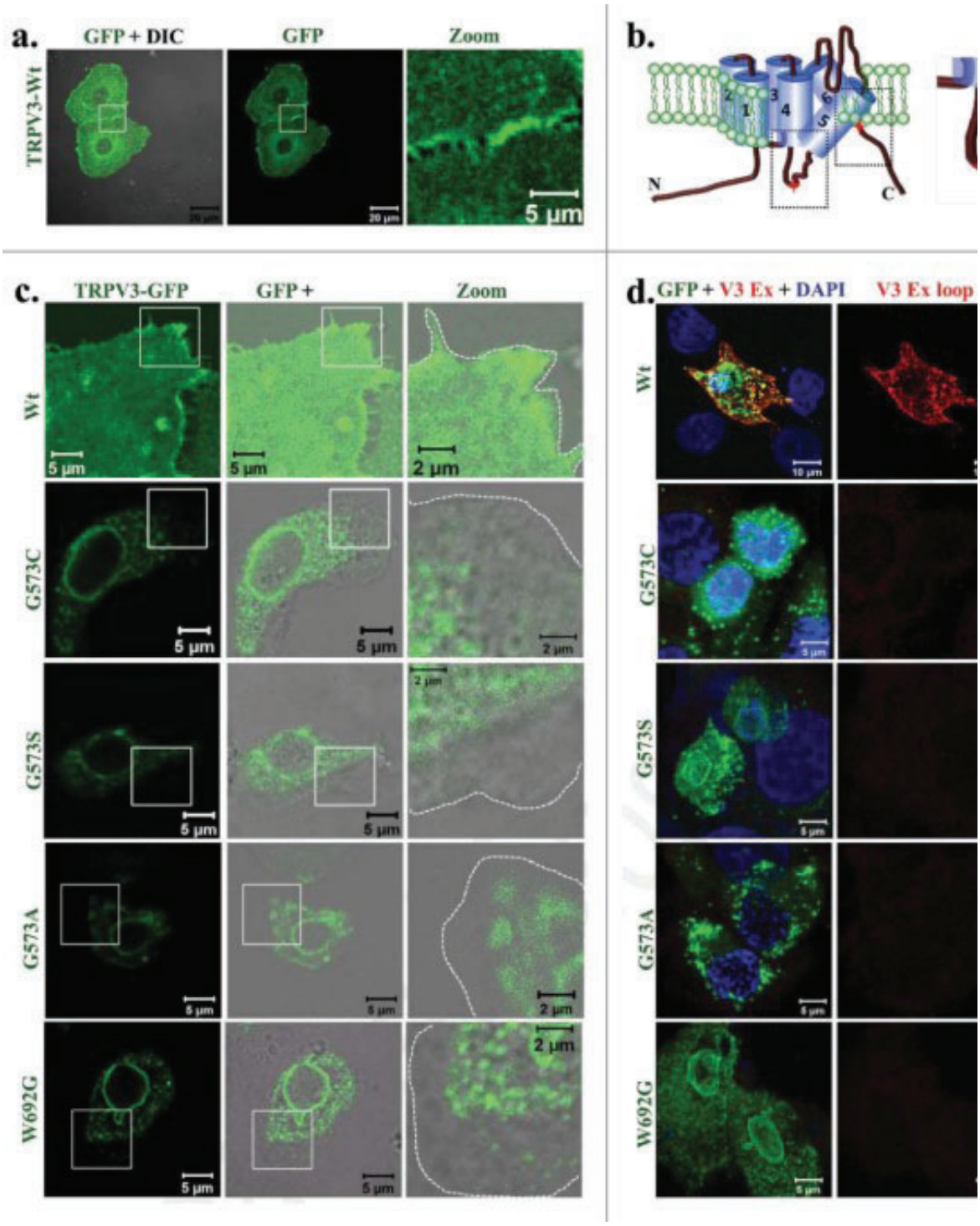

Figure 5. Confocal images of GFP-tagged OS-mutants and WT expressed in HaCaT cells.

OS-mutants but not WT have reduced surface expression. (A) Shown are the 3D-reconstituted confocal images of HaCaT cells transiently expressing WT-GFP. The enlarged image demonstrates the presence of TRPV3 at cell-cell contact sites. (B) Positions of point

mutations (G573A, G573S, G573C and W692G) are indicated. (C) The GFP fluorescence (green) alone or merged with DIC are shown. OS-mutants show no localization at the cell surface (cell boundary is indicated by dotted line) and accumulate at the ER. (D) An extracellular loop-specific antibody detects TRPV3 available at the cell surface (red) only in unpermeabilized cells expressing WT but not in unpermeabilized cells expressing OS-mutants. Intensity of TRPV3staining is provided in the right side. (E-G) expressing OS-mutants have much reduced cell periphery (E), area (F) and are more round in shape (in each case n = 70 cells and p value < 0.001 is considered as significant).
The figure and the description were published by Yadav *et al*. [286].

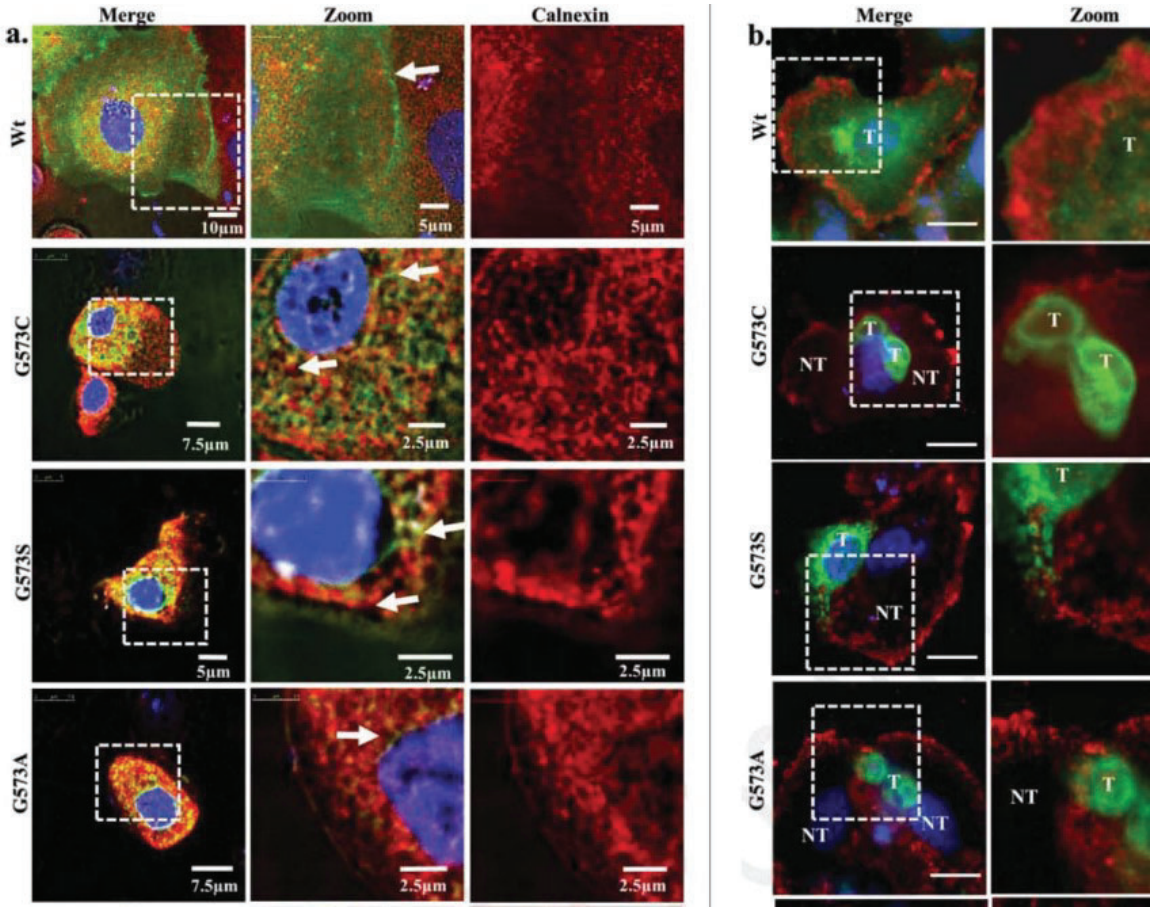

Figure 6. Confocal images of OS-mutants co-localized with E-calnexin in HaCaT cells
OS-mutants co-localize with calnexin, a chaperone that specifically retains unfolded or unassembled N-linked glycoproteins in the ER. OS-mutants did not co-localize with E-cadherin, a Ca^{2+}-dependent transmembrane glycoprotein for cell-cell adhesion. (A) Shown are the confocal images of HaCaT cells transiently expressing TRPV3-Wt-GFP or OS-mutants. Cells were fixed within 36 hours after transfection and the cells were stained for anti-Calnexin antibody. TRPV3-Wt shows discrete ER-labeling and TRPV3 localization on

membrane, while OS mutants shows co localization with ER (Merge image) suggesting that OS-mutants have reduced surface expression and are primarily retained in ER. (B) Immunolocalization of TRPV3-Wt-GFP and OS-mutants with membrane marker E-cadherin is shown. TRPV3-Wt-GFP shows proper E cadherin labeling and proper TRPV3 localization on membrane, while OS mutants are not localize on the membrane. In most cases, cells expressing OS mutants have much reduced E-cadherin staining (T and NT represent transfected and non-transfected cells respectively). Scale bar is 10mm and 5mm for merge and zoom images.

The figure and the description were published by Yadav *et al*. [286] but were adjusted slightly.

The hypothesis of Yadav is illustrated in **Figure 7** and visualized the proposed effect of the OS mutants. They suggest that their semi-quantative and qualitative data show the restriction of the OS mutants primarily to the ER regions and result in reduced surface expression. As a result, the HaCaT cells exhibited a loss of cell adhesion and contacts due to the lack of successful trafficked membrane proteins which stands in contrast to the hypothesis of Lin *et al.* of an increase of channel activity due to the gain-of-function mutation [140].

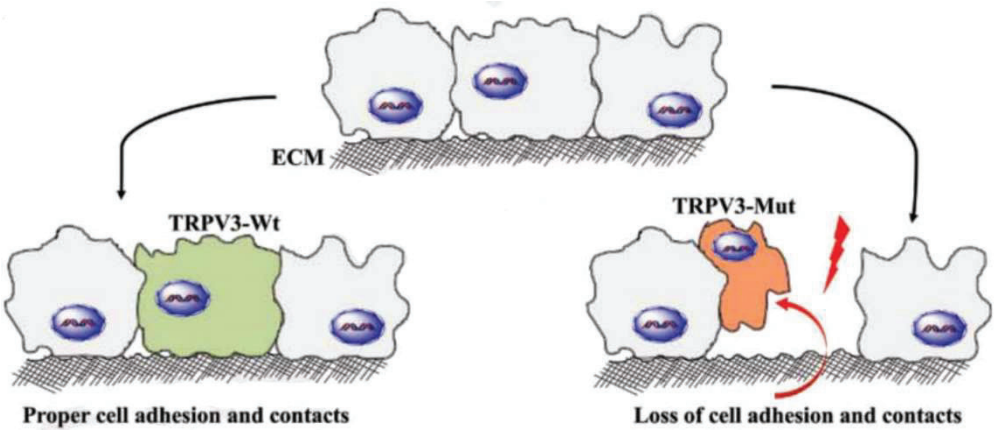

Figure 7. Schematic diagram demonstrating the loss of cell adhesion and cell-to-cell contacts due to expression of OS-mutants

The figure was published by Yadav *et al*. [286].

Prognosis

For OS patients, no reduced live expectancy has been reported but the progression of the ailment can lead to severe morbidities. The auto-amputation of digits and progressive keratoderma worsens the disease because it prevents patients from walking and grasping and can confine the subjects to a wheel-chair. Additionally, the severe pain and pruritus increases discomfort and may result in insomnia while corneal dystrophy can lead to blindness.

Management and treatment

Until very recently, there was no specific treatment for OS that was sufficiently tested and satisfactory. Skin lesions are usually refractory to therapy. Hyperkeratosis can be reduced with varying results using topical treatments like emollients (white etrolatum), keratolytics (salicylic acid, urea), wet dressing, boraic acid, tar, shale oil, corticosteroids, steroids, and retinoid acid. Skin grafting showed initial improvement but was followed by recurrence of the hyperkeratosis [19]. Poor to moderate relief could be observed in several OS patients after treatment with systemic retinoids, corticosteroids, or methotrexate [100,204,246,250]. Furthermore, symptomatic treatments are available that partially relieve the pain (painkillers, topical lidocaine, and others) or reduce the thickness of the keratotic palmoplanar skin lesions. All methods do not heal or slow down progression of the disease.

Recently, a very promising treatment option was suggested by Greco *et al.* [91] who used the epidermal growth factor receptor (EGFR) inhibitor Erlotinib. The drug is available as medication to treat non-small cell lung cancer (NSCLC) and pancreatic cancer. The 3 OS patients were treated with doses lower than those used in oncology with only moderate to mild adverse effects resulting in sustained improvements, with a marked reduction in pain and hyperkeratosis over a year and follow-up within 3 months of initial therapy. Similar observations were made by Zhang *et al.* who treated 4 children suffering from OS with erlotinib with highly promising results [294]. More research needs to be dedicated to this branch of treatment but the therapeutic success supports a model in which EGFR stimulates keratinocyte differentiation into corneocytes.

The development of new specific TRPV3 antagonists like dyclonine [143] to challenge the gain-of-function mutation may be another effective approach, which has so far only been tested in mouse models of the disease. More research is clearly needed to understand the role of the TRPV3 channel in health and disease, which might help OS patients harbouring such mutations. Understanding the mechanism how a vast array of different mutations leads to the same phenotype may also yield valuable insights for future strategies to cure this hereditary disease. Another promising approach may be discovered using gene therapy and CRISPR-Cas9, but this field clearly needs extensive further research and ethnical approval from society [70,134].

2.2. TRPV3 Channel

TRP

In 1969, the *trp* gene family was discovered in a *Drosophila* mutant with defective light sensing that exhibited only transient light-induced receptor potentials (TRP) and not the physiologically normal prolonged response [51]. Related proteins were subsequently found almost ubiquitously throughout the animal kingdom and the channels are now known to play important roles not only in insects, but also other species including mammals.

The TRP channel superfamily contains 28 mammalian members which are subdivided into seven subfamilies, most of which allow permeation of a variety of cations [174,175]. The seven subfamilies are TRPM (M for melastatin), TRPC (C for canonical), TRPA (A for ankyrin), TRPV (V for vanilloid), TRPP (P for polycystin), TRPML (ML for mucolipin) and TRPN (N for nonmechanoreceptor) [240]. After gene expression, the proteins assemble into hetero- or homotetramers that are located in the plasma membrane [83]. Activation of the non-selective members leads to influx of Na^+ and Ca^{2+} and efflux of K^+, thus depolarizing the membrane potential of cells at rest [185]. This can lead to an inactivation or activation of voltage-dependent ion channels and thereby modulates ion flux through transporters and channels. Furthermore, the influx of Ca^{2+} can lead to activation of numerous second messenger cascades [28]. Several members are selective for divalent cations over monovalent cations. Thus, TRPV5 and TRPV6 are known for their role in the absorption of Ca^{2+} across the renal tubule and the intestine [192], while TRPM6 and TRPM7 are involved in Mg^{2+} homeostasis [218]. It is also known that some TRP´s act as intracellular ion channels in several cell organelles such as endosomes, lysosomes, endoplasmatic reticulum, golgi network, and synaptic vessels where they mainly act as Ca^{2+} release channels [84].

TRP channels were found in the brain, heart, testis, kidney, liver, lung, ovary, spleen, placenta, uterus, prostate, intestine, and vascular tissue [163]. They are involved in a still growing number of cellular functions [256] like thermosensation, touch, pain, osmosensation, detection of pheromones, and taste [49,189] but also in vasorelaxation, metabolic stress, and immune function regulation [90,163]. Additionally, diverse members of the TRP family are linked to several human diseases [293] such as autosomal polycystic kidney disease [196], mucolipidosis [264], hereditary hypomagnesaemia and secondary hypocalcaemia [217], with less direct links to a range of autoimmune and inflammatory conditions like inflammatory bowel disease [25] and asthma [111]. In short, TRP channels have emerged as promising future therapeutic targets for diverse pathological conditions while being amenable to a wide range of modulators like changes in pH, temperature, mechanical stress, and Ca^{2+} concentrations [77].

TRPV

The vanilloid family of transient receptor potential (TRPV) channels belongs to one of the best studied subgroups in the TRP family, comprising the six channels TRPV1 to TRPV6 based on homology [173]. The family is named after its first mammalian member VR1 that binds vanilloids like capsaicin (**Figure 16D**) [262]. TRPV1, 2, 3, and 4 have striking temperature sensitivities ranging from 30 to 52 °C with permeability to both monovalent and divalent cations such as Ca^{+2} and are classically associated with sensory functions [260]. Conversely, TRPV5 and TRPV6 are highly Ca^{2+} selective and function as epithelial Ca^{2+} channels that are regulated by calcitropic hormones such as Vitamin D [253]. The channel function of all TRPV´s is tightly regulated by the intracellular Ca^{2+} concentration (abbreviated as $[Ca^{2+}]_i$) and phosphoinositides. All TRPV´s seem to share structural similarity with the cryo-electron microscopic structure of TRPV1 that exhibits fourfold symmetry and features two distinct regions: a compact transmembrane domain and a large intracellular basket-like domain [164].

TRPV3

The phylogenetic outsider TRPV3 (ENST00000301365.8, cryo-EM structure is illustrated in **Figure 8**.) shares only 43 % sequence homology with TRPV1 [172] and was originally cloned by three groups in 2002 [190,233,285]. Due to its thermosensitivity, the channel was thought to function as a thermosensor [173]. However, against expectations, the channel was not highly expressed in the sensory dorsal root or trigeminal ganglia in rodents but instead most abundantly expressed in epithelia including epidermal and hair follicle keratinocytes as well as in the tongue, testis, cornea, distal colon, human larynx, and inner ear [30,95,116,160,165,173,190,251,285]. The channel is notoriously promiscuous with a low selectivity for Ca^{2+} [191]. In contrast to other TRPV channels that desensitize during repetitive activation, uniquely, TRPV3 channel activity successively increases upon repeated stimulation which can be reduced by ATP [47,190,282,285]. TRPV3 has been identified as an interacting partner of calmodulin (CaM) [194], EGFR [43], A-kinase anchor protein 5 (AKAP-5) [297], and TRPV1 [233]. One of the most prominent features of TRPV3 is its high expression in keratinocytes of the skin, mainly in cells surrounding hair follicles [252].

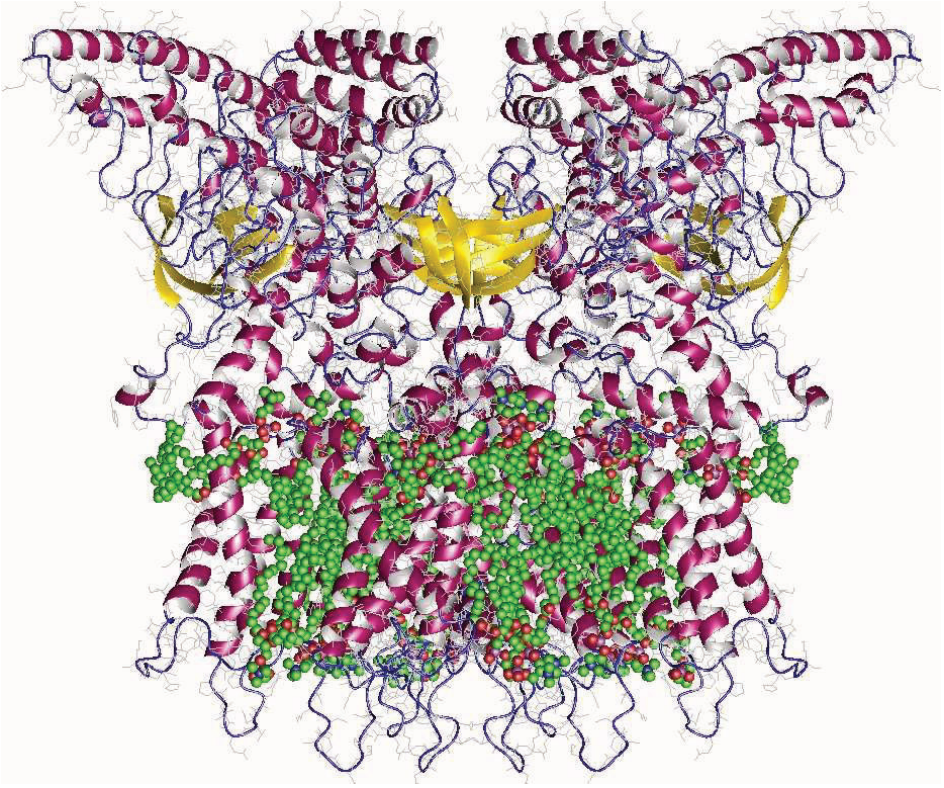

Figure 8. Protein structure of TRPV3

Structure of the TRPV3 homotetramer cation channel depicting the pore region on the top side and the intracellular domain on the bottom. This structure was published by Nadezhdin *et al.* in 2021 using data obtained using cryogenic electron microscopy (cryo-EM) [167].

TRPV3 modulators

TRPV3 is typically activated by innocuous warm temperatures above 33 °C [190,233,285]. Apart from this, the polymodal TRPV3 is also known to be stimulated by various pharmaceutical agonists (with corresponding EC_{50} values) like eugenol (2.3 mM) [65,284], carvacrol (0.49 ± 0.07 mM) [157,261,284], thymol (0.86 ± 0.07 mM) [183,261,284], camphor (6.03 ± 1.47 mM) [183,224,261], ethyl vanillin [13], menthol (1 mM, **Figure 16**) [150], the endogenous farnesyl pyrophosphate (0.13 µM) [15,281], and the synthetic 2-APB [50]. Notably, 2-APB plays a remarkable role due to its known inhibitory effect on various channels of the TRP family like TRPC1, 3, 5, 6, 7, TRPM3, 7, 8, TRPP2, and TRPV5 [50]. In contrast, 2-APB is known as a common activator of TRPV1, V2, and V3 with EC_{50} values of 114 ± 8, 129 ± 13, and 34 ± 12 µM respectively obtained using Ca^{2+} essays at 32 °C in HEK-293 cells transiently transfected with complementary DNA (cDNA) for the TRP channels [50]. Chung *et al.* [47] confirmed the EC_{50} value for TRPV3 by using HEK-293 cells expressing mouse TRPV3 (mTRPV3) and determined EC_{50} values of 28.3 µM at +80 mV and 41.6 µM at -80 mV with apparent saturation between 100 and 320 µM which are in range with the values obtained in

the Ca^{2+} essay of Colton *et al* [50]. This activation of TRPV3 has also been demonstrated in *Xenopus* laevis oocytes (*X.* oocytes) injected with cRNA for mTRPV3 where incubation with 300 µM 2-APB induced significant inward currents at -40 mV which was blocked by 3 µM ruthenium red (RR) but not by 10 µM capsazepine, the synthetic antagonist of the TRPV1 agonist capsaicin [110]. The same experiment demonstrated that a 40 °C temperature challenge did not invoke a significant current while application of 100 µM 2-APB at 40 °C invoked a current that was 35 ± 6 times in amplitude of that induced by the same concentration at 22 °C showing the immense potentiation of the thermal response of TRPV3 by 2-APB [110]. TRPV3 can be sensitized to warm temperatures by numerous pro-inflammatory agents like bradykinin, PGE_2, histamine, ATP, activation of protein kinase Cε, and receptor-coupled hydrolysis of phosphatidylinositol 4, 5-bisphosphate [172]. In contrast to the large number of known agonists, it has been more difficult to establish reliable blockers for TRPV3. Traditionally, RR has been shown to reliable block inward currents with an IC_{50} (half maximal inhibitory concentration) of 2.4 ± 0.4 µM [47] but it is non-specific [258]. Recently, the plant derived acridone alkaloid citrusinine-II from *Atalantia monophylla* has been shown to interact with Y564 within the S4 helix of TRPV3 to inhibit the channel with an IC_{50} of 12.43 µM and is currently investigated for its use in anti-pruritus pharmacology [97]. Additionally, the natural coumarin osthole from the *C. monnieri* plant which is commonly used in Chinese herbal medicines used for dermatitis and pruritus has also been identified to inhibit TRPV3 channels in transiently TRPV3 transfected HEK-293 cells in calcium fluorescent essays and whole-cell recordings [244]. Hang Qi *et al.* [197] demonstrated that the active components of the herb *Achillea alpine*, isochlorogenic acid A (IC_{50}: 2.7 ± 1.3 µM) and isochlorogenic acid B (IC_{50}: 0.9 ± 0.3 µM), can significantly decrease the open probability of TRPV3. Kewei Wang *et al.* [243] demonstrated the natural compound forsythoside B found in *Lamiophlomis rotata* as TRPV3 inhibitor (IC_{50}: 6.7 ± 0.7 µM) which can be used to alleviate acute and chronic itching. Several pharmaceutical companies have also developed an array of suitable compounds like Hydra Biosciences that reported a series of tetrahydroquinoline amides to selectively inhibit TRPV3. Their most promising compound #64 reportedly exhibited an IC_{50} value of 0.2 – 1 µM while also being highly selective (>40-fold vs. other TRP channels) just to name one example [46]. Despite extensive research and dedication, no commercial TRPV3 modulators are on the market so far. Possible reasons include poor reproducibility of effects, non-specific interactions leading to unwanted side effects and varying distribution mechanisms for humans and animals [240].

Role of TRPV3 and diseases

The role of TRPV3 as a thermosensor remains elusive. The expression pattern in epithelial cells and keratinocytes rather than in neurons tentatively argues against a primary role in

sensation [242,267,283]. Nevertheless, in a first investigation, Moqrich *et al.* [165] demonstrated that TRPV3 knockout mice exhibit strong deficits in response to innocuous and noxious heat but not in other sensory modalities. TRPV3 knockout mice also lacked the known activation of sensory nerve fibers due to heat-induced ATP release by keratinocytes [153]. Intriguingly, intragastric admission of natural TRPV3 agonists like thymol or ethyl vanillin did not have an effect on heat diffusion or thermogenesis which indicates a restricted effect on autonomic thermoregulation of TRPV3 [155]. In contrast to the initial findings, a re-investigation of TRPV3 knock-out mice with defined backgrounds showed no apparent alternations in thermal preference behavior which indicates limited involvement in thermoregulation [113]. There is thus some speculation that TRPV1, 3, and 4 exhibit significant functional redundancy which might explain the lacking thermosensory deficit in TRPV3 knock-out mice [172]. Human patients with a hereditary gain of function mutation of TRPV3, Olmsted syndrome, also do not exhibit defects in thermosensation, but show a severe and often disabling hyperkeratosis of the skin which is described in more detail in chapter **2.1 Olmsted syndrome**. Accumulating all evidence, TRPV3 should probably be omitted from the list of regulatory TRP thermosensors [173]. Notably, it is still interesting that TRPV3 seems to have played a role in the evolution of thermoregulation because in lower vertebrates such as the frog *Xenopus tropicalis*, TRPV3 is not activated by heat but detects noxious low temperatures of these cold blooded animals [211].

However, other non-sensory functional roles appear possible. Hair morphogenesis and epidermal development are orchestrated by an array of cytokines and growth factors [78]. Upregulation of transforming growth factor-α/ epidermal growth factor receptor (TGF-α/EGFR) signaling leads to the hairless phenotype in mice as shown by Schneider *et al* [219]. TRPV3 mice were found to have curly hair and whiskers, while a gain of function mutation of TRPV3 caused a hairless phenotype with itchy skin in mice [237].

TRPV3 is also associated with a variety of diseases like pruritic and atopic dermatitis [255,289,291], psoriasis [222], cutaneous pruritus [223,288], rosacea [241], cancer [136,238], myocardial hypertrophy [296], cardiac fibrosis [144], myocardial infarction [269], pain [7,89,112], and alopecia [290].

To elucidate the role of TRPV3 in the human skin, it is beneficial to read the overview in **2.3 The human skin**.

Additionally, Wang *et al.* proposed a model to explain the possible role of TRPV3 in itch and other related skin diseases which is shown in **Figure 9** [266]. They suggested the hypothesis that the influx of Ca^{2+} via TRPV3 leads to an elevation of Ca^{2+}-dependent production and

release of TGF-α or other EGFR ligands which in turn stimulate EGFR. They hypothesized a physically association between TRPV3 and EGFR to form a signaling complex which sensitizes the responses of TRPV3 to endogenous activation, which ultimately leads to a positive feedback loop that results in terminal differentiation of suprabasal keratinocytes and the release of numerous inflammatory molecules like histamine, TSLP, chemokines, and cytokines [266].

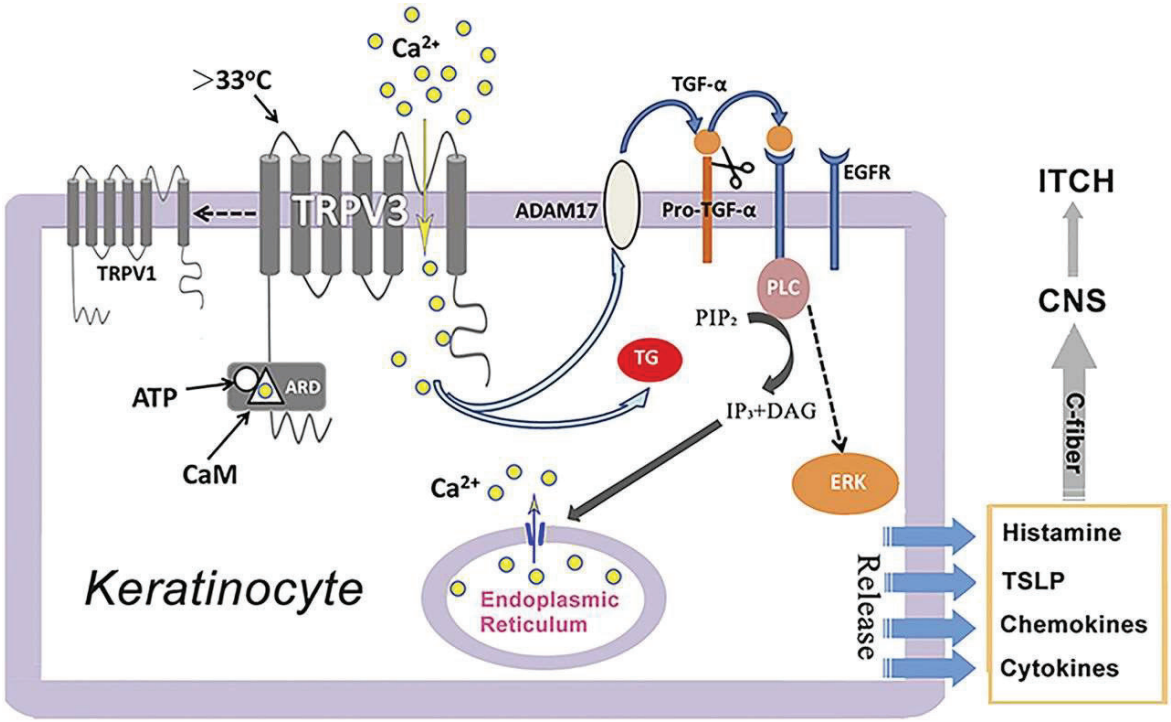

Figure 9. Proposed role of TRPV3 in itch signaling and hair growth

Proposed role of TRPV3 in itch signaling and hair growth. TRPV3 is abundantly expressed in keratinocytes, the predominant cell type comprising the layers of the epidermis in the skin. Keratinocytes release numerous inflammatory molecules such as histamine, TSLP, chemokines, and cytokines, accounting for enhanced pruriceptor sensitivity under chronic itch conditions. The TRPV3 channel is activated by mechanisms that include elevated intracellular acidification (protons), temperature, activators, and other unidentified cellular events, resulting in an elevation of Ca^{2+}-dependent production and release of TGF-α or other EGFR ligands. TGF-α in turn stimulates EGFR, which physically associates with TRPV3 to form a signaling complex, and consequently sensitizes the responses of TRPV3 to endogenous activation. Thus, a positive feedback loop is formed between TRPV3 and TGF-α/EGFR, likely resulting in terminal differentiation of suprabasal keratinocytes that are actively participated in reepithelialization, wound closure, and hair morphogenesis.

Coexpression of TRPV3 with TRPV1 enhances the capsaicin- or proton-evoked rise of intracellular Ca^{2+} concentrations, suggesting a physical association between the two proteins. Binding of ATP to conserved sites in the N-terminal ARD domains shared by TRPV3 and TRPV1 channels also suggests functional interactions between the two channels. ADAM17, metalloprotease ADAM17; ERK, extracellular signal-regulated kinase; CNS, central nervous system; DAG, diacylglycerol; IP3, inositol trisphosphate; PLC, phospholipase C; TSLP, thymic stromal lymphopoietin.

The figure and the description were published by Wang *et al* [266].

2.3. The human skin

The human skin is the largest organ if the body [18], functions as the protective barrier between the internal milieu and the environment, regulates temperature and fluid balance, and serves as the first line of defense against pathogens [270]. Its complex cellular network constitutes an immunological barrier [58,59]. The skin is composed of the three primary layers epidermis, dermis, and hypodermis (see **Figure 10**), although opinions differ whether the hypodermis should be considered to be a part of the skin [3] or not [126].

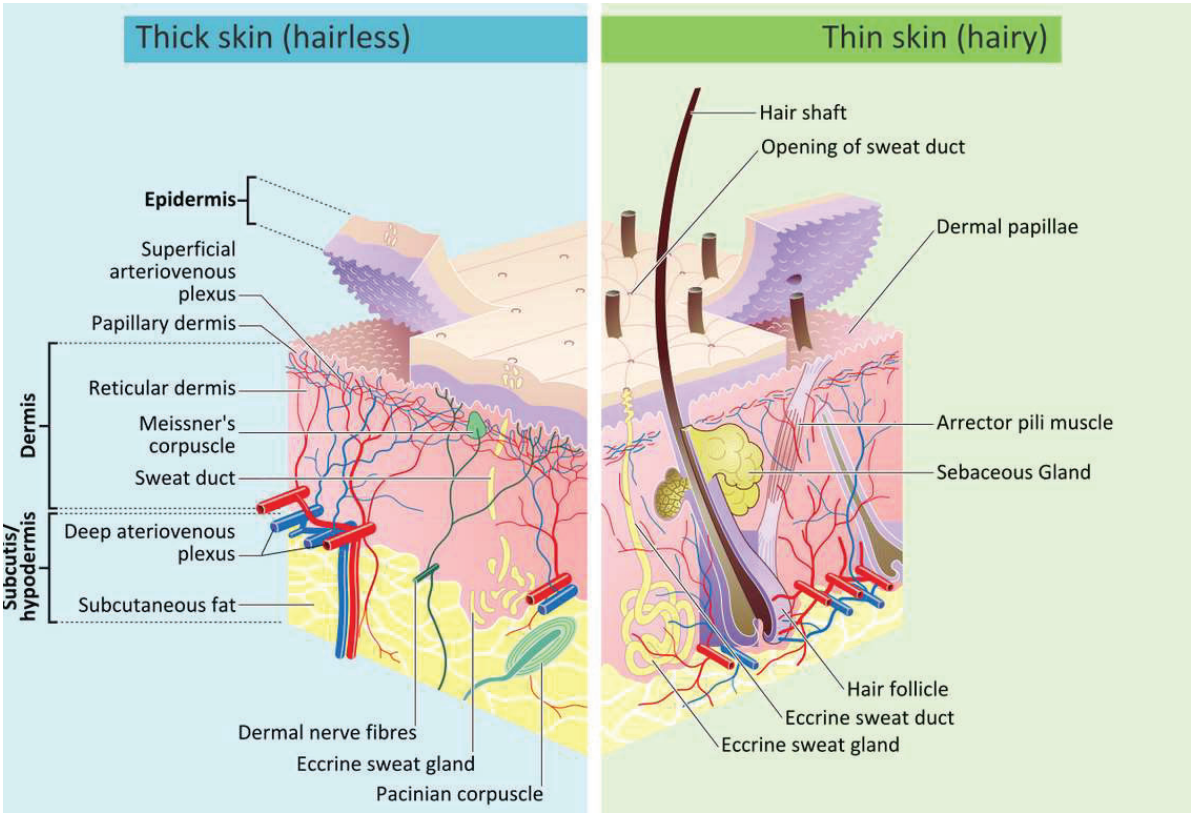

Figure 10. **Skin layers of hairy and hairless skin**

This illustration was published by Komorniczak *et al* [152].

The hypodermis connects the skin to underlying structures like muscles or bones and is commonly referred to as subcutaneous tissue [126]. It is composed of loose areolar and adipose tissue and provides additional cushion and insulation [126]. The dermis comprises the nerve endings, sweat glands, fibroblasts, and blood vessels among other structures [270]. It subdivides into the two layers superficial papillary dermis, which forms finger-like projections into the epidermis known as dermal papillae, and the deep reticular layer, which has dense connective tissue that forms a strong network [36]. The dermis provides elasticity and tensile

strength to the skin through an extracellular matrix which is composed of elastic fibers, collagen fibrils, and microfibrils [34]. These are embedded in hyaluronan and proteoglycans which are varied and have very specific locations [235]. A basement membrane separates and connects the dermis and the epidermis with anchoring epidermal mature melanocytes [270]. This membrane controls the traffic of cells and molecules while also serving as a reservoir for the controlled release of cytokines and growth factors during repair processes or physiological remodeling [115]. The outermost skin layer epidermis is composed of a network of keratinocytes with interconnected melanocytes and scattered inflammatory cells [270]. The epidermis is the frontier barrier of the body and can be subdivided into the five layers stratum corneum, stratum lucidum, stratum granulosum, stratum spinosum and stratum germinativum which is more commonly known as stratum basale [18]. The self-regeneration of the epidermis is achieved by accurate regulation of keratinocyte proliferation, migration, differentiation, and apoptosis [225,226]. The most crucial structural constituents of keratinocytes are the intermediate filaments called cytokeratins which play an essential role in the barrier function and development of the skin [231]. Proliferation of keratinocytes takes place in the basal layer and is stimulated by various growth factors [18,226,231]. Keratinocytes are stimulated to grow by members of the epidermal growth factors (EGF), fibroblast growth factors (FGF), nerve growth factors (NGF), granulocyte-macrophage colony stimulating factor (GM-CSF), and endothelin-1. On contrast, transforming growth factor-b, vitamin D3, and interferon-ɣ suppress their growth [18]. Keratinocytes are not only regulated by growth factors but they are also a source for various growth factors, chemokines, and cytokines themselves which is why they play a crucial role in the skins cytokine network [226]. Also, keratinocytes produce a vast array of hormones, neurotransmitters, and cytokines when stimulated by light, pain, temperature, or pressure [230]. These substances are mediators of inflammation and immune responses which are essentially connected to the pathophysiology of skin diseases and play an important role in skin wound healing [221,226]. The differentiation of keratinocytes occurs during the migration from the basal layer towards the skin surface which is followed by the cornification or keratinization where the cells progress from rounded cells to a flat form thereby building up the cornified outer layer of the skin [231]. This layer is most effected by external stimuli and is comprised of lipids, the cornified lipid envelope, cross-linked proteins, and the cornified cell envelope [32]. A visualization of the process of the terminal differentiation of the keratinocytes is shown in **Figure 11**.

The epidermal stem cells are located in the basal layer of the epidermis and in special niches of the hair follicles [8]. Proliferating keratinocytes generate cells that stop to divide and start terminal differentiation. Those cells move into the suprabasal layer or into suprabasal positions in the bulge of hair follicles. The keratinocytes change their gene expression profile after

detachment from the basement membrane [127,131]. Later during differentiation, the expression of the epidermal differentiation complex (EDC), a gene cluster, generates vital proteins such as involucrin and loricrin [104,131] which are cross-linked by enzymes of the transglutaminase family [41]. Transglutaminases can be for example activated by Ca^{2+} that could be released from degrading mitochondria or endoplasmatic reticulum [43,67]. Involucrin and loricrin form an insoluble cornified envelope close to the surface [41]. The EDC also encodes filaggrin, the main component of keratohyalin granules to which the granular layer owes his name. Filaggrin is dispersed and causes aggregation of the keratin intermediates [213]. At the same time, the nucleus is degraded and cell organelles disappear by an unknown mechanism [67]. At the end, keratins remain as the prevailing proteins inside the CE [179] and contribute strongly to the mechanical resistance of the stratum corneum [67].

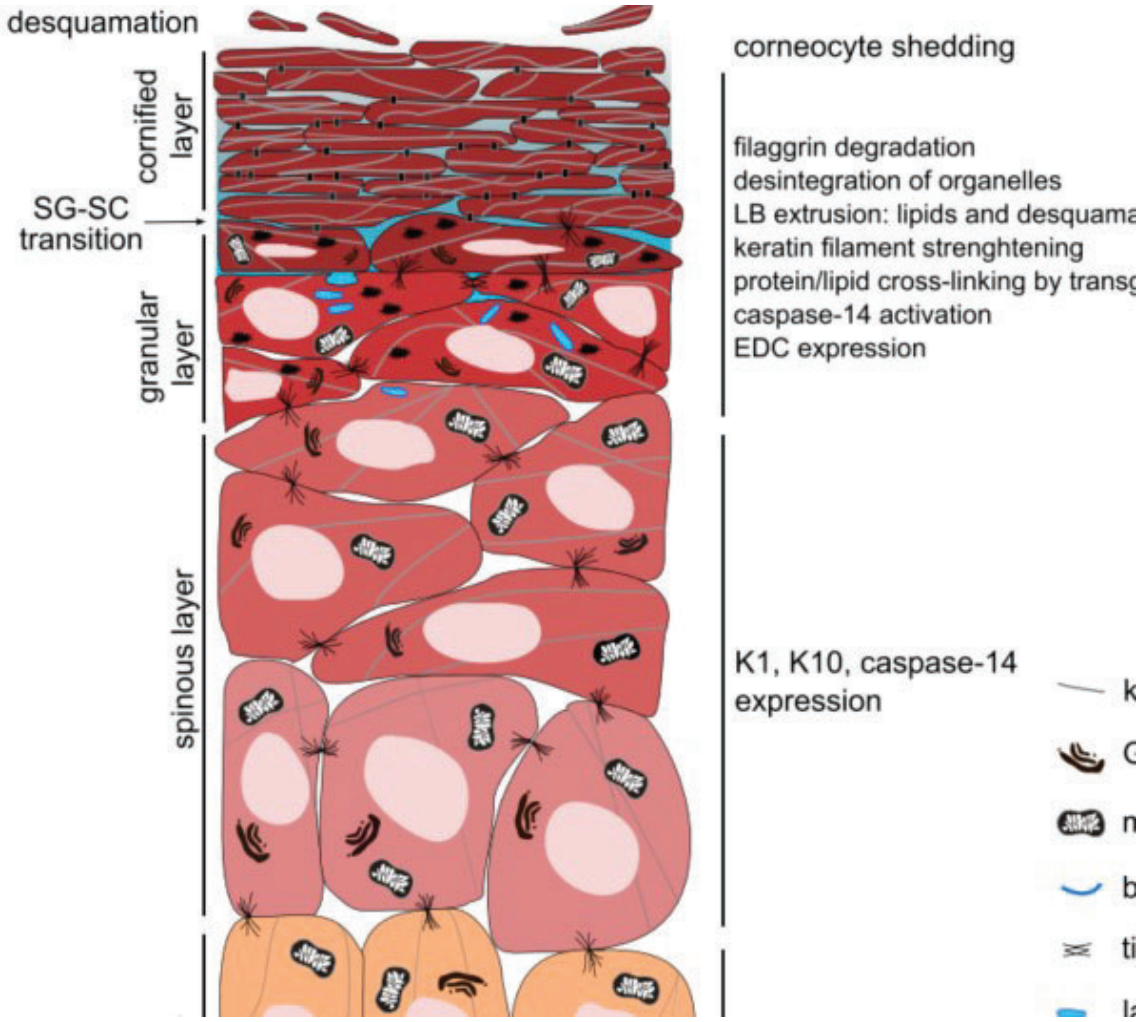

Figure 11. Visualization of the terminal differentiation process of keratinocytes

The epidermis consists of layers (indicated on the left) of different stages of keratinocyte differentiation distinguished by morphological hallmarks and expression markers. The cells

of the basal layer are attached to the basement membrane by hemidesmosomes, have the capacity to proliferate, and provide new cells that will differentiate towards the surface of the skin. Cells of the spinous layer no longer divide and express typical markers of differentiation such as keratins K1 and K10 and caspase-14. In the granular layer, keratohyalin granules are present and proteins of the epidermal differentiation complex (EDC) are expressed. At the transition from the granular to the cornified layer, a cascade of events occurs: caspase-14 becomes active and contributes to filaggrin degradation, and keratins and other proteins are cross-linked by transglutaminases. At this point the content of the lamellar bodies (LBs) is extruded into the intercellular space because the LBs fuse with the plasma membrane. At the cytoplasmic side of the plasma membrane cross-linking of proteins forms the cornified envelope (CE) that is tightly connected to neighboring CEs via corneodesmosomes. The actual physical skin barrier is formed by the tight junctions, which form strong intercellular interactions, and the lipids in the intercorneocyte spaces. Eventually the corneodesmosomes are proteolytically degraded by extracellular enzymes and the corneocytes are shed during desquamation.

The original figure was published by Eckhart *et al.* but edited slightly for an optimized length-width-ratio while the description was not altered [67].

The synthesis of key proteins like involucrin [228], loricrin [176], and filaggrin [35,107] requires glutamine, which can be produced intracellularly [68] from NH_4^+ and glutamate via the glutamine synthetase as seen in **Figure 12**.

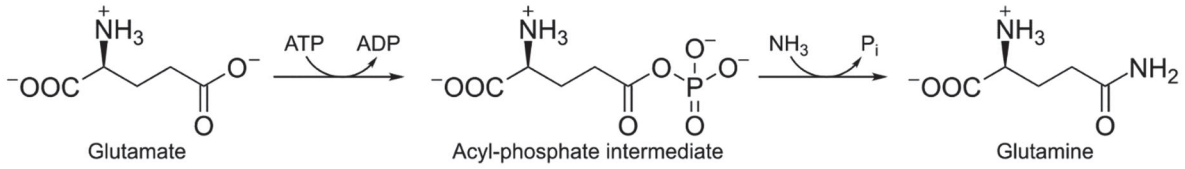

Figure 12. Glutamine synthetase

This enzyme plays an essential role in the metabolism of nitrogen by catalyzing the ATP-dependent condensation of ammonia and glutamate to yield glutamine.

2.4. TRPV3 in cattle

The bovine homologue of TRPV3 (bTRPV3) has also emerged as a candidate for the uptake of cations, including NH_4^+ and Ca^{2+}, from the rumen in cattle, a conclusion based on both functional evidence and mRNA data [198,209]. Due to the high demand involved in milk production, ruminants absorb considerable amounts of Ca^{2+} [278] and electrophysiological data postulated the existence of a ruminal Ca^{2+} channel [106,279]. However, the typical epithelial Ca^{2+} channels TRPV5 and TRPV6 are not expressed by the rumen [209,277]. The permeability of TRPV3 to Ca^{2+} is well documented [172,186,263,285]. Conversely, the permeability of the bovine homologue of TRPV3 to NH_4^+ has only been investigated once [220], with no information available on the human TRPV3. Further investigations are thus required.

Ammonia (NH_3) and its protonated form (NH_4^+) play a central role in the interconversion of amino acids for protein metabolism in the citrate cycle, for urea recycling in the rumino-hepatic circulation [99], and efficient protein supply which requires rapid transport across membranes of organelles and cells. Varying pathways describing the transport of nitrogen across the rumen epithelium have been published already [1] starting with the first observation made by Bödeker *et al*. in 1996 [29].

Classically, the uptake mechanism across cellular membranes had been characterized as simple diffusion of uncharged NH_3 [125,184]. However, considering the permanent electric dipole moment of NH_3 (~1.47 Debye or $4.90 \cdot 10^{-30}$ Cm [102]) due to its distorted tetrahedral structure resulting from the sp^3 hybridization of N (**Figure 13**), this mode of transportation seems unlikely.

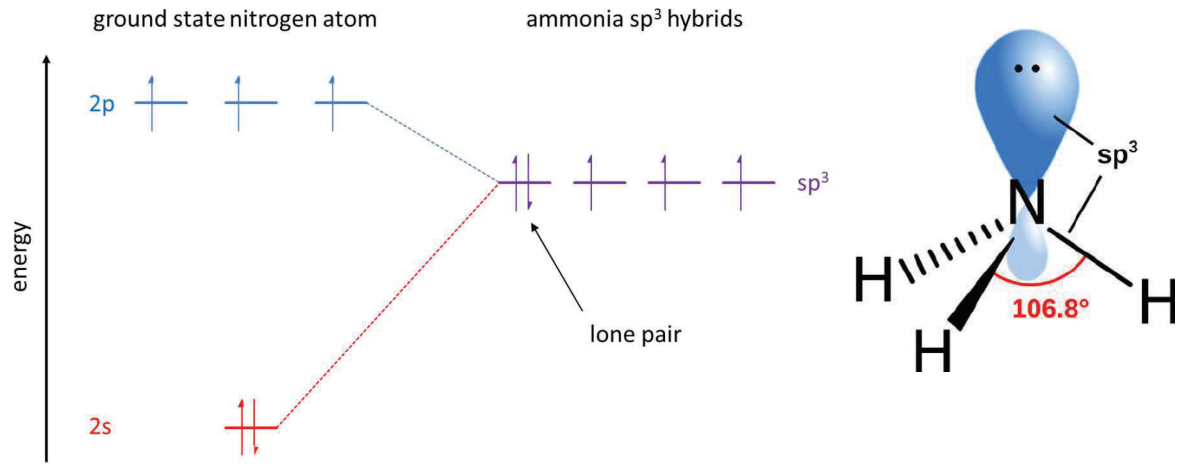

Figure 13. Structure of ammonia due to its electron configuration predicted by VSEPR

Ammonia has a permanent electric dipole moment due to its shape predicted by valence shell electron pair repulsion (VSEPR) theory [87]. According to the VSEPR, the shape of NH_3 is distorted tetrahedral. The electron configuration of the central nitrogen atom is [He]

$2s^2\ 2p^3$, meaning the nitrogen has five valence electrons in its ground state. During the formation of NH_3, the three 2p orbitals and the 2s orbital of nitrogen combine to create four equivalent energy hybrid orbitals, known as sp^3 hybridization (an orbital is the solution of the Schrödingers wave equation Ψ that describes the probability of finding an electron around a nucleus). Three of the five valence electrons of nitrogen form covalent bonds with the s orbitals of hydrogen atoms, filling three of the four sp^3 orbitals, while the two remaining electrons remain unpaired as the lone pair in the fourth sp^3 orbital. In accordance with VSEPR, lone pairs require more space than covalent bonds, resulting in the trigonal pyramidal or distorted tetrahedral shape of the molecule with a more positively charged "hydrogen bottom" and more negatively charged "nitrogen top" which explains the permanent electric dipole of ammonia. The illustration of the shape of ammonia on the right side was published by Behre *et al* [20].

Water has a comparable permanent electric dipole moment (1.85 Debye or $6.17 \cdot 10^{-30}$ Cm [102]) and is not able to diffuse biological membranes fast enough to explain biological observations without expression of aquaporins (AQP) [10,40,149]. This pathway also allows for regulation, as by the kidneys, something that is essential for water homeostasis. Saparov *et al.* [215] have demonstrated that AQP8 could transport NH_3 efficiently across an artificial planar bilayer membrane. AQP1, 3, 6, 7, 8, 9, and 10 have also been identified to transport NH_3 in humans [10,141,215,276]. Caner *et al*. [42] reported that rhesus-associated (Rh) glycoproteins RhAG, RhBG, and RhCG transport NH_3 in *X*. oocytes while RhAG and RhBG also transported NH_4^+. RhAG is expressed in erythrocytes and is widely known for its antigenicity while it is additionally involved in maintaining the stability and structure of the red cell membrane [42,171,254]. Both nonerythroid channels RhBG and RhCG are expressed *inter alia* in gastrointestinal organs [98] as well as in the liver and kidney [96] with roles associated to nitrogen and acid-base balance [42,273]. In ruminants, multiple channels have been suggested to be involved in nitrogen transport such as AQP3 [206,298], AQP7, 8, 9, 10 [21,206], various rhesus glycoproteins [42,156,274,275], and as mentioned prior bTRPV3 [220].

A better understanding of the mechanisms behind ammonia absorption and excretion have implications for diverse areas, including climate change. Thus, the agricultural sector, which includes livestock maintenance, accounts for the largest anthropogenic source (or 60%) of the highly potent climate gas N_2O [66,234,271]. This gas not only leads to human respiratory problems, but, due to nitrification of soils and surface water, also to eutrophication. Furthermore, nitrous oxides are powerful drivers of climate change [109]. The potential effect

of N_2O as climate gas (global warming potential – GWP) was estimated to be 298 times higher than CO_2 over a 100-year period even considering that just 10% of N_2O are converted to NO_2 and NO, which are known to be damaging to the ozone layer [66,200]. This detriment occurs through a catalyzed reaction, as illustrated in **Figure 14 A** and described by Crutzen *et al.* [52] and Johnston *et al* [120]. The high GWP of N_2O is primarily attributed to its relatively long atmospheric lifetime, averaging 114 years, compared to other greenhouse gases such as methane, which has a lifetime of 12 years, before being removed by chemical reactions or absorbed by soil or oceans [4].

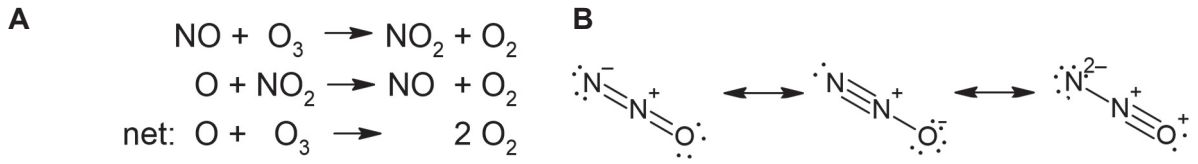

Figure 14. Nitrogen oxides contribute to the greenhouse effect
(A) Nitrogen oxides catalytically destroy ozone. (B) Lewis structures of N_2O.

Additionally, on a per-molecule basis, N_2O traps more heat than CO_2 due to its molecular structure and its infrared (IR) absorption bands. The complex structure of the unsymmetrical linear N_2O as illustrated in **Figure 14 B** gives the molecule more IR active degrees of freedom meaning more ways in which its atoms can move relative to each other. For IR spectroscopy, the relevant degrees of freedom are associated with the stretching and bending of bonds that result in a change of the dipole moment of the molecule. Generally, molecules with more atoms have more ways they can vibrate and absorb IR radiation. When IR radiation interacts with a molecule, it needs to match the difference between the molecule's vibrational energy levels, causing the molecule to absorb the light. This absorbed energy is later emitted as heat when the molecule returns to its original state. N_2O, with its complex asymmetrical structure, can absorb a wider range of IR wavelengths compared to symmetrical CO_2, enhancing its effectiveness in trapping heat and intensifying the greenhouse effect.

In cattle, the nitrogen originates from dietary protein that is broken down to NH_4^+ in the gut which can be used for microbial protein synthesis, but the larger fraction is absorbed, converted to urea, and excreted into the environment as illustrated in **Figure 15** with disastrous consequences.

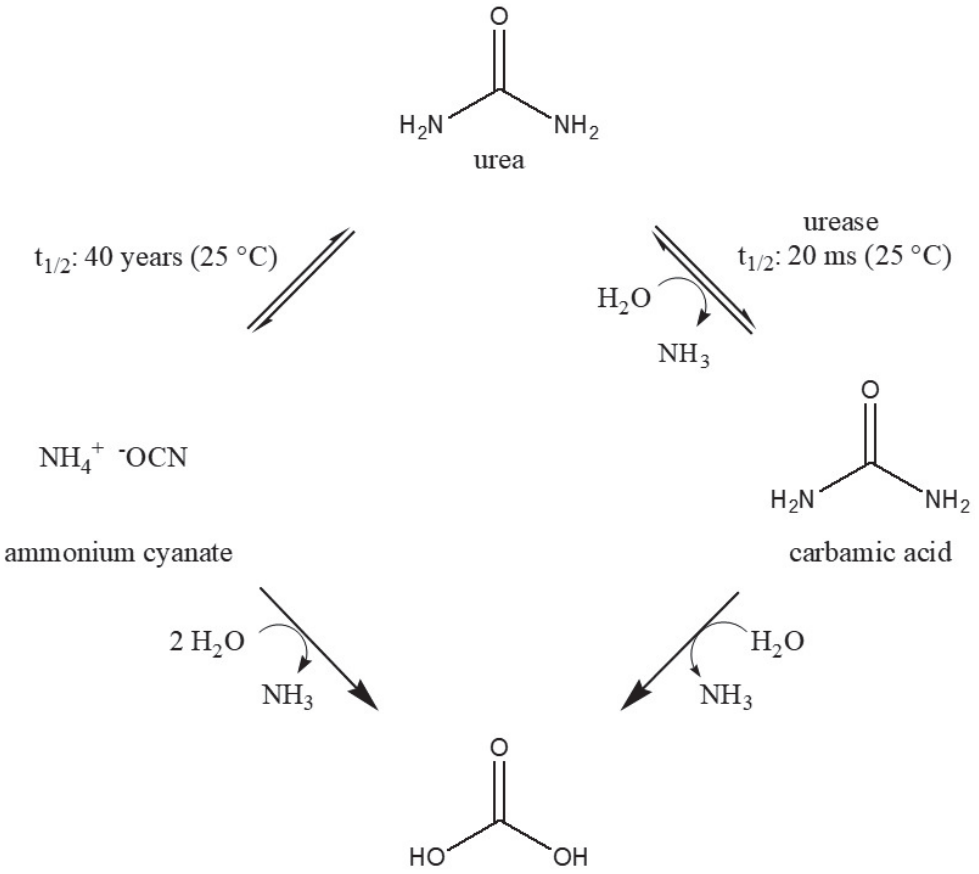

Figure 15. Urea decomposition pathways

Urea can be decomposed either in a sluggish un-catalyzed elimination reaction or the biological relevant fast urease-catalyzed hydrolysis [227]. The following hydrolysis is fast in both pathways and occurs spontaneously. In accordance to the Henderson-Hasselbach equation, the resulting NH_3 is mostly converted in an equilibrium to NH_4^+ in pH neutral soil (as described in more detail in the discussion section 5). This process of NH_3 emission into the environment is known as volatilization [229] and reportedly varies from 1.7% up to a staggering 56% ammonia loss of applied fertilizer depending on soil, moisture, temperature, soil pH, wind velocity, and fertilizer type [26,27,56,72,76,88,229]. At first glance, it appears contradictory that huge amounts of nitrogen can be lost via volatilization despite low NH_3 concentrations in the soil but this can be explained by the Le Chatelier principle (also known as equilibrium law [14]), meaning that even low concentrations of NH_3 would suffice because those would be emitted and thereby removed from the reaction shifting the equilibrium towards NH_3. In the soil, the remaining NH_4^+ can be oxidized to NO_3^- via nitrification by bacteria. Both NH_4^+ and NO_3^- can either be used by plants as crucial nutrients or get lost with water via so called leaching. NO_3^- can also be released into the environment via the denitrification process as N_2O, NO, or N_2 with consequences for the environment [229].

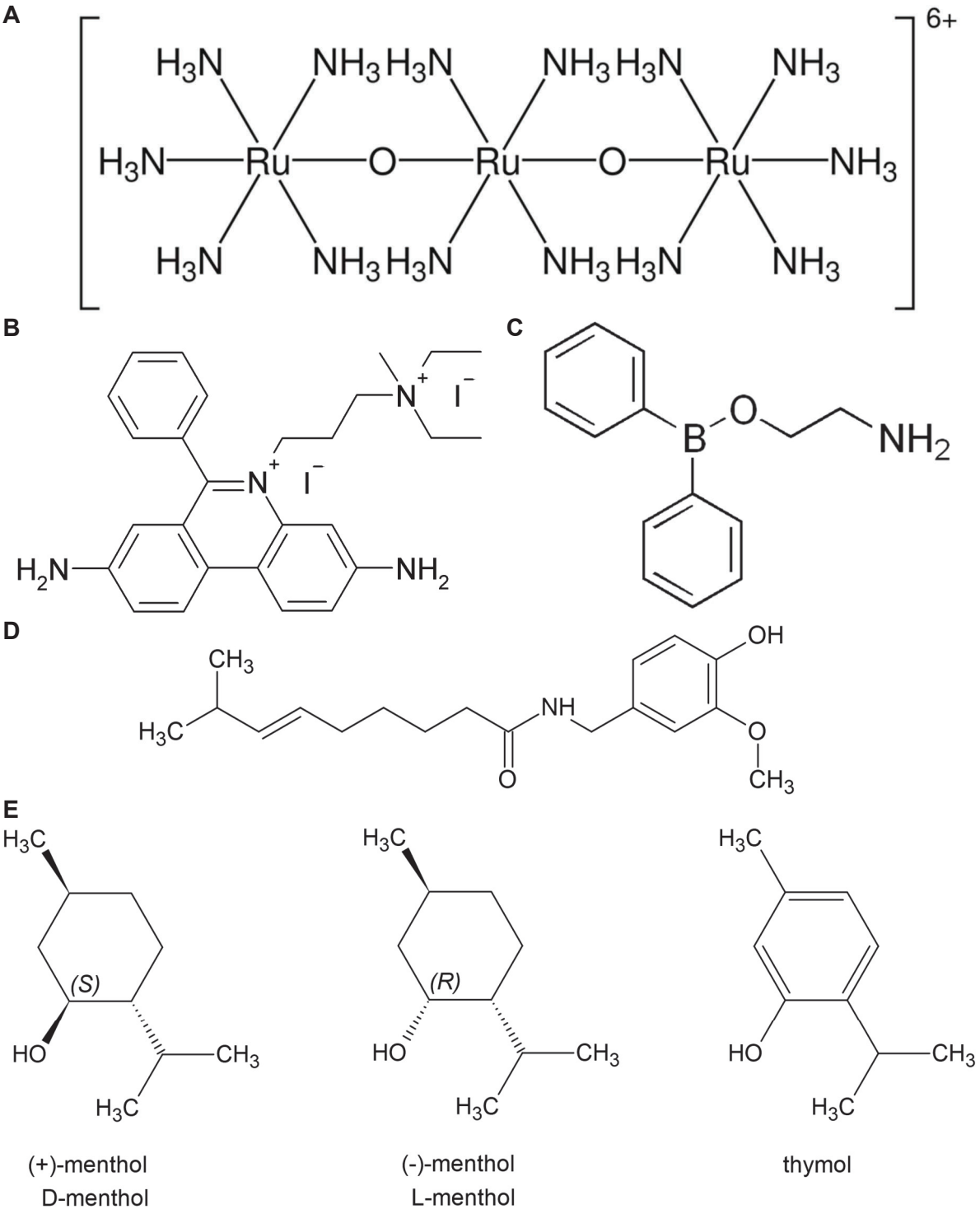

Figure 16. Chemical formula of selective substances

A) Ruthenium Red (RR), B) Propidiumiodid, C) 2-Aminoethoxydiphenyl borate (2-APB), D) Capsaicin, E) Menthol and thymol

3

Liebe *et al.* 2021

Pflügers Archiv - European Journal of Physiology
https://doi.org/10.1007/s00424-021-02616-0

ION CHANNELS, RECEPTORS AND TRANSPORTERS

Beyond Ca^{2+} signalling: the role of TRPV3 in the transport of NH_4^+

Hendrik Liebe[1,2] · Franziska Liebe[1] · Gerhard Sponder[1] · Sarah Hedtrich[3] · Friederike Stumpff[1]

Received: 2 June 2021 / Revised: 17 August 2021 / Accepted: 18 August 2021

Abstract
Mutations of TRPV3 lead to severe dermal hyperkeratosis in Olmsted syndrome, but whether the mutants are trafficked to the cell membrane or not is controversial. Even less is known about TRPV3 function in intestinal epithelia, although research on ruminants and pigs suggests an involvement in the uptake of NH_4^+. It was the purpose of this study to measure the permeability of the human homologue (hTRPV3) to NH_4^+, to localize hTRPV3 in human skin equivalents, and to investigate trafficking of the Olmsted mutant G573S. Immunoblotting and immunostaining verified the successful expression of hTRPV3 in HEK-293 cells and *Xenopus* oocytes with trafficking to the cell membrane. Human skin equivalents showed distinct staining of the apical membrane of the top layer of keratinocytes with cytosolic staining in the middle layers. Experiments with pH-sensitive microelectrodes on *Xenopus* oocytes demonstrated that acidification by NH_4^+ was significantly greater when hTRPV3 was expressed. Single-channel measurements showed larger conductances in overexpressing *Xenopus* oocytes than in controls. In whole-cell experiments on HEK-293 cells, both enantiomers of menthol stimulated influx of NH_4^+ in hTRPV3 expressing cells, but not in controls. Expression of the mutant G573S greatly reduced cell viability with partial rescue via ruthenium red. Immunofluorescence confirmed cytosolic expression, with membrane staining observed in a very small number of cells. We suggest that expression of TRPV3 by epithelia may have implications not just for Ca^{2+} signalling, but also for nitrogen metabolism. Models suggesting how influx of NH_4^+ via TRPV3 might stimulate skin cornification or intestinal NH_4^+ transport are discussed.

Keywords TRPV3 · Ammonia · NH_4^+ · Olmsted syndrome · Colon · Skin

Introduction

The multiple functions of channels of the transient receptor potential (TRP) family in general, and that of TRPV3 in particular, continue to be poorly understood [52]. The first TRP channel was cloned from a *Drosophila* fly mutant with visual impairment, resulting from a mutation that led to transient receptor potentials instead of the normal sustained response [47]. Since this time, 28 mammalian members of the family have been identified that form hetero- or homotetrameric assemblies and function as cation channels. Possibly owing to the initial discovery in the visual system of *Drosophila*, the family was initially associated exclusively with sensory perception. However, many members of the TRP channel family are highly expressed by non-sensory organs such as epithelial cells of the skin or the intestine [46, 52, 56, 74, 75], raising the question if sensory signalling is the end of the story.

From the first cloning of TRPV3 almost 20 years ago [57, 58, 71, 84], the high expression of TRPV3 in keratinocytes was noted in conjunction with a complete lack of expression in associated sensory dorsal root ganglion neurons. The channel is notoriously promiscuous with a low selectivity for Ca^{2+} [58]. Since TRPV3 is activated by warm temperatures above 33 °C, its primary function was initially thought to be in thermosensation, involving signalling via ATP or other molecules [45]. However, mice with a knockout of TRPV3 exhibited no obvious alterations in thermal preference behaviour [34] and instead, displayed a phenotype with curly hair and whiskers [17]. In mice, a gain of function mutation of TRPV3 caused a hairless phenotype with itchy

✉ Friederike Stumpff
stumpff@zedat.fu-berlin.de

1 Institute of Veterinary Physiology, Freie Universität Berlin, Oertzenweg 19b, 14163 Berlin, Germany

2 Department of Biology, Chemistry, and Pharmacy, Freie Universität Berlin, Oertzenweg 19b, 14163 Berlin, Germany

3 Faculty of Pharmaceutical Sciences, University of British Columbia, Vancouver, Canada

Published online: 19 October 2021

skin, while in humans with Olmsted syndrome (OS), gain of function mutants cause severe palmoplantar hyperkeratosis [22, 40].

Despite progress, it remains uncertain why a gain of function of TRPV3 leads to hyperkeratosis in humans [22]. The skin consists of several layers of cells that differentiate as they grow upwards from the stratum basale, forming the stratum spinosum, the stratum granulosum, and the stratum corneum. This final layer consists of terminally differentiated keratinocytes or corneocytes, the cytosol of which is surrounded by cross-linked proteins. In the epidermal skin, this protein envelope is tightly linked to a further envelope of complexly organized lipids that seal the intercellular space. The corneocytes have lost cytoplasmic organelles and cell nuclei, but are important for skin hydration and reportedly continue to participate in signalling cascades such as cytokine-mediated initiation of inflammation [48]. Cells in the lower parts of the stratum corneum are tightly adjoined by corneodesmosomes, which are the main intercellular adhesive structures found in this layer. In an attempt to explain the hyperkeratosis found in Olmsted syndrome, a simple hypothesis suggests that a higher influx of Ca^{2+} through mutant TRPV3 leads to apoptosis [24]. However, skin peeling formulations that induce apoptosis cause exfoliation with a loss of corneocytes, the precise opposite of what is observed in OS [14, 52]. Hyperkeratosis occurs when the enzymatic disruption of the corneodesmosomes does not keep pace with the speed at which new corneocytes are formed [23].

The therapeutic success of targeting the epidermal growth factor receptor (EGFR) in OS [27, 86] supports a model in which EGFR stimulates keratinocyte differentiation into corneocytes. According to this concept, EGFR increases the activity of TRPV3, leading to influx of Ca^{2+} from the extracellular space into the stratum granulosum. Ca^{2+} activates transglutaminases [17, 23], which catalyse the cross-linking of glutamine and lysine residues of involucrin and loricrin, a key reaction in the formation of the highly resistant protein envelope. Synthesis of involucrin, loricrin, and a third important corneocyte protein, filaggrin, requires glutamine, which is produced intracellularly from NH_4^+ and glutamate via glutamine synthetase. A steady supply of ammonia is required both as a substrate and to activate glutamine synthetase [2, 19].

The model outlined above has been challenged by a study [85] of four separate TRPV3 mutants associated with the OS phenotype, including the most prominent point mutation glycine-573-serine (G573S) [22]. In that study [85], it was proposed that mutation of the TRPV3 channel interferes with the trafficking of the protein to the cellular membrane. This would prevent influx of Ca^{2+} into the cell, rather than enhancing it. Furthermore, it has been suggested that Ca^{2+} does not enter from the extracellular space but is released from intracellular stores after activation of calcium-sensing receptors [37]. It is also not quite clear why a non-selective cation channel such as TRPV3 is involved when the skin expresses a number of channels with a much higher selectivity to Ca^{2+}, such as Orai1, TRPV6, or TRPA1 [37, 55]. The question arises if the low selectivity of TRPV3 might possibly also play a role in keratinocyte differentiation—for instance, by providing NH_4^+ for the production of the glutamine required for synthesis of involucrin, loricrin, and filaggrin as building blocks of the corneocyte envelope.

Apart from the skin, TRPV3 is also highly expressed by the apical membrane of enterocytes in intestinal epithelia such as the colon and the caecum, suggesting a role in the apical uptake of cations [46, 75]. A role in inflammatory signalling has been postulated, but attempts to correlate clinical findings in ulcerative colitis with expression of TRPV3 have been inconclusive [63]. A primary function in the absorption of Ca^{2+} can be ruled out since this clearly occurs in the small intestine via the highly selective Ca^{2+} channels TRPV5 and TRPV6, although transport of Ca^{2+} is possible [43]. However, the colon and the caecum absorb large quantities of ammonia [2]. Since NH_3 is a highly polar molecule, it cannot simply diffuse through the lipid bilayer. Instead, it has been suggested that transport of ammonia (NH_3) is facilitated by transport proteins such as the Rhesus-like glycoproteins or certain types of aquaporins [26, 30, 51]. Furthermore, functional studies have shown that both the colon and the caecum express an electrogenic pathway for the uptake of NH_4^+ via divalent-sensitive, non-selective cation conductances with permeability to NH_4^+ [46, 70], correlating with the apical expression of TRPV3 by both tissues [46, 75].

Our own interest in TRPV3 was sparked when looking for the pathway mediating the uptake of NH_4^+ from the rumen of cattle [39, 66, 69]. Having evolved from the oesophagus, the ruminal epithelium is a stratified squamous epithelium that, like the skin of many amphibians, has transporting properties [1, 8, 76]. In what is known as nitrogen recycling, urea is secreted from blood into the lumen, where microbes break up urea into ammonia which is then protonated and reabsorbed [31, 62, 72]. The same mechanism is found in the colon and caecum of monogastric species such as humans [72]. Since mammalian enzymes cannot break down urea, secretion of this waste product into a space colonized by microbes allows the host to reclaim the nitrogen contained in urea for the synthesis of glutamine and other non-essential amino acids in situations where dietary protein intake is low.

Intriguingly, the skin also secretes large quantities of urea, mostly via sweat [2, 5, 83]. While high concentrations of urea have keratolytic properties that are used to treat hyperkeratosis, the low concentrations (~7%) contained in sweat or in cosmetic products are generally considered to enhance skin hydration and barrier function via pathways that are incompletely understood [15]. Since many dermal

bacteria express ureases [68], ammonia is released in large quantities, exceeding those in breath [38, 77]. It would certainly enhance evolutionary survival if at least part of this ammonia could be reabsorbed—e.g. via TRPV3—and utilized by dermal glutamine synthetase to produce glutamine as a precursor of the proteins required for keratin synthesis. In line with this hypothesis, inhibition of dermal urea transport inhibits production of transglutaminase, involucrin, loricrin, and filaggrin as proteins central to the process of cornification, although down-regulation of gene activity has been suggested as the mode of action [28].

The first purpose of the current study was therefore to investigate whether the human homologue of TRPV3 can conduct NH_4^+, as we have previously shown for the bovine homologue [39, 69]. A further purpose was to localize TRPV3 in a human skin equivalent [42] and, finally, to investigate the trafficking of the G573S mutant [85].

Materials and methods

Cloning of hTRPV3

Cloning was essentially performed as previously described [39, 69]. The human sequence of *TRPV3* (*hTRPV3*, NM_001258205.1) was obtained from Thermo Fisher Scientific GENEART (Regensburg, Germany) and tagged with a Hemagglutinin (HA) and a streptavidin (Strep) tag. The dual tag was placed at the N-terminus to prevent possible interference with a C-terminal PDZ binding motif found in some TRP-channels [60].

A number of experiments were performed using *Xenopus laevis* oocytes (referred to as *X.* oocytes or simply oocytes in the following, see below). For transfection, the HA-Strep-*hTRPV3* construct was subcloned into pGEM-HE-MCS (kindly donated by Prof. Blanche Schwappach, Georg-August-Universität, Göttingen, Germany) using the restriction sites HindIII and XbaI. The vector was linearized with the restriction enzyme MluI. RiboMAX Large Scale RNA Production System-T7 (Promega, Mannheim, Germany) was used for in vitro transcription to cRNA according to the manufacturer's instructions.

For transfection of HEK-293 cells, the HA-Strep-*hTRPV3* construct was subcloned into pIRES2-AcGFP1 (Takara BioEurope, Saint-Germain-en-Laye, France) using the restriction sites NheI and XhoI. In the vector arrangement, the hTRPV3 coding sequence lies upstream, followed by an IRES sequence and, finally, the green fluorescent protein (GFP) coding sequence. Accordingly, hTRPV3 and GFP were separately expressed. The same method was utilized to construct a vector using a mutated sequence of the *hTRPV3* gene (Thermo Fisher Scientific GENEART) containing the point mutation G573S.

Harvesting and injection of Xenopus laevis oocytes

X. oocytes were harvested and processed from the same frogs as in Liebe et al. [39] (supplement part A, permit G0025/16). Xenopus laevis frogs were anaesthetized in a bath solution containing 0.2% MS222 (ethyl 3-aminobenzoate methanesulfonate, Sigma-Aldrich, Taufkirchen, Germany) for 5–10 min at 20 °C. After sufficient anaesthesia was reached, ovarian lobes were obtained by partial ovariectomy [10, 78]. *X.* oocytes were injected with 50 nl RNAse-free water containing 15 to 30 ng of HA-Strep-*hTRPV3* cRNA (WPI Nanoliter 2010, World Precision Instruments, Sarasota, FL, USA) to overexpress hTRPV3. Control *X.* oocytes were injected with 50 nl RNAse-free water only. Experiments alternated strictly between hTRPV3, the bovine analogue bTRPV3, and control oocytes. This made it possible to directly compare the two TRPV3 proteins with each other. Note that the control *X.* oocytes in microelectrode and inside-out measurements were the same as in the previous study from our group in which bTRPV3 was investigated [39].

Generation of human skin equivalents

Interfollicular primary human fibroblasts and keratinocytes were isolated from juvenile foreskin following circumcision at age 2 to 11 years (permit EA1/081/13). After cultivation for 3–4 days, they were used to generate human skin equivalents (hsEq) as described previously [42].

Cell culture and transfection of HEK-293 cells

HEK-293 cells (DSMZ, Braunschweig, Germany, 2016/06/08) were cultivated under standard conditions (37 °C, 5% CO_2 in humidified air) in Dulbecco's modified Eagle's medium (FG 0445) supplemented with 10% foetal bovine serum and 100 units · mL^{-1} of penicillin and streptomycin (all Biochrom). For seeding, the supernatant of an 80% confluent T-25 flask was removed including non-attached cells. Living cells adhering to the flask bottom were washed with phosphate-buffered saline (PBS; 5 mL; Sigma-Aldrich, St. Louis, MO, USA). After trypsinization for 5 min (1 mL; 0.05% trypsin + 0.02% EDTA (Merck, Darmstadt, Germany)), cells were incubated with trypan blue (0.4%, Sigma-Aldrich) at a ratio of 1:1 to identify non-vital cells. Viable, non-stained cells were counted manually using a hemocytometer (Paul Marienfeld GmbH & Co. KG, Germany) and a binocular inverse microscope. Subsequently, $1.2 \cdot 10^6$, $6 \cdot 10^5$, or $3 \cdot 10^5$ HEK-293 cells were seeded into a new T-25 flask with 5 mL medium for experiments after 1, 2, or 3 days, respectively. Alternatively, cells were seeded onto coverslips for immunofluorescence staining. Polyethylenimine (PEI, linear, MW

25,000, Polysciences, Inc., Hirschberg an der Bergstrasse, Germany) was used to transiently transfect the cells with pIRES2-*AcGFP*1-HA-Strep-*hTRPV3* (hTRPV3 or wild-type), with pIRES-AcGFP1-HA-Strep-*hTRPV3*-G573S (G573S), or with the empty pIRES2-*AcGFP*1 (control) vector using the website "http://www.cytographica.com/lab/PEItransfect.html" for calculations. The medium was refreshed 24 h prior to experiments.

Immunoblotting

Proteins were prepared, denatured, electrophoresed, and blotted onto membranes as described in supplement part B. A primary mouse antibody directed against an epitope (AA 458–474) in the first extracellular loop of hTRPV3 was used at a dilution of 1:3000 ("Anti-TRPV3"; ID: ABIN863127, antibodies-online GmbH, Aachen, Germany). This antibody was previously validated in our group for staining of the bovine homologue of TRPV3 [39]. For detection of the Strep-tag, a primary mouse antibody ("Anti-Strep"; ID: 34,850, Qiagen, Hilden, Germany) was used at the dilution of 1:2500. After blocking, the membranes were incubated with the primary antibodies (in 2.5% milk in Tris-buffered saline with Tween-20 (0.1 vol%; TBST) supplemented with NaN_3 (0.01%)) overnight (4 °C). Horseradish peroxidase conjugated secondary antibody (anti-mouse, 1:1000 in 2.5% milk in TBST; 45 min; room temperature, Cell Signaling Technology, Frankfurt, Germany) was used to detect the primary antibodies on the membranes. Proteins were visualized by use of the Clarity Western ECL Substrate (Bio-Rad Laboratories GmbH, Munich, Germany).

Immunofluorescence staining

All preparation steps were performed as described in [39, 73] or in the supplement part C. Anti-TRPV3 was diluted 1:1000 in goat serum (5% in PBS; PAN-Biotech GmbH, Aidenbach, Germany) to stain *X.* oocytes and HEK-293 cells (1:250 for human skin equivalents). Treated slices were incubated overnight (4 °C). Secondary antibody controls were performed with goat serum (5% in PBS) only. On the next day, slices of *X.* oocytes and human skin equivalents were incubated with Alexa Fluor® 488 conjugated goat anti-mouse IgG (1:1000; Thermo Fisher Scientific, Waltham, MA, USA) as secondary antibody (60 min, 37 °C). HEK-293 cells were stained with Alexa Fluor® 594 conjugated goat anti-mouse IgG (1:1000; Thermo Fisher Scientific) due to GFP emitting green light with peak emission at 509 nm [16]. Images were obtained using a confocal laser-scanning microscope (LSM 510, Axiovert200M, Zeiss, Jena, Germany) at 405, 488, and 543 nm.

Double-barrelled pH-sensitive microelectrode measurements

Experiments were performed as described previously in Liebe et al. [39] and in the supplement part D. The method was used to simultaneously determine the membrane potential (U_{mem}) and the intracellular pH (pH_i) of *X.* oocytes superfused with varying solutions. Calibration was performed before and after each measurement. All experiments were performed in parallel to those on the bovine homologue (bTRPV3, [39]) at 23 °C, alternating between overexpressing *X.* oocytes and controls, with the latter also used in [39]. The following solutions were used (in $mmol \cdot L^{-1}$): "NaCl" (85 NaCl), "KCl" (81 KCl, 5 NaCl), "NaGlu" (80 sodium D-gluconate (NaGlu), 5 NaCl, 10 (2*R*,3*R*,4*R*,5*S*)-6-(Methylamino)hexane-1,2,3,4,5-pentol chloride (NMDGCl)), "NH_4Cl" (5 NaCl, 80 NH_4Cl), "NH_4Cl-EDTA" (5 NaCl, 80 NH_4Cl, 5 NMDGCl, 5 EDTA, no $CaCl_2$ and no $MgCl_2$), and "NMDGCl" (80 NMDGCl, 5 NaCl). In addition, all solutions contained (in $mmol \cdot L^{-1}$) 5 4-(2-hydroxyethyl)-1-piperazineethanesulfonic acid (HEPES), 1 $CaCl_2$, 1 $MgCl_2$, and 1 KCl and were adjusted to an osmolality of 223 $mOsm \cdot kg^{-1}$ (D-mannitol) and to pH 7.4 (Tris), except for "NaCl-6.4" (85 NaCl), which was adjusted to pH 6.4 and contained 5 2-(*N*-morpholino)ethanesulfonic acid (MES) instead of HEPES.

The relative permeability ratio was calculated from the membrane potentials (see supplement part E). Slopes were calculated from the regression in a 5-s interval around the point of interest.

Inside-out patch-clamp experiments

Inside-out experiments were performed as previously described [25, 69] in a continuously perfused bath chamber at 23 °C, alternating between overexpressing *X.* oocytes and controls. Pipettes were pulled with a DMZ Universal Puller (Zeitz Instruments, Munich, Germany). Currents were recorded by an EPC 9 patch-clamp amplifier (HEKA Electronic, Lambrecht, Germany) using Patchmaster Software (HEKA Electronic). Data were sampled at 10 kHz and filtered at 250 Hz. Currents were clamped at the potentials − 60 to + 60 mV in 10 mV steps for six seconds each.

As described in Liebe et al. [39], *X.* oocytes were placed in a cell culture dish with frog oocyte Ringer (in $mmol \cdot L^{-1}$: 96 NaCl, 5 HEPES, 2.5 2-oxopropanoic acid, 1 KCl, 1 $CaCl_2$, 1 $MgCl_2$) to which D-mannitol was added incrementally. After dissociation of the vitelline membrane from the oolemma, it was removed with two sharpened forceps under a dissecting microscope. The stripped *X.* oocyte was then placed in a conventional flow chamber over an inverted microscope (Axiovert.A1, Zeiss) with subsequent seal formation and patch excision.

Solutions for patch-clamping were based on Doerner et al. [21] and contained (in mmol·L^{-1}) 20 HEPES, 5 CsCl, 1 ethylene glycol-bis(β-aminoethyl ether)-*N*,*N*,*N*′,*N*′-tetraacetic acid (EGTA), and 1 KCl. The pipette and the "NH_4Cl" bath solution additionally contained NH_4Cl (96 mmol·L^{-1}). In "NaCl", "KCl," and "NMDGCl" bath solutions, NH_4^+ was replaced by the same amount (96 mmol·L^{-1}) of Na^+, K^+, or $NMDG^+$, respectively. "NH_4Glu" bath solution substituted 81 mmol·L^{-1} NH_4Cl with NH_4-Glu. Solutions were adjusted to an osmolality of 223 mOsm · kg^{-1} (D-mannitol) and a pH of 7.4 (Tris and HCl).

Single-channel data were analysed using Igor Pro Software (6.37, WaveMetrics Inc., Lake Oswego, Oregon, USA) as described previously [39] and in the supplement part F.

Whole-cell experiments

Whole-cell experiments with HEK-293 cells were performed at 23 °C as previously described [39, 69] using Patchmaster Software (HEKA Electronic) with automatic correction of capacitance and series resistance. For continuous monitoring (66 s), we used a pulse protocol ("pulse protocol I") with a low sampling rate (100 Hz), starting from a holding potential of − 40 mV and cycling from + 100 to − 120 mV in 10 mV steps. Afterwards, a protocol with a high sampling rate (5 kHz, "pulse protocol II") was applied to assess channel kinetics. Only measurements with a series resistance between 3 and 12 MOhm were included in the evaluation. After each overexpressing HEK-293 cell, a control was measured. For analysis, type I protocols were merged.

All whole-cell solutions were adjusted to an osmolality of 300 mOsm · kg^{-1} using D-mannitol and to a pH of 7.4 with Tris and HCl. Pipette solutions for the first series of experiments in NaCl Ringer were based on Macpherson et al. [44] and contained (in mmol·L^{-1}) 140 CsCl, 10 HEPES, 5 EGTA, and 1 MgATP. Extracellular solutions ("NaCl") contained 140 NaCl or NMDGCl, respectively, in addition to 10 HEPES, 5 KCl, 2 $MgCl_2$, and 5 EGTA. In a second series of experiments, the conductance to NH_4^+ was investigated using a pipette solution containing (in mmol·L^{-1}) 120 NaGlu, 15 NaCl, 5 KCl, 5 EGTA, and 10 HEPES. Extracellular solutions in this series contained either 130 NaCl ("NaCl") or 135 NH_4Cl ("NH_4Cl") in addition to 5 KCl, 2 $CaCl_2$, 2 $MgCl_2$, 10 HEPES, and 10 glucose.

Stock solutions were prepared by dissolving menthol and thymol in ethanol, while 2-APB was dissolved in methanol and stored at − 20 ºC. Immediately prior to the experiments, they were added to the extracellular solution at a ratio of 1:1000 yielding the following end concentrations (in mmol·L^{-1}): 1 menthol (2-Isopropyl-5-methyl-cyclohexanol1, racemic), 1 D-menthol (1S,2R,5S)-(+)-menthol), 1 L-menthol (1R,2S,5R)-(−)-menthol) (all from Sigma-Aldrich), 1 thymol (Carl Roth), and 0.3 2-APB (Merck).

For statistical evaluation, clamped pipette potentials were corrected for the liquid junction potential (JPCalcWin software, School of Medical Sciences, Sydney, Australia) [3]. Current densities were calculated by dividing the absolute current values obtained from pulse protocol II by the capacitance. Positive or "outward" currents reflect cations flowing out of the cell or anions flowing into it. Reversal potentials were calculated by linear interpolation between the values above and below a current of zero in the corresponding IV-curve.

Cell viability experiments with HEK-293 cells using ruthenium red

T-25 flasks ($N = 18$) were seeded with $3 \cdot 10^5$ HEK-293 cells each. After 2 days, the cells were transfected according to procedure with the wild-type hTRPV3, G573S mutant, or empty control vector (6 flasks for each vector). Afterwards, half of the flasks of each group were supplemented with ruthenium red (RR; 20 µmol·L^{-1}; Sigma-Aldrich) for 20 h. The cell concentration in each flask was determined 4 times independently via hemocytometer as described above.

Statistical analysis

All data were statistically evaluated using SigmaStat 11.0. After testing for normality using the Shapiro–Wilk test, comparisons between two groups were performed using the Mann–Whitney Rank Sum Test. Comparisons between three groups (see supplement) were performed using the Kruskal–Wallis One Way Analysis of Variance on Ranks followed by pairwise comparisons (Mann–Whitney Rank Sum Test). In cases where different solutions were applied consecutively, differences were evaluated using Friedman Repeated Measures Analysis of Variance on Ranks (ANOVA on Ranks) followed by the Student–Newman–Keuls method for multiple comparisons or the Wilcoxon Signed Rank Test for pairwise comparisons. A significant difference was assumed for $p \leq 0.05$. Obtained values were given as means ± SEM, rounding as recommended by the DIN 1333 [20].

The *n* value represents the amount of individual experiments, whereas *N* refers to the number of different frogs, T-25 flasks, or donors (in the case of the skin equivalent).

Results

Immuno-detection of hTRPV3

To study the role of hTRPV3 in ammonia transport, HEK-293 cells were transfected with either pIRES2-*AcGFP*1-Strep-*hTRPV3*- (hTRPV3) or the empty vector (control),

while *X.* oocytes were injected with pGEM-HE-MCS-Strep-*hTRPV3*-cRNA (hTRPV3) or water (control).

In immunoblots (Fig. 1), staining against the Strep-tag showed a band at the predicted molecular weight of hTRPV3 (~95 kDa) both in HEK-293 cells overexpressing hTRPV3 ($n=14$) or its mutant G573S ($n=8$) and in hTRPV3 overexpressing *X.* oocytes ($n=7$), all in line with a successful expression of the Strep-tagged protein. No staining occurred in controls for either HEK-293 cells ($n=19$) or *X.* oocytes ($n=8$). In HEK-293 cells only, a faint additional band appeared at ~60 kDa, most likely reflecting a degradation product, since it was not observed in the controls. Using the commercial Anti-TRPV3 antibody, all protein samples from overexpressing cells showed staining at the expected height of ~95 kDa (hTRPV3 HEK 293, $n=10$; G573S, $n=11$; hTRPV3 *X.* oocytes, $n=7$). Degradation products were stained in hTRPV3 *X.* oocytes at ~80 kDa, with a band of similar height appearing in hTRPV3 HEK-293 cells at higher exposition times (data not shown). In G573S HEK-cells, a strong band appeared at ~50 kDa and a weaker one at ~60 kDa. Controls again showed no staining (c-HEK 293, $n=15$; c-*X.* oocytes, $n=7$). Note that the Strep-tag was attached to the N-terminal end of the protein, while the anti-TRPV3 antibody stained an epitope near S1-S2 in the middle of the protein (AA 458–474). This suggests that the fragments did not contain the N-terminus.

In protein from a model of human keratinocytes (human skin equivalent, 12 replicates from 2 donors), the ~95 kDa band was weak, requiring high exposure times. The intense band at ~60 kDa may correspond to a previously described splice variant first reported in human keratinocytes [74] but also found in bovine rumen [39], porcine intestine, and porcine and murine skin [46] or to a degradation product.

In immunofluorescence staining, *X.* oocytes overexpressing hTRPV3 showed membrane staining ($n=24$), which was absent in controls ($n=20$) (Fig. 2, green). Successfully transfected HEK-293 cells showed green fluorescence in the cytosol ($n=4$ cultures, Fig. 3). Anti-TRPV3 (in red) primarily stained the cell membrane of overexpressing HEK-293 cells indicating unimpaired expression and trafficking of the hTRPV3 channel protein. Control cells ($n=12$, data not shown) and non-fluorescent HEK-293 cells (Fig. 3a, bottom) failed to show staining for hTRPV3.

In immunofluorescence staining of the human skin equivalent ($n=10$, Fig. 4), no staining of the fibroblasts growing on the support near the basolateral side could be observed. Strong staining of the cytosol was observed in the middle of the keratinocytic layers. Intriguingly, in the topmost layer of cells, staining was clearly visible in the apical membrane, while the cytosol was almost devoid of staining. This suggests a process of differentiation with increasing trafficking of the TRPV3 protein into the apical cellular membrane, as observed in native preparations of human skin [56]. Note that the topmost cell layer reflects an equivalent of the stratum granulosum since the human skin equivalent was immersed in medium throughout, preventing cornification.

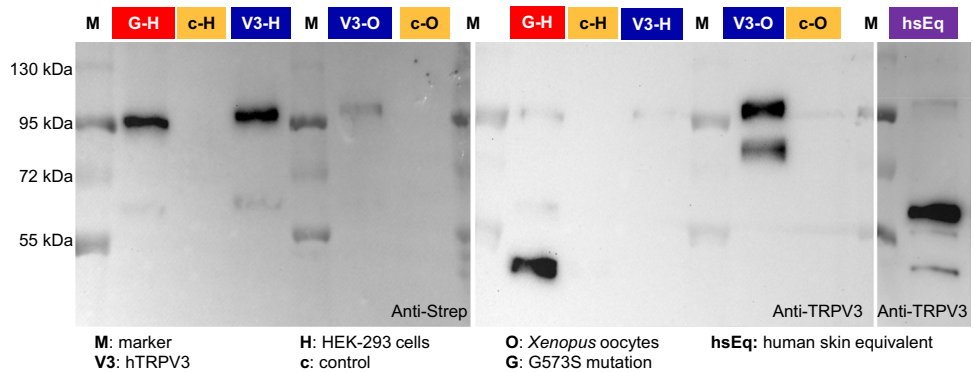

Fig. 1 Immunoblots: detection of hTRPV3 in overexpressing HEK-293 cells, *X.* oocytes, and in human keratinocytes. Following the marker lane (M) and from left to right, lanes were loaded with protein samples extracted from G573S HEK-293 cells (1 µg; typical example of $n=8$ replicates), control HEK-293 cells (10 ng; $n=19$), hTRPV3 HEK-293 cells (10 ng; $n=14$), hTRPV3 *X.* oocytes (5 µg; $n=7$), control *X.* oocytes (5 µg; $n=8$), G573S HEK-cells (1 µg; $n=11$), control HEK-cells (20 ng; $n=15$), hTRPV3 HEK-cells (20 ng; $n=10$), hTRPV3 *X.* oocytes (1 µg; $n=7$), control *X.* oocytes (1 µg; $n=7$), and keratinocytes obtained from human skin equivalents (1 µg; $n/N=12/2$). Staining with Anti-Strep, a band at the height of full-length TRPV3 (~95 kDa) can be seen in all overexpressing cells. At ~60 kDa, an additional weaker band was found in overexpressing HEK 293 cells only. Staining with Anti-TRPV3, all overexpressing cells showed the full-length band at ~95 kDa. *X.* oocytes expressed an additional band at ~80 kDa. Various breakdown products were stained at different heights in cells expressing the mutant G573S (see "Discussion" section). Control cells showed no staining. The keratinocyte protein extracted from human skin equivalents showed a weak band at ~95 kDa needing longer exposure times than normal in addition to various bands ≤60 kDa

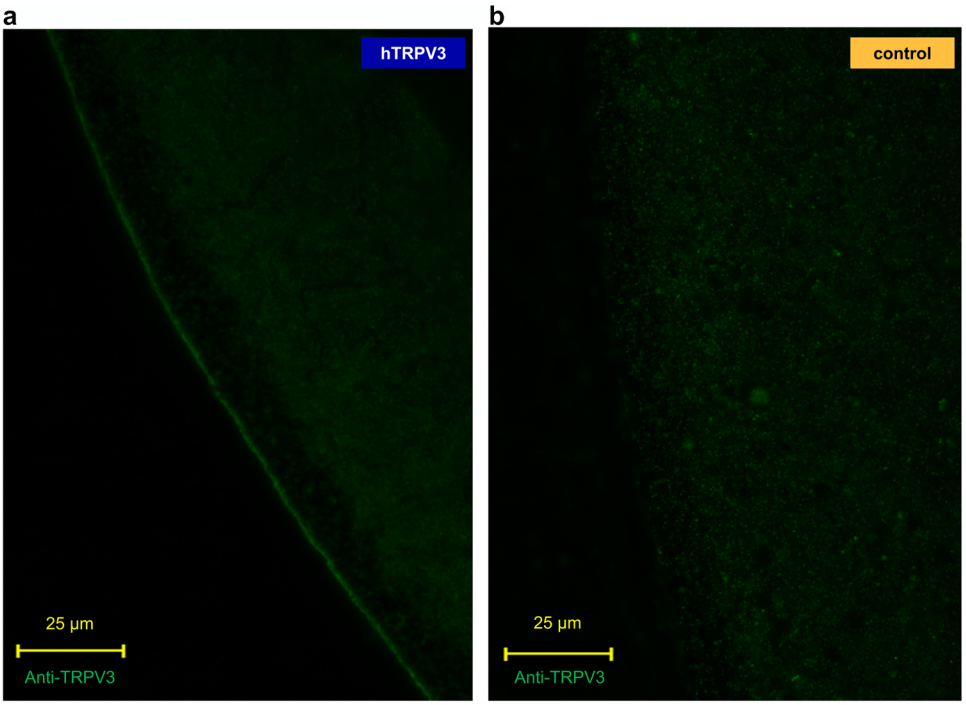

Fig. 2 Confocal laser microscopy: localization of hTRPV3 in *X.* oocytes overexpressing hTRPV3. **a** Anti-TRPV3 distinctly stained the cell membrane of hTRPV3 *X.* oocytes ($n = 24$), confirming successful expression and trafficking. **b** Controls ($n = 20$) injected with RNA-free water showed no signal after staining with the anti-TRPV3 antibody [39]

Experiments with pH-sensitive double-barrelled microelectrodes

Classical theories hold that NH_3 passes into cells via lipid diffusion [54]. Since ammonia is a strong base, influx primarily in the form of NH_3 into the cytosol should increase intracellular pH (pH_i), with a subsequent removal of ammonia leading to a rapid steep drop in pH_i [49]. Conversely, influx primarily in the form of NH_4^+ with dissociation and subsequent removal of NH_3 via sequestration in subcompartments, metabolism, or efflux should have an acidifying effect on pH_i [49]. As the system approaches the electrochemical equilibrium [50, 65], acid loading via influx of NH_4^+ will gradually decrease until pH regulatory

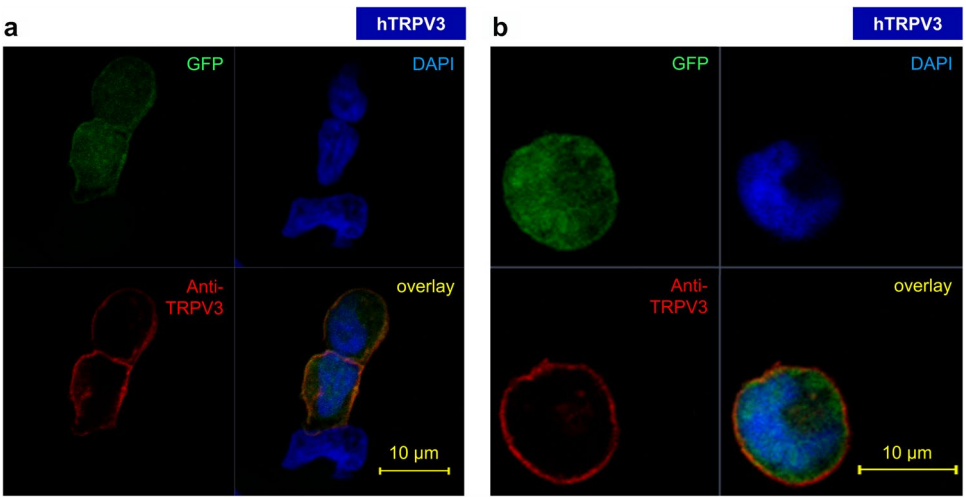

Fig. 3 Confocal laser microscopy: localization of hTRPV3 in HEK-293 cells overexpressing hTRPV3. **a** Staining of three adjacent HEK-293 cells, two of which have been transfected successfully. The green fluorescent signal marks cells overexpressing GFP, which was expressed downstream of hTRPV3. Since the GFP protein was not fused to the channel protein, cytoplasmic staining is observed. Conversely, hTRPV3 was primarily localized to the cell membrane (Anti-TRPV3, red). Cell nuclei were stained with DAPI (blue). Cells expressing GFP also stained for hTRPV3 and unsuccessful transfection led to no staining. **b** Close-up of one isolated HEK-293 cell overexpressing hTRPV3. (number of replicates: hTRPV3 HEK-293 cells, $n = 4$ cultures; control HEK-293 cells, $n = 12$ cultures)

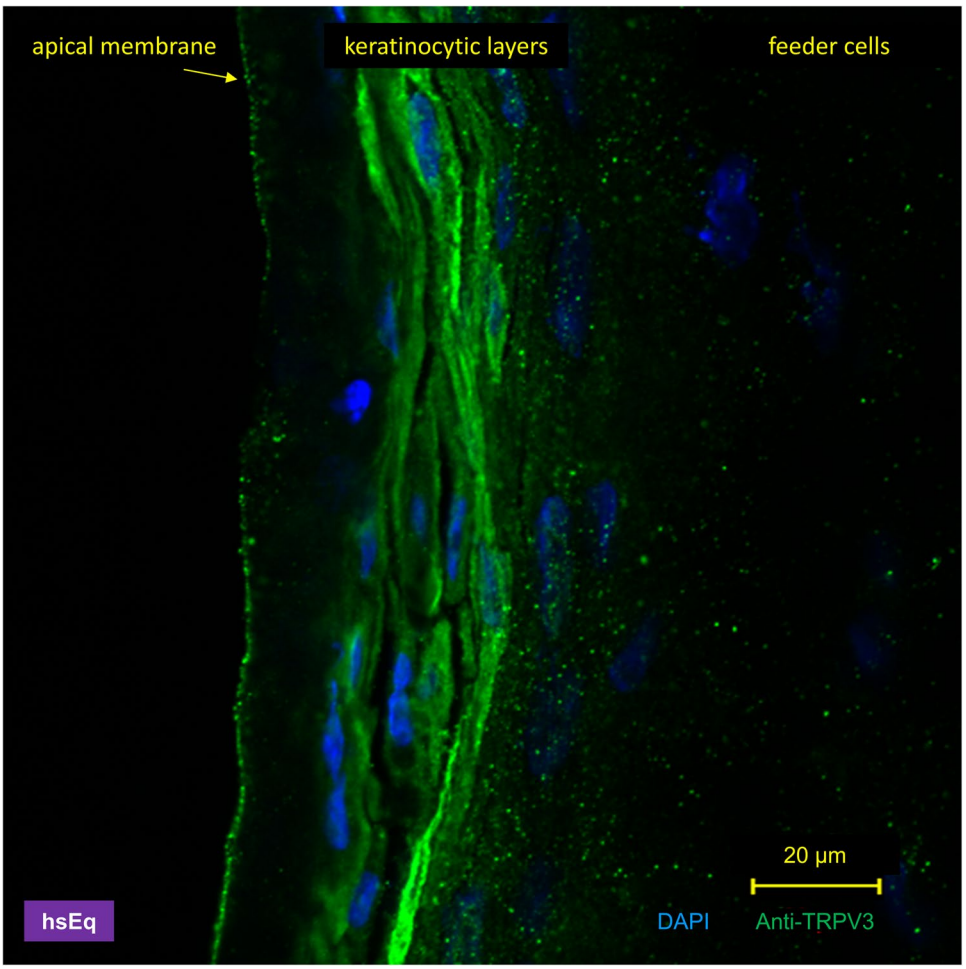

Fig. 4 Confocal laser microscopy: localization of hTRPV3 in a human skin equivalent. Interfollicular primary human fibroblasts and keratinocytes were isolated from juvenile foreskin and grown in culture to obtain human skin equivalents, as described in detail elsewhere [42]. Staining with Anti-TRPV3 ($n = 10$) is shown in green. Cell nuclei are shown in blue (DAPI), allowing identification of the basal feeder cells (fibroblasts) to the right, which showed no staining for TRPV3. Conversely, keratinocytes showed strong staining of the cytosol, except for the top layer on the left of the image, where staining for hTRPV3 was almost exclusively observed in the apical membrane. Note that since the skin equivalent was covered with cell culture medium throughout, it did not form the equivalent of a stratum corneum

mechanisms of the cell can compensate for the residual influx of protons via NH_4^+. Accordingly, an enhanced permeability to NH_4^+ should increase the speed of acidification, while the pH_i minimum should decrease. Simultaneously, it should be possible to observe a depolarization of the membrane potential (U_{mem}), the magnitude of which will depend not on the absolute influx of NH_4^+ but on its magnitude relative to other conductances.

In accordance with the latter scenario, preliminary screening experiments on four hTRPV3 expressing *X.* oocytes showed that application of NH_4Cl led to an acidification and depolarization of each oocyte studied. After washout, a very slow pH increase could be observed, clearly distinct from the rapid drop in pH associated with an efflux of NH_3 (see supplement part H, Fig. S1). Possible reasons for the remarkably slow recovery will be discussed further down.

Transport primarily in the form of NH_4^+ is supported by subsequent more rigorously performed investigations (Fig. 5 and Table 1). The experiments were conducted in parallel with another project [39], alternating between hTRPV3 ($n/N = 13/3$), the bovine homologue bTRPV3 ($n/N = 14/3$), and control *X.* oocytes ($n/N = 16/3$) (see supplement part H, Fig. S2 and Table S2). To prevent damage to *X.* oocytes overexpressing hTRPV3 due to influx of Na^+, all groups of oocytes were incubated in NMDGCl solution prior to the experiment and in its initial phase. A switch to NaCl resulted in a depolarization that was significantly higher in the hTRPV3 group, reflecting greater permeability to Na^+ with a higher $p(Na^+)/p(NMDG^+)$. Conversely, the depolarizing effects of NH_4^+ were larger in control oocytes. This suggested that in addition to non-selective cation channels as previously assumed [11], endogenous K^+ channels may have contributed to the NH_4^+ response of the control oocytes in our study [18, 33, 82]. Alternately, the permeability of the endogenous non-selective cation channels to Na^+ may have been lower than that to K^+. Note that U_{mem} only measured the permeability ratio relative to other ions (as indicated by the Goldman-Hodgkin-Katz equation) and not the absolute influx rate, which may be why significant differences did not emerge.

Influx of NH_4^+ is confirmed by analysing the pH_i data. Application of NH_4^+ induced a strong acidification with a final pH_i in NH_4Cl solution that was significantly lower in hTRPV3 oocytes than in controls, confirming a higher

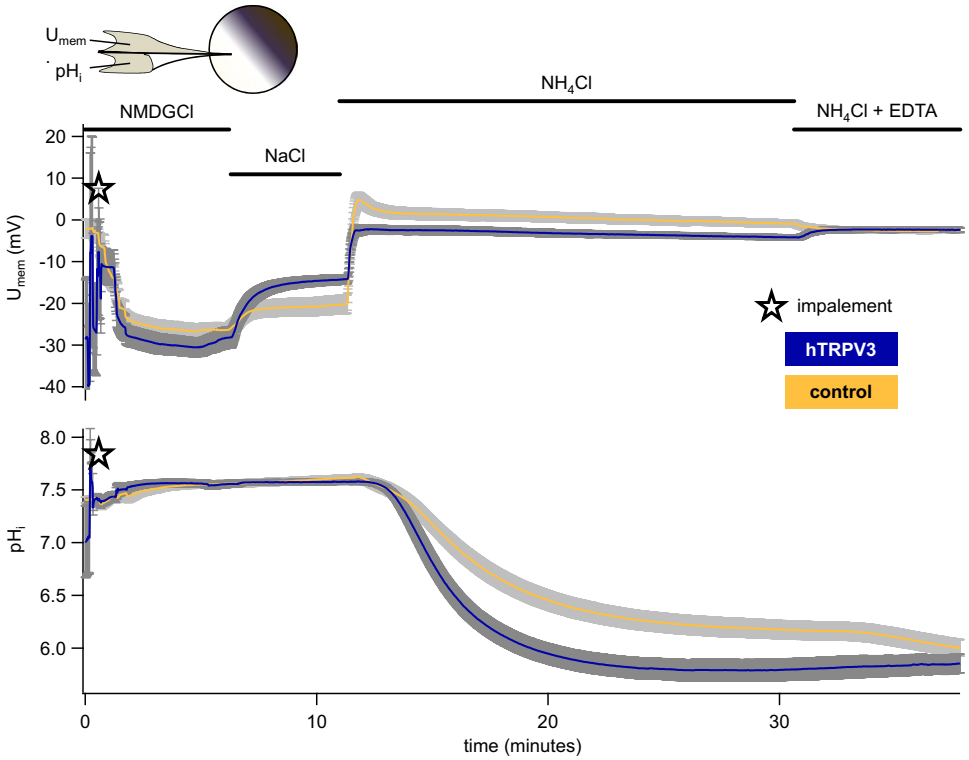

Fig. 5 Double-barrelled pH-sensitive microelectrodes: response of control *X. oocytes* and *X. oocytes* expressing hTRPV3 to NH_4Cl solution (means ± SEM). The blue traces show the means ± SEM of hTRPV3 *X. oocytes* (*n/N* = 12/3), while the orange traces represent the means of the controls (*n/N* = 16/3) [39], with SEM values shown in shades of grey. Impalement is marked by the star and the sharp drop in U_{mem}. *X. oocytes* were incubated in NMDGCl containing solution in the days before the experiment and in its initial phase. Subsequently, the bath solution was switched to various solutions as indicated by the bars. Acidification occurred after application of NH_4Cl with a stronger effect in hTRPV3 *X. oocytes*, reflecting greater influx of NH_4^+

Table 1 Double-barrelled pH-sensitive microelectrodes: effects of NH_4^+ on the pH_i and the membrane potential of *X. oocytes* expressing hTRPV3. The table shows means ± SEM of measurements using hTRPV3 (hV3, *n/N* = 13/3) and control *X. oocytes* (ctrl, *n/N* = 16/3) consecutively exposed to various solutions. Values were measured 5 min after exposure unless indicated otherwise. The last column shows the statistical comparison of the two groups using the Mann–Whitney Rank Sum Test. Within columns, different superscripts indicate significant differences with $p \leq 0.05$ (ANOVA on Ranks)

Bath solution	hTRPV3	Control	*p* (hV3 vs. ctrl)
Membrane potential (mV)			
NMDGCl	−30.6 ± 2.2[a]	−27.2 ± 1.8[a]	0.4
NaCl	−14.4 ± 1.1[b]	−20.3 ± 2.2[b]	0.03
NH_4Cl (3.5 min)	−2.5 ± 1.0[c]	1.5 ± 1.4[c]	0.03
NH_4Cl (20 min)	−4.1 ± 0.6[d]	−0.9 ± 0.8[d]	0.003
NH_4Cl-EDTA	−2.3 ± 0.6[c]	−2.7 ± 0.5[e]	0.7
Intracellular pH (pH_i)			
NMDGCl	7.56 ± 0.04[a]	7.56 ± 0.04[a]	0.9
NaCl	7.58 ± 0.03[a]	7.61 ± 0.03[b]	0.5
NH_4Cl (3.5 min)	6.76 ± 0.09[b]	7.14 ± 0.06[c]	0.004
NH_4Cl (20 min)	5.81 ± 0.11[c]	6.18 ± 0.09[d]	0.007
NH_4Cl-EDTA	5.85 ± 0.09[c]	6.05 ± 0.08[e]	0.07
Change of pH_i (slope in ΔpH/min)			
NMDGCl	0.03 ± 0.02[a]	0.01 ± 0.01[a]	0.5
NaCl	0.00 ± 0.00[a]	0.00 ± 0.01[a]	0.6
NH_4Cl (3.5 min)	−0.39 ± 0.04[b]	−0.22 ± 0.04[b]	0.006
NH_4Cl (20 min)	0.02 ± 0.01[a]	0.00 ± 0.01[a]	0.05
NH_4Cl-EDTA	−0.004 ± 0.02[a]	−0.04 ± 0.02[c]	0.01
Relative permeability ratio p(X) / $p(NMDG^+)$			
Ion X			
Na^+	1.98 ± 0.18[a]	1.37 ± 0.12[a]	0.005
NH_4^+ (20 min)	2.93 ± 0.24[b]	2.93 ± 0.23[b]	1.0
NH_4^+ (in EDTA)	3.15 ± 0.25[c]	2.70 ± 0.18[c]	0.3

permeability to NH_4^+ in the hTRPV3 group (Fig. 5 and Table 1). Prior to NH_4Cl application, an alkaline drift was observed that led to a significant difference in the absolute pH_i values between NaCl and NMDGCl. It is tempting to speculate on an involvement of NHE, but the lack of an impact of the solution change on the slope of the pH_i curve indicates that any involvement of endogenous NHE was weak (Fig. 5 and Table 1).

In both groups, the speed of acidification after application of NH_4^+ was initially high with influx driven both by the negative membrane potential and a high concentration gradient for NH_4^+, but levelled off as the oocytes approached an equilibrium distribution (Table 1 and Fig. 5). Twenty minutes after application of NH_4^+, the pH_i of hTRPV3 oocytes started to recover slightly, suggesting a situation near equilibrium. Accordingly, opening of hTRPV3 channels after removal of Ca^{2+} showed no significant effect on pH_i ($p = 0.2$). Conversely, the rate of acidification increased after application of EDTA in control oocytes, suggesting that equilibrium had not been reached. Most likely, removal of Ca^{2+} opened endogenous NH_4^+ permeable non-selective cation channels [11, 82].

The effects of a removal of Ca^{2+} on the membrane potential were inverse in hTPRV3 and control oocytes. All hTRPV3 oocytes depolarized significantly with a significant rise in $p(NH_4^+)/p(NMDG^+)$, suggesting a greater influx of NH_4^+ through hTRPV3 channels that were opened by the removal of Ca^{2+}. Conversely, all control oocytes hyperpolarized. *X.* oocytes express rather unique endogenous Cl^- channels that open when Ca^{2+} is removed [61, 82]. It appears likely that in control oocytes, the corresponding hyperpolarization overrode the opening of endogenous non-selective cation channels, while in oocytes overexpressing hTRPV3, the effect on hTRPV3 channels predominated. Note that the corresponding relative permeability ratios (which were calculated from the membrane potentials) contain contributions of this Ca^{2+} inactivated Cl^- conductance and must therefore be considered with caution.

In conjunction, these results suggest that both groups of *X.* oocytes expressed conductances to Na^+ and NH_4^+, but that permeability to Na^+ was greater and influx of NH_4^+ more rapid in hTRPV3 oocytes than in controls. In both groups, any permeability to NH_3 was much smaller than that to NH_4^+. The comparison with the bovine homologue [39]

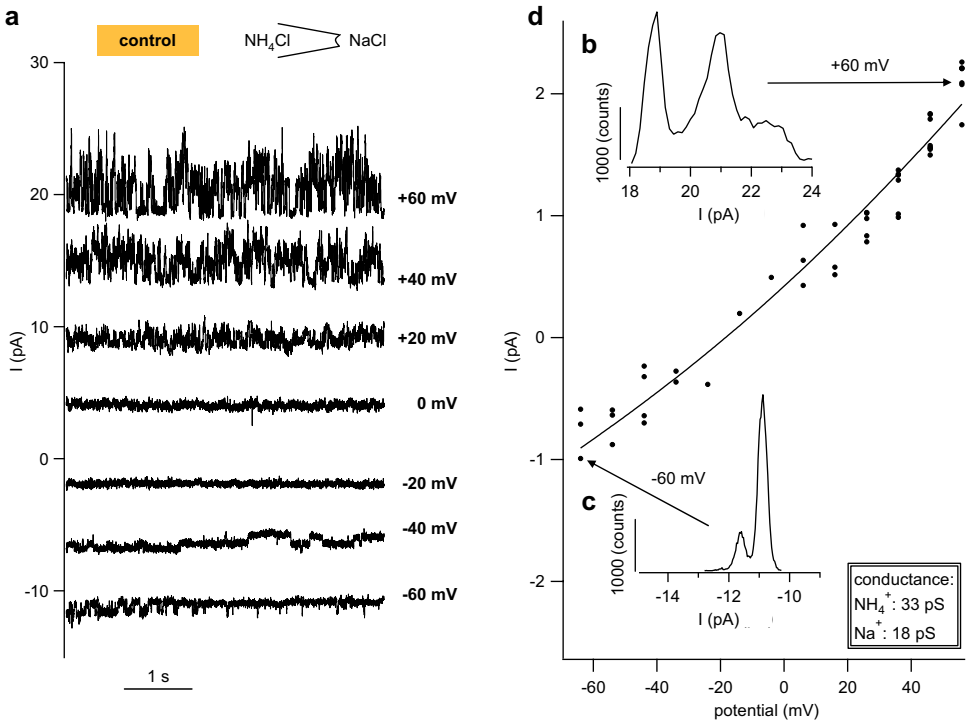

Fig. 6 Single-channel recordings of a patch from a control *X.* oocyte showing channels permeable to NH_4^+ and Na^+. This measurement was performed in the inside-out configuration with NaCl in the bath (facing the cytosolic side) and NH_4Cl in the pipette (external side), with pipette potentials as indicated. **a** Original recording showing channel events that were visibly smaller at negative potentials (influx of Na^+ from the bath) than at positive potentials (efflux of NH_4^+ from the pipette). **b** Amplitude histogram of the trace at +60 mV. The distance between the two large peaks was used to determine the unitary conductance. The noisy residue above 22 pA most likely reflects very brief openings of additional channels. **c** Amplitude histogram of the trace at −60 mV, the peak distance is smaller than in (**b**). **d** All unitary currents (black circle) from this patch were plotted against the potential. The data were fitted with a GHK fit (black line) yielding a higher conductance for NH_4^+ than Na^+ (also see the histogram in Fig. 9)

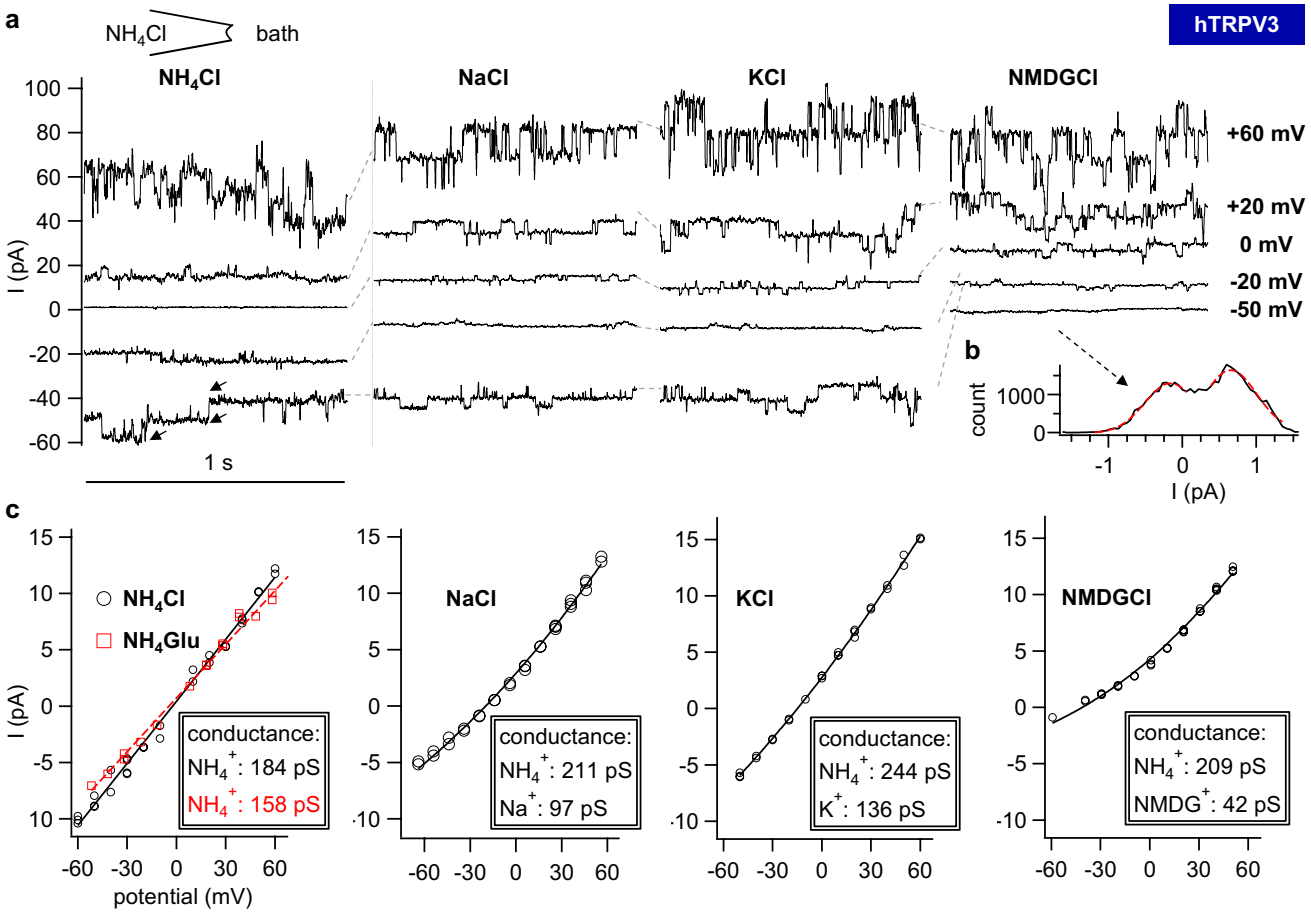

Fig. 7 Single-channel recordings of a patch from a hTRPV3 *X. oocyte* in symmetrical NH_4^+ solution. This measurement was performed in the inside-out configuration with NH_4Cl in the pipette and consecutively applied bath solutions as indicated. **a** Traces at pipette potentials of +60 mV, +20 mV, 0 mV, −20 mV, and −50 mV. In symmetrical NH_4Cl solution at −50 mV, the arrows indicate three different current levels corresponding to the opening of two channels. Channel openings of similar size were visible at positive and negative potentials. In NMDGCl, reduction in the amplitude of channel openings was clearly visible at −50 mV with channel activity reduced to a flicker. The absolute current level also dropped sharply suggesting that much of the baseline current in the previous traces was channel-mediated. Conversely, at +60 mV, unitary currents remained at the same level, reflecting efflux of NH_4^+ from the pipette into the bath. **b** Amplitude histogram of the trace at −50 mV in NMDGCl solution. The red broken lines represent two Gauss fits. The distance between their peaks was used to estimate the unitary current. **c** Unitary currents (white circle) from amplitude histograms as exemplarily in (**b**) were plotted over the potential. A linear fit was used for data from NH_4Cl solution (black) and NH_4-Glu solution (red, no traces shown above). All other data were fitted with the GHK equation for two cations to yield the conductances as indicated (also see the histogram in Fig. 9)

is shown in the Supplement (part H and Fig. S2) and will be discussed below.

Inside-out patch-clamp experiments

In total, patches from 30 hTRPV3 and 21 control *X. oocytes* from three frogs were investigated, alternating between hTRPV3, bTRPV3, and control *X. oocytes* [39]. In all groups, there was a tendency for single-channel events to occur in one solution and vanish in another without apparent reason. Channel activity mostly rose with the duration of the experiment.

The pipette solution contained NH_4Cl, and the bath was changed from NaCl to NH_4Cl and NH_4Glu. In control *X. oocytes*, 14 out of 21 patches showed single-channel activity in at least one solution (supplement, Fig. S4). Unitary events were not altered by the replacement of Cl- by the larger anion, Glu^-, arguing against an anion conductance. In an asymmetrical configuration with NaCl in the bath, channel openings were visible at negative potentials, reflecting influx of Na^+. At positive potentials, larger channel openings could be observed, reflecting efflux of NH_4^+ (Fig. 6a). The results of the GHK-analysis (Fig. 6b) varied from patch to patch. The mean conductance of this diverse group of

channels was previously reported in Liebe et al. [39] (43 ± 9 pS for NH_4^+ ($n = 13$) and 33 ± 10 pS for Na^+ ($n = 11$)).

Of 30 hTRPV3 patches, six showed no channel activity (supplement Fig. S4). In total, hTRPV3 patches showed a channel conductance in NH_4Cl solution that was three times higher than in controls (132 ± 68 pS $n/N = 19/3$, $p = 0.001$). The sharp decline of current at negative potentials in NMDGCl solution suggests that much of the baseline current in the other traces reflects continuously open cation channels (Fig. 7). Five patches showed small channel events with a conductance (G) for NH_4^+ of 62 ± 49 pS ($p = 0.6$ vs. control). Ten other patches showed both large and small channel events, sometimes appearing simultaneously in the same trace (Fig. 8). In nine patches, activity of channels was initially lacking or small with $G(NH_4^+) < 100$ pS, although later, larger channels with $G(NH_4^+) > 100$ pS became visible.

Since channel events yielding a conductance > 100 pS were almost exclusively observed in hTRPV3 *X. oocytes*, they were considered to reflect hTRPV3 channel activity (Fig. 9), with the scatter possibly reflecting formation of heteromers with endogenous channels. The conductance of these larger channels was $G(Na^+) = 91 \pm 27$ pS and $G(NH_4^+) = 190 \pm 53$ pS. A further histogram in the supplement includes bTRPV3 conductances (Fig. S3). These values were obtained in oocyte Ringer, which contained lower concentrations of Na^+ and NH_4^+ than the standard Ringer solutions used when working with HEK-293 cells. Assuming that the independence principle applies, the corresponding values for 145 mmol·L^{-1} can be obtained using Eq. 4 in supplement part F, yielding $G(Na^+) = 137 \pm 42$ pS and $G(NH_4^+) = 287 \pm 80$ pS, respectively.

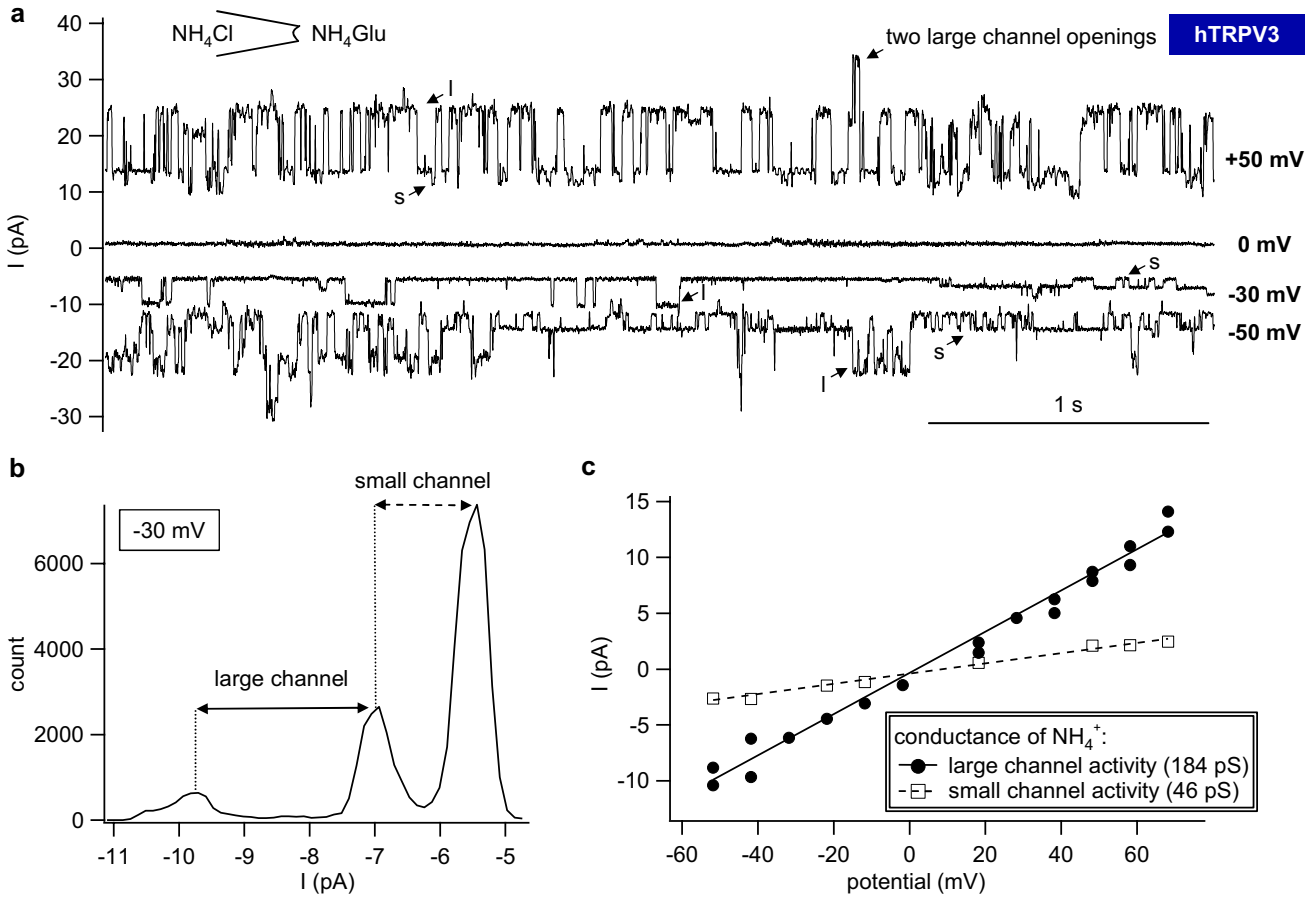

Fig. 8 Single-channel recordings of a patch from an hTRPV3 *X. oocyte* showing both endogenous channels and hTRPV3. This measurement was performed with NH_4Cl in the pipette and NH_4Glu in the bath. **a** At +50 mV, 0 mV, −30 mV, and −50 mV pipette potential, both large (l) and small (s) channel openings occurred in the same trace as indicated by the arrows. At 0 mV, there is no electrochemical gradient for NH_4^+, and no channel activity could be observed. At +50 mV, two large channels opened at the same time leading to a higher current response. **b** In the amplitude histogram corresponding to the trace shown in Fig. 8a at −30 mV, three peaks were clearly visible with unitary currents indicated by the double arrows. The small channel was usually open, while the large channel had a much lower open probability but higher unitary current. **c** All unitary currents were plotted against the clamped potentials. The data of large and small channels were fitted separately to yield the conductances for NH_4^+

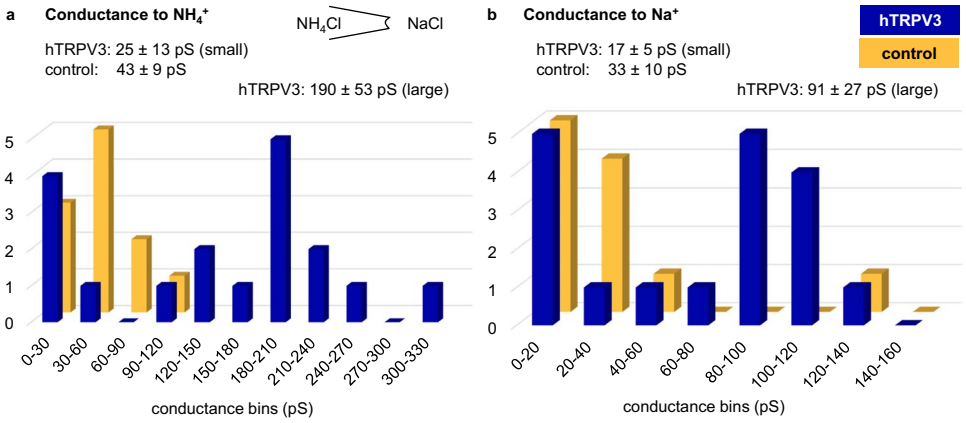

Fig. 9 Inside-out patch-clamp measurements: histograms of all NH_4^+ and Na^+ conductances from *X.* oocytes. The conductances visualized in the histograms were obtained in asymmetrical configuration with NH_4Cl in the pipette and NaCl in the bath. The vertical axis yields the number of patches in which the conductance fell into a particular conductance bin as shown on the horizontal axis. **a** All NH_4^+ conductances from control patches (orange) were below 100 pS. Patches of hTRPV3 *X.* oocytes showed both small NH_4^+ conductances such as those observed in controls and larger NH_4^+ conductances ranging up to 303 pS, possibly reflecting formation of heteromers of hTRPV3 with endogenous channels. **b** Corresponding histogram of all Na^+ conductances. Although channels were smaller, a similar pattern emerged as in (**a**), with a cluster of channels below 60 pS in both groups and a second larger cluster emerging in hTRPV3 *X.* oocytes. Interestingly, one solitary control patch expressed a very large conductance to Na^+ reflecting what is clearly a very diverse population of channels expressed by the native *X.* oocyte [82]. Note that these measurements were performed in oocyte Ringer (96 mmol·L^{-1}), yielding lower conductances than would have been expected in mammalian Ringer (145 mmol·L^{-1})

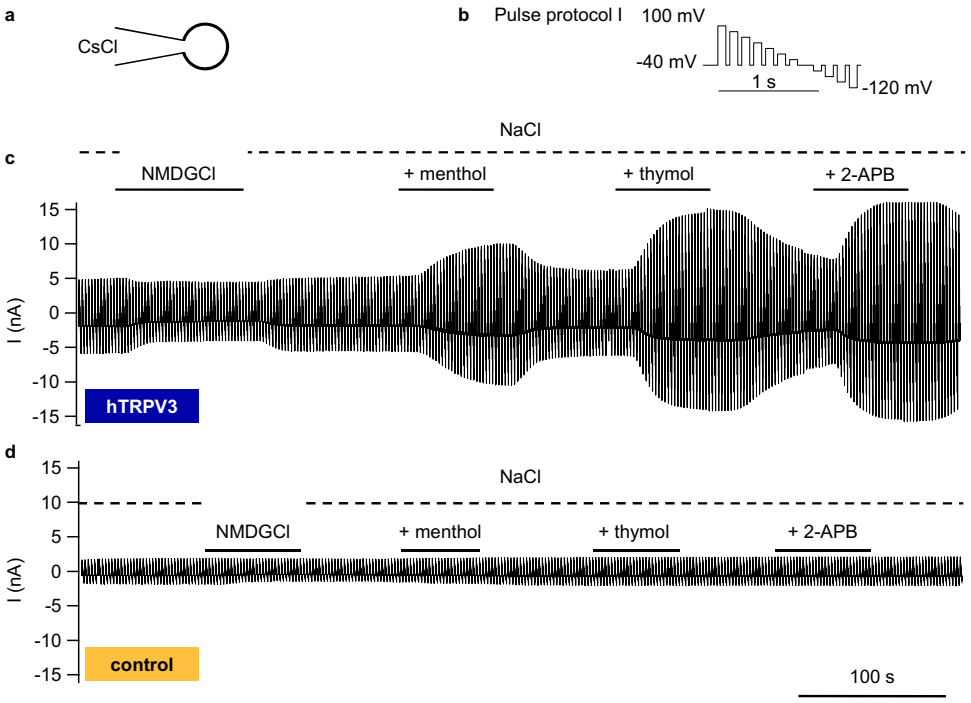

Fig. 10 Whole-cell recordings: response of hTRPV3 HEK-293 cells to TRP channel agonists in NaCl solution. To confirm functional expression of hTRPV3, measurements were performed in a standard configuration using divalent-free solutions with CsCl in the pipette and NaCl in the bath (**a**). Cells were stimulated with the continuous pulse protocol I shown in (**b**). Pulse protocols were merged to visualize whole-cell currents measured in one hTRPV3 HEK-293 cell (**c**) and a control cell (**d**). Both cells showed a reduction in inward current at negative pipette potentials when extracellular Na^+ was exchanged for the poorly permeable $NMDG^+$, indicating the presence of cation channels. After return to NaCl, the three TRPV3 agonists menthol (1 mmol·L^{-1}), thymol (1 mmol·L^{-1}), and 2-APB (1 mmol·L^{-1}) were consecutively applied with significant effects in overexpressing cells, while no observable impact was detectable in controls. Washout significantly reduced the currents (hTRPV3, $n = 19$; control, $n = 13$, see also Table 2)

Table 2 Whole-cell measurements: effects of menthol, thymol, and 2-APB on Na^+ currents and the reversal potential of HEK-293 cells expressing hTRPV3. The table shows means ± SEM of whole-cell measurements of hTRPV3 (hV3, $n = 19$) and control (ctrl, $n = 13$) HEK-293 cells consecutively exposed to various solutions. Both the pipette solution (CsCl) and the bath solution (NaCl) were divalent-free resulting in large current densities. Numbers in parentheses reflect repeated application of the same bath solution. The last column gives the p values between the two groups (Mann–Whitney Rank Sum Test). Different superscripts indicate significant differences ($p \le 0.05$) between different solutions within one group (ANOVA on Ranks)

Bath (pipette: CsCl)	hTRPV3	Control	p (hV3 vs. ctrl)
Outward current (pA · pF^{-1}) at + 100 mV			
NaCl	135 ± 24^a	64 ± 22^a	0.04
NMDGCl	145 ± 29^a	57 ± 21^b	0.01
NaCl (2)	141 ± 26^a	60 ± 21^a	0.03
Menthol in NaCl	327 ± 99^b	64 ± 22^a	0.001
NaCl (3)	172 ± 34^c	67 ± 22^a	0.03
Thymol in NaCl	575 ± 139^d	67 ± 23^a	≤ 0.001
NaCl (4)	338 ± 106^e	69 ± 24^a	0.004
2-APB in NaCl	1058 ± 140^f	70 ± 24^a	≤ 0.001
NaCl (5)	615 ± 115^d	70 ± 26^a	≤ 0.001
Inward current (pA · pF^{-1}) at − 120 mV			
NaCl	-129 ± 28^a	-67 ± 26^a	0.16
NMDGCl	-85 ± 20^b	-47 ± 19^b	0.22
NaCl (2)	-111 ± 26^c	-61 ± 22^a	0.18
Menthol in NaCl	-255 ± 88^d	-66 ± 25^a	0.05
NaCl (3)	-129 ± 29^a	-71 ± 26^a	0.14
Thymol in NaCl	-481 ± 123^e	-72 ± 27^a	≤ 0.001
NaCl (4)	-306 ± 112^d	-72 ± 27^a	0.05
2-APB in NaCl	-993 ± 122^f	-75 ± 28^a	≤ 0.001
NaCl (5)	-634 ± 130^e	-102 ± 39^a	≤ 0.001
Reversal potential (mV)			
NaCl	-12.0 ± 4.6^a	-8.2 ± 2.8^a	0.9
NMDGCl	-27 ± 4.2^b	-21.8 ± 4.4^b	0.4
NaCl (2)	-8.9 ± 1.3^c	-10.4 ± 4^a	0.8
Menthol in NaCl	-10.9 ± 2.4^d	-7.9 ± 2.5^a	0.4
NaCl (3)	-10.3 ± 3.6^{ae}	-7.3 ± 2.7^a	0.7
Thymol in NaCl	-10.1 ± 1.1^c	-7.7 ± 2.8^a	0.05
NaCl (4)	-13.3 ± 3.8^c	-8.3 ± 3.2^a	0.3
2-APB in NaCl	-18.5 ± 4.2^f	-7.6 ± 2.8^a	0.002
NaCl (5)	-11.7 ± 2.8^c	-7.8 ± 3.0^a	0.1

Whole-cell patch-clamp experiments

NaCl

Functional expression of hTRPV3 in HEK-293 cells was investigated using a CsCl pipette solution and a Ca^{2+}- and Mg^{2+}-free NaCl bath solution [44]. After stabilization of current, agonists of hTRPV3 [44, 79] were applied, namely, menthol (racemic form; 1 mmol·L^{-1}), thymol (1 mmol·L^{-1}), and 2-APB (0.3 mmol·L^{-1}), with subsequent NaCl-washout (Fig. 10 and Table 2).

In the initial NaCl solution, hTRPV3 cells ($n = 19$) showed a higher outward current density at + 100 mV than the controls ($n = 13$), reflecting a higher efflux of Cs^+ through hTRPV3. When Na^+ was replaced by $NMDG^+$, current at − 120 mV in controls changed by − 18 ± 7 pA·pF^{-1}, slightly lower than in hTRPV3 cells (− 44 ± 10 pA·pF^{-1}, $p = 0.06$). the relative permeability ratios ($p(Na^+)$/$p(NMDG^+)$) were not different at 1.8 ± 0.2 (controls) and 1.9 ± 0.3 (hTRPV3) ($p = 0.8$). As reported by Macpherson et al. [44], highly significant differences between the two groups emerged after exposure to the agonists (Table 2).

NH_4Cl

In subsequent experiments, the permeability to NH_4^+ was investigated with a NaGlu pipette solution. Cells were initially superfused with a NaCl solution, with equal concentrations of Na^+ inside and outside. The external solution contained physiological amounts of divalent cations, leading to significantly lower currents than in the Ca^{2+}- and Mg^{2+}-free solutions used above (Tables 2 and 3).

In the initial NaCl solution, any difference between hTRPV3 and control cells did not test for significance (Figs. 11 and 12 and Table 3). In both cell types, a switch to NH_4Cl bath solution resulted in a significant rise in inward current level at − 120 mV in conjunction with a significant depolarization of the reversal potential, reflecting influx of

Table 3 Whole-cell measurements: effects of D-menthol on NH_4^+ currents and the reversal potential of HEK-293 cells expressing hTRPV3. The table shows means ± SEM of measurements of hTRPV3 (hV3) and control (ctrl) HEK-293 cells consecutively exposed to various solutions that contained physiological amounts of Ca^{2+} and Mg^{2+}, resulting in smaller current densities than in Table 2. Numbers in parentheses reflect repeated application of the same bath solution. The last column gives the *p* values between the two groups within the same solution (Mann–Whitney Rank Sum Test). Different superscripts indicate significant differences ($p \le 0.05$) between values measured in different solutions within the same cell type (ANOVA on Ranks)

Bath (pipette: NaGlu)	hTRPV3	*n*	Control	*n*	*p* (hV3 vs. ctrl)
Outward current (pA · pF^{-1}) at + 100 mV					
NaCl	9 ± 3^a	18	6 ± 2^a	12	0.9
NH_4Cl	16 ± 4^b	18	17 ± 3^b	12	0.3
NH_4Cl + D-menthol	116 ± 42^c	18	20 ± 3^b	12	0.01
NH_4Cl (2)	98 ± 44^d	16	19 ± 2^c	10	0.7
NaCl (2)	86 ± 42^b	16	10 ± 2^d	10	0.3
Inward current (pA · pF^{-1}) at -120 mV					
NaCl	-11 ± 4^a	18	-5 ± 2^a	12	0.4
NH_4Cl	-21 ± 6^b	18	-9 ± 2^b	12	0.6
NH_4Cl + D-menthol	-102 ± 62^c	18	-10 ± 3^b	12	0.05
NH_4Cl (2)	-85 ± 42^c	16	-13 ± 4^c	10	0.2
NaCl (2)	-67 ± 38^b	16	-9 ± 3^d	10	0.5
Reversal potential (mV)					
NaCl	-1 ± 7^a	18	10 ± 7^a	12	0.2
NH_4Cl	19 ± 5^b	18	26 ± 4^b	12	0.2
NH_4Cl + D-menthol	15 ± 2^b	18	28 ± 4^b	12	0.01
NH_4Cl (2)	14 ± 3^b	16	27 ± 5^b	10	0.11
NaCl (2)	-1 ± 5^a	16	19 ± 7^a	10	0.03

NH_4^+. A concomitant rise in outward current at + 100 mV was observed (see discussion). From the reversal potentials, relative permeability ratios were calculated, yielding ratios for $p(NH_4^+)/p(Na^+)$ of 2.3 ± 0.5 (hTRPV3) and 2.0 ± 0.3 (control) ($p = 0.9$).

In hTRPV3 cells only, application of D-menthol led to a significant rise in inward and outward currents, reflecting an activation of hTPRV3 channels with influx of NH_4^+ (at − 120 mV) and efflux of Na^+ (at + 100 mV). Additionally, relative permeability $p(NH_4^+)/p(Na^+)$ rose significantly to 3.1 ± 0.7 ($p < 0.05$). In controls, $p(NH_4^+)/p(Na^+)$ remained at 2.5 ± 0.6 ($p > 0.05$) with no significant difference between groups. The hTRPV3 currents had interesting kinetics with a time-dependent activation after depolarization and tail currents after a return to the holding potential of − 40 mV (Fig. 12), reflecting influx of NH_4^+ that decreased with time. Most likely, both the activation at high positive potentials followed by tail currents after repolarization were caused by voltage-dependent interaction with external Ca^{2+}. Note that internal Ca^{2+} was buffered by EGTA, preventing an internal block by Ca^{2+}.

Interestingly, in two control cells, a reversible reduction in inward current level could be observed. L-menthol inhibits cardiac L-type channels [4], which have a certain pharmacological similarity to endogenous Ca^{2+} channels expressed by HEK-293 cells [7].

While effects of L-menthol on TRPV3 are classical [44], we are not aware of studies using D-menthol. In order to compare the effects of D- and L-menthol, experiments were performed in which both agonists were consecutively applied. The sequence of the application of the two forms of menthol was altered between experiments so that five cells were first treated with D-menthol and then with L-menthol, while in further 5 cells, the order was inverse (Fig. 13c,d). While the effects of the second application of menthol were always significantly larger, no difference between the two enantiomers emerged (Fig. 13e).

Investigation of the Olmsted mutant G573S of hTRPV3

Since conflicting reports are found in the literature, a final goal of the current study was to investigate whether the G573S mutation of hTRPV3 (G573S) is trafficked to the cell membrane [22, 40]. Immunoblots suggested successful but weak expression of G573S in HEK-293 cells (Fig. 1). Individual G573S HEK-293 showed Anti-TRPV3 immunofluorescence staining in the cytosol. Even fewer cells showed staining within the cell membrane (Fig. 14a). However, it should be stressed that in the 26 cultures investigated, only very few cells could be shown to have any staining for G573S, and of those that did, most deviated

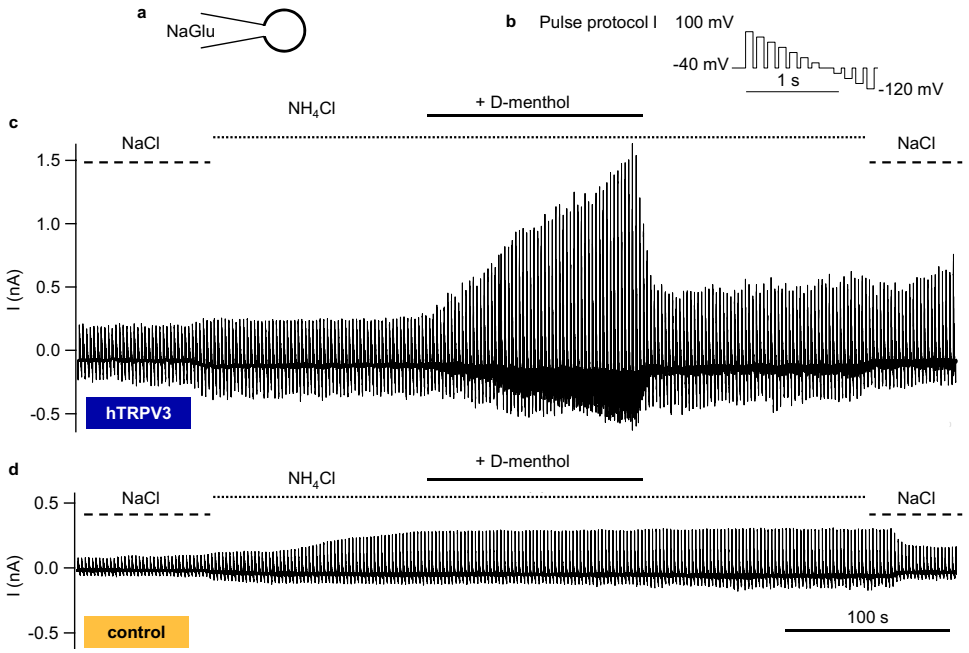

Fig. 11 Whole-cell recordings: effects of D-menthol on NH_4^+ mediated currents in HEK-293 cells. Measurements were performed with a NaGlu pipette solution (**a**) using pulse protocol I (**b**) with physiological concentrations of divalent cations in the bath solution. Merged pulse protocols show the current responses for one hTRPV3 HEK-293 cell (**c**) and for one control cell (**d**). Note the increase in inward current at negative potential in both groups after the change from NaCl to NH_4Cl. In hTRPV3 expressing cells, but not in controls, application of D-menthol (1 mmol·L^{-1}) strongly increased both inward current (carried by NH_4^+) and outward current (carried by Na^+). Washout significantly reduced the currents (hTRPV3, $n = 18$; control, $n = 12$; see also Table 3)

morphologically from non-expressing controls, and all failed to express significant amounts of GFP. Furthermore, large numbers of detached and deformed cells were found floating in the supernatant. In order to enhance the viability of HEK-293 cells expressing the mutant, we attempted various approaches, which included reducing the concentration of free Ca^{2+} in the medium, changing the concentration of foetal bovine serum or altering incubation times after transfection that are summarized in supplement part G. All of these attempts were unsuccessful.

Transfection with the *G573S* vector resulted in a significantly reduced HEK-293 cell count in comparison to wild-type hTRPV3 ($p \leq 0.001$; Fig. 14b). In a next step, the TRP antagonist ruthenium red (RR) was added to the medium, which should block channels from the external side. In cells expressing G573S, RR induced a significant ($p = 0.04$) increase in the cell count. Conversely, the wild-type hTRPV3 cell count was significantly reduced by RR ($p \leq 0.05$). Note that the effect of RR on G573S cells was significantly ($p \leq 0.001$) stronger in comparison to hTRPV3 cells. Cell counts of controls responded to RR in a similar way as wild-type hTRPV3, although the difference induced by ruthenium red was not significant ($p = 0.2$). Despite the RR treatment, the number of successfully transfected G573S cells remained very low, and staining for GFP was insufficient. For this reason, attempts to patch-clamp HEK-293 cells with the G573S mutation of hTRPV3 failed.

Discussion

Using the whole-cell and inside-out configuration of the patch-clamp technique and double-barrelled pH-sensitive microelectrodes in two different expression systems, the present study clearly shows that the human homologue of TRPV3 channel (hTRPV3) conducts NH_4^+. It may be argued that this is hardly surprising in light of the low ability of TRPV3 to discriminate between different cations [58] and our previous findings concerning the bovine homologue [39], but a conductance of hTRPV3 to NH_4^+ has to be shown rigorously before any further deliberations are possible. Parts of the study were performed in a manner to allow a direct comparison between the human and the bovine TRPV3, but the data of this study do not support a significant functional difference between the two homologues.

In a further step, we demonstrated that both the native hTRPV3 of human keratinocytes and the OS mutant G573S are trafficked to the cellular membrane, in line with established models [17, 52, 53]. However, there are also signs of an expression in intracellular organelles. We conclude that

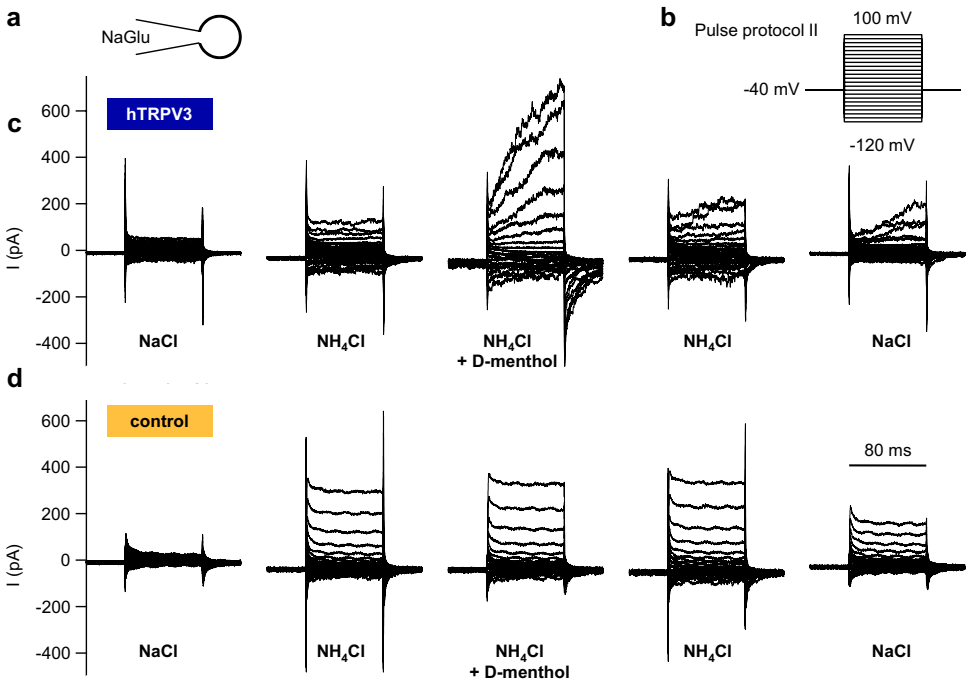

Fig. 12 Whole-cell recordings: kinetics of NH_4^+ currents in HEK-293 cells. Measurements were performed with cells filled with NaGlu pipette solution (**a**) using pulse protocol II (**b**). Cells were superfused with NaCl, NH_4Cl, supplemented D-menthol in NH_4Cl, and washout, consecutively. **c** Original recording of a HEK-293 cell overexpressing hTRPV3. Note the typical current kinetics after application of D-menthol (1 mmol·L^{-1}) with strong current activation at depolarizing potentials and subsequent tail currents after return to −40 mV. These tail currents reflect NH_4^+ that is entering the cell via previously opened hTRPV3 channels. **d** Original recording of a control cell, showing a strong induction of outward current in response to application of NH_4Cl, but no further stimulation by D-menthol (hTRPV3, $n = 18$, control, $n = 12$; see also Table 3)

while hTRPV3 is certainly important for Ca^{2+} signalling as classically proposed [17, 52], it may also mediate relevant exchanges of monovalent cations such as NH_4^+ both between organelles and the cytoplasm and between the cytoplasm and the extracellular space, with consequences for nitrogen exchanges and protein metabolism.

It may be argued that ammonia can simply diffuse through the lipid membrane, so why is a transport protein needed? However, ammonia (NH_3) is a very polar molecule which strongly binds H^+ so that at physiological pH, over 98% is found in the form of ammonium (NH_4^+). Both the strong dipole moment and the low concentrations of NH_3 argue against sizable transport rates via lipid diffusion. Instead, the strong alkalinization observed in many types of cells exposed to NH_4Cl reflects expression of Rhesus-like glycoproteins (AMT/Rh) [30] and aquaporins [9], which catalyse the deprotonation of NH_4^+, so that NH_3 is formed, which then passes through these protein pores into the cell [51]. In other preparations, uptake occurs primarily as ammonium (NH_4^+). In the thick ascending loop of Henle, uptake of ammonium occurs via a K^+ channel (ROMK) [18] and the NKCC cotransporter, which is not surprising since the hydration radii and, thus, the hydration energies of NH_4^+ and K^+ are similar [36]. In native *X.* oocytes [11, 39] and the ruminal epithelium, non-selective cation channels have emerged as the primary uptake route for NH_4^+ [1, 8, 59, 66]. Since uptake is driven by the negative membrane potential, this mechanism should be particularly useful if nitrogen needs to be scavenged for synthesis of non-essential amino acids. This is certainly the case in ruminants on traditional diets, but it is also possible to speculate that *X.* oocytes might profit from being able to take up ammonia from degradation processes within a pond.

Detection of the protein

In the current study, hTRPV3 channels were expressed in HEK-293 and *X.* oocytes. Immunoblots (Fig. 1) with staining against the Strep-tag showed bands at the predicted height (~95 kDa) in the hTRPV3 and G573S overexpressing cells, but not in controls. A weak band (~60 kDa) could be seen in the hTRPV3 and G573S HEK-293 cells, most likely reflecting a degradation product since it was not seen in the controls. This band was not seen either in *X.* oocytes or in our previous study of HEK-293 cells expressing the bovine TRPV3 for reasons that are unclear [39].

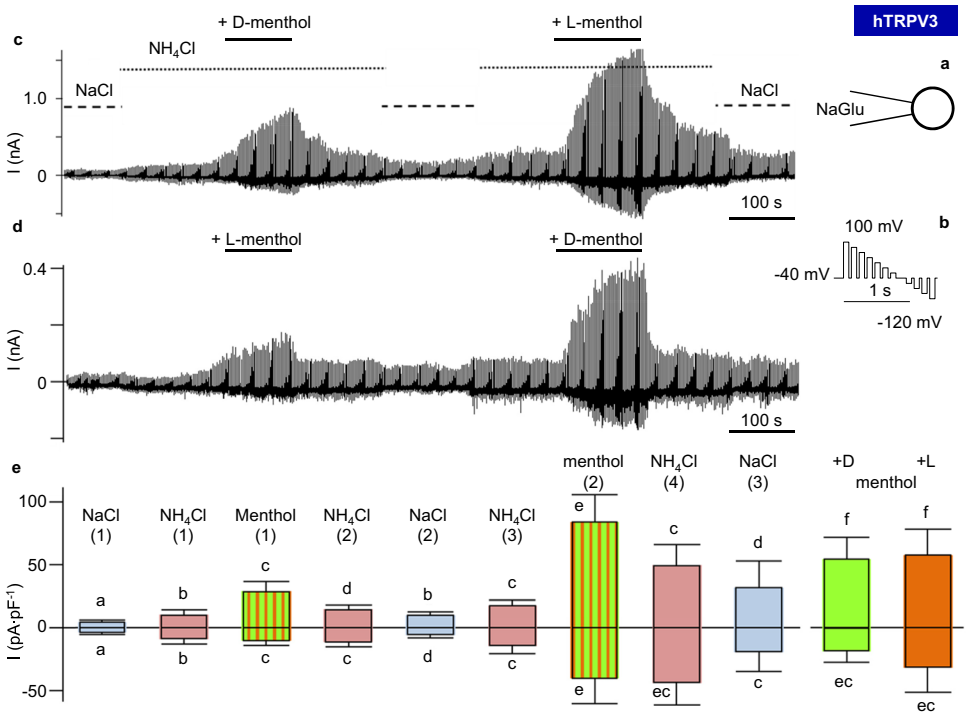

Fig. 13 Whole-cell recordings: comparison of the effects of D- and L-menthol on NH_4^+ currents in HEK-293 cells. In order to compare the effects of two menthol enantiomers on NH_4^+ currents through hTRPV3, measurements were performed with cells filled with NaGlu pipette solution (**a**) using pulse protocol I (**b**) and bath solutions as indicated. The order in which D-menthol (1 mmol·L^{-1}) and L-menthol (1 mmol·L^{-1}) were applied was switched after every successful experiment. **c** Original recording of one of 5 hTRPV3 HEK-293 cells first exposed to D-menthol and then to L-menthol. **d** Original recording of one of 5 hTRPV3 HEK-293 cells first exposed to L-menthol and then to D-menthol. **e** Statistical evaluation (boxplot). The numbers in parentheses reflect repeated application of the same bath solution so that "menthol (1)" designates the response to the first application of menthol as either D- or L-menthol, while "menthol (2)" designates the response to the second application of either enantiomer. The two boxes in green ("+D") and red ("+L") show separate evaluation of data for each of the two enantiomers. Different letters indicate significant differences ($p < 0.05$) within the same group ($n = 10$, ANOVA on Ranks)

A similar pattern emerged after staining overexpressing HEK-293 cells and *X.* oocytes with Anti-TRPV3. In addition to the ~ 95 kDa band, a second strong band was observed in overexpressing *X.* oocytes at ~ 80 kDa. Again, no staining could be observed in the controls, arguing against non-specific effects. Although a weak band could be seen at ~ 95 kDa, the most prominent band of the G573S HEK-293 cells had a molecular weight of ~ 50 kDa followed by several lower weight bands. Possibly, these bands reflect breakdown products within apoptotic cells. Cleavage of the N-terminally placed Strep-tag would explain why these bands could not be seen in the immunoblots stained with Anti-Strep. At the exposure times used for the expressing systems, only the ~ 60 kDa band was visible in proteins from human keratinocytes, although at high exposure times, the full-length protein (~ 95 kDa) could be detected in addition to some smaller bands (Fig. 1). In our previous study of the rumen [39] and in an unrelated study of cultured keratinocytes [74], the ~ 60 kDa band was also stronger than the ~ 95 kDa band, although the difference in staining intensity was not as pronounced. Furthermore, we observed that the ~ 60 kDa band was always more pronounced than the ~ 95 kDa band in various parts of the porcine intestine, the porcine skin and in murine skin [46]. While this band may reflect a breakdown product, sequences for a ~ 60 kDa splice variant of TRPV3 are available for the bovine species (AAI46079.1) and for mice (XP_006533411.1) and suggest that the protein is truncated after amino acid 527 (mouse) or 526 (bovine) (for alignment, see the supplement of [46]). This is in the middle of the third transmembrane domain (S3) so that the pore region (S5 and S6, > aa580) is missing [81]. It thus appears unlikely that the short variant functions as an ion channel, but it may have regulatory properties that clearly need to be explored.

In immunofluorescence staining, hTRPV3 was clearly targeted to the cell membrane in hTRPV3 overexpressing cells (Figs. 2 and 3), which, in the case of HEK-293 cells, coincided with the expression of cytosolic GFP. Control HEK-293 cells and control *X.* oocytes showed no staining so that the antibody appears specific for hTRPV3. The functional expression of hTRPV3 in HEK-293 cells was cross-checked using whole-cell experiments demonstrating

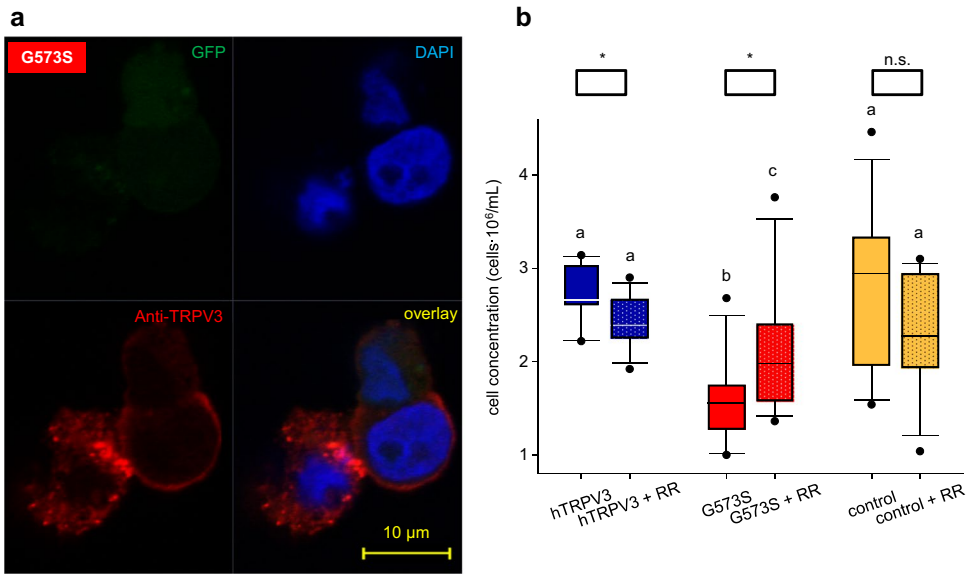

Fig. 14 Expression of the Olmsted mutant G573S in HEK-293 cells. **a** HEK-293 cells expressing the hTRPV3 mutant G573S were immunostained 22 h after transfection (for details, see supplement part G ($n = 26$)). As in Fig. 3, DAPI (blue) was used to stain the cell nuclei. All three cells showed staining with the anti-TRPV3 antibody (red), with one cell showing clear trafficking of the protein to the cell membrane. Conversely, the HEK-293 cell that can be seen on the left showed strong cytosolic staining. Using transmitted-light microscopy, signs of a general structural degradation with partial loss of the cell membrane were observed in this cell. The GFP (green), which should be co-expressed as in Fig. 3, was too low for detection in all three cells. **b** Boxplots show the cell viability of hTRPV3, G573S, and control HEK-293 cells. Half of the passages were incubated with the TRP antagonist RR ($n/N = 12/3$). A significantly lower number of cells transfected with G573S (red) was found to be intact in comparison to cells transfected with hTRPV3 (blue) and controls (orange). Supplementing RR, cell viability was lower in the hTRPV3 and control groups and significantly higher in G573S. Different letters indicate significant differences determined using ANOVA on Ranks with Student–Newman–Keuls method. For the effect of RR, differences were determined using Mann–Whitney Rank Sum Test (*: $p < 0.05$; n.s.: not significant)

currents sensitive to menthol, thymol, and 2-APB in overexpressing cells, but not in controls (Fig. 10 and Table 2) [44]. The permeability of hTRPV3 to NH_4^+ was unambiguously shown using both expression systems and three different experimental approaches.

Experiments on X. oocytes

A first series of experiments was performed using *X.* oocytes as a well-established expression system [13, 26]. Experiments were performed both with pH-sensitive microelectrodes and with the single-channel configuration of the patch-clamp technique. Experiments on the bovine homologue of TRPV3 (bTRPV3) were conducted in parallel and published previously [39]. Comparative results are shown in the supplement (parts H and I).

In both overexpressing oocytes and controls, experiments with pH-sensitive microelectrodes showed a depolarization and a clear acidification of the cytosol after incubation with NH_4^+ (Fig. 5 and Table 1) with a slow recovery of pH_i after washout (Fig. S1). Despite their frequent use as a system for studying ammonia transport, it thus appears that native *X.* oocytes amply express endogenous pathways for the uptake of NH_4^+. This finding confirms previous reports [11, 35, 49] and may have contributed to the controversy surrounding the preferred substrates of members of the AMT/Rh transporter family [51].

The response of native *X.* oocytes to NH_4^+ containing solutions was first studied in depth by Burkhardt and Frömter [11]. These authors demonstrated that NH_4^+ produced a depolarization and acidification that could not be blocked by either K^+ channel blockers such as Cs^+ or TEA (triethylamine) or by blockers of NKCC such as bumetanide [11]. Furthermore, the removal of NH_4Cl did not lead to the anticipated rapid acidification of the cytosol due to efflux of NH_3, but to a pH recovery towards a more alkaline pH. The authors concluded that the *X.* oocyte membrane was almost completely impermeable to NH_3 and that, instead, NH_4^+ was being taken up via non-selective cation channels. These observations were basically confirmed in a later publication by Keicher and Meech [35], although in that study, evidence emerged that transporter expression varied with the stage of oocyte maturation.

In what is arguably the most in depth study of the issue by Musa-Aziz et al. from the Boron laboratory [49], *X.* oocytes were impaled by one electrode for the membrane potential (U_{mem}) and by another for pH_i, while a third blunt pH electrode was pushed against the oocyte from the outside so that

surface pH (pH_s) could additionally be monitored. Although a depolarization was again observed, it was much slower than in the current study or previous ones [11, 35, 39] for reasons that are not clear. Again as described previously, an intracellular acidification was observed. Paradoxically, pH_S also dropped. The authors concluded in their excellent discussion that NH_3 was clearly entering the oocyte. However, they had no definite explanation for the NH_4^+ induced changes in pH_i and U_{mem}. They also pointed out that pH_s data predicted a flux ratio of $J_{NH3}/J_{NH4}^+ > 2/100$, while pH_i data supported $J_{NH3}/J_{NH4}^+ < 0.5/100$. These contradicting fluxes are clearly impossible unless the *X.* oocyte is surrounded by two separate membranes. Indeed, *X.* oocytes are surrounded not only by a lipid membrane (or oolemma), but also by a stabilizing network of protein fibres (the vitelline membrane) that is permeable to water and solutes. A removal of the vitelline membrane was not reported [49] and does not appear likely, since this would have made the oocyte preparation too unstable for manipulation with three electrodes (own observations). We suggest that diffusion of the small NH_3 molecule through the vitelline membrane should be more rapid than that of the heavily hydrated NH_4^+ ion, explaining the changes in pH_s [49]. In a subsequent step, NH_4^+ could then leave the perivitelline space and pass into the cytosol via a channel of the oolemma, explaining the changes in pH_i and U_{mem} measured by the cytosolic electrodes.

Another important insight to emerge from the study of Musa-Aziz et al. [49] is that incubation of *X.* oocytes in as little as 0.5 mmol·L^{-1} NH_4Cl solution for 30 min leads to an accumulation of cytosolic [NH_3/NH_4^+] to a level of over 3.3 mmol·L^{-1}. The U_{mem} was at ~ − 40 mV, and the pH_i was at 7.17 so that the cytosolic concentration of NH_4^+ clearly exceeded the equilibrium concentration of ~ 2.4 mmol·L^{-1} for NH_4^+ alone (with the contribution of NH_3 to total ammonia negligible). Conversely, no evidence for glutamine synthesis could be found by Musa-Aziz et al. after a 10-min incubation [49] so that this aspect does not contribute to the observations within the timeframe of these experiments.

In conjunction, a relatively consistent model emerges. While the vitelline membrane appears to be more permeable to NH_3 than to NH_4^+, the inverse is true for the lipid bilayer surrounding the *X.* oocyte, which is, in fact, almost impermeable to NH_3. The presence of NH_4^+ permeable channels in the oolemma is clearly supported the changes in pH_i and U_{mem} and by our single-channel data. Within the cytosol, a fraction of the NH_4^+ dissociates into a proton and NH_3, with the latter sequestered in intracellular vesicles [49]. Acidification will slow down as the system approaches the equilibrium distribution for NH_4^+. After washout, repolarization is almost immediate, but the alkalinization will be much slower than the initial acidification for a number of reasons. Firstly, the release of NH_3 trapped in the intracellular stores may require time [49]. Secondly, while uptake of NH_4^+ is supported by the electrical gradient, efflux of NH_4^+ from the repolarized oocyte has to occur against the electrical gradient. Thirdly, many non-selective cation channels (such as TRPV3) are outwardly rectifying so that the permeability of the channel is lower at negative than at positive potentials. For this reason, the rate of efflux of NH_4^+ from the repolarized oocyte in NaCl solution will be slower than the rate of influx measured after depolarization by application of NH_4Cl. Functionally, the native *X.* oocyte is thus able to scavenge ammonia–nitrogen, which might be useful for protein synthesis.

In the current study, initial values of pH_i (7.56) and U_{mem} (~ − 30 mV) of hTRPV3 *X.* oocytes were similar to those of the control oocytes (Table 1 and Fig. 5). Previous studies of native *X.* oocytes have reported a pH_i of ~ 7.5 [12] and U_{mem} within the range of − 40 to − 60 mV [11, 35, 49]. The higher U_{mem} in the current study possibly reflects the fact that after injection, the *X.* oocytes were incubated in NMDGCl solution. This approach was adopted to avoid excessive influx of Na^+ in the hTRPV3 oocytes, but it may have compromised uptake of K^+ by the Na^+/K^+-ATPase in both groups. The initial rate of acidification after application of NH_4^+ was significantly higher in hTRPV3 oocytes than in controls (Table 1). A slight recovery could be observed after 20 min, most likely reflecting a situation at the equilibrium point at which net influx of NH_4^+ had ceased so that pH regulatory mechanisms became effective [65]. Since control oocytes did not acidify as quickly, the pH_i was significantly higher after 20 min than in oocytes overexpressing hTRPV3. It appears that at this point, residual NH_4^+ influx and the pH regulatory mechanisms were roughly in balance so that no acidification and no recovery of pH_i was observed.

Apart from these differences, a very striking difference versus controls was the inverse response to replacement of Ca^{2+} by EDTA (Fig. 5 and Table 1). This manoeuvre opens many non-selective cation channels, including TRPV3. For hTRPV3 *X.* oocytes, removal of Ca^{2+} induced no change in pH_i, which is to be expected if NH_4^+ is at equilibrium [65]. Conversely, control oocytes, which had obviously not yet reached the Nernst equilibrium for NH_4^+, began to acidify again. In line with this hypothesis, all hTRPV3 *X.* oocytes depolarized significantly, reflecting the opening of TRPV3 channels. Unexpectedly, all control *X.* oocytes hyperpolarized. This most likely reflects the expression of rather unique endogenous Cl^- channels that open when Ca^{2+} is removed [61, 82]. We suggest that in the hTRPV3 expressing oocytes, this effect was obscured by the larger effect due to the opening of hTRPV3.

For inside-out experiments, the vitelline membrane was removed to expose the lipid membrane of the *X.* oocyte, which subsequently had to be handled very carefully. The

experiments clearly demonstrate the presence of non-selective cation channels with a permeability to NH_4^+ in both native *X.* oocytes and in the oocytes overexpressing hTRPV3. However, channels with $G(NH_4^+) > 100$ pS were only found in the hTRPV3 *X.* oocytes (Figs. 7, 8, and 9). Conductance levels were very variable, most likely explained by formation of heteromers with endogenous channels expressed by the *X.* oocyte. Intra-family heteromerization of TRPV3 with other TRP channels has long been known [71].

Single-channel conductances were comparable, while acidification of hTRPV3 was stronger than in bovine TRPV3. This probably reflects a higher level of expression in the hTRPV3 *X.* oocytes rather than a more fundamental functional difference (supplement, Fig. S4).

In whole-cell experiments, both hTRPV3 HEK-293 cells and controls expressed channels permeable to NH_4^+ with a significant increase in influx at − 120 mV pipette potential and a higher reversal potential (Table 3). Outward current at + 100 mV also increased. This may reflect efflux of Na^+, influx of Cl^-, or a combination of both, induced by changes in pH_i or swelling. Furthermore, an increase in current is frequently seen when the concentration of a permeant ion rises [33]. Significant differences in NH_4^+ influx emerged after hTRPV3 cells and controls were stimulated by application of D-menthol ((+)-menthol) (Figs. 11 and 12 and Table 3). Cells overexpressing hTRPV3 not only showed different current amplitudes but also different current kinetics (Fig. 12 and Table 3). The most likely explanation is that depolarization repels positively charged Ca^{2+} and Mg^{2+} ions from the mouth of the hTRPV3 channel pore (voltage-dependent block by divalent cations [39, 55, 58]) leading to the time-dependent increase in current observed at positive potentials. At negative potentials, the inverse happens and influx of NH_4^+ decreases as divalent cations are drawn into the channel. In line with this explanation, strong tail currents followed the depolarizing pulses, reflecting an influx of NH_4^+ that decreased as more and more divalent cations returned to the channel mouth. Furthermore, we showed that D-menthol and L-menthol had similar effects on hTRPV3 so that the activation mechanism appears to be independent of the chirality (Fig. 13). As observed previously, pre-activation of the channel by either form increased the subsequent response to the agonist [44], despite washout between the applications.

One goal of the study was to investigate the G573S mutant, which causes Olmsted syndrome (OS) with hyperkeratinization in humans. This dominant mutation is localized in the linker region between the S4 and S5 segment of the TRPV3 subunit, interfering with normal channel gating so that in the mutant, the channel is locked in an open conformation [22, 40, 81]. In one previous study, expression of OS-mutants in HaCaT cells caused impaired vesicular trafficking that resulted in reduced surface localization of these hTRPV3 mutants and other membrane proteins [85], suggesting that Olmsted syndrome might be primarily a lysosomal disorder. Conversely, other studies using HEK-293 cells have reported successful membrane expression of G573S [40] and a number of other OS associated mutants [87] in the cell membrane. We confirm that at least when expressed in HEK-293, the G573S mutation can be trafficked to the membrane in individual cells (Fig. 14a). However, it was also clearly apparent that the number of cells that showed staining was extremely low and of these few cells, many showed marked staining within the cytosol and severely impaired structural morphology. Interestingly, none of the cells showed visible staining for GFP, which is in marked contrast to the observations using the wild-type hTRPV3 or bTRPV3 construct. The most likely explanation for these observations is that the expression of the mutant G573S induced cell death immediately after insertion of the channel protein in the membrane and before sufficient expression of GFP could occur.

The problem of significantly increased death rate in cells expressing gain of function hTRPV3 mutants was described earlier by Lin et al. [40] and most likely reflects apoptosis or necrosis due to Ca^{2+} influx [64]. This may explain why despite extensive attempts (supplement part G), we were unable to obtain a sufficient number of cells that successfully co-expressed GFP to identify G573S cells for patch-clamping. Possibly, this problem might have been prevented using a vector with fusion of G573S to GFP, as in the study by Lin et al. [40]. On the other hand, we purposely avoided this approach since the fusion of the channel to a large marker protein may be one reason why the mutant channel was not correctly trafficked to the membrane in the study of Yadav et al. [85]. Furthermore, we were concerned that fusion of GFP to the mutant channel might alter its properties. In this context, it is possible to speculate that a decrease in conductance due to the fusion protein enhanced cell viability in the study of Lin et al. [40]. As reported by this group, we confirm that expression of G573S severely impairs cell survival and that cells can be partially rescued by ruthenium red (RR) (Fig. 14b) [40]. RR is a large cation that is thought to block the extracellular mouth of the mutant channel, thus preventing influx of cations. These experiments support the hypothesis that expression in the extracellular membrane is crucial to the ability of G573S to cause cell death under in vitro conditions.

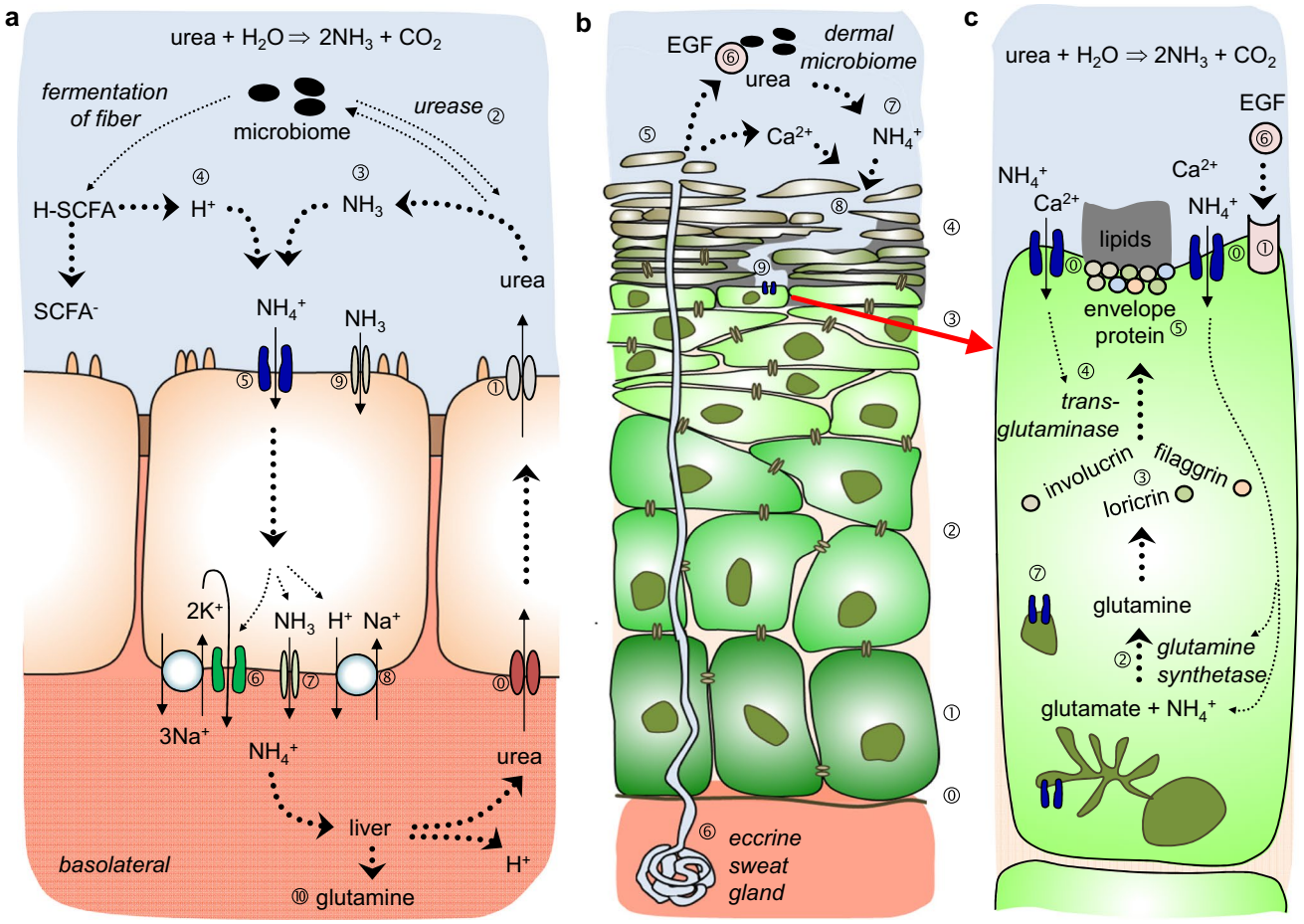

Fig. 15 Model: TRPV3—an epithelial ammoniumtransporter? **a** Simplified model of nitrogen recycling across the colonic epithelium. While mammalian enzymes cannot break down urea to salvage the nitrogen, large quantities enter the colonic lumen via transporters such as UT-B, UT-A6, or aquaglyceroporins (⓪ and ①). Within the colonic lumen, the resident microbiome produces ureases that break up urea, forming ammonia (NH_3, ③). Bacterial enzymes also degrade complex carbohydrates, forming short-chain fatty acids (H-SCFA) that release protons (④). Removal of these protons is important for colonic homeostasis. One possibility is absorption of NH_4^+ via electrogenic pathways that include TRPV3 (⑤). Basolateral efflux may involve K^+ channels (⑥) or Rhesus-like glycoproteins such as RhBG (⑦) coupled to basolateral pH regulatory mechanisms such as NHE (⑧) or Na^+-HCO_3^--cotransporters. Conversely, efflux from the lumen in the form of NH_3 (e.g. via apical RhCG (⑨)) will not remove protons from the lumen. Within the liver, ammonia can be used for the formation of urea for colonic buffering. In particular, in situations where dietary intake of protein is low, synthesis of glutamine and other non-essential amino acids may enhance survival (⑩). **b** Simplified model of human skin. The basement membrane (⓪) is followed by the cells of the stratum basale (①). Differentiation of these cells consecutively yields the stratum spinosum (②), stratum granulosum (③), and the stratum corneum (④). The cytosolic compartment of the fully differentiated corneocytes is filled with water and electrolytes, but lacks cell nuclei and organelles, while the lipid membrane is replaced by a protein envelope that binds intercellular lipids, forming a tight barrier separating the inside of the body from the outside. In shedding (⑤), the corneodesmosomes that adjoin the corneocytes are lysed so that desquamation can occur. Hyperkeratosis occurs when formation of corneocytes exceeds desquamation. Primarily in humans, thermoregulation involves formation of eccrine sweat that contains Na^+, Cl^-, Ca^{2+}, urea, and epidermal growth factor (EGF; ⑥). Urea is degraded to NH_4^+ (⑦) by urealytic bacteria that colonize the skin. Small defects in the stratum corneum (⑧) provide access to the apical membrane of the stratum granulosum (⑨). **c** Detail from (**b**) showing an apical cell from the stratum granulosum. The apical membrane of the top layer of the stratum granulosum expresses TRPV3 channels (⓪), which form a signalling complex with the epidermal growth factor receptor (①). EGF, Ca^{2+}, and NH_4^+ from eccrine sweat enter through defects in the *stratum corneum*. Entry of NH_4^+ facilitates cytosolic formation of glutamine from glutamate and NH_4^+ (②). Glutamine is required for the synthesis of involucrin, loricrin, and filaggrin (③). Entry of Ca^{2+} via TRPV3 activates the transglutaminases (④) that are required for the cross-linking of these proteins, forming the corneocyte envelope (⑤). EGF (⑥) regulates the open probability of TRPV3, fine-tuning the process. Especially in the middle of the stratum spinosum and stratum granulosum, TRPV3 is also expressed by cytosolic structures (⑦), which may reflect recruitment of channels in vesicles for trafficking to the apical membrane or other functions

Staining of a skin equivalent consisting of human fibroblasts and keratinocytes clearly showed that expression of hTRPV3 primarily occurs in keratinocytes with expression in the apical membrane of the top layer of cells (Fig. 4). Skin equivalents from cultured human keratinocytes are increasingly used as human-based test systems for basic and preclinical research [42]. Such skin equivalents do not express cells of neuronal origin, and it is possible to obtain very thin preparations, ensuring good optical properties for confocal laser microscopy. Since the construct was kept covered with cell culture medium throughout, the stratum corneum was not formed, which might be useful for future transport studies. Cells in the middle of the keratinocyte layer showed strong staining of the cytosol, most likely reflecting expression of hTRPV3 by the endoplasmic reticulum, as previously reported not just for hTRPV3 [85], but also for many other TRP channels [32]. Cells in the top layer showed a strikingly hTRPV3-free cytosol with staining for hTRPV3 almost exclusively visible in the apical membrane, suggesting a function in the apical uptake of ions. On the whole, the expression pattern of hTRPV3 in the skin equivalent remarkably resembled that found in native human skin [56] or the rumen [39]. In the colonic epithelium, which consists of only one layer of cells, staining for hTRPV3 is also localized primarily within the apical membrane [46, 75], with very little cytosolic staining. Notably, both the colonic and the ruminal epithelium functionally express a divalent-sensitive conductance to NH_4^+ that can be stimulated by agonists of TRPV3 [46, 66].

So what role might a very promiscuous channel with remarkably low selectivity to Ca^{2+} play in the apical membrane of an epithelium? Certainly, uptake of Ca^{2+} is important—in the skin, to activate the transglutaminases; in the case of the rumen, to supply the animal with Ca^{2+}; and in the colon or the caecum, for reasons that may include inflammatory signalling. However, it is interesting to note that all three epithelia also secrete large quantities of urea, a product that is degraded by the microbiota living on the surface, yielding ammonia [2, 5, 72, 83] (Fig. 15).

In the case of the skin, more work clearly needs to be done. However, some speculation is possible (Fig. 15 b and c). After secretion of urea with sweat and degradation by the dermal microbiome [68, 77], NH_4^+ is released. Small lesions in the stratum corneum may facilitate access to the apical membrane of the underlying stratum granulosum, signalling a need for local replacement of corneocytes. What follows has already been outlined: Influx of NH_4^+ through TRPV3 stimulates the formation of glutamine from glutamate, allowing synthesis of proteins important for cornification such as filaggrin, involucrin, and loricrin [19]. Influx of Ca^{2+} via TRPV3 activates transglutaminases, which catalyse the cross-linking of involucrin and loricrin, forming the corneocyte envelope [17, 23]. Activation of the TRPV3 signalling complex by EGF—which intriguingly is also contained in eccrine sweat [67]—completes the picture. The importance of a cytosolic production of glutamine from NH_4^+ is highlighted by the pathophysiology of newborns with an inherited systemic deficiency of glutamine synthetase, which leads to numerous lethal defects that include necrolytic erythema of the skin [29]. Whether or not excessive influx of NH_4^+ via TRPV3 plays any role in OS remains to be determined, but it is interesting to note that the full-fledged clinical picture is found only in humans and there, mostly in the palms and the soles of the feet [22]. Humans produce more eccrine sweat than other mammals, with secretion highest in the palmo-plantar skin.

In the case of the colon, the function of TRPV3 is clearer (Fig. 15a). Within the colonic lumen, microbes utilize the nitrogen contained in amino acids and urea for protein synthesis, but also set free large quantities of ammonia that are absorbed into the portal blood [41, 72, 80]. In evolutionary terms, the absorption of nitrogen in the form of ammonia from the gut must be considered advantageous, since it can be re-utilized for the synthesis of urea and non-essential amino acids such as glutamine in situations where protein intake is low [72]. In part, this may certainly occur in the form of NH_3 (e.g. via the ammonia transporter RhCG [30, 51]). However, uptake in the form of NH_4^+ via divalent sensitive cation channels such as TRPV3 has also been observed [46]. Uptake in the protonated form should help with the pH homeostasis of the colonic lumen, which is challenged by acids set free in the fermentation process [6]. On the downside, well-known problems arise when ammonia cannot be detoxified by the liver in hepatic disease [2, 5, 72]. In this context and others, identifying the proteins that mediate transport of ammonia represents a first step in finding new options for intervention.

Supplementary Information The online version contains supplementary material available at https://doi.org/10.1007/s00424-021-02616-0.

Acknowledgements We wish to express our profound gratitude to Gisela Manz and Susanne Trappe, who participated in all technical aspects of the study and gave us expert advice in many cases. Without them, this project would not have been completed. We would further like to thank Katharina Söllig and Patrick Graff for their expertise and technical help. Prof. Dr. Dorothee Günzel and Dr. Jörg Piontek, Institute of Clinical Physiology, University Medicine, Charité, Berlin, are thanked for the support in confocal laser microscopy in the first phase of the study. Our gratitude also extends to Prof. Salah Amasheh, Dr. Constanze Vitzthum, and N. Brunner who provided us with *Xenopus laevis* oocytes and shared expertise in handling them. We also wish to thank Prof. Dr. Aschenbach for his continuous support.

Author contribution Conceived and designed study: F. Stumpff and H. Liebe. Performed research: H. Liebe, F. Liebe, G. Sponder, F. Stumpff. Analysed data: H. Liebe, F. Liebe, G. Sponder, F. Stumpff. Software: F. Stumpff. Contributed human skin equivalent: S. Hedtrich. Wrote the paper: H. Liebe, F. Stumpff. Corrected draft: F. Liebe, G. Sponder.

Funding We would like to express our gratitude for funding by the Sonnenfeld Stiftung and the Deutsche Forschungsgemeinschaft (DFG STU 258/7–1).

Data availability All data generated and/or analysed during the current study are available from the corresponding author on reasonable request.

Code availability Available on reasonable request from F.S.

Declarations

Ethics approval The treatment of *Xenopus laevis* frogs was in accordance with the guidelines of German legislation, with approval by the animal welfare officer for the Freie Universität Berlin and the Veterinary Health Inspectorate (Landesamt für Gesundheit und Soziales Berlin, permit G0025/16). Human keratinocytes were obtained from juvenile foreskin following circumcision at age 2 to 11 years (approved by ethics committee of the Charité – Universitätsmedizin Berlin, EA1/081/13).

Consent to participate Consent to participate does not apply, except as outlined immediately above (EA1/081/13).

Consent for publication Consent for publication does not apply, except as outlined immediately above (EA1/081/13).

Conflict of interest The authors declare no competing interests.

References

1. Abdoun K, Stumpff F, Wolf K, Martens H (2005) Modulation of electroneutral Na transport in sheep rumen epithelium by luminal ammonia. Am J Physiol Gastrointest Liver Physiol 289:G508-520. https://doi.org/10.1152/ajpgi.00436.2004
2. Adeva MM, Souto G, Blanco N, Donapetry C (2012) Ammonium metabolism in humans. Metabolism 61:1495–1511. https://doi.org/10.1016/j.metabol.2012.07.007
3. Barry PH, Lynch JW (1991) Liquid junction potentials and small cell effects in patch-clamp analysis. J Membr Biol 121:101–117. https://doi.org/10.1007/BF01870526
4. Baylie RL, Cheng H, Langton PD, James AF (2010) Inhibition of the cardiac L-type calcium channel current by the TRPM8 agonist, (-)-menthol. J Physiol Pharmacol 61:543–550
5. Bergen WG, Wu G (2009) Intestinal nitrogen recycling and utilization in health and disease. J Nutr 139:821-825. doi:jn.109.104497 [pii]; https://doi.org/10.3945/jn.109.104497
6. Bergman EN (1990) Energy contributions of volatile fatty acids from the gastrointestinal tract in various species. Physiol Rev 70:567–590. https://doi.org/10.1152/physrev.1990.70.2.567
7. Berjukow S, Doring F, Froschmayr M, Grabner M, Glossmann H, Hering S (1996) Endogenous calcium channels in human embryonic kidney (HEK293) cells. Br J Pharmacol 118:748–754. https://doi.org/10.1111/j.1476-5381.1996.tb15463.x
8. Bödeker D, Kemkowski J (1996) Participation of NH4+ in total ammonia absorption across the rumen epithelium of sheep (Ovis aries). Comp Biochem Physiol A Physiol 114:305–310. https://doi.org/10.1016/0300-9629(96)00012-6
9. Boron WF (2010) Sharpey-Schafer lecture: gas channels. Exp Physiol 95:1107–1130. https://doi.org/10.1113/expphysiol.2010.055244
10. Brunner N, Stein L, Cornelius V, Knittel R, Fallier-Becker P, Amasheh S (2020) Blood-brain barrier protein claudin-5 expressed in paired Xenopus laevis oocytes mediates cell-cell interaction. Frontiers in Physiology 11. https://doi.org/10.3389/fphys.2020.00857
11. Burckhardt BC, Fromter E (1992) Pathways of NH3/NH4+ permeation across Xenopus laevis oocyte cell membrane. Pflugers Arch 420:83–86. https://doi.org/10.1007/BF00378645
12. Burckhardt BC, Kroll B, Fromter E (1992) Proton transport mechanism in the cell membrane of Xenopus laevis oocytes. Pflugers Arch 420:78–82. https://doi.org/10.1007/BF00378644
13. Caner T, Abdulnour-Nakhoul S, Brown K, Islam MT, Hamm LL, Nakhoul NL (2015) Mechanisms of ammonia and ammonium transport by rhesus-associated glycoproteins. Am J Physiol Cell Physiol 309:C747-758. https://doi.org/10.1152/ajpcell.00085.2015
14. Cao X, Yang F, Zheng J, Wang K (2012) Intracellular proton-mediated activation of TRPV3 channels accounts for the exfoliation effect of alpha-hydroxyl acids on keratinocytes. J Biol Chem 287:25905–25916. https://doi.org/10.1074/jbc.M112.364869
15. Celleno L (2018) Topical urea in skincare: A review. Dermatol Ther 31:e12690. https://doi.org/10.1111/dth.12690
16. Chalfie M, Tu Y, Euskirchen G, Ward W, Prasher D (1994) Green fluorescent protein as a marker for gene expression. 263:802-805. https://doi.org/10.1126/science.8303295 %J Science
17. Cheng X, Jin J, Hu L, Shen D, Dong XP, Samie MA, Knoff J, Eisinger B, Liu ML, Huang SM, Caterina MJ, Dempsey P, Michael LE, Dlugosz AA, Andrews NC, Clapham DE, Xu H (2010) TRP channel regulates EGFR signaling in hair morphogenesis and skin barrier formation. Cell 141:331–343. https://doi.org/10.1016/j.cell.2010.03.013
18. Chepilko S, Zhou H, Sackin H, Palmer LG (1995) Permeation and gating properties of a cloned renal K+ channel. Am J Physiol 268:C389-401. https://doi.org/10.1152/ajpcell.1995.268.2.C389
19. Danielyan L, Zellmer S, Sickinger S, Tolstonog GV, Salvetter J, Lourhmati A, Reissig DD, Gleiter CH, Gebhardt R, Buniatian GH (2009) Keratinocytes as depository of ammonium-inducible glutamine synthetase: age- and anatomy-dependent distribution in human and rat skin. PLoS ONE 4:e4416. https://doi.org/10.1371/journal.pone.0004416
20. DIN e.V. (Hrsg.) (DIN 1333–1992–02): Zahlenangaben, Kapitel 4 (Runden), Beuth-Verlag, Berlin, 2019. doi:https://dx.doi.org/https://doi.org/10.31030/2426986
21. Doerner JF, Hatt H, Ramsey IS (2011) Voltage- and temperature-dependent activation of TRPV3 channels is potentiated by receptor-mediated PI(4,5)P2 hydrolysis. J Gen Physiol 137:271–288. https://doi.org/10.1085/jgp.200910388
22. Duchatelet S, Hovnanian A (2015) Olmsted syndrome: clinical, molecular and therapeutic aspects. Orphanet J Rare Dis 10:33. https://doi.org/10.1186/s13023-015-0246-5

23. Eckhart L, Lippens S, Tschachler E, Declercq W (2013) Cell death by cornification. Biochim Biophys Acta 1833:3471–3480. https://doi.org/10.1016/j.bbamcr.2013.06.010
24. Elsholz F, Harteneck C, Muller W, Friedland K (2014) Calcium–a central regulator of keratinocyte differentiation in health and disease. Eur J Dermatol 24:650–661. https://doi.org/10.1684/ejd.2014.2452
25. Georgi MI, Rosendahl J, Ernst F, Gunzel D, Aschenbach JR, Martens H, Stumpff F (2014) Epithelia of the ovine and bovine forestomach express basolateral maxi-anion channels permeable to the anions of short-chain fatty acids. Pflugers Arch 466:1689–1712. https://doi.org/10.1007/s00424-013-1386-x
26. Geyer RR, Parker MD, Toye AM, Boron WF, Musa-Aziz R (2013) Relative CO(2)/NH(3) permeabilities of human RhAG, RhBG and RhCG. J Membr Biol 246:915–926. https://doi.org/10.1007/s00232-013-9593-0
27. Greco C, Leclerc-Mercier S, Chaumon S, Doz F, Hadj-Rabia S, Molina T, Boucheix C, Bodemer C (2020) Use of epidermal growth factor receptor inhibitor erlotinib to treat palmoplantar keratoderma in patients with Olmsted syndrome caused by TRPV3 mutations. JAMA Dermatol 156:191–195. https://doi.org/10.1001/jamadermatol.2019.4126
28. Grether-Beck S, Felsner I, Brenden H, Kohne Z, Majora M, Marini A, Jaenicke T, Rodriguez-Martin M, Trullas C, Hupe M, Elias PM, Krutmann J (2012) Urea uptake enhances barrier function and antimicrobial defense in humans by regulating epidermal gene expression. J Invest Dermatol 132:1561–1572. https://doi.org/10.1038/jid.2012.42
29. Haberle J, Gorg B, Toutain A, Rutsch F, Benoist JF, Gelot A, Suc AL, Koch HG, Schliess F, Haussinger D (2006) Inborn error of amino acid synthesis: human glutamine synthetase deficiency. J Inherit Metab Dis 29:352–358. https://doi.org/10.1007/s10545-006-0256-5
30. Handlogten ME, Hong SP, Zhang L, Vander AW, Steinbaum ML, Campbell-Thompson M, Weiner ID (2005) Expression of the ammonia transporter proteins Rh B glycoprotein and Rh C glycoprotein in the intestinal tract. Am J Physiol Gastrointest Liver Physiol 288:G1036-1047. https://doi.org/10.1152/ajpgi.00418.2004
31. Harmeyer J, Martens H (1980) Aspects of urea metabolism in ruminants with reference to the goat. J Dairy Sci 63:1707–1728. https://doi.org/10.3168/jds.S0022-0302(80)83132-8
32. Haustrate A, Prevarskaya N, Lehen'kyi V (2020) Role of the TRPV channels in the endoplasmic reticulum calcium homeostasis. Cells 9. https://doi.org/10.3390/cells9020317
33. Hille B, Schwarz W (1978) Potassium channels as multi-ion single-file pores. J Gen Physiol 72:409–442. https://doi.org/10.1085/jgp.72.4.409
34. Huang SM, Li X, Yu Y, Wang J, Caterina MJ (2011) TRPV3 and TRPV4 ion channels are not major contributors to mouse heat sensation. Mol Pain 7:37. https://doi.org/10.1186/1744-8069-7-37
35. Keicher E, Meech R (1994) Endogenous Na(+)-K+ (or NH4+)-2Cl- cotransport in Rana oocytes; anomalous effect of external NH4+ on pHi. J Physiol 475:45–57. https://doi.org/10.1113/jphysiol.1994.sp020048
36. Knepper MA, Packer R, Good DW (1989) Ammonium transport in the kidney. Physiol Rev 69:179–249. https://doi.org/10.1152/physrev.1989.69.1.179
37. Lee SE, Lee SH (2018) Skin Barrier and Calcium Ann Dermatol 30:265–275. https://doi.org/10.5021/ad.2018.30.3.265
38. Li M, Weschler CJ, Beko G, Wargocki P, Lucic G, Williams J (2020) Human ammonia emission rates under various indoor environmental conditions. Environ Sci Technol 54:5419–5428. https://doi.org/10.1021/acs.est.0c00094
39. Liebe F, Liebe H, Kaessmeyer S, Sponder G, Stumpff F (2020) The TRPV3 channel of the bovine rumen: localization and functional characterization of a protein relevant for ruminal ammonia transport. Pflügers Arch Eur J Physiol 472:693–710. https://doi.org/10.1007/s00424-020-02393-2
40. Lin Z, Chen Q, Lee M, Cao X, Zhang J, Ma D, Chen L, Hu X, Wang H, Wang X, Zhang P, Liu X, Guan L, Tang Y, Yang H, Tu P, Bu D, Zhu X, Wang K, Li R, Yang Y (2012) Exome sequencing reveals mutations in TRPV3 as a cause of Olmsted syndrome. Am J Hum Genet 90:558–564. https://doi.org/10.1016/j.ajhg.2012.02.006
41. Liu J, Lkhagva E, Chung HJ, Kim HJ, Hong ST (2018) The pharmabiotic approach to treat hyperammonemia. Nutrients 10. https://doi.org/10.3390/nu10020140
42. Löwa A, Vogt A, Kaessmeyer S, Hedtrich S (2018) Generation of full-thickness skin equivalents using hair follicle-derived primary human keratinocytes and fibroblasts. J Tissue Eng Regen Med 12:e2134–e2146. https://doi.org/10.1002/term.2646
43. Lutz T, Scharrer E (1991) Effect of short-chain fatty acids on calcium absorption by the rat colon. Exp Physiol 76:615–618. https://doi.org/10.1113/expphysiol.1991.sp003530
44. Macpherson LJ, Hwang SW, Miyamoto T, Dubin AE, Patapoutian A, Story GM (2006) More than cool: promiscuous relationships of menthol and other sensory compounds. Mol Cell Neurosci 32:335–343. https://doi.org/10.1016/j.mcn.2006.05.005
45. Mandadi S, Sokabe T, Shibasaki K, Katanosaka K, Mizuno A, Moqrich A, Patapoutian A, Fukumi-Tominaga T, Mizumura K, Tominaga M (2009) TRPV3 in keratinocytes transmits temperature information to sensory neurons via ATP. Pflugers Arch 458:1093–1102. https://doi.org/10.1007/s00424-009-0703-x
46. Manneck D, Braun HS, Schrapers KT, Stumpff F (2021) TRPV3 and TRPV4 as candidate proteins for intestinal ammonium absorption. Acta Physiol (Oxf):e13694. doi:https://doi.org/10.1111/apha.13694
47. Montell C (2011) The history of TRP channels, a commentary and reflection. Pflugers Arch 461:499–506. https://doi.org/10.1007/s00424-010-0920-3
48. Murphrey MB, Miao JH, Zito PM (2021) Histology, stratum corneum. In: StatPearls. Treasure Island (FL),
49. Musa-Aziz R, Jiang L, Chen LM, Behar KL, Boron WF (2009) Concentration-dependent effects on intracellular and surface pH of exposing Xenopus oocytes to solutions containing NH3/NH4(+). J Membr Biol 228:15–31. https://doi.org/10.1007/s00232-009-9155-7
50. Nagaraja TN, Brookes N (1998) Intracellular acidification induced by passive and active transport of ammonium ions in astrocytes. Am J Physiol 274:C883-891. https://doi.org/10.1152/ajpcell.1998.274.4.C883
51. Neuhauser B, Dynowski M, Ludewig U (2014) Switching substrate specificity of AMT/MEP/ Rh proteins. Channels (Austin) 8:496–502. https://doi.org/10.4161/19336950.2014.967618
52. Nilius B, Biro T (2013) TRPV3: a "more than skinny" channel. Exp Dermatol 22:447–452. https://doi.org/10.1111/exd.12163
53. Nilius B, Biro T, Owsianik G (2014) TRPV3: time to decipher a poorly understood family member! J Physiol 592:295–304. https://doi.org/10.1113/jphysiol.2013.255968
54. Overton CE (1901) Studien über die Narkose zugleich ein Beitrag zur allgemeinen Pharmakologie. Gustav Fischer, Jena
55. Owsianik G, Talavera K, Voets T, Nilius B (2006) Permeation and selectivity of TRP channels. Annu Rev Physiol 68:685–717. https://doi.org/10.1146/annurev.physiol.68.040204.101406
56. Park CW, Kim HJ, Choi YW, Chung BY, Woo SY, Song DK, Kim HO (2017) TRPV3 channel in keratinocytes in scars with post-burn pruritus. Int J Mol Sci 18. https://doi.org/10.3390/ijms18112425
57. Peier AM, Moqrich A, Hergarden AC, Reeve AJ, Andersson DA, Story GM, Earley TJ, Dragoni I, McIntyre P, Bevan S, Patapoutian A (2002) A TRP channel that senses cold stimuli and menthol. Cell 108:705–715. https://doi.org/10.1016/s0092-8674(02)00652-9

58. Peier AM, Reeve AJ, Andersson DA, Moqrich A, Earley TJ, Hergarden AC, Story GM, Colley S, Hogenesch JB, McIntyre P, Bevan S, Patapoutian A (2002) A heat-sensitive TRP channel expressed in keratinocytes. Science 296:2046–2049. https://doi.org/10.1126/science.1073140
59. Rabbani I, Braun HS, Akhtar T, Liebe F, Rosendahl J, Grunau M, Tietjen U, Masood S, Kaessmeyer S, Gunzel D, Rehman H, Stumpff F (2018) A comparative study of ammonia transport across ruminal epithelia from Bos indicus crossbreds versus Bos taurus. Anim Sci J 89:1692–1700. https://doi.org/10.1111/asj.13107
60. Ramsey IS, Delling M, Clapham DE (2006) An introduction to TRP channels. Annu Rev Physiol 68:619–647. https://doi.org/10.1146/annurev.physiol.68.040204.100431
61. Reifarth FW, Amasheh S, Clauss W, Weber W (1997) The Ca2+-inactivated Cl- channel at work: selectivity, blocker kinetics and transport visualization. J Membr Biol 155:95–104. https://doi.org/10.1007/s002329900161
62. Reynolds CK, Kristensen NB (2008) Nitrogen recycling through the gut and the nitrogen economy of ruminants: an asynchronous symbiosis. J Anim Sci 86:E293-305. https://doi.org/10.2527/jas.2007-0475
63. Rizopoulos T, Papadaki-Petrou H, Assimakopoulou M (2018) Expression profiling of the transient receptor potential vanilloid (TRPV) channels 1, 2, 3 and 4 in mucosal epithelium of human ulcerative colitis. Cells 7. https://doi.org/10.3390/cells7060061
64. Rizzuto R, Pinton P, Ferrari D, Chami M, Szabadkai G, Magalhães PJ, Virgilio FD, Pozzan T (2003) Calcium and apoptosis: facts and hypotheses. Oncogene 22:8619–8627. https://doi.org/10.1038/sj.onc.1207105
65. Roos A, Boron WF (1981) Intracellular pH. Physiol Rev 61:296–434. https://doi.org/10.1152/physrev.1981.61.2.296
66. Rosendahl J, Braun HS, Schrapers KT, Martens H, Stumpff F (2016) Evidence for the functional involvement of members of the TRP channel family in the uptake of Na(+) and NH4 (+) by the ruminal epithelium. Pflugers Arch 468:1333–1352. https://doi.org/10.1007/s00424-016-1835-4
67. Saga K, Jimbow K (2001) Immunohistochemical localization of activated EGF receptor in human eccrine and apocrine sweat glands. J Histochem Cytochem 49:597–602. https://doi.org/10.1177/002215540104900506
68. Scharschmidt TC, Fischbach MA (2013) What lives on our skin: ecology, genomics and therapeutic opportunities of the skin microbiome. Drug Discov Today Dis Mech 10. https://doi.org/10.1016/j.ddmec.2012.12.003
69. Schrapers KT, Sponder G, Liebe F, Liebe H, Stumpff F (2018) The bovine TRPV3 as a pathway for the uptake of Na+, Ca2+, and NH4+. PLoS ONE 13:e0193519. https://doi.org/10.1371/journal.pone.0193519
70. Sellin JH, Dubinsky WP (1994) Apical nonspecific cation conductances in rabbit cecum. Am J Physiol 266:G475-484. https://doi.org/10.1152/ajpgi.1994.266.3.G475
71. Smith GD, Gunthorpe MJ, Kelsell RE, Hayes PD, Reilly P, Facer P, Wright JE, Jerman JC, Walhin JP, Ooi L, Egerton J, Charles KJ, Smart D, Randall AD, Anand P, Davis JB (2002) TRPV3 is a temperature-sensitive vanilloid receptor-like protein. Nature 418:186–190. https://doi.org/10.1038/nature00894
72. Stewart GS, Smith CP (2005) Urea nitrogen salvage mechanisms and their relevance to ruminants, non-ruminants and man. Nutr Res Rev 18:49–62. https://doi.org/10.1079/NRR200498
73. Stumpff F, Georgi MI, Mundhenk L, Rabbani I, Fromm M, Martens H, Günzel D (2011) Sheep rumen and omasum primary cultures and source epithelia: barrier function aligns with expression of tight junction proteins. J Exp Biol 214:2871–2882. https://doi.org/10.1242/jeb.055582
74. Szollosi AG, Vasas N, Angyal A, Kistamas K, Nanasi PP, Mihaly J, Beke G, Herczeg-Lisztes E, Szegedi A, Kawada N, Yanagida T, Mori T, Kemeny L, Biro T (2018) Activation of TRPV3 regulates inflammatory actions of human epidermal keratinocytes. J Invest Dermatol 138:365–374. https://doi.org/10.1016/j.jid.2017.07.852
75. Ueda T, Yamada T, Ugawa S, Ishida Y, Shimada S (2009) TRPV3, a thermosensitive channel is expressed in mouse distal colon epithelium. Biochem Biophys Res Commun 383:130–134. https://doi.org/10.1016/j.bbrc.2009.03.143
76. Ussing HH, Zerahn K (1951) Active transport of sodium as the source of electric current in the short-circuited isolated frog skin. Acta Physiol Scand 23:110–127. https://doi.org/10.1111/j.1748-1716.1951.tb00800.x
77. Verhulst NO, Andriessen R, Groenhagen U, Bukovinszkine Kiss G, Schulz S, Takken W, van Loon JJ, Schraa G, Smallegange RC (2010) Differential attraction of malaria mosquitoes to volatile blends produced by human skin bacteria. PLoS ONE 5:e15829. https://doi.org/10.1371/journal.pone.0015829
78. Vitzthum C, Stein L, Brunner N, Knittel R, Fallier-Becker P, Amasheh S (2019) Xenopus oocytes as a heterologous expression system for analysis of tight junction proteins. Federation of American Societies for Experimental Biology Journal 33:5312–5319. https://doi.org/10.1096/fj.201801451RR
79. Vogt-Eisele AK, Weber K, Sherkheli MA, Vielhaber G, Panten J, Gisselmann G, Hatt H (2007) Monoterpenoid agonists of TRPV3. Br J Pharmacol 151:530–540. https://doi.org/10.1038/sj.bjp.0707245
80. Walker V (2014) Ammonia metabolism and hyperammonemic disorders. Adv Clin Chem 67:73–150. https://doi.org/10.1016/bs.acc.2014.09.002
81. Wang G, Wang K (2017) The Ca(2+)-permeable cation transient receptor potential TRPV3 channel: an emerging pivotal target for itch and skin diseases. Mol Pharmacol 92:193–200. https://doi.org/10.1124/mol.116.107946
82. Weber W (1999) Ion currents of Xenopus laevis oocytes: state of the art. Biochim Biophys Acta 1421:213–233. https://doi.org/10.1016/s0005-2736(99)00135-2
83. Xie L, Jin L, Feng J, Lv J (2017) The expression of AQP5 and UTs in the sweat glands of uremic patients. Biomed Res Int 2017:8629783. https://doi.org/10.1155/2017/8629783
84. Xu H, Ramsey IS, Kotecha SA, Moran MM, Chong JA, Lawson D, Ge P, Lilly J, Silos-Santiago I, Xie Y, DiStefano PS, Curtis R, Clapham DE (2002) TRPV3 is a calcium-permeable temperature-sensitive cation channel. Nature 418:181–186. https://doi.org/10.1038/nature00882
85. Yadav M, Goswami C (2017) TRPV3 mutants causing Olmsted syndrome induce impaired cell adhesion and nonfunctional lysosomes. Channels (Austin) 11:196–208. https://doi.org/10.1080/19336950.2016.1249076
86. Zhang A, Duchatelet S, Lakdawala N, Tower RL, Diamond C, Marathe K, Hill I, Richard G, Diab Y, Kirkorian AY, Watanabe F, Siegel DH, Hovnanian A (2020) Targeted inhibition of the epidermal growth factor receptor and mammalian target of rapamycin signaling pathways in Olmsted syndrome. JAMA Dermatol 156:196–200. https://doi.org/10.1001/jamadermatol.2019.4141
87. Zhong W, Hu L, Cao X, Zhao J, Zhang X, Lee M, Wang H, Zhang J, Chen Q, Feng C, Duo L, Wang X, Tang L, Lin Z, Yang Y (2020) Genotype phenotype correlation of TRPV3-related Olmsted syndrome. J Invest Dermatol. https://doi.org/10.1016/j.jid.2020.06.035

3.1. Supplementary material (Liebe et al. 2021)

Online Resource

Beyond Ca^{2+} signalling: a role for TRPV3 in the transport of NH_4^+

Pflügers Archiv – European Journal of Physiology

Hendrik Liebe[1,2], Franziska Liebe[1], Gerhard Sponder[1], Sarah Hedtrich[3], Friederike Stumpff[1]
stumpff@zedat.fu-berlin.de

[1]Institute of Veterinary Physiology, Freie Universität Berlin, Berlin, Germany

[2]Department of Biology, Chemistry, and Pharmacy, Freie Universität Berlin, Germany

[3]Faculty of Pharmaceutical Sciences, University of British Columbia, Vancouver, Canada

A) Harvesting and processing of *Xenopus laevis* oocytes

Xenopus laevis oocytes (*X.* oocytes) were obtained and prepared as described by Vitzthum *et. al*. [11] and in [1]. After surgical removal, ovarian lobes were placed in oocyte Ringer's solution (180 mOsm·kg^{-1} adjusted with D-mannitol), shaken mechanically for 90 minutes, and transferred into calcium-free oocyte Ringer's solution for 10 minutes. Defolliculated stage V-VI *X*. oocytes were stored in oocyte culture solution at +16 °C until the following day, when they were injected (see methods). Injected *X.* oocytes were incubated for at least three days in modified low-sodium oocyte Ringer's solution (NMDGCl Ringer solution, 16 °C) before use in experiments (in mmol·L^{-1}: 80 N-methyl-D-glucamine chloride (NMDGCl), 5 NaCl, 5 4-(2-hydroxyethyl)-1-piperazineethanesulfonic acid (HEPES), 2.5 2-Oxopropanoic acid, 1 KCl, 1 $CaCl_2$, 1 $MgCl_2$, 50 units·mL^{-1} penicillin, 0.05 mg·mL^{-1} streptomycin, pH 7.4 adjusted with tris(hydroxymethyl)aminomethane (Tris), 223 mOsm·kg^{-1} adjusted with D-mannitol).

B) Preparation for immunoblotting

Both the solvents and the samples were cooled throughout the experiments to minimize protein degradation and processed essentially as in Liebe *et al* [7]. In brief, injected *X.* oocytes were incubated for four days, lysed mechanically in oocyte lysis buffer (500 µL; in mmol·L^{-1}: 5 $MgCl_2$, 5 NaH_2PO_4, 1 EDTA, 80 sucrose, pH 7.4 (Tris)), and centrifuged at 200 rpm (10 min, 4 °C). The supernatant was centrifuged using the same settings, and subsequently, at 13,000 rpm (40 min, 4 °C). The precipitate was suspended in fresh oocyte lysis buffer (40 µL). Cultivated to confluence in a T-25 flask, HEK-293 cells were washed with PBS, harvested by scraping, and centrifuged (500 g, 5 min). The cell pellet was suspended in PBS (1 mL), centrifuged (700 g, 4 min) and resuspended in RIPA buffer (100 µL). Lysis was performed for 30 min with gentle agitation and 5 min in an ultrasound bath, followed by a clarifying spin (20 min, 15,000 g) using a new tube for each step. Human skin equivalents were lysed in RIPA buffer (supplemented with phosphatase and protease inhibitors) [5].

All protein samples were stored at -80 °C. Concentrations were determined prior to the experiment using a Pierce™ 660 nm protein assay kit (Thermo Fisher Scientific, Waltham, MA, USA). All samples were denatured in SDS sample loading buffer (10 %) and electrophoresed on polyacrylamide-gels (7.5 %, SDS-PAGE) in Tris-Glycine buffer (0.1 % SDS). Electroblotting was performed onto polyvinylidene difluoride membranes (PVDF, Immun-Blot®, Bio-Rad) in Tris-Glycine buffer (0.3 % SDS, 20 % methanol, 4 °C). The membranes were blocked in milk (5 %) in Tris-buffered saline supplemented with Tween20 (0.1 vol%) for 45 min.

C) Preparation for immunofluorescence staining

Immunofluorescence staining was performed according to the procedure previously described [1]. *X.* oocytes were fixed in paraformaldehyde (4 %, 3 h) and washed twice with PBS. After dehydration in increasing concentrations of ethanol (2 times in 70 % (1 h), 70 % (overnight), 3 times in 80 % (1 h), 80 % (72 h), 2 times in 96 % (10 min), 3 times in 99.9 % (10 min)) and immersion in Xylene (2 times for

10 min), *X.* oocytes were embedded in paraffin (2 times for 30 min), cut (5 µm) and mounted (Superfrost® Plus Menzel-Gläser, Carl Roth). Subsequently, slides were deparaffinized overnight (Roti®-Histol, Carl Roth) and rehydrated in descending concentrations of ethanol (99.9 %, 96 %, 90 %, 80 %, 70 %, demineralized water, 5 minutes each). After washing (PBS, 5 min) and boiling (EDTA buffer, 1 mmol·L^{-1}; pH 8.0, 15 min), the slides were rinsed in PBS for 1, 5, and 5 minutes respectively.

One hour after seeding HEK-293 cells on coverslips, these were washed twice in PBS, transferred to Roti®-Histofix (4 %, 30 min), and washed again twice in PBS.

Human skin equivalents were submerged in tissue freezing media, flash frozen, and cut into cross sections (8 µm) on a cryotome (Leica Biosystems, PLACE, Wetzlar, Germany) as described previously [5]. Samples were stored at -80 °C. Cryo-embedded human skin equivalents were defrosted at room temperature for 45 min. The tissue was fixated in paraformaldehyde for 5 min and washed 2 times with PBS for 5 min.

X. oocytes, HEK-293 cells, and human skin equivalents were all permeabilized in Triton X-100 (0.5 %, 5 min; Merck KGaA, Darmstadt, Germany) and washed twice in PBS. Afterwards, all preparations were incubated in blocking solution (BS, goat serum (5 %; PAN-Biotech GmbH, Aidenbach, Germany) in PBS) in a closed container for 1 hour. Samples were then stained with primary antibody diluted in BS as stated in methods or in BS only for secondary antibody controls (both 4 °C, overnight). After washing with BS (3 times for 5 min), the slides were incubated with diluted secondary antibodies as stated in methods (in BS supplemented with 4′, 6-diamidine-2′-phenylindole dihydrochloride (1 µg/mL; DAPI, Roche, Mannheim, Germany), 37 °C, 1 h). Afterwards, samples were washed with demineralized water and ethanol, followed by embedding (Mount Flour, Biocyc GmbH & Co. KG, Potsdam, Germany) on a microscopic slide.

D) Double-barrelled pH-sensitive microelectrode measurements

Experiments with pH-sensitive microelectrodes were prepared essentially as described previously [1,7]. For pH-measurements, SUTTER BF 150-86-10 glass tubing (Science Products GmbH, Hofheim, Germany) was used. The reference barrel was made of filamented bisected GC150F 15 glass tubing (Harvard Apparatus, Kent, UK). Two core cable ends (4×10, 611889, Conrad Bauelemente, Conrad Elektronik, Hirschau, Germany) were pushed into tightly fitting shrink tubing (Ø 3 mm) and used to adjoin the two barrels, leaving the middle section free (~ 3 cm). A small piece of shrink tubing (1 mm; Deray-H-set 1/8″, DSG-Canusa, Meckenheim, Germany) was slipped over the end of the reference barrel, slightly separating the barrels at one end. After baking (180 °C, 10 min), the piggyback electrodes were pulled with a programmable multipipette puller (PMP-107, Microdata Instrument, South Plainfield, NJ, USA) to give a resistance of ~ 50 MΩ. Subsequently, the reference barrel was perfused with pressurized dry air via plastic tubing pushed over one end (~ 0.9 bar). The pH-sensitive barrel was pushed into a rubber insert in the lid of a heated glass jar and exposed to the vapour formed by a drop (200 µl) of fresh dichlorodimethylsilane (Sigma-Aldrich) for 30 min. Pipettes were then baked at 180 °C for 2 h. The pH-sensitive barrel was filled with Hydrogen Ionophore I-Cocktail A (0.2 µl; Sigma Aldrich) via a Microliter

syringe (type 7000.50C, Hamilton Company, Reno, NV, USA). The electrodes could be stored in a plastic container with silica gel (P077.2, Carl Roth) and light protection for many months. Once opened, Dichlorodimethylsilane had to be replaced frequently.

On the experimental day, the reference barrel was filled with KCl solution (0.5 mol·L^{-1}) via a MicroFil micropipette (34Gauge/67 mm, World Precision Instruments, Sarasota, FL, USA), while the pH-sensitive barrel was filled with KCl/HEPES-buffer (in mmol·L^{-1}: 500 KCl, 20 HEPES, pH 7.2 adjusted with Tris). Microelectrodes were then trimmed (0.5-30 MΩ) to remove clogging silane residues using a beveller (BV-10, Sutter Instrument, Novato, CA, USA).

Measurements were performed in a continuously perfused bath chamber (23 °C). Via chlorinated silver wires, the two barrels were connected to an amplifier (F-223 A Dual Electrometer, World Precision Instruments). The bath was grounded to a common technical earth via a chlorinated silver wire. In addition, the bath was connected to a commercial electrode (Metrohm, Filderstadt, Germany) via a KCl (3 mol·L^{-1}) agar bridge to minimize liquid junction potential effects (ground signal) [2]. All three signals were measured versus the technical earth and recorded using LabChart 7 software (ADintruments Ltd, Oxford, UK). The potential difference between the two barrels was used to determine the intracellular pH (pH_i), while the potential difference between the reference barrel and the ground signal from the bath corresponded to the membrane potential (U_{mem}). Electrodes were calibrated before and after each measurement using NaCl (pH 7.4) and NaCl-6.4 (pH 6.4) solutions. Suitable electrodes showed a stable potential difference of 45 mV or higher measured by the pH-sensitive barrel with effects at the reference electrode < 0.3 mV. A micromanipulator (Mini 25, Luigs & Neumann, Ratingen, Germany) was used to insert the microelectrode into the *X.* oocyte. Impalement was considered to be successful if a sharp drop in the potential across the reference channel to values under -10 mV could be observed. Drift correction was used to compensate for small variations in the pH-response of the electrode to the calibration solutions before and after the experiment, but cells were excluded when ΔpH was greater than 0.05.

E) Relative permeability ratio

To calculate relative permeability ratios, the assumption was made that leak currents were low and that the contribution of extracellular K^+ and intracellular Cl^- to total membrane potential was low. The Goldman-Hodgkin-Katz (GHK) theory then yields the following expression [6]:

$$(1) \qquad U_A - U_B \approx -\frac{R \cdot T}{F} \cdot \ln\left(\frac{P_A \cdot [A]_o}{P_B \cdot [B]_o}\right)$$

Here, U_x designates the membrane potential in solution X, F the Faraday constant, and T the absolute temperature, while P_x designates the permeability, and $[X]_o$ the outside concentration of ion X.

F) Analysis of Inside-out patch-clamp data via Goldman-Hodgkin-Katz theory

Igor (Igor Pro 6.2.2.2; WaveMetrics Inc., Lake Oswego, USA) was used to fit amplitude histograms to a Gaussian distribution as described previously [4,10,7]. The unitary current was determined from the

distance of the maxima and cross-checked by direct measurements. Current-Voltage plots (IV-plots) were obtained by plotting the obtained unitary currents against the clamped pipette potentials, which were corrected for liquid junction potentials throughout (JPCalcWin software, School of Medical Sciences, Sydney, Australia) [2]. The GHK theory was used to fit the IV-plot via Igor, yielding the permeability for two ions (P_A and P_B) as described in detail in [10].

$$(2)\ \mathrm{I} = \frac{U_{mem} \cdot \mathrm{F}^2}{\mathrm{R} \cdot \mathrm{T}} \cdot \left(\frac{\mathrm{P_A} \cdot [\mathrm{A}]_\mathrm{i} + \mathrm{P_B} \cdot [\mathrm{B}]_\mathrm{i} - (\mathrm{P_A} \cdot [\mathrm{A}]_\mathrm{o} + (\mathrm{P_B} \cdot [\mathrm{B}]_\mathrm{o}) \cdot \mathrm{e}^{-U_{mem} \cdot \frac{\mathrm{F}}{\mathrm{R} \cdot \mathrm{T}}}}{1 - \mathrm{e}^{-U_{mem} \cdot \frac{\mathrm{F}}{\mathrm{R} \cdot \mathrm{T}}}} \right)$$

If pipette and bath solutions were identical (symmetrical configuration), the slope of the linear regression of the IV-plot was used to determine the conductance (G_x) of a given ion X. Equation (3) was used to yield P_x, the permeability of the ion X, while [C] is the concentration of the major cation in used solutions (96 mmol·L^{-1}).

$$(3)\quad \mathrm{G_X} = \frac{\mathrm{I}}{U_{mem}} = \frac{\mathrm{F}^2}{\mathrm{R} \cdot \mathrm{T}} \cdot \mathrm{P_X} \cdot [\mathrm{C}]$$

To compare these conductance values with data obtained with HEK-293 cells, where mammalian Ringer solutions containing 145 mmol·L^{-1} of the main cation, the conductance G_x in oocyte solution was multiplied by the concentration ratio yielding:

$$(4)\ \mathrm{G_X}\ (145\ \mathrm{mmol \cdot L^{-1}}) = \mathrm{G_X}\ (96\ \mathrm{mmol \cdot L^{-1}}) \times \frac{145\ \mathrm{mmol \cdot L^{-1}}}{96\ \mathrm{mmol \cdot L^{-1}}}$$

For comparison of single-channel data from overexpressing cells and controls, data were plotted in amplitude histograms (Fig. 9 and Fig. S3). After collecting data from all patches, the total conductance range of all measurements was divided into a number of equidistant bins, which were plotted on the horizontal axis. The vertical axis was used to plot the number of patches with a conductance falling into the corresponding bin on the X-axis. Accordingly, the bars in these histograms do not correspond to discrete conductance steps.

G) Attempts to enhance cell viability of HEK-293 cells overexpressing G573S

In order to enhance the viability of G573S HEK-293 cells for patch-clamping, we attempted various approaches to reduce the concentration of free Ca^{2+} by diluting the medium (DMEM, FG 0445; Ca^{2+}-concentration: 200 mg·L^{-1} = 0.91 mmol·L^{-1}) with PBS (no Ca^{2+} or Mg^{2+}; Sigma-Aldrich) or by supplementing EGTA in PBS (10 mmol·L^{-1}). Furthermore, we tried out different concentrations of foetal bovine serum (FBS, Biochrom). The different strategies are summarised in Table S1 but no approach yielded the desired outcome of cells emitting a visible fluorescent signal allowing selection for patch-clamping.

Additionally, the duration for transfection with the vector was altered. We transfected HEK-293 cells with the G573S mutant and control vector for 22 h, 93 h, 2 h, and 1 h, respectively, but no fluorescent signal emerged despite successful parallel expression of wild type hTRPV3. Most likely, the cells started to disintegrate immediately after expression of the G573S mutant but prior to the downstream expression of observable quantities of GFP.

This hypothesis was confirmed via subsequent immunofluorescence. A few cells could be shown to express the G573S mutant with traces of visible GFP fluorescence. In addition, disintegrated cells could be seen (see Fig. 14a; 22 h transfection). It is likely that the majority of cells successfully expressing the G573S mutant rapidly became apoptotic and detached from the coverslip before the downstream expression of GFP could occur. It was therefore not possible to select successfully expressing cells for patch-clamping.

#	Medium [mL]	$PBS^{-/-}$ [mL]	EGTA [$mmol \cdot L^{-1}$]	FBS [µL]	Free Ca^{2+} [$mmol \cdot L^{-1}$]
1	2.5	2.5	0	250	0.5
2	3.75	1.25	0	125	0.7
3	4.5	0.5	0	50	0.8
4	1	1	0	100	0.5
5	1.5	0.5	0	50	0.7
6	1.8	0.2	0	20	0.8
7	1	0	0	0	0.9
8	1	0	0.2	4	0.7
9	1	0	0.4	0	0.5
10	1	0	0.6	8	0.3
11	1	0	0.8	10	0.07
12	1	0	1.0	20	0.006
13	1	0	5.0	100	0.0001

Table S1. Composition of different media to enhance the vitality of for G573S HEK-293 cells

H) Supplemental microelectrode data: hTRPV3, bTRPV3, and control *X.* oocytes

The double-barrelled pH-sensitive microelectrode experiments (Fig. 5 and Fig. S1) were performed in parallel to our study of the bovine homologue of TRPV3 (bTRPV3), alternating between hTRPV3, bTRPV3, and control *X.* oocytes [7].

Screening experiments

In preliminary screening experiments on four hTRPV3 overexpressing *X.* oocytes, Na^+ in the bath solution was consecutively replaced by K^+, NH_4^+, or $NMDG^+$ while Cl^- was replaced by Glu^- (Fig. S1).

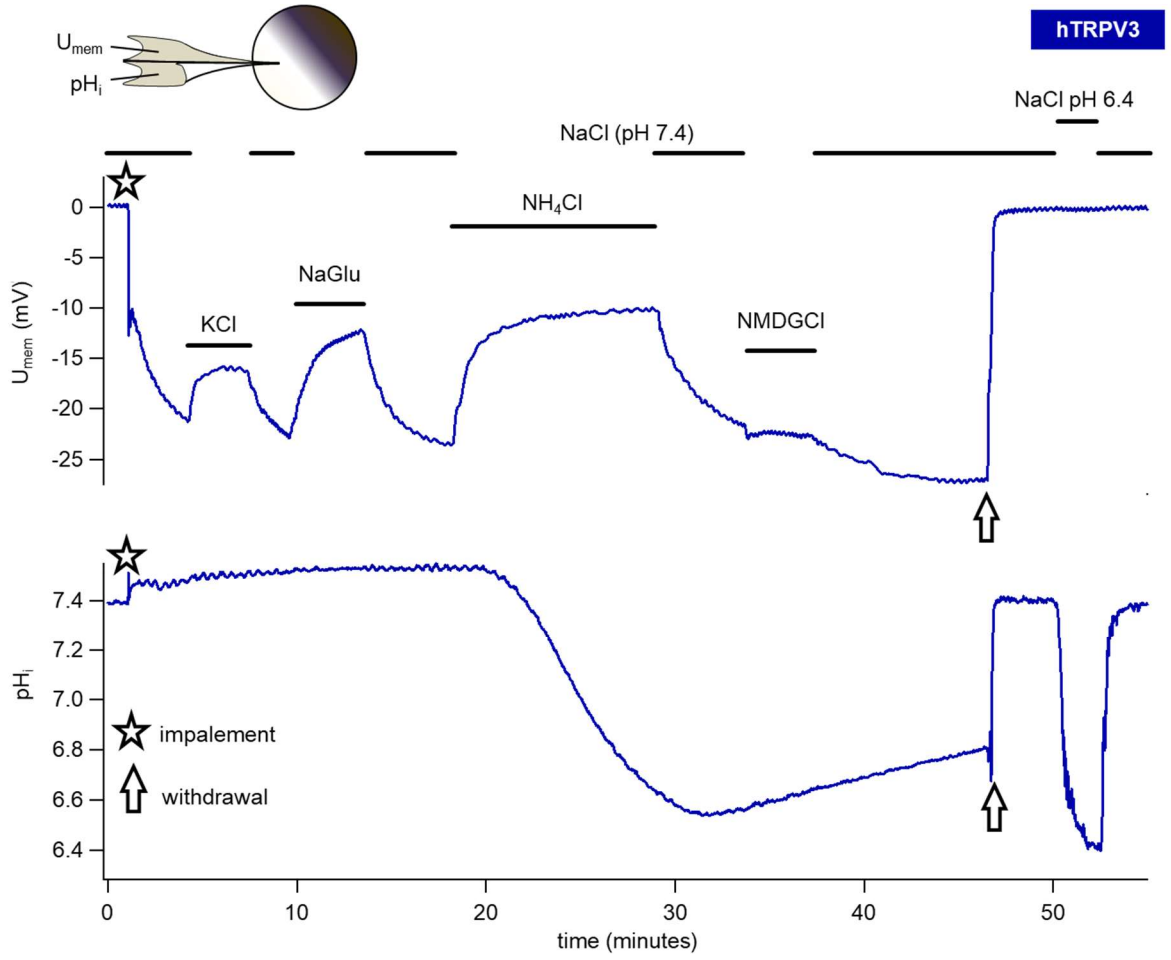

Fig. S1 Double-barrelled pH-sensitive microelectrodes: original recording showing the response of an hTRPV3 *X.* oocyte to various solutions

At the beginning of the measurement, impalement (star) can be seen, which resulted in a sharp drop in U_{mem} with a small rise in pH_i. Opposite effects visible after withdrawal of the pipette (arrow) at the end. Replacement of Na^+ by K^+ or Cl^- by Glu^- led to a reversible depolarisation of U_{mem} with no impact on pH_i. Conversely, NH_4^+ led to both a rapid depolarisation of U_{mem} and a slower decrease in pH_i, arguing for influx of NH_4^+. In line with this, return to NaCl solution led to a rapid repolarization of U_{mem} although recovery of pH_i was very slow (see discussion). Replacement of Na^+ by $NMDG^+$ had no effect on the recovery of pH_i, arguing against an involvement of NHE in pH regulation. Effects of $NMDG^+$ on U_{mem} were variable

X. oocytes (n/N = 4/1) depolarised after application of KCl (-12.1 ± 1.8 mV), NaGlu (-7.8 ± 2.0 mV), or NH_4Cl (-4.9 ± 1.9 mV) with recovery after each return to NaCl solution (-17 ± 3 mV). However, only the depolarisation in NaGlu ($p = 0.03$) and NH_4Cl ($p = 0.006$) tested for significance. From the reversal

potentials, relative permeability ratios could be calculated ([6] and supplement part E), yielding a $p(Cl^-)/p(Glu^-)$ of 1.62 ± 0.25. Permeability to NH_4^+ ($p(NH_4^+)/p(Na^+)$ = 1.79 ± 0.22) was significantly higher than that to K^+ ($p(K^+)/p(Na^+)$ = 1.33 ± 0.12, p = 0.03).

In NaCl, pH_i was 7.40 ± 0.05 and solution changes to KCl (p = 0.9) or NaGlu (p = 0.8) showed no significant effect. Application of NH_4Cl solution resulted in a significant acidification (6.64 ± 0.09 after 10 minutes, p ≤ 0.001) with a slow recovery after return to NaCl solution (6.72 ± 0.08 after 15 minutes). This recovery was not interrupted by removal of Na^+, so that any involvement of NHE seems unlikely. In response to $NMDG^+$, two cells showed hyperpolarisation (ΔU_{mem} = -3.8 ± 0.5 mV), in line with a reduction of Na^+ influx. Surprisingly, two other cells depolarised (ΔU_{mem} = 2.4 ± 1.7 mV). Similar effects have been observed by others and possibly reflect membrane leakage induced by full substitution of Na^+ by $NMDG^+$ [7,8]. Such high concentrations of $NMDG^+$ can induce pore dilation of TRP channels with influx of large molecular substrates [10,3]. It is possible to speculate that this leads to uptake of $NMDG^+$, swelling and bursting of cells, but further work is clearly necessary. For the preliminary experiments, observations were similar to those seen in bTRPV3 and control oocytes [7].

Comparison between bRPV3, hTRPV3, and control oocytes

The acidification by NH_4Cl could be confirmed in more rigorously performed experiments. Membrane potentials, intracellular pH (pH_i), and relative permeabilities are visualised in Fig. S2 and statistically evaluated in Table S2. The relative permeability ratio of Na^+ versus $NMDG^+$ was comparable between hTRPV3 and bTRPV3 (p = 0.5), but significantly higher than that of the controls (p = 0.002 ctrl vs bTRPV3 [7] and p = 0.005 vs hTRPV3 (main text)), reflecting expression of TRPV3. After application of NH_4Cl solution, all *X.* oocytes depolarised strongly and acidified, reflecting expression of NH_4^+ conducting channels by all three groups. However, after 3.5 minutes of incubation with NH_4Cl, both hTRPV3 and bTRPV3 *X.* oocytes showed a lower value of pH_i than controls (p = 0.004 and p = 0.04 [7], respectively), reflecting a higher influx rate of NH_4^+. The pH_i dropped most rapidly in hTRPV3, showing a slight recovery towards the end of the measurement which suggests that an equilibrium distribution had been reached in this group of oocytes. This may explain why a removal of Ca^{2+} had no further effect on pH_i in this group. However, both hTRPV3 and bTRPV3 oocytes depolarised after removal of Ca^{2+} as to be expected after opening of a divalent-sensitive cation channel such as TRPV3. Conversely, control cells hyperpolarised, possibly reflecting expression of Ca^{2+} inactivated chloride channels [12,9]. For further discussion of the differences between hTRPV3 and bTRPV3, see the main text and supplement part I, Fig. S4.

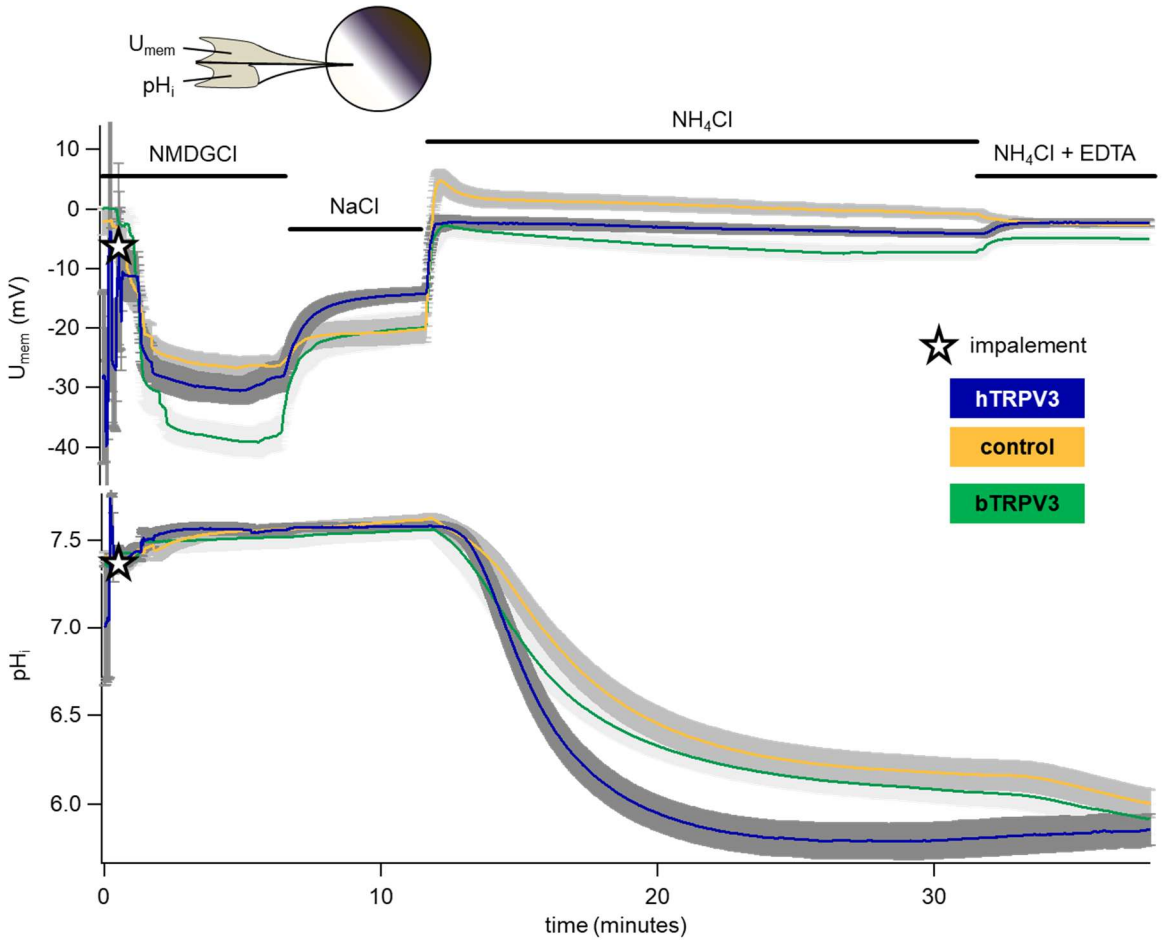

Fig. S2 Double-barrelled pH-sensitive microelectrode measurement of *X.* oocytes

Shown are the mean of the membrane potential and pH_i of X. oocytes expressing hTRPV3 (n/N = 12/3, blue), bTRPV3 (n/N = 14/3, green) [7], and controls (n/N = 16/3, orange). The SEM is visualised in different shades of grey. The differences between hTRPV3 and bTRPV3 most likely reflect a higher expression efficiency in hTRPV3, as discussed in supplement part I, Fig. S4

Membrane potential [mV]							
Bath solution	hTRPV3	control	bTRPV3	ANOVA	bV3 vs ctrl	hV3 vs ctrl	hV3 vs bV3
NMDGCl	-30.6 ± 2.2[a]	-27.2 ± 1.8[a]	-39.2 ± 2.6[a]	0.003	0.001	0.4	0.02
NaCl	-14.4 ± 1.1[b]	-20.3 ± 2.2[b]	-20.1 ± 2.8[b]	0.02	0.6	0.03	0.009
NH_4Cl (3.5 min)	-2.5 ± 1.0[c]	1.5 ± 1.4[c]	-4.4 ± 1.5[c]	0.005	0.003	0.03	0.3
NH_4Cl (20 min)	-4.1 ± 0.6[d]	-0.9 ± 0.8[d]	-7.2 ± 1.3[d]	<0.001	<0.001	0.003	0.2
NH_4Cl-EDTA	-2.3 ± 0.6[c]	-2.7 ± 0.5[e]	-5.0 ± 1.1[c]	0.03	0.03	0.7	0.02
Intracellular pH (pH_i)							
	hTRPV3	control	bTRPV3	ANOVA	bV3 vs ctrl	hV3 vs ctrl	hV3 vs bV3
NMDGCl	7.56 ± 0.04[a]	7.56 ± 0.04[a]	7.52 ± 0.07[a]	1.0	1.0	0.9	0.9
NaCl	7.58 ± 0.03[a]	7.61 ± 0.03[b]	7.56 ± 0.05[b]	0.8	0.9	0.5	0.8
NH_4Cl (3.5 min)	6.76 ± 0.09[b]	7.14 ± 0.06[c]	6.90 ± 0.08[c]	< 0.001	0.04	0.004	0.3
NH_4Cl (20 min)	5.81 ± 0.11[c]	6.18 ± 0.09[d]	6.08 ± 0.08[d]	0.02	0.6	0.007	0.03
NH_4Cl-EDTA	5.85 ± 0.09[c]	6.05 ± 0.08[e]	5.96 ± 0.09[e]	0.2	0.6	0.07	0.3
Change of pH_i (slope in ΔpH/min)							
	hTRPV3	control	bTRPV3	ANOVA	bV3 vs ctrl	hV3 vs ctrl	hV3 vs bV3
NMDGCl	0.03 ± 0.02[a]	0.01 ± 0.01[a]	-0.02 ± 0.02[a]	0.7	0.7	0.5	0.6
NaCl	0.00 ± 0.00[a]	0.00 ± 0.01[a]	0.03 ± 0.01[b]	0.009	0.02	0.6	0.003
NH_4Cl (3.5 min)	-0.39 ± 0.04[b]	-0.22 ± 0.04 [b]	-0.22 ± 0.03[c]	0.004	0.7	0.006	0.002
NH_4Cl (20 min)	0.02 ± 0.01[a]	0.00 ± 0.01[a]	-0.01 ± 0.01[a]	0.13	0.9	0.05	0.2
NH_4Cl-EDTA	-0.004± 0.02[a]	-0.04 ± 0.02 [c]	-0.02 ± 0.01[a]	0.02	0.3	0.01	0.05
Relative permeability ratio p(X) / p($NMDG^+$)							
Ion X	hTRPV3	control	bTRPV3	ANOVA	bV3 vs ctrl	hV3 vs ctrl	hV3 vs bV3
Na^+	1.98 ± 0.18[a]	1.37 ± 0.12[a]	2.25 ± 0.20[a]	0.002	0.002	0.005	0.5
NH_4^+ (20 min)	2.93 ± 0.24[b]	2.93 ± 0.23[b]	3.62 ± 0.25[b]	0.08	0.06	1.0	0.05
NH_4^+ (EDTA)	3.15 ± 0.25[c]	2.70 ± 0.18[c]	4.01 ± 0.33[c]	0.008	0.003	0.3	0.07

Table S2. Double-barrelled pH-sensitive microelectrodes: Effects of NH_4^+ on the pH_i and the membrane potential of *Xenopus* oocytes expressing hTRPV3 (hV3, n/N = 13/3), bTRPV3 (bV3, n/N = 14/3) [7] and controls (ctrl; n/N = 16/3)

Solutions were applied consecutively and values were measured 5 minutes after exposure unless indicated otherwise. Within columns, different superscripts indicate significant differences with $p \leq 0.05$. The fifth column gives the p-value of the ANOVA (Kruskal-Wallis) between the three groups, followed by the p-values for pairwise comparisons (Mann-Whitney) in column 6, 7, and 8

I) Comparison of single-channel patch-clamp data: hTRPV3, bTRPV3, and control *X.* oocytes

Single-channel patch-clamp experiments of *X.* oocytes overexpressing hTRPV3 were performed in parallel to our study of bTRPV3 [7], again allowing a direct comparison. The resulting histograms are shown in Fig. S3 and discussed in context with the microelectrode results in Fig. S4.

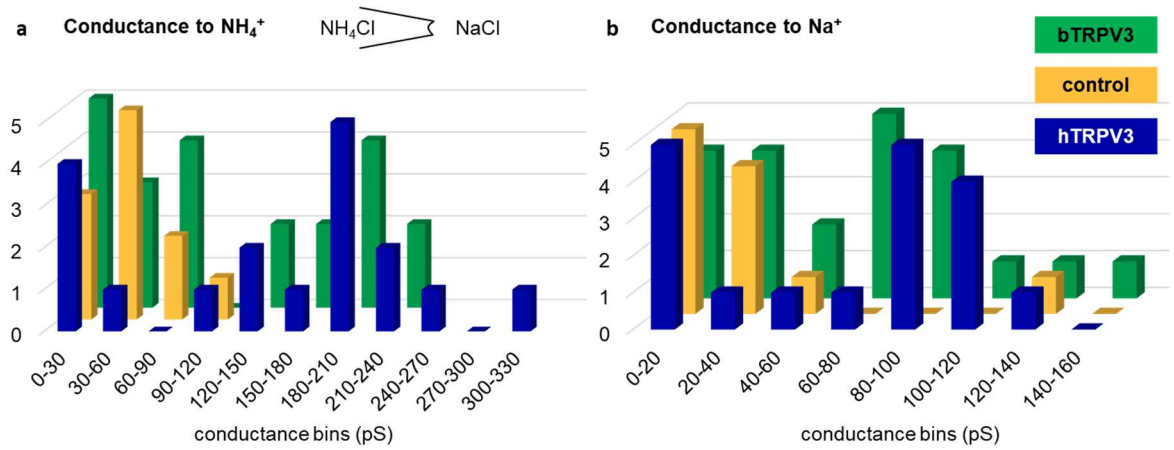

Fig. S3. Histograms of single-channel conductances from *X.* oocytes overexpressing hTRPV3, bTRPV3 [7], and controls

a) Histogram of all single-channel conductances for NH_4^+, determined from GHK fits of IV-plots of experiments in the asymmetrical configuration with NH_4Cl in the pipette and NaCl in the bath. The vertical axis shows the number of patches (n) falling into the corresponding conductance range or bin shown on the horizontal axis. Patches from control *X.* oocytes only showed NH_4^+ conductances below 100 pS. In contrast, *X.* oocytes expressing hTRPV3 or bTRPV3 (published in Liebe et al. [7]) showed both small channels such as those observed in the control *X.* oocytes and larger conductances ranging up to 303 pS. These larger conductances probably reflected heteromers of endogenous channels with TRPV3. b) Corresponding histogram of all single-channel conductances for Na^+. A similar pattern emerged as in a), with a cluster of channels below 60 pS in patches from both control and TRPV3 *X.* oocytes, and a second, larger cluster emerging in hTRPV3 and bTRPV3 *X.* oocytes. Interestingly, one solitary control patch expressed a very large conductance to Na^+ reflecting what is clearly a very diverse population of channels expressed by the native *X.* oocytes [12]. Any differences between bTRPV3 and hTRPV3 did not test for significance

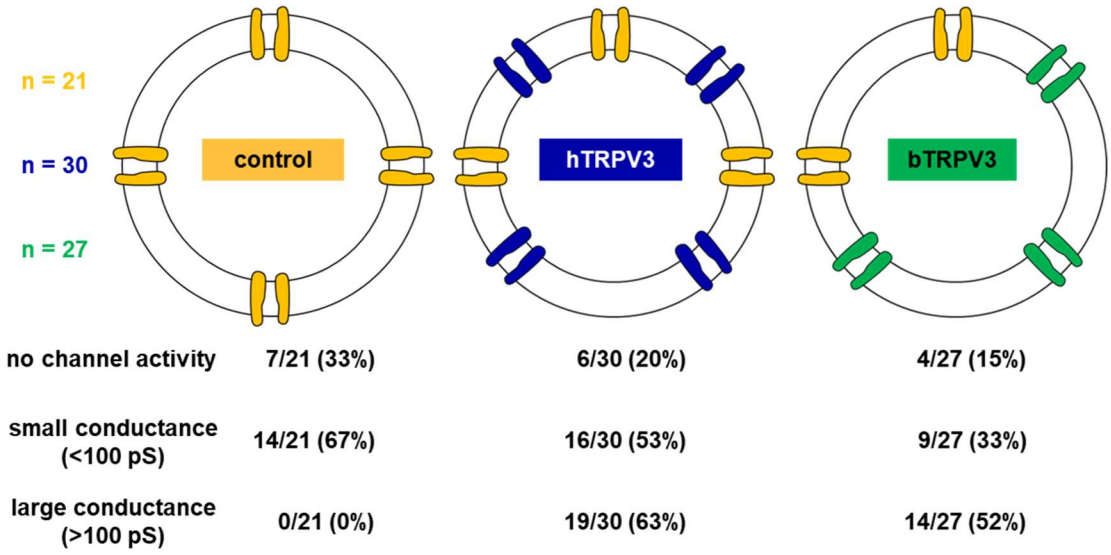

	control	hTRPV3	bTRPV3
no channel activity	7/21 (33%)	6/30 (20%)	4/27 (15%)
small conductance (<100 pS)	14/21 (67%)	16/30 (53%)	9/27 (33%)
large conductance (>100 pS)	0/21 (0%)	19/30 (63%)	14/27 (52%)

Fig. S4. Schematic representation showing the relative abundance of small and large conductances in single-channel patch-clamp experiments for hTRPV3, bTRPV3 [7], and control *X.* oocytes in symmetrical NH_4Cl solution

Small channels (<100 pS) were primarily expressed by control *X.* oocytes and are shown in yellow. Large channels (>100 pS) are shown in blue if expressed by hTRPV3 oocytes and green if expressed by bTRPV3 oocytes. The number n of patches with either no single-channel events, small channels (<100 pS), or large channels (>100 pS) is given in relation to the total number N of patches measured as a ratio (n/N) followed by the percentage. 15 hTRPV3 and 8 bTRPV3 membrane patches simultaneously expressed both small and large conductances. The hTRPV3 *X.* oocytes showed both a higher number of channels in individual patches and a larger percentage of large channels than bTRPV3 *X.* oocytes.

We suggest that expression of hTRPV3 or bTRPV3 significantly enhanced the single-channel conductance of individual channels, with the scatter in values reflecting the formation of heteromers with endogenous channels. Furthermore, expression of endogenous channels was suppressed by either hTRPV3 or bTRPV3, with effects more pronounced in the case of bTRPV3. It also appears that expression of hTRPV3 was more efficient than expression of bTRPV3. Both the lower number of bTRPV3 channels and the lower number of endogenous channels might explain why bTRPV3 oocytes did not acidify as rapidly in response to NH_4Cl as hTRPV3 oocytes in the microelectrode experiments (supplement part H).

References

1. Abdoun K, Stumpff F, Rabbani I, Martens H (2010) Modulation of urea transport across sheep rumen epithelium in vitro by SCFA and CO2. American journal of physiology Gastrointestinal and liver physiology 298:G190-202. doi:10.1152/ajpgi.00216.2009
2. Barry PH, Lynch JW (1991) Liquid junction potentials and small cell effects in patch-clamp analysis. J Membr Biol 121:101-117. doi:10.1007/BF01870526
3. Ferreira LG, Faria RX (2016) TRPing on the pore phenomenon: what do we know about transient receptor potential ion channel-related pore dilation up to now? J Bioenerg Biomembr 48:1-12. doi:10.1007/s10863-015-9634-8
4. Georgi MI, Rosendahl J, Ernst F, Gunzel D, Aschenbach JR, Martens H, Stumpff F (2014) Epithelia of the ovine and bovine forestomach express basolateral maxi-anion channels permeable to the anions of short-chain fatty acids. Pflugers Arch 466:1689-1712. doi:10.1007/s00424-013-1386-x
5. Giulbudagian M, Yealland G, Hönzke S, Edlich A, Geisendörfer B, Kleuser B, Hedtrich S, Calderón M (2018) Breaking the Barrier - Potent Anti-Inflammatory Activity following Efficient Topical Delivery of Etanercept using Thermoresponsive Nanogels. Theranostics 8:450-463. doi:10.7150/thno.21668
6. Hille B (2001) Ion Channels of Excitable Membranes. 3rd edn. Sinauer Associates, Sunderland, Mass. doi:10.4236/jbm.2020.82005
7. Liebe F, Liebe H, Kaessmeyer S, Sponder G, Stumpff F (2020) The TRPV3 channel of the bovine rumen: localization and functional characterization of a protein relevant for ruminal ammonia transport. Pflügers Archiv - European Journal of Physiology 472:693-710. doi:10.1007/s00424-020-02393-2
8. Ochoa-de la Paz LD, Espino-Saldana AE, Arellano-Ostoa R, Reyes JP, Miledi R, Martinez-Torres A (2013) Characterization of an outward rectifying chloride current of Xenopus tropicalis oocytes. Biochim Biophys Acta 1828:1743-1753. doi:10.1016/j.bbamem.2013.03.013
9. Reifarth FW, Amasheh S, Clauss W, Weber W (1997) The Ca2+-inactivated Cl- channel at work: selectivity, blocker kinetics and transport visualization. J Membr Biol 155:95-104. doi:10.1007/s002329900161
10. Schrapers KT, Sponder G, Liebe F, Liebe H, Stumpff F (2018) The bovine TRPV3 as a pathway for the uptake of Na+, Ca2+, and NH4+. PLoS One 13:e0193519. doi:10.1371/journal.pone.0193519
11. Vitzthum C, Stein L, Brunner N, Knittel R, Fallier-Becker P, Amasheh S (2019) Xenopus oocytes as a heterologous expression system for analysis of tight junction proteins. Federation of American Societies for Experimental Biology Journal 33:5312-5319. doi:10.1096/fj.201801451RR
12. Weber W (1999) Ion currents of Xenopus laevis oocytes: state of the art. Biochim Biophys Acta 1421:213-233. doi:10.1016/s0005-2736(99)00135-2

4

Liebe *et al.* 2020

Pflügers Archiv - European Journal of Physiology (2020) 472:693–710
https://doi.org/10.1007/s00424-020-02393-2

ION CHANNELS, RECEPTORS AND TRANSPORTERS

The TRPV3 channel of the bovine rumen: localization and functional characterization of a protein relevant for ruminal ammonia transport

Franziska Liebe[1] · Hendrik Liebe[1,2] · Sabine Kaessmeyer[3] · Gerhard Sponder[1] · Friederike Stumpff[1]

Received: 13 February 2020 / Revised: 31 March 2020 / Accepted: 6 May 2020 / Published online: 26 May 2020

Abstract

Large quantities of ammonia (NH_3 or NH_4^+) are absorbed from the gut, associated with encephalitis in hepatic disease, poor protein efficiency in livestock, and emissions of nitrogenous climate gasses. Identifying the transport mechanisms appears urgent. Recent functional and mRNA data suggest that absorption of ammonia from the forestomach of cattle may involve TRPV3 channels. The purpose of the present study was to sequence the bovine homologue of *TRPV3* (*bTRPV3*), localize the protein in ruminal tissue, and confirm transport of NH_4^+. After sequencing, bTRPV3 was overexpressed in HEK-293 cells and *Xenopus* oocytes. An antibody was selected via epitope screening and used to detect the protein in immunoblots of overexpressing cells and bovine rumen, revealing a signal of the predicted ~ 90 kDa. In rumen only, an additional ~ 60 kDa band appeared, which may represent a previously described bTRPV3 splice variant of equal length. Immunohistochemistry revealed staining from the ruminal *stratum basale* to *stratum granulosum*. Measurements with pH-sensitive microelectrodes showed that NH_4^+ acidifies *Xenopus* oocytes, with overexpression of bTRPV3 enhancing permeability to NH_4^+. Single-channel measurements revealed that *Xenopus* oocytes endogenously expressed small cation channels in addition to fourfold-larger channels only observed after expression of bTRPV3. Both endogenous and bTRPV3 channels conducted NH_4^+, Na^+, and K^+. We conclude that bTRPV3 is expressed by the ruminal epithelium on the protein level. In conjunction with data from previous studies, a role in the transport of Na^+, Ca^{2+}, and NH_4^+ emerges. Consequences for calcium homeostasis, ruminal pH, and nitrogen efficiency in cattle are discussed.

Keywords TRPV3 · Ammonia transport · Microelectrode · Climate gas · Rumen · *Xenopus* oocyte

Introduction

Ammonia in its two forms (NH_3 and NH_4^+) plays a central role in the interconversion of amino acids for protein metabolism, requiring rapid transport across membranes of cells and organelles. Surprisingly, little information is currently available concerning the transport of this metabolite by epithelia of the gut. Given that more than half of the ammonia found in peripheral blood is of gastrointestinal origin [31], understanding the mechanisms responsible for ammonia absorption might help with a better management of hyperammonemia in patients suffering from hepatic disease. However, the most urgent task may be to find strategies to reduce the vast amounts of nitrogen that are excreted by livestock worldwide, leading to human respiratory problems, eutrophication, and climate change [28]. Livestock production represents the largest anthropogenic source of the highly potent climate gas N_2O [56]. The nitrogen in this compound originates from dietary protein that is broken down to ammonia in the gut. This ammonia can be utilized for microbial protein synthesis, but unfortunately, the larger fraction of this toxin is absorbed, converted to urea, and excreted into the environment with disastrous consequences.

So why are the losses of ammonia from the gut so high? As recently as two decades ago, it was widely believed that

Franziska Liebe and Hendrik Liebe contributed equally to this work.

A Commentary to this article is available online at https://doi.org/10.1007/s00424-020-02394-1

Electronic supplementary material The online version of this article (https://doi.org/10.1007/s00424-020-02393-2) contains supplementary material, which is available to authorized users.

✉ Friederike Stumpff
stumpff@zedat.fu-berlin.de

[1] Institute of Veterinary Physiology, Freie Universität Berlin, Oertzenweg 19b, 14163 Berlin, Germany

[2] Department of Biology, Chemistry, and Pharmacy, Freie Universität Berlin, Arnimallee 22, 14195 Berlin, Germany

[3] Institute of Veterinary Anatomy, Freie Universität Berlin, Koserstraße 20, 14195 Berlin, Germany

epithelial ammonia transport occurred by simple diffusion of the uncharged form (NH_3) through the lipid bilayer of the cell membrane [57]. However, like water, NH_3 has a strong dipole moment and it has become increasingly clear that proteins are required to mediate transport. In the collecting duct of the kidney, it has been established that aquaporins are required for the transport of water. Likewise, Rh-glycoproteins are necessary to mediate ammonia transport. The apical ammonia transporter RhCG is considered to be highly selective for NH_3 while the substrate (NH_3 or NH_4^+) of the basolateral RhBG has not yet been clarified [12, 24, 35]. Far less information is available on intestinal absorption of ammonia. In analogy to the collecting duct, electroneutral apical uptake of NH_3 via RhCG and basolateral efflux via RhBG has been proposed for the intestine of mice [25] or toadfish [10]. Conversely, exchange of NH_4^+ with H^+ via sodium-proton exchange (NHE) has been suggested in rat colon [13]. In pig caecum and trout intestine, NH_4^+ is taken up in an unclear, electrogenic mechanism [46, 52].

Comparatively, more information is available concerning ammonia transport across the forestomach of ruminants. The interest is old [22, 33] and triggered by the low protein efficiency of cattle [20, 26]. In the largest of the forestomachs, the rumen, the cellulose-rich diet is broken up into digestible components by resident microbial populations. Microbial protein is produced from any nitrogen source available, including ammonia and urea [1, 43]. Unfortunately, large quantities of ammonia are absorbed from the rumen before they can be utilized. However, the ruminal epithelium expresses transport proteins through which urea can reenter the rumen and serve as a source of nitrogen for microbial protein synthesis [2, 43, 50, 65]. Since this protein can be fully digested in the following parts of the gastrointestinal tract, this recycling of nitrogen allows ruminants to subsist on low-grade, poorly digestible fodder while yielding milk and meat. Problems emerge when cattle are fed large quantities of high-quality protein required for maximal yields in industrial farming. In this scenario, blood urea levels rise and nitrogen recycling leads to secretion of some 10 mol day^{-1} of urea into the rumen, where it is degraded to ammonia, reabsorbed, and again converted to urea and resecreted, requiring ~ 40 mol day^{-1} of ATP for hepatic detoxification. Despite recycling, up to 70% of dietary nitrogen is eventually excreted into the environment with urine and feces [20].

Clearly, a clarification of the mechanism responsible for the high efflux of ammonia from the rumen is overdue. The expression profile in the ovine rumen does not appear to support the involvement of either RhCG or RhCB [65]. Systematic studies of ruminal transport of ammonia have established that electroneutral transport of NH_3 is predominant at an alkaline pH of 7.4. At a physiological pH of 6.4, transport primarily involves electrogenic uptake of NH_4^+ [3, 4, 7, 22, 40]. Thus, studies with microelectrodes and in Ussing chambers have shown that exposure to NH_4^+ depolarizes both the apical membrane and the intact ruminal epithelium in toto with acidification of the cytosolic space [32, 45], resulting in stimulation of NHE [3, 4].

Based on both functional evidence and mRNA data, the bovine homologue of the non-selective transient receptor potential cation channel, subfamily V, member 3 (bTRPV3) has recently emerged as a candidate for uptake of cations from the rumen, including NH_4^+ and Ca^{2+} [40, 45]. Like most other members of the large family of TRP channels [39], both the human and the bovine homologue of TRPV3 are known to be permeable to a number of monovalent and divalent cations, including Na^+ and Ca^{2+} [48, 63]. Given that certain plant-derived compounds modulate the activity of TRPV3 [55], this has implications both for the development of new drugs and for new feeding strategies [8]. Ruminants absorb considerable amounts of Ca^{2+} from the rumen to meet the high demand involved in milk production [61]. Based on electrophysiological data, a ruminal channel for Ca^{2+} has long been postulated [27, 62], although the typical epithelial calcium channels TRPV5 and TRPV6 are not expressed in the ruminal epithelium [45, 60]. Intriguingly, TRPV3 channels are activated by intracellular protons [36], which may explain the well-documented stimulatory effects of short-chain fatty acids on ruminal calcium uptake [61].

In contrast to a wealth of data concerning the permeability of TRPV3 to Ca^{2+} [36, 39, 55, 63], the permeability of TRP channels in general and TRPV3 in particular to NH_4^+ had never been investigated before our recent patch-clamp study of HEK-293 cells [48]. One goal of the present study was to confirm transport of NH_4^+ by bTRPV3 using a different expression system (*Xenopus* oocytes) and a different method (pH-sensitive microelectrodes), both as established in studies of other ammonia transporters [12, 24]. Furthermore, a confirmed sequence and detection on the protein level are lacking. The major aim of the current study was therefore to properly sequence the bTRPV3, to establish a suitable antibody, and finally to localize the channel in the ruminal epithelium.

Materials and methods

Animal welfare

The maintenance and surgical treatment of *Xenopus laevis* frogs was in accordance with the guidelines of German legislation, with approval by the animal welfare officer for the Freie Universität Berlin and under the governance of the Berlin Veterinary Health Inspectorate (Landesamt für Gesundheit und Soziales Berlin, permit G0025/16).

Bovine ruminal epithelium was obtained from Holstein-Friesian cattle slaughtered for meat production in a commercial abattoir (Beelitz, Germany), also under control of the German authorities.

Ruminal tissue

Pieces of the bovine rumen were removed about 10 min after death and immediately stripped, rinsed twice with PBS, and dissected into pieces of 1 to 2 cm^2. Samples were shock-frozen in liquid nitrogen and stored at − 80 °C or transferred into formaldehyde solution (Roti®-Histofix 4%, Carl Roth, Karlsruhe, Germany). Unless indicated otherwise, only ventral rumen was used as the locus with maximal absorptive capacity.

Sequencing and cloning of *bTRPV3*

Shock-frozen bovine ruminal epithelium was used for mRNA extraction with subsequent reverse transcription to cDNA, which was used to sequence the bovine representative of the *TRPV3* channel (*bTRPV3*). The construct was tagged with a streptavidin (Strep) tag (ShineGene Bio-Technologies Inc., Shanghai, China), which was placed at the N terminus to prevent possible interference with a C-terminal PDZ binding motif found in some TRP channels [41]. This Strep-*bTRPV3* construct was then subcloned into pIRES2-*AcGFP*1 (Takara BioEurope, Saint-Germain-en-Laye, France) or into pcDNA5/TO (Life Technologies, Darmstadt, Germany) as described previously [48]. Cells successfully transfected with Strep-*bTRPV3*-pIRES2-*AcGFP*1 showed green fluorescence.

For expression of *bTRPV3* in *Xenopus* oocytes, the restriction enzymes PasI and XbaI were used to replace the last 716 bp of the Strep-*bTRPV3*-pcDNA5/TO construct with a 713-bp fragment lacking the stop codon. The resulting construct was then cut out from Strep-*bTRPV3*-pcDNA5/TO and subcloned into pGEM-HE-MCS (kindly donated by Prof. Blanche Schwappach, Georg-August-Universität, Göttingen, Germany) via the restriction sites HindIII and XbaI. The restriction enzyme MluI was used for linearization and RiboMAX Large Scale RNA Production System-T7 (Promega, Mannheim, Germany) was used for in vitro transcription to cRNA according to the manufacturer's instructions.

Harvesting and injection of *Xenopus* oocytes

Xenopus laevis oocytes were obtained and prepared as described by Vitzthum et al. [54] After surgical removal, ovarian lobes were placed in oocyte Ringer's solution (180 mOsm kg^{-1} adjusted with D-mannitol) [54], shaken mechanically for 90 min, and transferred into calcium-free oocyte Ringer's solution for 10 min. Defolliculated stage V–VI oocytes were stored in oocyte culture solution at 16 °C until the following day, when they were injected with 50 nL RNAse free water containing 15–30 ng of *bTRPV3*-Strep cRNA (WPI Nanoliter 2010, World Precision Instruments, Sarasota, FL, USA). Control oocytes were injected with 50 nL RNAse free water. Injected oocytes were incubated for at least 3 days in modified low-sodium oocyte culture solution before use in experiments (in mmol L^{-1}: 80 N-methyl-D-glucamine chloride (NMDGCl), 5 NaCl, 5 4-(2-hydroxyethyl)-1-piperazineethanesulfonic acid (HEPES), 2.5 2-Oxopropanoic acid, 1 KCl, 1 $CaCl_2$, 1 $MgCl_2$, 50 units mL^{-1} penicillin, 0.05 mg mL^{-1} streptomycin, pH 7.4 adjusted with tris (hydroxymethyl) aminomethane (Tris), 223 mOsm kg^{-1} adjusted with D-mannitol).

Cell culture and transfection of HEK-293 cells

HEK-293 cells (DSMZ, Braunschweig, Germany, 2016/06/08) were cultivated at 37 °C in Dulbecco's modified Eagle's medium (FG 0445) supplemented with 10% fetal bovine serum and 100 units mL^{-1} of penicillin and streptomycin (all Biochrom, Berlin, Germany). Polyethylenimine (PEI, linear, MW 25000, Polysciences, Inc., Hirschberg an der Bergstrasse, Germany) was used to transiently transfect the cells with the Strep-*bTRPV3*-pIRES2-*AcGFP*1 vector or with the empty pIRES2-*AcGFP*1 vector as control (http://www.cytographica.com/lab/PEItransfect.html). Experiments were performed 48 h after transfection.

Immunoblotting

Both the solvents and the samples were cooled throughout the experiments to minimize protein degradation.

Bovine rumen

RIPA buffer (500 μL; in mmol L^{-1}: 25 HEPES, 2 EDTA, 25 NaF, protease inhibitor (cOmplete™, mini, Roche, Basel, Switzerland), 1% sodium dodecyl sulfate (SDS)) was added to the defrosted tissue (200 mg) together with two metal beads. The tissue was homogenized in a mixer mill (30 × 2 min; MM 200, Retsch GmbH, Haan, Germany), followed by a clarifying spin (15 min, 20,000 g, 4 °C). The supernatant containing the protein was transferred into a new tube.

Xenopus oocytes

After the removal of the culture medium, ten oocytes of each transfected group were lysed mechanically in oocyte lysis buffer (500 μL; in mmol L^{-1}: 5 $MgCl_2$, 5 NaH_2PO_4, 1 EDTA, 80 sucrose, pH 7.4 (Tris)). The suspension was centrifuged (200 rpm, 10 min, 4 °C) and the supernatant was transferred to a new tube, after which the centrifugation step was repeated. The supernatant was then centrifuged a third time (13,000 rpm, 40 min, 4 °C). The precipitate was suspended in fresh oocyte lysis buffer (40 μL).

HEK-293 cells

After washing with phosphate-buffered saline (PBS), HEK-293 cells were harvested mechanically by scraping in PBS. After centrifugation (500 g, 5 min), the cell pellet was suspended in PBS (1 mL) and transferred into a new tube. PBS was removed via centrifugation (700 g, 4 min) and the cell pellet was suspended in RIPA buffer (100 μL). Lysis was performed for 30 min with gentle agitation and 5 min in an ultrasound bath, followed by a clarifying spin (20 min, 15,000 g), and supernatant with protein was stored at − 80 °C.

The protein concentration of each suspension was determined using the Pierce™ 660 nm protein assay kit (Thermo Fischer Scientific, Waltham, MA, USA). Proteins were denatured in SDS sample loading buffer (10%) and electrophoresed on polyacrylamide gels (7.5%, SDS-PAGE) in Tris-Glycine buffer (0.1% SDS). Electroblotting was performed onto polyvinylidene difluoride membranes (PVDF, Immun-Blot®, Bio-Rad Laboratories GmbH, Munich, Germany) in Tris-Glycine buffer (0.3% SDS, 20% methanol, 4 °C).

Antibodies against bTRPV3

After the first attempts to stain ruminal tissues with a commercial antibody against the human homologue (ab63148, abcam, Cambridge, UK) had failed, epitopes of several commercial antibodies against the human TRPV3 channel were aligned with the sequence of the bovine homologue. A primary mouse antibody directed against an epitope (AA 458-474) from the first extracellular loop of the human TRPV3 channel was selected as the most promising candidate and used at a dilution of 1:3000 (ID: ABIN863127, antibodies-online GmbH, Aachen, Germany). The human epitope (SYYRPREEEA**I**PHPLA) showed almost complete homology with the bovine sequence (SYYRPREEEA**L**PHPLA). For control purposes, a primary mouse antibody directed against the Strep-tag of the clones (1:2500; ID: 34850, Qiagen, Hilden, Germany) was used. Horseradish peroxidase conjugated secondary antibody (anti-mouse, 1:1000; Cell Signaling Technology, Frankfurt, Germany) was used to detect the primary antibodies on the membrane. Proteins were visualized by use of the Clarity Western ECL Substrate (Bio-Rad Laboratories GmbH, Munich, Germany).

These experiments yielded an additional prominent band below the expected molecular weight of full-length bTRPV3. To test for binding via the domains specific for the target epitope [9], additional immunoblots with primary TRPV3 antibody were performed in the presence and absence of the peptide used to produce the TRPV3 antibody (referred to as specific immunizing peptide or SIP, smc 334d_peptide, antibodies online GmbH, Aachen, Germany) and a control peptide (CP, anti SLC41A3, Santa Cruz Biotechnology, Heidelberg, Germany), all at 1:1000. Exposure time was optimized via the ImageLab software (BioRad), which was also used to calculate the relative quantities (see Supplement).

Immunohistological staining

All preparation steps were performed as described in detail in the Supplement or as described in [51]. Samples from both the ventral and the dorsal rumen were stained with primary antibody diluted in goat serum (5% in PBS; PAN-Biotech GmbH, Aidenbach, Germany) according to Table 1 (4 °C, overnight). Secondary antibody controls were performed with goat serum (5% in PBS) only. To test for specificity of binding, adjacent slices from the same sample of ruminal tissue were incubated in parallel either with the primary mouse TRPV3 antibody only or with a mix of this antibody and its corresponding antigenic peptide (SIP) (Table 1). Images were obtained using a confocal laser-scanning microscope (LSM 510, Axiovert200M, Zeiss, Jena, Germany) at 405, 488, and 543 nm.

Double-barrelled pH-sensitive microelectrode measurements

pH-sensitive microelectrodes were prepared as described in detail previously [2] and in the Supplement. The potential difference between the pH-sensitive barrel and the reference barrel was used to determine the intracellular pH (pH_i), while the potential difference between the reference barrel and the ground signal from the bath corresponded to the membrane potential (U_{mem}). Electrodes were calibrated before and after each measurement (23 °C). After each measurement of an oocyte expressing bTRPV3, a control oocyte was measured.

All microelectrode solutions were adjusted to an osmolality of 223 mOsm kg^{-1} using D-mannitol, and were adjusted to pH 7.4 (Tris) and contained (in mmol L^{-1}) 5 HEPES, 1 $CaCl_2$, 1 $MgCl_2$, and 1 KCl. The following solutions were used (in mmol L^{-1}): NaCl (85 NaCl), KCl (81 KCl, 5 NaCl), NaGlu (80 sodium D-gluconate (NaGlu), 5 NaCl, 10 NMDGCl), NH_4Cl (5 NaCl, 80 NH_4Cl), NH_4Cl-EDTA (5 NaCl, 80 NH_4Cl, 5 NMDGCl, no $CaCl_2$ and no $MgCl_2$), NMDGCl (80 NMDGCl, 5 NaCl), and NaCl-6.4 (85 NaCl, 5 2-(*N*-morpholino) ethanesulfonic acid (MES), pH 6.4, no HEPES).

Inside-out patch-clamp experiments

Single-channel experiments were performed as previously described [23, 48] in a continuously perfused bath chamber at 23 °C. Pipettes were pulled with a DMZ Universal Puller (Zeitz Instruments, Munich, Germany). Currents were recorded by an EPC 9 patch-clamp amplifier (HEKA Electronic, Lambrecht, Germany) using the Patchmaster Software (HEKA Electronic). Data were sampled at 10 kHz and filtered at 250 Hz. Currents were clamped at the potentials − 60 to +

Table 1 Primary and secondary antibodies used for immunohistochemical staining

	HEK-293 cells	Ruminal tissue	*Xenopus* oocytes
Primary antibody 1	mouse TRPV3 antibody (1:1000)[§]	mouse TRPV3 antibody (1:1000)[§]	mouse TRPV3 antibody (1:1000) [§]
Primary antibody 2		rabbit claudin-4 antibody (1:250)[&]	
Secondary antibody 1	594 goat anti-mouse IgG (1:1000)*	488 goat anti-mouse IgG (1:1000)*	488 goat anti-mouse IgG (1:1000)*
Secondary antibody 2		594 goat anti-rabbit IgG (1:1000)*	
Immunizing Peptide		smc-334d_peptide (1:330)[#]	

[§] ABIN863127, antibodies-online GmbH, Aachen, Germany

*Alexa Fluor®, Thermo Fischer Scientific, Waltham, MA, USA

[&] AB53156, Abcam, Cambridge, UK

[#] smc-334d_peptide, antibodies-online GmbH, Aachen, Germany

60 mV in 10 mV steps for 6 s each. After each oocyte over-expressing bTRPV3, a control oocyte was measured.

All single-channel patch-clamp solutions were adjusted to an osmolality of 223 mOsm kg^{-1} using D-mannitol and had a pH of 7.4 adjusted with Tris and HCl. Initially, oocytes were incubated (5–10 min) in oocyte Ringer (in mmol L^{-1}: 96 NaCl, 5 HEPES, 2.5 2-Oxopropanoic acid, 1 KCl, 1 $CaCl_2$, 1 $MgCl_2$). Oocytes were then placed in a cell culture dish under a dissecting microscope and D-mannitol was added incrementally until the vitelline membrane began to dissociate so that it could be manually removed with sharpened forceps. Care was taken not to damage the plasma membrane. After allowing the stripped oocyte to settle on the glass bottom of a conventional flow chamber over an inverted microscope (Axiovert.A1, Zeiss), a seal was formed and a membrane patch excised and measured in the usual manner. Solutions were based on those used by Doerner et al. [18] and contained (in mmol L^{-1}) 20 HEPES, 5 CsCl, 1 ethylene glycol-bis(β-aminoethyl ether)-*N*,*N*,*N*′,*N*′-tetraacetic acid (EGTA), and 1 KCl. The pipette and the NH_4Cl bath solution additionally contained NH_4Cl (96 mmol·L^{-1}). In NaCl, KCl, and NMDGCl bath solutions, NH_4^+ was replaced by the same amount of Na^+, K^+, or $NMDG^+$ respectively. NH_4Glu bath solution substituted 81 mmol L^{-1} NH_4Cl with NH_4-gluconate.

Data analysis

Data processing was performed using Igor Pro 6.2.2.2 (WaveMetrics Inc., Lake Oswego, USA) and Sigma Plot 11.0 (Systat Software 11.0, Erkrath, Germany). All potentials were corrected for liquid junction potential using the JPCalcWin software (School of Medical Sciences, Sydney, Australia) [6].

In the microelectrode experiments, relative permeability ratios were calculated according to standard methods from the membrane potentials using Goldman-Hodgkin-Katz theory (GHK) [39, 45].

$$U_A - U_B \approx - \frac{R \cdot T}{F} \cdot \ln\left(\frac{P_A \cdot [A]_o}{P_B \cdot [B]_o}\right) \quad (1)$$

Here, U_x designates the membrane potential in solution X, F is the Faraday constant, and T is the absolute temperature, while P_x designates the permeability, $[X]_i$ the inside, and $[X]_o$ the outside concentration of ion X. Note that this equation assumes that the leak current is low as are the contributions of extracellular K^+ and intracellular Cl^-.

Single-channel data were analyzed as described previously [23, 48] and in the Supplement. To gain an overview of the conductances determined from the analysis of different patches, data were plotted in amplitude histograms. For this, data from all patches were collected, after which the conductance range was divided into a number of equidistant bins, which were plotted on the horizontal axis. The vertical axis gives the number of patches with a conductance falling into the corresponding bin on the *X*-axis. Note that the bars in these histograms do not correspond to discrete conductance steps.

Statistical analysis

All data were statistically evaluated using SigmaStat 11.0. After testing for normality using the Shapiro-Wilk test, comparisons between two groups were performed using the Mann-Whitney rank sum test. In cases where different solutions were applied consecutively, differences were evaluated using ANOVA on ranks followed by the Student-Newman-Keuls method for multiple comparisons or the Wilcoxon

signed-rank test for pairwise comparisons. A significant difference was assumed if $p \leq 0.05$.

Obtained values were given as means ± SEM, rounding as recommended by the DIN 1333 [17]. The *n* value represents the amount of individual experiments whereas *n*/*N* refers to the number of experiments (*n*) from different animals (*N*).

Results

Immunohistochemical detection of bTRPV3 in the ruminal epithelium

In a first step, the bovine gene for *TRPV3* was sequenced from ruminal tissue (GenBank: MF063038.1; https://www.ncbi.nlm.nih.gov/nuccore/1220516332). The resulting sequence of 2397 base pairs (bp) showed ~ 90% homology with human *TRPV3*. Via epitope screening, a promising TRPV3 antibody was selected and its suitability controlled in the two expression systems *Xenopus laevis* oocytes and HEK-293 cells. Successful bTRPV3 expression was confirmed by an immunoblot with detection of the Strep-tag (*n* = 8, Fig. 1a), demonstrating a band at the predicted molecular weight of bTRPV3 (~ 90 kDa) in overexpressing cells, but not in controls. In a second step, the TRPV3 antibody was tested in both expression systems and in protein samples from bovine rumen (*n*/*N* = 7/5, Fig. 1b). Both overexpressing and ruminal samples showed a band at ~ 90 kDa. Controls showed no staining. In protein from native ruminal epithelium, the TRPV3 antibody stained a second, stronger band at ~ 60 kDa. The blot was repeated in the absence and presence of the specific peptide (SIP) used to produce the TRPV3 antibody. Co-incubation with SIP markedly reduced staining intensity, proving binding of the TRPV3 antibody via the domains specific for the target epitope (see methods and the Supplement).

For imaging, HEK-293 cells (*n* = 2, Fig. 2) and oocytes (*N* = 3, Fig. 3) were stained with the TRPV3 antibody. In both cases, the cell membrane showed staining for bTRPV3 in overexpressing cells, but not in cells treated with the secondary antibody only or in control cells. Finally, native bovine ruminal tissue from four different animals was stained using the TRPV3 antibody (Fig. 4). Epithelial layers from the *stratum basale* to the *stratum granulosum* were strongly stained, with detection both in the cellular membrane and in the cytosol. In addition, a number of cells within the lower parts of the *stratum corneum* showed staining. Conversely, staining of structures within the subepithelial layers was weak. Treatment with the secondary antibody only did not result in staining. Co-incubation with SIP strongly reduced staining (Fig. 4e, f).

Experiments with pH-sensitive microelectrodes

Since *Xenopus* oocytes are an established system for studying ammonia transport [12, 24], the intracellular pH (pH_i) and the membrane potential (U_{mem}) of oocytes expressing bTRPV3

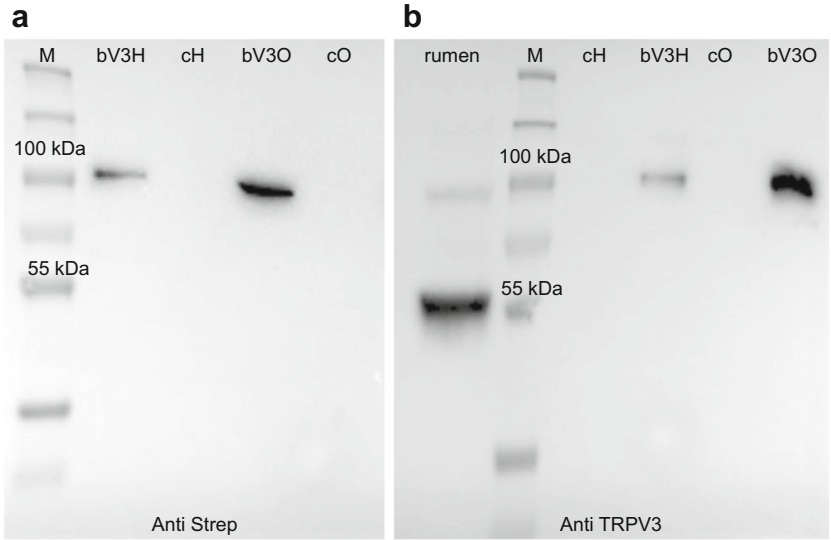

Fig. 1 Comparative immunoblots to validate specific binding of the TRPV3 antibody. **a** Identification via Strep antibody: the marker lane (M) is followed by HEK-293 cells transfected with the Strep-tagged bTRPV3 construct (bV3H) or the control vector (cH), followed by oocytes injected with Strep-tagged bTRPV3 (bV3O) or water (cO). A strong band can be seen at ~ 90 kDa in the overexpressing samples but not in controls, representing Strep-tagged bTRPV3. **b** Identification via TRPV3 antibody: the four lanes to the right of the marker lane (M) represent bTRPV3 and controls as in **a**. On the left-hand side, bovine ruminal protein (rumen) has been added, showing a band at about ~ 90 kDa. A second, more prominent band is observed at ~ 60 kDa. (protein loading: HEK-293 0.02 μg, oocytes 0.20 μg, rumen 50 μg)

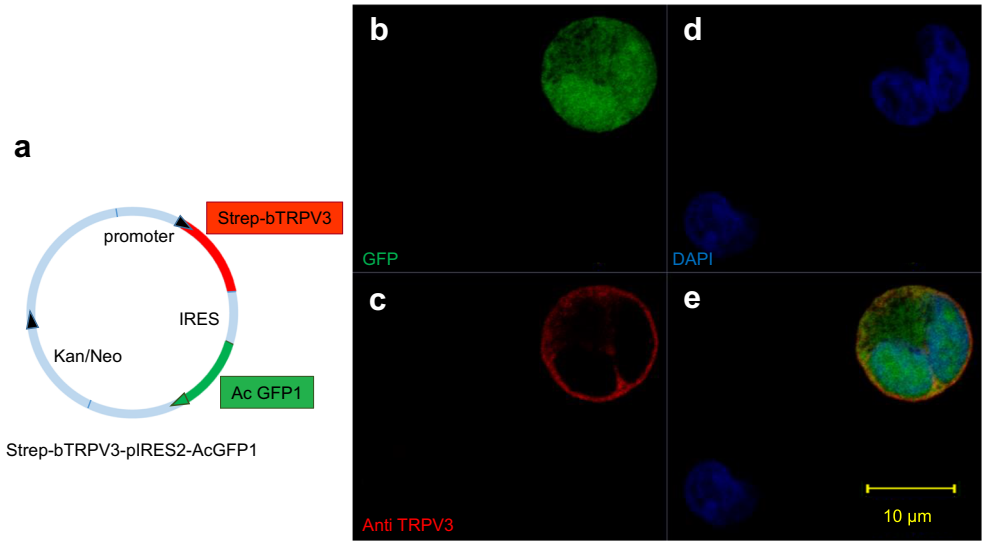

Fig. 2 Immunohistological staining of overexpressing bTRPV3 HEK-293 cells. **a** Vector used for transfection. The *bTRPV3* gene is fused to a Strep-tag, but not to green fluorescent protein (GFP). **b** Immunohistological staining reveals successful expression of cytosolic GFP. **c** Staining with the TRPV3 antibody (red) shows expression in the cellular membrane. **d** All cell nuclei were stained with DAPI (blue). **e** Overlay of **b**, **c**, and **d**. The cell in the top right-hand corner is in the process of division with both halves expressing bTRPV3 and GFP. The cell in the lower left-hand corner was not successfully transfected

and controls were investigated using pH-sensitive double-barrelled microelectrodes.

In a first set of screening experiments on oocytes, the effect of a replacement of bath Na^+ by K^+, NH_4^+, and $NMDG^+$ was investigated, as well as the effect of a replacement of Cl^- by gluconate (Glu^-). All successfully impaled bTRPV3 oocytes responded to the application of KCl solution with a depolarization (from − 20 ± 4 mV to − 12 ± 4 mV, $n/N = 6/1$, $p = 0.006$) with recovery to − 18 ± 3 mV (Fig. 5 a and b). Responses to Glu^- were variable, with little impact on U_{mem} in three of the six oocytes studied (Fig. 5a). The other three oocytes were depolarized by $\Delta U_{mem} = 14 \pm 4$ mV (Fig. 5b), reflecting expression of Cl^- channels [38, 42]. However, overall, effect of Glu^- did not pass testing for significance (p = 0.6), so that U_{mem} appears to be primarily determined by the cation conductances:

$$U_{mem} = \frac{R \cdot T}{F} \cdot \ln\left(\frac{P_{Na} \cdot [Na^+]_o + P_K \cdot [K^+]_o}{P_{Na} \cdot [Na^+]_i + P_K \cdot [K^+]_i}\right) \approx \frac{R \cdot T}{F} \cdot \ln\left(\frac{P_{Na} \cdot [Na^+]_o}{P_K \cdot [K^+]_i}\right) \quad (2)$$

Mean pH_i was not visibly affected by these solution changes, but rose continuously from 7.39 ± 0.12 after impalement to 7.61 ± 0.10 after washout of Glu^- (p = 0.07). Subsequent application of NH_4Cl solution resulted in a rapid depolarization of all bTRPV3 oocytes studied (− 4.0 ± 2.2 mV, p = 0.008) with a highly significant pH_i decline to 6.22 ± 0.18

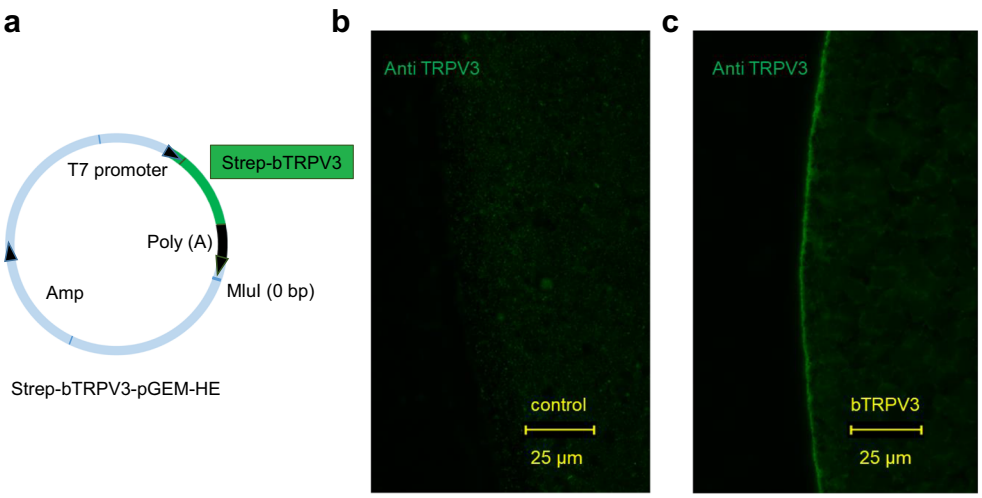

Fig. 3 Immunohistological staining of bTRPV3 in *Xenopus* oocytes. **a** pGEM construct containing a Strep-tagged *bTRPV3* sequence for *in vitro* transcription to cRNA. **b** and **c** Immunohistological staining of two oocytes 4 days after injection of **b** water or **c** *bTRPV3* cRNA. Cells were stained with TRPV3 antibody and investigated using the same microscope settings. Only overexpressing oocytes **c** show staining of the cellular membrane with the TRPV3 antibody

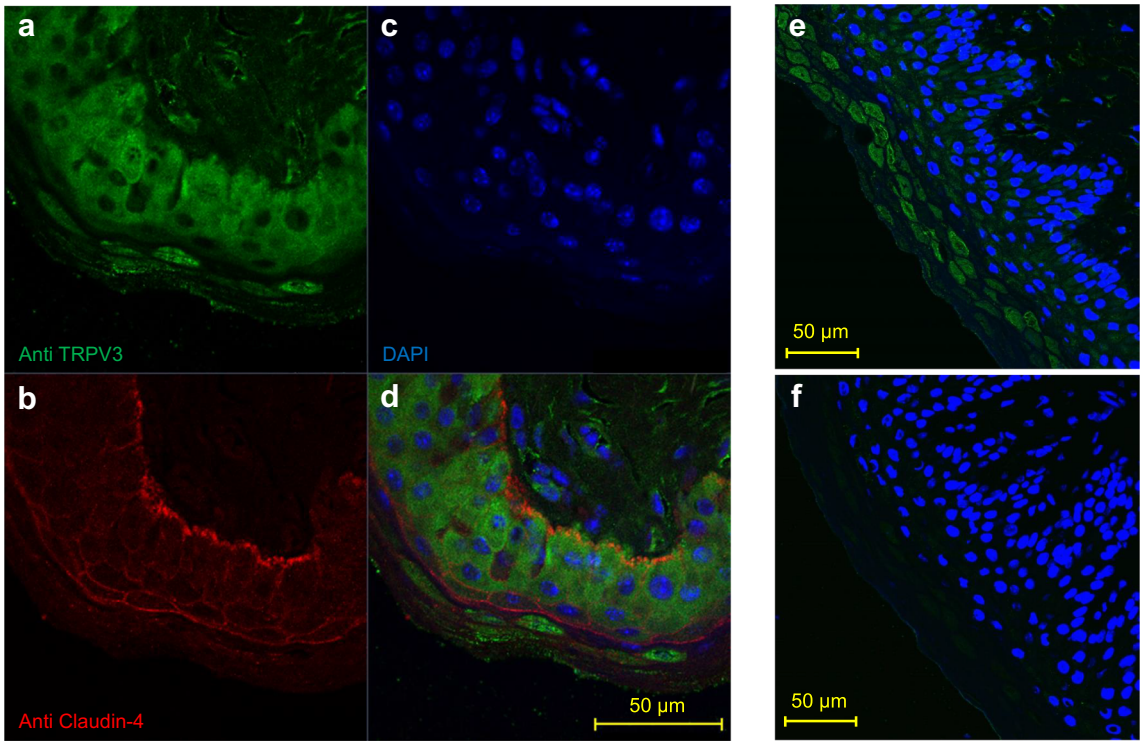

Fig. 4 Immunohistological staining of native ruminal epithelium. **a** Staining of ventral rumen with the antibody against bTRPV3 (green), demonstrating strong staining of all epithelial layers. Although staining of peripheral structures (most likely representing the cellular membrane) could be clearly seen, cytosolic staining was intense throughout. **b** Claudin-4 (red) forms junctions between the cells. **c** Cell nuclei are shown in blue (DAPI). **d** Overlay of **a**, **b**, and **c**. **e** Staining of dorsal rumen with the bTRPV3 antibody and DAPI. **f** Using the same rumen sample and same microscope settings as in **e**, treatment with both the TRPV3 antibody and its immunizing peptide (SIP) prevented most of the staining for bTRPV3

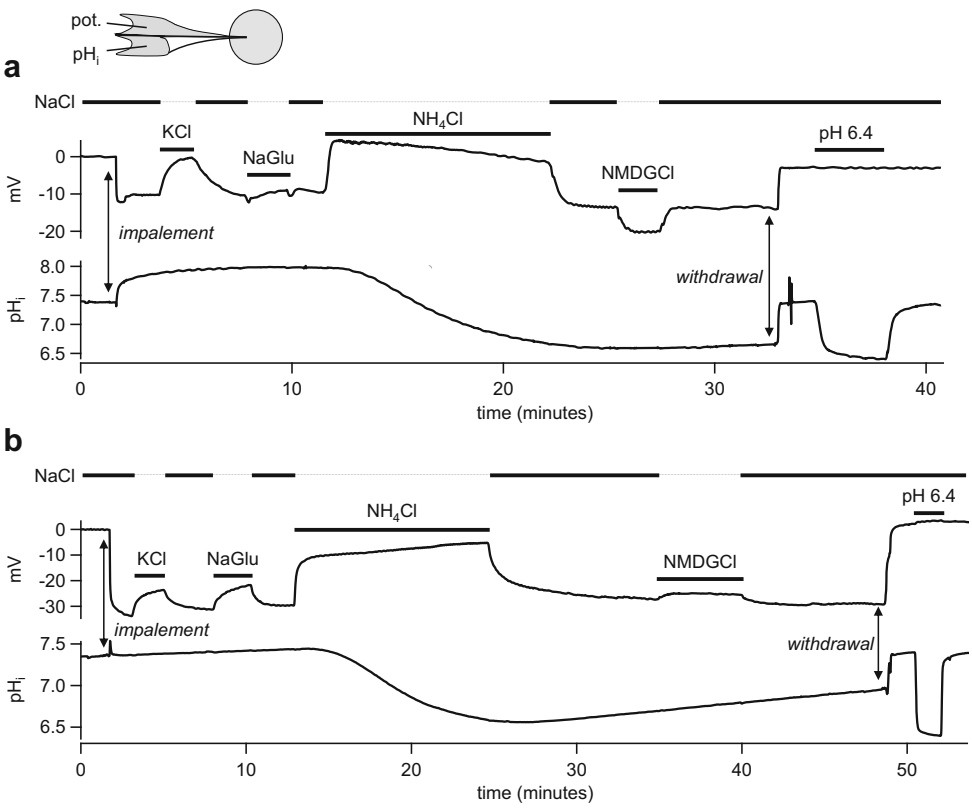

Fig. 5 Original recordings of two oocytes expressing bTRPV3 measured via pH-sensitive, double-barreled microelectrodes. All oocytes uniformly responded to KCl and NH_4Cl with a rapid and reversible depolarization. Only application of NH_4Cl induced a strong and reversible acidification. Responses to NaGlu and NMDGCl varied, as shown in **a** and **b** and discussed in the text

($p = 0.006$). Return to NaCl solution resulted in an immediate repolarization of all oocytes to − 17 ± 3 mV. Intracellular pH recovered more gradually, reaching 6.27 ± 0.14 after 10 min. Replacement of Na^+ by $NMDG^+$ during the recovery phase had no impact on pH_i, but induced a strong reversible hyperpolarization in three oocytes (ΔU_{mem} = 10 ± 4 mV, Fig. 5a), reflecting reduced influx of cations. Unexpectedly, the three other bTRPV3 oocytes responded with a slight depolarization (ΔU_{mem} = 2.7 ± 0.3 mV, Fig. 5b). This may reflect induction of membrane leakage by high concentrations of $NMDG^+$ as described previously [38]. Due to converse reactions, the overall effect of $NMDG^+$ was not significant ($p = 0.5$). In seven control oocytes from the same frog, effects were not significantly different, although interestingly, six of them responded to $NMDG^+$ with a hyperpolarization.

In a second set of experiments, the effect of NH_4^+ was studied more rigidly in *Xenopus* oocytes from three animals, strictly alternating between bTRPV3 and control oocytes (Fig. 6 and Table 2). To assess leak currents, experiments started in an NMDGCl solution, in which bTRPV3 oocytes had a significantly lower U_{mem} than controls. This undoubtedly reflects higher efflux of K^+ through bTRPV3 channels, resulting in a lower resting potential. A slight continuous alkaline drift was observed. Replacement of $NMDG^+$ by Na^+ did not change this drift in pH_i, suggesting that any baseline activity of NHE was discrete. Addition of Na^+ resulted in a strong depolarization of all oocytes studied, with a potential jump significantly higher in the bTRPV3 group, but reaching the same end level as in the controls. According to GHK theory, this is to be expected if overexpression of bTRPV3 increases both the permeability to K^+ (i.e., K^+ efflux) and the permeability to Na^+ (i.e., Na^+ influx) by the same factor. While absolute currents should increase, the U_{mem} (Eq. 2) should remain roughly the same.

Application of NH_4^+ caused a further depolarization in both cell types. Relative to the potential in NMDGCl, the magnitude of depolarization was significantly higher in oocytes expressing bTRPV3, suggesting higher influx of NH_4^+. However, in absolute terms, the resulting U_{mem} in NH_4^+ was lower in bTRPV3 expressing oocytes, again reflecting higher K^+ efflux. From these potentials, relative permeability ratios can be determined that are given in Table 2, which showed that relative to $NMDG^+$, bTRPV3 expressing oocytes showed significantly higher conductances to both Na^+ and NH_4^+. In line with this, after application of NH_4^+, an acidification was observed in all oocytes that was significantly faster in bTRPV3 oocytes than in controls, suggesting a higher absolute influx of NH_4^+ ions. However, final

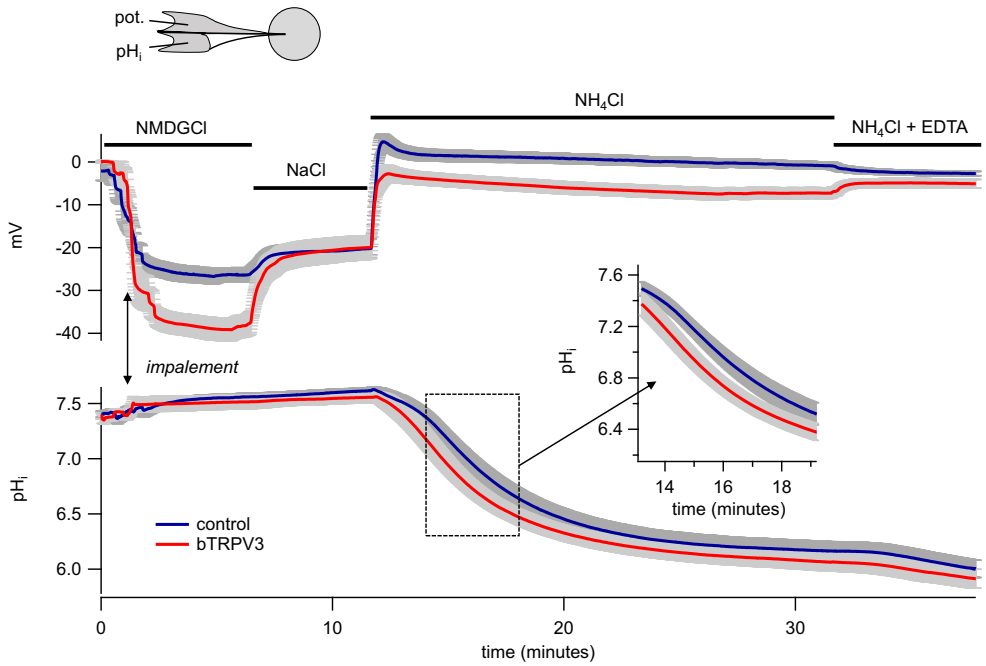

Fig. 6 Intracellular pH (pH_i) and membrane potential (in mV) of oocytes expressing bTRPV3 (n/N = 14/3) and control oocytes (n/N = 16/3). The blue traces show the means (± SEM in gray) of all control oocytes, the red traces the means (± SEM in gray) of all bTRPV3 oocytes. Overexpressing bTRPV3 oocytes had a significantly lower membrane potential in NMDGCl than controls, reflecting higher efflux of K^+ through bTRPV3 channels. Subsequent application of NaCl led to a stronger potential jump in oocytes expressing bTRPV3. The final potential was equal to that of controls, reflecting both a higher influx of Na^+ and a higher efflux of K^+. Relative to NMDGCl, NH_4Cl solution induced a stronger depolarization in bTRPV3 oocytes than in controls, reflecting higher influx of NH_4^+. However, the final potential was slightly lower in bTRPV3 oocytes, suggesting a relatively higher efflux of K^+ in bTRPV3 oocytes. Acidification after application of NH_4^+ was significantly faster in bTRPV3 oocytes. Ultimately, both systems reached similar pH_i. Note the inverse responses in membrane potential after a switch to a divalent cation-free NH_4Cl solution (EDTA) (details see text and Table 2)

Table 2 Membrane potential, intracellular pH and relative permeability ratios of bTRPV3 expressing (bV3, n/N = 14/3) and control *Xenopus* oocytes (ctrl, n/N = 16/3). Solutions were applied consecutively and values were measured 5 min after exposure unless indicated otherwise. Relative permeability ratios were calculated from Eq. 1 and contain contributions of leak currents. The last column gives the p values for differences between the two columns. Within columns, different superscripts indicate significant differences with $p < 0.05$

Membrane potential (mV)

	bTRPV3	control	p (bV3 vs. ctrl)
NMDGCl	-39.2 ± 2.6[a]	-27.2 ± 1.8[a]	0.001
NaCl	-20.1 ± 2.8[b]	-20.3 ± 2.2[b]	0.6
NH_4Cl (3.5 min)	-4.4 ± 1.5[d]	1.5 ± 1.4[c]	0.003
NH_4Cl (20 min)	-7.2 ± 1.3[c]	-0.9 ± 0.8[d]	≤0.001
NH_4Cl-EDTA	-5.0 ± 1.1[d]	-2.7 ± 0.5[e]	0.03

Intracellular pH

	bTRPV3	control	p (bV3 vs. ctrl)
NMDGCl	7.52 ± 0.07[a]	7.56 ± 0.04[a]	1.0
NaCl	7.56 ± 0.05[b]	7.61 ± 0.03[b]	0.9
NH_4Cl (3.5 min)	6.90 ± 0.08[c]	7.14 ± 0.06[c]	0.04
NH_4Cl (20 min)	6.08 ± 0.08[d]	6.18 ± 0.09[d]	0.6
NH_4Cl-EDTA	5.96 ± 0.09[e]	6.05 ± 0.08[e]	0.6

Relative permeability ratio p(X) / p($NMDG^+$)

Ion X	bTRPV3	control	p (bV3 vs. ctrl)
Na^+	2.16 ± 0.19[a]	1.35 ± 0.11[a]	0.002
NH_4^+ (20 min)	3.41 ± 0.22[b]	2.78 ± 0.21[b]	0.06
NH_4^+ (EDTA)	3.76 ± 0.30[c]	2.58 ± 0.17[c]	0.003

pH_i did not differ, possibly reflecting an equilibrium primarily determined by the potential, the concentration gradients, and the pH regulatory mechanisms rather than by the permeability.

Subsequent removal of Ca^{2+} from the solution with buffering by EDTA had inverse effects on bTPRV3 expressing and control oocytes. As expected, all bTRPV3 oocytes were depolarized by removal of Ca^{2+} in line with greater influx of NH_4^+ through bTRPV3 after removal of Ca^{2+}, which permeates the pore of bTRPV3 with high affinity, thus interfering with the entry of monovalent cations. More surprising was the observation that all control oocytes were hyperpolarized. Most likely, this reflects a lower expression of divalent-sensitive cation channels in conjunction with an opening of calcium-inactivated Cl^- channels that are endogenously expressed by *Xenopus* oocytes [42]. In both groups of oocytes, application of EDTA resulted in a further slight acidification. In bTRPV3 oocytes, speed of acidification rose from (− 8 ± 4) 10^{-3} pH units/min before application of EDTA to (− 34 ± 6) 10^{-3} pH units/min ($p \leq 0.001$) 5 min later, in controls, from (− 3.2 ± 1.7) 10^{-3} pH units/min to (− 41 ± 9) 10^{-3} pH units/min ($p = 0.006$), with no significant difference between the groups ($p = 0.11$). Likewise, the end value of pH_i did not differ between the two groups.

In conjunction, these results suggest that both groups of oocytes express conductances to K^+, Na^+, and NH_4^+, with permeability relative to $NMDG^+$ (plus leak currents) higher in bTRPV3 oocytes (Table 2). In both groups, any permeability to NH_3 is much smaller than that to NH_4^+.

Patch-clamp experiments

Subsequent inside-out patch-clamp experiments on membrane patches of oocytes confirmed this hypothesis, with both groups showing a conductance to NH_4^+ on the single-channel level. In total, patches from 27 bTRPV3 and 21 control oocytes from the same three frogs used in microelectrode experiments were investigated in the inside-out configuration, alternating between the two groups. To allow an assessment of the NH_4^+ conductance under symmetrical conditions, the experiments were carried out with NH_4^+ in the pipette.

Throughout and in both groups, there was a tendency for single-channel events to occur in one solution and vanish in another solution without apparent reason. Typically, activity of channels increased with the duration of the measurement. Patches were frequently silent in the first solution (NaCl), and showed activity after application of the second solution (NH_4Cl). Those patches that survived a return to NaCl remained active, arguing against a selective conductance to NH_4^+.

Of the 27 patches from bTRPV3 expressing oocytes, all but four showed channel activity in at least one trace (Fig. 7). The conductance could be determined using linear fits for symmetrical (Fig. 7 c and e) or the GHK equation for asymmetrical configurations (Fig. 7g, see methods). Ion replacement showed that the conductance depended on the cation, but not on the anion in the bath. Over all patches, single-channel conductance to NH_4^+ in symmetrical solution was 92 ± 15 pS, (n = 18).

In control oocytes, only 14 out of 21 patches showed channel activity in at least one solution (Fig. 8). In asymmetrical solution with NaCl in the bath, the conductance of these small channels was about half of those found in bTRPV3 oocytes (48 ± 9 pS, n = 11, p = 0.04). An almost identical NH_4^+ conductance was determined from linear fits after switching to symmetrical NH_4Cl solution (43 ± 9 pS, n = 13, p = 0.7). In four patches, it was possible to switch to KCl and NMDGCl solutions, yielding similar values for NH_4^+ (p = 0.7). The conductances to the other ions Na^+ (33 ± 10 pS, n = 11, p = 0.11), K^+ (23.8 ± 1.3 pS, n = 2, p = 0.4), and $NMDG^+$ (9.2 ± 2.1 pS, n = 3, p = 0.10) were numerically smaller than the NH_4^+ conductance.

Compared with the control oocytes, the channel population in patches from bTRPV3 oocytes was visibly much more diverse. While 14 patches showed large conductances similar to those in Fig. 7, nine other patches showed smaller channels comparable with those seen in the control oocytes. In eight patches, both small and large channels could be observed in

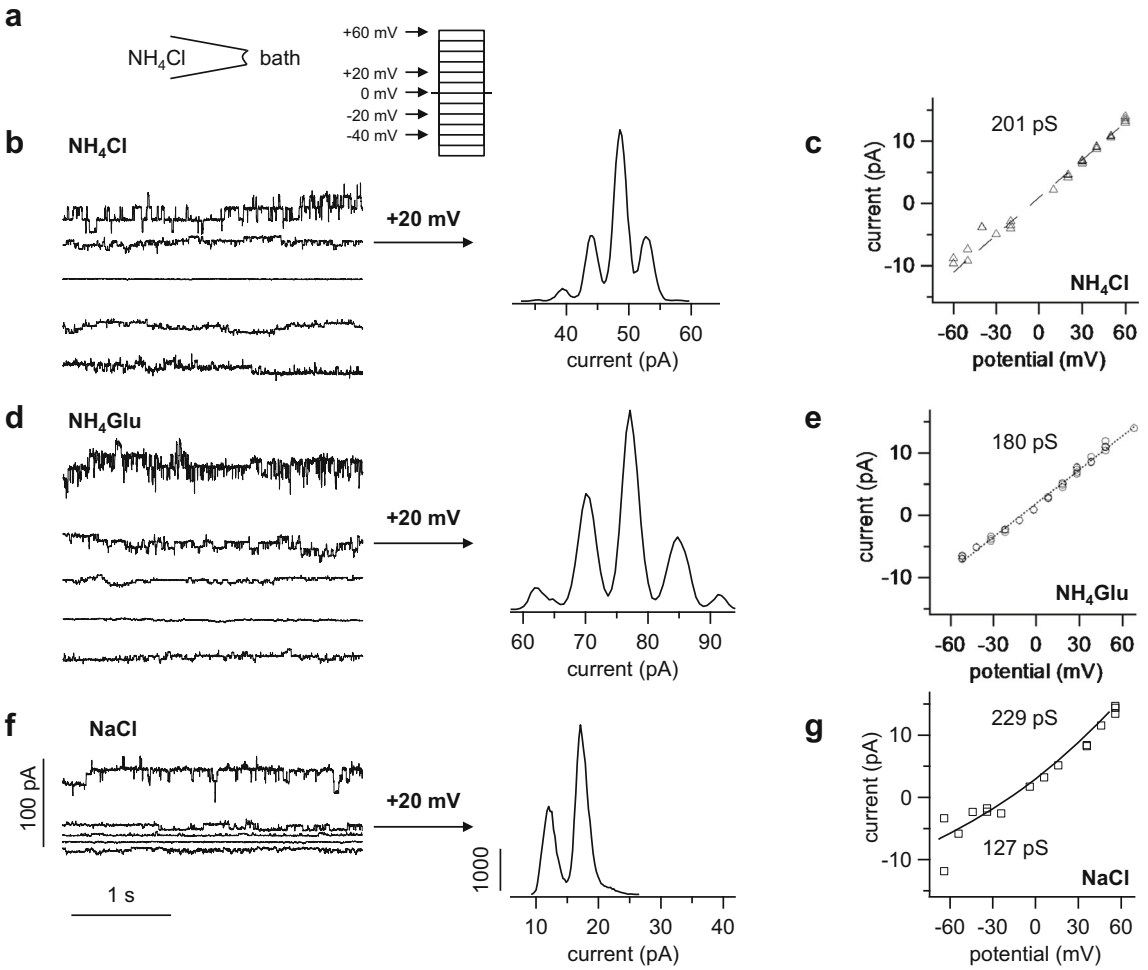

Fig. 7 Single-channel measurements from a bTRPV3 expressing oocyte (inside-out). **a** Measurements were performed with NH_4Cl in the pipette. The cytosolic side of the patch was consecutively exposed to different bath solutions as indicated and exposed to potentials between − 60 and + 60 mV in steps of 10 mV. For clarity, only the current responses to the potentials indicated by the arrows are shown. **b** Original recording in NH_4Cl bath solution (same scaling as in **f**). The amplitude histogram at + 20 mV can be seen in the middle showing three distinct channels. **c** IV-plot corresponding to **b**, yielding a linear relationship with the slope of the fit as indicated in the figure. **d** Channel openings were not affected by the replacement of chloride by the much larger anion gluconate, proving cation selectivity (same scaling as in **a** and **f**). The histogram in the middle shows four distinct channels. **e** IV-plot from **d**, with the GHK fit yielding a similar conductance as in **c**. **f** In NaCl solution, channel openings at positive potentials are comparable with **b** and **d**, whereas channel openings at negative potentials were smaller. **g** IV-plot from **f**, fitted with the GHK equation by variation of the permeability to the two ions Na^+ and NH_4^+. The conductance was then calculated from the GHK fit to the data and from the concentrations (see Supplement, equation 2). The negative reversal potential of the fit reflects a higher conductance to NH_4^+

the same experiment and three of them simultaneously showed large and small channel activity in the same trace. The conductance of bTRPV3 for K^+ could be investigated in two of such patches (Fig. 9). The large channels in these patches had a conductance of 216 ± 2 pS for NH_4^+ and 116 ± 13 pS for K^+ and most likely reflected bTRPV3 channels. The smaller conductances of 52 ± 11 pS for NH_4^+ and of 43 ± 14 pS for K^+ ($n = 5$) appeared to reflect endogenous channels.

Despite some overlap, the two populations of channels become apparent in the amplitude histogram of NH_4^+ conductances (Fig. 10c). The vertical height of the bars represents the number of patches falling into a certain conductance range, which is given on the horizontal axis. While control oocytes had one peak at conductances around 50 pS, oocytes expressing bTRPV3 showed a second peak over 150 pS. In the corresponding histogram for Na^+ conductances, a similar distribution was observed with one peak at ~ 20 pS for both groups and a second peak at ~ 80 pS in bTRPV3 oocytes only (Fig. 10d). In the further analysis, we assumed that channel activity smaller than 100 pS for NH_4^+ reflects expression of endogenous non-selective channels, which were excluded from subsequent statistical evaluation. Under these circumstances, the mean NH_4^+ conductances from these traces were 144 ± 12 pS ($n = 9$) for symmetrical NH_4Cl solution, 185 ± 14 pS ($n = 6$, $p = 0.7$ vs. NH_4Cl) for the NH_4Glu bath solution, and 182 ± 12 pS ($n = 10$, $p = 0.04$ vs. NH_4Cl) for the NaCl bath solution. The latter also yielded a conductance to Na^+ (98 ± 10 pS), significantly lower than that for NH_4^+ ($p \leq 0.001$).

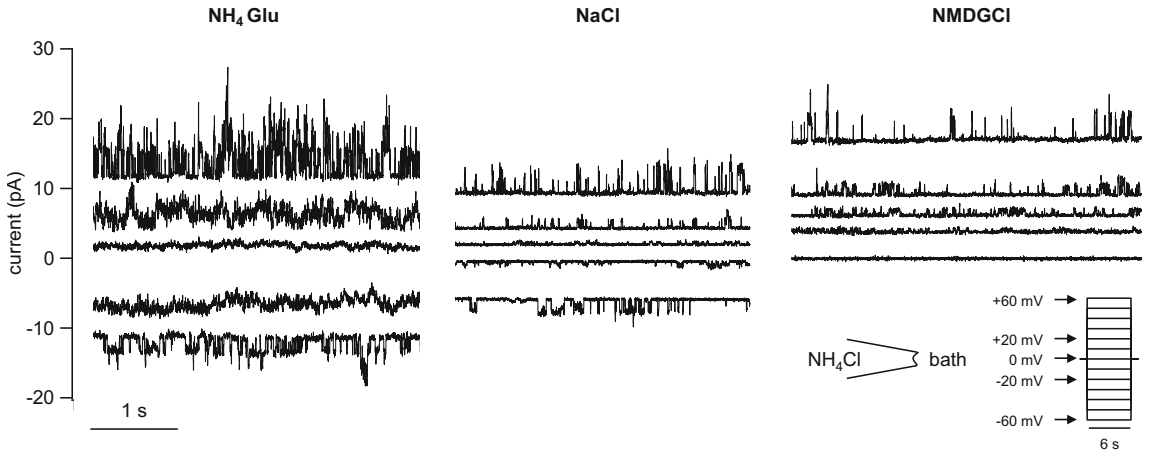

Fig. 8 Original recordings from an inside-out patch from a control oocyte (same scaling). Measurements were performed with NH_4Cl in the pipette. Only the current responses to the potentials indicated by the arrows are shown in the traces. Measurement in NH_4Glu solution showed small channel openings at positive and negative potentials, with the fit yielding a conductance of 41 pS for NH_4^+ in this patch. After switching to NaCl solution, channel openings at negative potentials were visibly smaller, reflecting influx of Na^+ (here: conductance of 59 pS for NH_4^+ and 31 pS for Na^+). After replacement of Na^+ with the much larger cation $NMDG^+$, channel openings were only visible at positive potentials. The GHK fit yielded a conductance for NH_4^+ of 53 pS and 11 pS for $NMDG^+$

The current study was performed in modifications of oocyte Ringer solution and accordingly, the conductances differed from those obtained in mammalian Ringer solution. However, after adjusting for the different concentrations of NH_4^+ (Supplement, equation 3), the conductance of the large channels in the bTRPV3 group could be statistical compared with the data which we obtained in a previous study of bTRPV3 expressed in HEK-293 cells [48]. For symmetrical

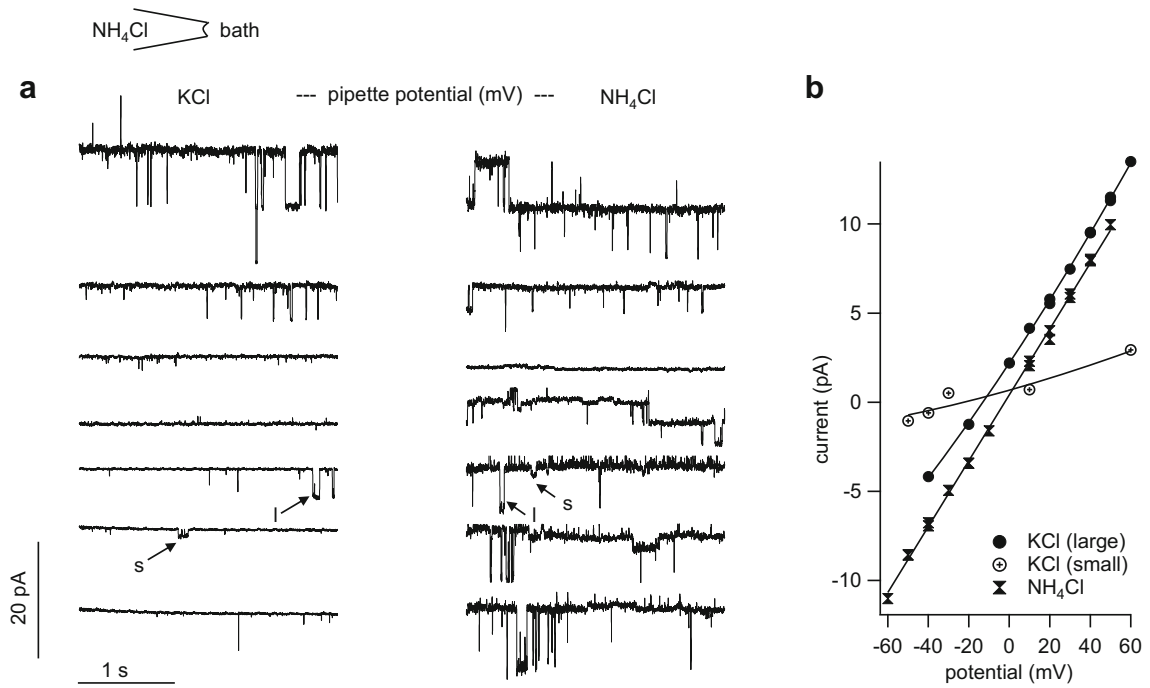

Fig. 9 Inside-out measurement of a patch from a bTRPV3 oocyte expressing two different types of channels. The pipette was filled with NH_4Cl. **a** Original recordings, showing consecutive exposure to KCl (traces to the left) and NH_4Cl (traces to the right, same scaling). Small (s) and large (l) populations of channels were observed, most likely representing endogenous and bTRPV3 channels respectively. **b** IV-plot of unitary currents from amplitude histograms of the patch in **a**. Data from the symmetrical NH_4Cl configuration were fitted linearly and yielded a conductance of 185 pS, with a reversal potential ~ 0 mV. In the asymmetrical KCl configuration, data from large and small channels were fitted separately to the GHK equation by variation of the permeability to the two ions NH_4^+ and K^+. The conductance was calculated from the permeability and the concentrations (see Supplement, equation 2). The fit of the large channel openings yielded a conductance to NH_4^+ of 215 pS and to K^+ of 129 pS. The smaller openings could be fitted with a conductance of 45 pS for NH_4^+ and 18 pS for K^+. Both reversal potentials were shifted to ~ − 15 mV, confirming the higher conductance to NH_4^+

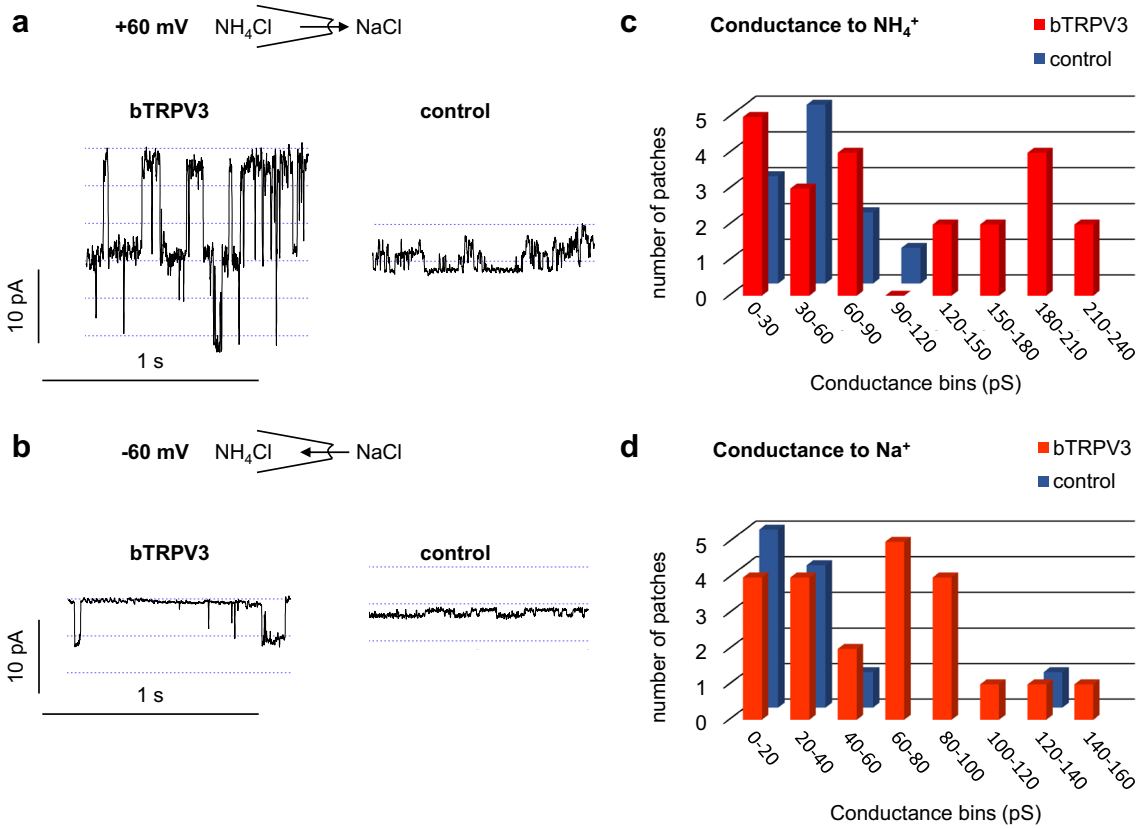

Fig. 10 Original inside-out recordings and histograms from control and bTRPV3 oocytes in asymmetrical solution with NH_4Cl in the pipette and NaCl in the bath. **a** Original recordings from one overexpressing bTRPV3 oocyte and one control oocyte at a pipette potential of + 60 mV, reflecting efflux of NH_4^+ (same scaling). **b** Corresponding traces at − 60 mV, reflecting Na^+ influx. Data from all voltages were fitted as in Figs. 7 and 8 to yield a conductance to NH_4^+ and Na^+ for each patch. **c** Histogram giving an overview of all conductance values for NH_4^+ determined from patches showing channel activity in asymmetrical solution. The total conductance range was divided into a number of equidistant bins, which are given on the *X*-axis. The *Y*-axis gives the number of patches with a conductance falling into the corresponding bin on the *X*-axis. The histogram shows one cluster of NH_4^+ conductances for control oocytes (blue) around 50 pS, while for bTRPV3 oocytes (red), a second cluster of conductances can be seen around 150 pS. Three bTRPV3 patches expressed both small and large channels. **d** Corresponding histogram of all measurements of the conductance to Na^+. One peak emerges at ~ 20 pS for both groups of oocytes and a second peak at ~ 80 pS in bTRPV3 oocytes only

NH_4Cl solution, no significant differences were found (p = 0.8). In asymmetrical solution, there was a slight trend for a lower NH_4^+ conductance in oocytes (p = 0.08). The Na^+ conductance did not differ (p = 0.9).

Discussion

The current study provides clear evidence for expression of the bovine homologue of TRPV3 by the epithelial layers of the bovine rumen. We confirmed the permeability of this channel to NH_4^+, Na^+, and K^+ in Ringer solutions with physiological concentrations of Ca^{2+} and Mg^{2+}. In conjunction with previous studies of our group [8, 40, 45, 48], we conclude that bTRPV3 is involved in the ruminal uptake of NH_4^+, Na^+, and Ca^{2+} and contributes to the apical conductance of K^+ [29] (Fig. 11).

In a first step, the bovine *TRPV3* was sequenced. After epitope screening, a commercial murine antibody was selected with binding affinity to a conserved epitope in the first extracellular loop of TRPV3. In immunoblots of protein from overexpressing HEK-293 and *Xenopus* oocytes, the antibody stained a band at the predicted height of ~ 90 kDa (Fig. 1). In non-expressing controls from both groups, no band was observed proving that staining was caused by binding of the antibody to bTRPV3. Corresponding immunohistochemistry confirmed expression of the channel protein primarily in the cellular membrane (Figs. 2 and 3). Immunoblots of ruminal protein show a band of equivalent molecular weight (~ 90 kDa), clearly arguing for expression of bTRPV3 by the rumen. However, a second, stronger band was visible at ~ 60 kDa (Fig. 1b). In a previous study, a ~ 60 kDa band could also be observed in human epidermal keratinocytes stained with a goat-polyclonal antibody directed against the epitope AA 461-487 of TRPV3 [53]. In that study, knockdown of TRPV3 showed that the ~ 60 kDa band was a splice variant. Blasting the epitope sequence with alignment in NCBI yields only three splice variants of bTRPV3, two at ~ 90 kDa, and

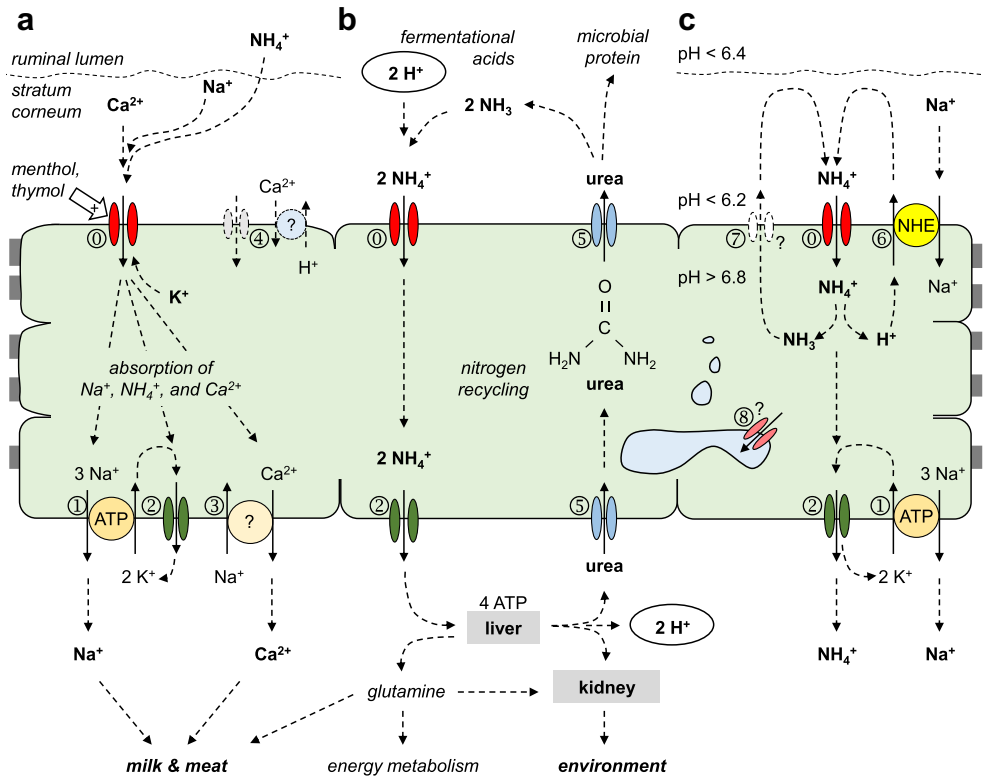

Fig. 11 Model showing the function of bTRPV3 in the rumen. The ruminal epithelium is a multilayered, *squamous* epithelium of cells that are interconnected by gap junctions, thus forming a functional syncytium. **a** bTRPV3 (⓪) is a non-selective cation channel that can serve as a pathway for the uptake of nutrients such as Na^+ and Ca^{2+}, and contributes to the apical conductance for K^+. Uptake of cations is stimulated by certain monoterpenoids such as menthol and thymol. Basolateral extrusion involves the sodium-potassium pump (ATP1A1,①), basolateral K^+ channels (②), and sodium-calcium exchangers (③). In the model, NH_4^+ is taken up by the same pathway as K^+ (⓪,②). Other TRP channels and exchangers may be involved (④). **b** Within the ruminal lumen, large quantities of fermentational acids are produced, releasing protons that can partially be removed via efflux of NH_4^+ via bTRPV3 (⓪) and basolateral K^+ channels (②). In the liver, NH_4^+ is converted to non-toxic metabolites, mostly urea, but also some glutamine. Only glutamine can be utilized by mammalian enzymes for protein synthesis. Conversely, urea must be excreted. This can occur renally, resulting in nitrogen losses and environmental damage. Alternately, urea can be secreted into the rumen via urea transporters such as UT-B or aquaporin 3 (⑤). After degradation by the microbiota within, NH_3 is released and can be utilized by microbial enzymes for protein synthesis. NH_3 also functions as a buffer, binding protons to form NH_4^+ that is again removed via bTRPV3 (⓪). This "nitrogen recycling" can reach 20 mol day^{-1} in cattle. **c** At physiological pH gradients across the apical membrane, NH_4^+ stimulates sodium transport via NHE (SLC9A3,⑥) with apical recirculation of NH_3 via an unknown pathway (⑦). Electrogenic transport of NH_4^+ across the basolateral membrane continues (②). Specific staining for bTRPV3 can also be found within the cytosol, possibly reflecting expression of bTRPV3 or its splice variant in intracellular membranes such as those of the ER (⑧)

only one with a predicted length of 60.25 kDa (NP_001092494.1). This splice variant contains the epitope for binding of the antibody and thus appears as the most likely explanation for the additional ~ 60 kDa band in Fig. 1b.

In particular in immunohistochemical staining, antibodies may occasionally bind by their constant domains rather than via the high affinity binding domains for the target epitope [9]. For this reason, immunochemical stainings and immunoblots were repeated in presence of the peptide used to produce the TRPV3 antibody. If the antibody is functional, this peptide should interfere with specific binding via the high affinity binding domains. Non-specific binding via other domains should continue unimpaired. In our case, a quenching of staining was observed (Fig. 4 f and Supplement). However, it should be emphasized that ultimately, this observation does not rule out that binding might have occurred to another protein via a structure similar to the target epitope [9].

TRPV3 emerged as a candidate gene when searching for the apical divalent-sensitive, non-selective cation channel of the rumen [30, 45, 49, 59]. Traditionally, TRP channels have been primarily regarded as channels involved in neuronal signaling rather than in epithelial transport. However, both spontaneous and induced mutations of TRPV3 primarily interfere with the function of keratinocytes, inducing skin lesions rather than neurological symptoms [36]. In line with this, ruminal tissue showed a strong immunohistochemical staining of bTRPV3 within the epithelium while subepithelial staining was weak (Fig. 4). Staining was observed not only in the cellular membranes of the ruminal epithelium, but also in the cytosol. This is in line with findings in human

keratinocytes or intact epidermis, where similar staining patterns were found [53].

Research in recent years has established that almost all TRP channels studied so far are expressed not only by the plasma membrane as previously thought, but also by intracellular vesicular membranes [19]. Thus, a recent study of the skin suggests expression of TRPV3 by the endoplasmic reticulum (ER) [64] and an involvement of TRPV3 in lysosomal function. It should also be noted that in the course of cell differentiation in stratified squamous epithelia, granules dissociate from the ER via blebbing and grow in size until they become visible as the keratohyalin granules that give the *stratum granulosum* its name [21]. Here, the proteins needed for keratinization are produced, requiring high quantities of glutamine. Accordingly, glutamine synthetase is highly expressed by the skin [16] and the rumen [47]. Within the ER, this enzyme catalyzes formation of glutamine from NH_4^+, possibly requiring additional uptake routes from the cytosolic space. TRPV3 would certainly fulfill this role (Fig. 11c).

However this may be, there is convincing evidence to suggest that bTRPV3 mediates transport of NH_4^+ across the ruminal epithelium. In Ussing chamber experiments, TRPV3 channel agonists stimulate currents carried by Na^+ and NH_4^+ and enhance Ca^{2+} flux [40, 45] (Fig. 11a). Furthermore, at physiological ruminal pH, exposure to NH_4^+ acidifies the cytosolic space of native ruminal epithelia from sheep and cattle as measured by pH-sensitive microelectrodes [32, 45]. Flux measurements confirm concomitant stimulation of NHE [3] (Fig. 11c). This has profound implications for the role of this channel in maintaining the pH of the ruminal fluid (Fig. 11b). As mentioned, large quantities of urea are secreted by the rumen and degraded according to:

$$(NH_2)_2CO + H_2O \rightarrow 2\ NH_3 + CO_2 \quad (3)$$

At physiological ruminal pH of 6.4, over 99.9% of NH_3 is immediately converted to NH_4^+. Absorption of NH_4^+ via TRPV3 results in a permanent removal of these protons from the rumen. In cattle on high-energy diets with production of large quantities of fermentational acids, influx of urea and efflux of NH_4^+ via bTRPV3 might represent an essential mechanism for ruminal pH homeostasis [5], explaining the high levels of nitrogen recycling observed in these animals, and the large quantities of ammonia that they excrete into the environment (Fig. 11b).

The current study confirms that bTPRV3 can serve as a pathway for protons bound in the form of NH_4^+. Microelectrode studies show a strong acidification of the cytosol of *Xenopus* oocytes expressing bTRPV3 (Fig. 5). Although NH_4Cl generally leads to an increase of the pH_i via influx of NH_3, an acidification has been observed in a number of systems such as astrocytes [34] or the ruminal epithelium [32, 45] and is generally attributed to influx of NH_4^+ with subsequent dissociation to H^+ and NH_3 [11] (Fig. 11c). Depending on the pH gradients present across the cellular membrane, NH_3 can diffuse back into the extracellular space [34], or accumulate in subcellular organelles where it can be detoxified [11]. In our study, we were tempted to calculate the relative permeability ratio of NH_4^+ vs. NH_3 from the equilibrium pH_i reached in steady state. In principle, this should be possible but would require knowledge of the distribution of ammonia inside and outside of the cell (Eq. 15 in [44] and Fig. 8 in [34]). Furthermore, the system is not in equilibrium but must have ill-defined mechanisms for pH regulation and detoxification of ammonia, further complicating matters.

It should be stressed that control oocytes were also strongly acidified by application of NH_4^+, albeit somewhat less rapidly than in oocytes expressing bTPV3 (Fig. 6). Given that *Xenopus* oocytes have been widely used as expression systems for ammonia-transporting proteins such as Rh-like proteins [12, 24], we did not anticipate the magnitude of the response. It has been noted previously that the lack of a robust expression system for functional analysis of ammonia transport has generally hampered research in the area [35]. Burckhardt and Frömter [11] were among the first to report transport of NH_4^+ by native *Xenopus* oocytes. In a careful study using pH-sensitive microelectrodes, the authors showed that endogenously expressed non-selective cation channels were involved. Our single-channel patch-clamp measurements confirm the findings of these authors [11] and clearly demonstrate that native *Xenopus* oocytes robustly express channels that are permeable not only to K^+ and Na^+, but also to NH_4^+. However, it should also be stressed that these endogenous channels were distinct from the larger channels that were only observed in bTRPV3 overexpressing cells. The conductance values from both groups of channels showed considerable scatter. This certainly reflects both stochastic effects and imprecisions involved with the evaluation and fitting of single-channel data. However, this finding may also reflect the formation of heteromeric channels consisting of bTRPV3 subunits and subunits of smaller endogenous *Xenopus* channels, leading to intermediate conductance levels as previously reported for TRPV1 [14, 15].

In summary, we provide clear evidence for the expression of bTRPV3 by the ruminal epithelium. In conjunction with previous functional studies of the ruminal epithelium [3, 40, 45], a role of this channel in mediating the ruminal transfer of NH_4^+ can be assumed. The finding that complex proteins are required to mediate ruminal transport not only of urea [50, 65] but also of ammonium across the ruminal wall should end the concept of ruminal nitrogen recycling as the result of a "leaky" epithelium. Instead, nitrogen recycling appears an efficient mechanism to remove protons from the rumen with the energy coming from the liver (Fig. 11b). Given the robust evidence supporting transport of Ca^{2+} by TRPV3 [37, 45, 48, 63], bTRPV3 also clearly emerges as a candidate mediating electrogenic Ca^{2+} transport by the ruminal epithelium [27, 61, 62].

Certainly, bTRPV3 is not the only NH_4^+ transporting channel and there is good reason to believe that in the rumen, in *Xenopus* oocytes, and in other parts of the gut, multiple types of non-selective cation channels should be considered when searching for pathways for the uptake of ammonium [58].

Acknowledgments Open Access funding provided by Projekt DEAL. We wish to express our gratitude to Prof. Dr. Dorothee Günzel and Dr. Jörg Piontek, Institute of Clinical Physiology, University Medicine, Charité, Berlin for the support in histological imaging. We would also like to thank Gisela Manz, Katharina Söllig, Susanne Trappe, Barbara Drewes, and Edith Gröninger for their expertise and technical help. We would like to cordially thank Prof. Salah Amasheh and Dr. Constanze Vitzthum for providing *Xenopus* oocytes and sharing expertise in handling them. We are also grateful to Prof. Dr. Aschenbach for his continuous support.

Author contributions Friederike Stumpff, Franziska Liebe, Hendrik Liebe, and Gerhard Sponder all contributed to the study conception and design, material preparation, data collection, and analysis. The first draft of the manuscript was written by Friederike Stumpff, Franziska Liebe, and Hendrik Liebe. All authors were involved in editing the manuscript and approved the final version.

Funding information The study received funding from Deutsche Forschungsgemeinschaft (DFG STU 258/7-1) and Sonnenfeld Stiftung.

Compliance with ethical standards

Conflict of interest The authors declare that they have no conflicts of interest. Friederike Stumpff is the holder of a patent that was transferred to a startup company.

Ethics approval The maintenance and surgical treatment of *Xenopus laevis* frogs was in accordance with the guidelines of German legislation, with approval by the animal welfare officer for the Freie Universität Berlin and under the governance of the Berlin Veterinary Health Inspectorate (Landesamt für Gesundheit und Soziales Berlin, permit G0025/16). Bovine ruminal epithelium was obtained from Holstein-Friesian cattle slaughtered for meat production in a commercial abattoir (Beelitz, Germany), also under control of the German authorities.

References

1. Abdoun K, Stumpff F, Martens H (2006) Ammonia and urea transport across the rumen epithelium: a review. Anim Health Res Rev 7:43–59. https://doi.org/10.1017/S1466252307001156
2. Abdoun K, Stumpff F, Rabbani I, Martens H (2010) Modulation of urea transport across sheep rumen epithelium in vitro by SCFA and CO2. Am J Physiol Gastrointest Liver Physiol 298:G190–G202. https://doi.org/10.1152/ajpgi.00216.2009
3. Abdoun K, Stumpff F, Wolf K, Martens H (2005) Modulation of electroneutral Na transport in sheep rumen epithelium by luminal ammonia. Am J Physiol Gastrointest Liver Physiol 289:G508–G520. https://doi.org/10.1152/ajpgi.00436.2004
4. Abdoun K, Wolf K, Arndt G, Martens H (2003) Effect of ammonia on Na+transport across isolated rumen epithelium of sheep is diet dependent. Br J Nutr 90:751–758. https://doi.org/10.1079/BJN2003957
5. Aschenbach JR, Penner GB, Stumpff F, Gabel G (2011) Ruminant Nutrition Symposium: role of fermentation acid absorption in the regulation of ruminal pH. J Anim Sci 89:1092–1107. https://doi.org/10.2527/jas.2010-3301
6. Barry PH, Lynch JW (1991) Liquid junction potentials and small cell effects in patch-clamp analysis. J Membr Biol 121:101–117. https://doi.org/10.1007/BF01870526
7. Bödeker D, Kemkowski J (1996) Participation of NH4+ in total ammonia absorption across the rumen epithelium of sheep (Ovis aries). Comp Biochem Physiol A Physiol 114:305–310. https://doi.org/10.1016/0300-9629(96)00012-6
8. Braun HS, Schrapers KT, Mahlkow-Nerge K, Stumpff F, Rosendahl J (2018) Dietary supplementation of essential oils in dairy cows: evidence for stimulatory effects on nutrient absorption. Animal : an international journal of animal bioscience:1-6. https://doi.org/10.1017/S1751731118001696
9. Brownjohn PW, Ashton JC (2014) What can be concluded from blocking peptide controls? Appl Immunohistochem Mol Morphol 22:634. https://doi.org/10.1097/PAI.0b013e3182a77fe5
10. Bucking C, Edwards SL, Tickle P, Smith CP, McDonald MD, Walsh PJ (2013) Immunohistochemical localization of urea and ammonia transporters in two confamilial fish species, the ureotelic gulf toadfish (Opsanus beta) and the ammoniotelic plainfin midshipman (Porichthys notatus). Cell Tissue Res 352:623–637. https://doi.org/10.1007/s00441-013-1591-0
11. Burckhardt BC, Frömter E (1992) Pathways of NH3/NH4+ permeation across Xenopus laevis oocyte cell membrane. Pflugers Arch 420:83–86. https://doi.org/10.1007/bf00378645
12. Caner T, Abdulnour-Nakhoul S, Brown K, Islam MT, Hamm LL, Nakhoul NL (2015) Mechanisms of ammonia and ammonium transport by rhesus-associated glycoproteins. Am J Phys Cell Phys 309:C747–C758. https://doi.org/10.1152/ajpcell.00085.2015
13. Cermak R, Lawnitzak C, Scharrer E (2000) Influence of ammonia on sodium absorption in rat proximal colon. Pflugers Arch 440:619–626. https://doi.org/10.1007/s004240000309
14. Cheng W, Yang F, Liu S, Colton CK, Wang C, Cui Y, Cao X, Zhu MX, Sun C, Wang K, Zheng J (2012) Heteromeric heat-sensitive transient receptor potential channels exhibit distinct temperature and chemical response. J Biol Chem 287:7279–7288. https://doi.org/10.1074/jbc.M111.305045
15. Cheng W, Yang F, Takanishi CL, Zheng J (2007) Thermosensitive TRPV channel subunits coassemble into heteromeric channels with intermediate conductance and gating properties. J Gen Physiol 129:191–207. https://doi.org/10.1085/jgp.200709731
16. Danielyan L, Zellmer S, Sickinger S, Tolstonog GV, Salvetter J, Lourhmati A, Reissig DD, Gleiter CH, Gebhardt R, Buniatian GH (2009) Keratinocytes as depository of ammonium-inducible glutamine synthetase: age- and anatomy-dependent distribution in human and rat skin. PLoS One 4:e4416. https://doi.org/10.1371/journal.pone.0004416
17. Denning GM, Ostedgaard LS, Cheng SH, Smith AE, Welsh MJ (1992) Localization of cystic fibrosis transmembrane conductance regulator in chloride secretory epithelia. J Clin Investig 89:339–349. https://doi.org/10.1172/JCI115582

18. Doerner JF, Hatt H, Ramsey IS (2011) Voltage- and temperature-dependent activation of TRPV3 channels is potentiated by receptor-mediated PI(4,5)P2 hydrolysis. J Gen Physiol 137:271–288. https://doi.org/10.1085/jgp.200910388
19. Dong XP, Wang X, Xu H (2010) TRP channels of intracellular membranes. J Neurochem 113:313–328. https://doi.org/10.1111/j.1471-4159.2010.06626.x
20. Foskolos A, Moorby JM (2018) Evaluating lifetime nitrogen use efficiency of dairy cattle: a modelling approach. PLoS One 13: e0201638. https://doi.org/10.1371/journal.pone.0201638
21. Freeman SC, Sonthalia S (2020) Histology, keratohyalin granules. In: StatPearls. StatPearls Publishing, Treasure Island (FL),
22. Gärtner K, Decker P, Hill H (1961) Untersuchungen über die Passage von Harnstoff und Ammoniak durch die Pansenwand von Ziegen. Pflugers Arch 274:281–288. https://doi.org/10.1007/BF00362319
23. Georgi MI, Rosendahl J, Ernst F, Gunzel D, Aschenbach JR, Martens H, Stumpff F (2014) Epithelia of the ovine and bovine forestomach express basolateral maxi-anion channels permeable to the anions of short-chain fatty acids. Pflugers Arch 466:1689–1712. https://doi.org/10.1007/s00424-013-1386-x
24. Geyer RR, Parker MD, Toye AM, Boron WF, Musa-Aziz R (2013) Relative CO(2)/NH(3) permeabilities of human RhAG, RhBG and RhCG. J Membr Biol 246:915–926. https://doi.org/10.1007/s00232-013-9593-0
25. Handlogten ME, Hong SP, Zhang L, Vander AW, Steinbaum ML, Campbell-Thompson M, Weiner ID (2005) Expression of the ammonia transporter proteins Rh B glycoprotein and Rh C glycoprotein in the intestinal tract. Am J Physiol Gastrointest Liver Physiol 288:G1036–G1047. https://doi.org/10.1152/ajpgi.00418.2004
26. Hartinger T, Gresner N, Sudekum KH (2018) Does intra-ruminal nitrogen recycling waste valuable resources? A review of major players and their manipulation. J Anim Sci Biotechnol 9:33. https://doi.org/10.1186/s40104-018-0249-x
27. Holler H, Breves G, Kocabatmaz M, Gerdes H (1988) Flux of calcium across the sheep rumen wall in vivo and in vitro. Q J Exp Physiol 73:609–618. https://doi.org/10.1113/expphysiol.1988.sp003180
28. Hristov AN, Bannink A, Crompton LA, Huhtanen P, Kreuzer M, McGee M, Noziere P, Reynolds CK, Bayat AR, Yanez-Ruiz DR, Dijkstra J, Kebreab E, Schwarm A, Shingfield KJ, Yu Z (2019) Invited review: nitrogen in ruminant nutrition: a review of measurement techniques. J Dairy Sci 102:5811–5852. https://doi.org/10.3168/jds.2018-15829
29. Leonhard-Marek S, Martens H (1996) Effects of potassium on magnesium transport across rumen epithelium. Am J Phys 271:G1034–G1038
30. Leonhard-Marek S, Stumpff F, Brinkmann I, Breves G, Martens H (2005) Basolateral Mg2+/Na+ exchange regulates apical nonselective cation channel in sheep rumen epithelium via cytosolic Mg2+. Am J Physiol Gastrointest Liver Physiol 288:G630–G645. https://doi.org/10.1152/ajpgi.00275.2004
31. Levitt MD, Levitt DG (2019) Use Of quantitative modelling to elucidate the roles of the liver, gut, kidney, and muscle in ammonia homeostasis and how lactulose and rifaximin alter this homeostasis. Int J Gen Med 12:367–380. https://doi.org/10.2147/IJGM.S218405
32. Lu Z, Stumpff F, Deiner C, Rosendahl J, Braun H, Abdoun K, Aschenbach JR, Martens H (2014) Modulation of sheep ruminal urea transport by ammonia and pH. Am J Physiol Regul Integr Comp Physiol 307:R558–R570. https://doi.org/10.1152/ajpregu.00107.2014
33. McDonald IW (1948) The absorption of ammonia from the rumen of the sheep. Biochem J 42:584–587
34. Nagaraja TN, Brookes N (1998) Intracellular acidification induced by passive and active transport of ammonium ions in astrocytes. Am J Phys 274:C883–C891. https://doi.org/10.1152/ajpcell.1998.274.4.C883
35. Neuhauser B, Dynowski M, Ludewig U (2014) Switching substrate specificity of AMT/MEP/ Rh proteins. Channels (Austin) 8:496–502. https://doi.org/10.4161/19336950.2014.967618
36. Nilius B, Biro T (2013) TRPV3: a 'more than skinny' channel. Exp Dermatol 22:447–452. https://doi.org/10.1111/exd.12163
37. Nilius B, Biro T, Owsianik G (2014) TRPV3: time to decipher a poorly understood family member! J Physiol 592:295–304. https://doi.org/10.1113/jphysiol.2013.255968
38. Ochoa-de la Paz LD, Espino-Saldana AE, Arellano-Ostoa R, Reyes JP, Miledi R, Martinez-Torres A (2013) Characterization of an outward rectifying chloride current of Xenopus tropicalis oocytes. Biochim Biophys Acta 1828:1743–1753. https://doi.org/10.1016/j.bbamem.2013.03.013
39. Owsianik G, Talavera K, Voets T, Nilius B (2006) Permeation and selectivity of TRP channels. Annu Rev Physiol 68:685–717. https://doi.org/10.1146/annurev.physiol.68.040204.101406
40. Rabbani I, Braun HS, Akhtar T, Liebe F, Rosendahl J, Grunau M, Tietjen U, Masood S, Kaessmeyer S, Gunzel D, Rehman H, Stumpff F (2018) A comparative study of ammonia transport across ruminal epithelia from Bos indicus crossbreds versus Bos taurus. Animal science journal = Nihon chikusan Gakkaiho. https://doi.org/10.1111/asj.13107
41. Ramsey IS, Delling M, Clapham DE (2006) An introduction to TRP channels. Annu Rev Physiol 68:619–647. https://doi.org/10.1146/annurev.physiol.68.040204.100431
42. Reifarth FW, Amasheh S, Clauss W, Weber W (1997) The Ca2+-inactivated Cl- channel at work: selectivity, blocker kinetics and transport visualization. J Membr Biol 155:95–104. https://doi.org/10.1007/s002329900161
43. Reynolds CK, Kristensen NB (2008) Nitrogen recycling through the gut and the nitrogen economy of ruminants: an asynchronous symbiosis. J Anim Sci 86:E293–E305. https://doi.org/10.2527/jas.2007-0475
44. Roos A, Boron WF (1981) Intracellular pH. Physiol Rev 61:296–434. https://doi.org/10.1152/physrev.1981.61.2.296
45. Rosendahl J, Braun HS, Schrapers KT, Martens H, Stumpff F (2016) Evidence for the functional involvement of members of the TRP channel family in the uptake of Na(+) and NH4 (+) by the ruminal epithelium. Pflugers Arch 468:1333–1352. https://doi.org/10.1007/s00424-016-1835-4
46. Rubino JG, Wilson JM, Wood CM (2019) An in vitro analysis of intestinal ammonia transport in fasted and fed freshwater rainbow trout: roles of NKCC, K(+) channels, and Na(+), K(+) ATPase. J Comp Physiol B 189:549–566. https://doi.org/10.1007/s00360-019-01231-x
47. Salem HA, Devlin TJ, Marquardt RR (1973) Effects of urea on the activity of glutamate dehydrogenase, giutamine synthetase, carbamyl phosphate synthetase, and carbamyl phosphokinase in ruminant tissues. Can J Anim Sci 53:503–511
48. Schrapers KT, Sponder G, Liebe F, Liebe H, Stumpff F (2018) The bovine TRPV3 as a pathway for the uptake of Na+, Ca2+, and NH4+. PLoS One 13:e0193519. https://doi.org/10.1371/journal.pone.0193519
49. Schultheiss G, Martens H (1999) Ca-sensitive Na transport in sheep omasum. Am J Phys 276:G1331–G1344
50. Stewart GS, Graham C, Cattell S, Smith TP, Simmons NL, Smith CP (2005) UT-B is expressed in bovine rumen: potential role in ruminal urea transport. Am J Physiol Regul Integr Comp Physiol 289:R605–R612. https://doi.org/10.1152/ajpregu.00127.2005
51. Stumpff F, Georgi MI, Mundhenk L, Rabbani I, Fromm M, Martens H, Günzel D (2011) Sheep rumen and omasum primary cultures and source epithelia: barrier function aligns with expression of tight junction proteins. J Exp Biol 214:2871–2882. https://doi.org/10.1242/jeb.055582

52. Stumpff F, Lodemann U, Van Kessel AG, Pieper R, Klingspor S, Wolf K, Martens H, Zentek J, Aschenbach JR (2013) Effects of dietary fibre and protein on urea transport across the cecal mucosa of piglets. J Comp Physiol B 183:1053–1063. https://doi.org/10.1007/s00360-013-0771-2
53. Szollosi AG, Vasas N, Angyal A, Kistamas K, Nanasi PP, Mihaly J, Beke G, Herczeg-Lisztes E, Szegedi A, Kawada N, Yanagida T, Mori T, Kemeny L, Biro T (2018) Activation of TRPV3 regulates inflammatory actions of human epidermal keratinocytes. J Invest Dermatol 138:365–374. https://doi.org/10.1016/j.jid.2017.07.852
54. Vitzthum C, Stein L, Brunner N, Knittel R, Fallier-Becker P, Amasheh S (2019) Xenopus oocytes as a heterologous expression system for analysis of tight junction proteins. FASEB journal : official publication of the Federation of American Societies for Experimental Biology 33:5312–5319. https://doi.org/10.1096/fj.201801451RR
55. Vriens J, Nilius B, Vennekens R (2008) Herbal compounds and toxins modulating TRP channels. Curr Neuropharmacol 6:79–96. https://doi.org/10.2174/157015908783769644
56. Wang Y, Li X, Yang J, Tian Z, Sun Q, Xue W, Dong H (2018) Mitigating greenhouse gas and ammonia emissions from beef cattle feedlot production: a system meta-analysis. Environ Sci Technol 52:11232–11242. https://doi.org/10.1021/acs.est.8b02475
57. Weiner ID, Verlander JW (2011) Role of NH3 and NH4+ transporters in renal acid-base transport. Am J Physiol Ren Physiol 300:F11–F23. https://doi.org/10.1152/ajprenal.00554.2010
58. Weiner ID, Verlander JW (2019) Emerging features of ammonia metabolism and transport in acid-base balance. Semin Nephrol 39:394–405. https://doi.org/10.1016/j.semnephrol.2019.04.008
59. Wilkens M, Kunert-Keil C, Brinkmeier H, Schröder B (2008) Expression of calcium channel TRPV6 in ovine epithelial tissue. Vet J 182:294–300. https://doi.org/10.1016/j.tvjl.2008.06.020
60. Wilkens MR, Mrochen N, Breves G, Schroder B (2011) Gastrointestinal calcium absorption in sheep is mostly insensitive to an alimentary induced challenge of calcium homeostasis. Comp Biochem Physiol B Biochem Mol Biol 158:199–207. https://doi.org/10.1016/j.cbpb.2010.11.008
61. Wilkens MR, Nelson CD, Hernandez LL, McArt JAA (2020) Symposium review: transition cow calcium homeostasis-health effects of hypocalcemia and strategies for prevention. J Dairy Sci 103:2909–2927. https://doi.org/10.3168/jds.2019-17268
62. Wilkens MR, Praechter C, Breves G, Schroder B (2016) Stimulating effects of a diet negative in dietary cation-anion difference on calcium absorption from the rumen in sheep. J Anim Physiol Anim Nutr 100:156–166. https://doi.org/10.1111/jpn.12296
63. Xu H, Ramsey IS, Kotecha SA, Moran MM, Chong JA, Lawson D, Ge P, Lilly J, Silos-Santiago I, Xie Y, DiStefano PS, Curtis R, Clapham DE (2002) TRPV3 is a calcium-permeable temperature-sensitive cation channel. Nature 418:181–186. https://doi.org/10.1038/nature00882
64. Yadav M, Goswami C (2017) TRPV3 mutants causing Olmsted Syndrome induce impaired cell adhesion and nonfunctional lysosomes. Channels (Austin) 11:196–208. https://doi.org/10.1080/19336950.2016.1249076
65. Zhong C, Farrell A, Stewart GS (2020) Localization of aquaporin-3 proteins in the bovine rumen. J Dairy Sci 103:2814–2820. https://doi.org/10.3168/jds.2019-17735

Supplementary Material

The TRPV3 channel of the bovine rumen - localization and functional characterization of a protein relevant for ruminal ammonia transport

Pflügers Archiv – European Journal of Physiology

Franziska Liebe[1]*, Hendrik Liebe[1,2*], Sabine Kaessmeyer[3], Gerhard Sponder[1], Friederike Stumpff[1]

email: stumpff@zedat.fu-berlin.de

[1]Institute of Veterinary Physiology, Freie Universität Berlin, Berlin, Germany
[2]Department of Biology, Chemistry, and Pharmacy, Freie Universität Berlin, Germany
[3]Institute of Veterinary Anatomy, Freie Universität Berlin, Berlin, Germany

*) both authors contributed equally to this study

Methods (Supplement)

Immunohistochemical staining

Xenopus laevis oocytes were fixed in paraformaldehyde (4 %, 3 h), washed with PBS (2 times), and dehydrated in increasing concentrations of ethanol (2 times in 70 % (1 h), 70 % (overnight), 3 times in 80 % (1 h), 80 % (72 h), 2 times in 96 % (10 min), 3 times in 99.9 % (10 min)). Xylene was used as intermedium (2 times for 10 min) and finally, oocytes were embedded in paraffin (2 times for 30 min).

Frozen bovine tissue was defrosted in methanol (-20 °C, 1 h). Afterwards, tissue was fixated in formaldehyde (4 % in PBS, 4 °C, 24 h) and dehydrated in increasing ethanol concentrations as follows: 70 % (4 times, each 1 h; last overnight), 80 % (3 times, each 1 h; last overnight), then 80 % (once, 24 h), 96 % (2 times, each 45 min), 99.9 % (3 times, 45 min), methyl benzoate (2 h). Fresh bovine tissues were fixed immediately in formaldehyde and dehydrated with a shorter protocol (70 %, 80 %, 96 %, 99.9 % for 50 min).

For all bovine samples, Xylene was used as intermedium (2x 30 min). The samples were then infiltrated overnight in the incubator at 59°C in paraffin I, afterwards for 2.5h each in paraffin II and III; and finally the samples were embedded in fresh paraffin and

stored in the refrigerator. Slices of 5 µm were cut and mounted on glass slides (Superfrost® Plus Menzel-Gläser, Carl Roth GmbH & Co. KG, Karlsruhe, Germany).

Deparaffinization of cuts of ruminal tissues or oocytes was performed in Roti®-Histol (Carl Roth, Karlsruhe, Germany) overnight. Rehydration was completed by incubating the slides in descending ethanol concentration (99.9 %, 96 %, 90 %, 80 %, 70 %, demineralized water) for 5 minutes respectively.

The slides were washed in PBS (5 min) and boiled in EDTA buffer (1 mmol·L^{-1}; oocytes: pH 8.0 adjusted with NaOH; rumen: pH 9.0 adjusted with Tris) for 15 min. Afterwards, the slides were rinsed thrice with PBS (for 1 min and 2 times for 5 min).

HEK-293 cells were seeded onto coverslips, transfected, washed in PBS (2 times), incubated in Roti®-Histofix (4 %, 30 min), and washed again twice in PBS.

Permeabilization of all fixed samples was achieved via incubation in Triton X-100 (0.5 %, 5 min; Merck KGaA, Darmstadt, Germany). After two washing steps with PBS, followed by incubation in blocking solution (BS, goat serum (5 %; PAN-Biotech GmbH, Aidenbach, Germany) in PBS) in a closed container with humidified atmosphere for 1 hour. Samples were then stained with primary antibody diluted in BS (4 °C, overnight) according to Table 1. Secondary antibody controls were performed with BS only.

To test for binding to the epitope, adjacent slices from the same sample of ruminal tissue were incubated in parallel either with the primary mouse TRPV3 antibody (AB_{V3}) only or with a mix of this antibody and its corresponding specific immunizing peptide (SIP) (Table 1).

According to Table 1, samples and secondary antibody controls were incubated in diluted secondary antibodies (in BS supplemented with 4′, 6-diamidine-2′-phenylindole dihydrochloride (1 µg/mL; DAPI, Roche, Mannheim, Germany), 37 °C, 1 h). Slices were washed with BS (2 times for 5 min), demineralized water, and ethanol, followed by embedding (Mount Flour, Biocyc GmbH & Co. KG, Potsdam, Germany) and covering.

Double-barrelled pH-sensitive microelectrode measurements

pH-sensitive microelectrodes were prepared essentially as described previously [1] with a few alterations. For pH-measurements, SUTTER BF 150-86-10 glass tubing (Science Products GmbH, Hofheim, Germany) was used. The reference barrel was made of filamented bisected GC150F 15 glass tubing (Harvard Apparatus, Kent, UK). Two core cable ends (4×10, 611889, Conrad Bauelemente, Conrad Elektronik, Hirschau, Germany) were pushed into tightly fitting shrink tubing (Ø 3 mm) and used to adjoin the two barrels, leaving the middle section free (~ 3 cm). A small piece of shrink tubing (1 mm; Deray-H-set 1/8″, DSG-Canusa, Meckenheim, Germany) was slipped over the end of the reference barrel, slightly separating the barrels at one end. After baking (180°C, 10 min), the piggyback electrodes were pulled with a programmable multipipette puller (PMP-107, Microdata Instrument, South Plainfield, NJ, USA) to give a resistance of ~ 50 MΩ (measured with EPC 9, Heka Elektronik, Lambrecht, Germany). Subsequently, the reference barrel was perfused with pressurized dry air via plastic tubing pushed over one end (~ 0.9 bar). The pH-sensitive barrel was pushed into a rubber insert in the lid of a heated glass jar and exposed to the vapour formed by a drop (200 µl) of fresh dichlorodimethylsilane (Sigma-Aldrich) for 30 min. Pipettes were then baked at 180 °C for 2 h. The pH-sensitive barrel was filled with Hydrogen Ionophore I-Cocktail A (0.2 µl; Sigma Aldrich, St. Louis, MO, USA) via a Microliter syringe (type 7000.50C, Hamilton Company, Reno, NV, USA). The electrodes could be stored in a plastic container with silica gel (P077.2, Carl Roth) and light protection for many months. Once opened, Dichlorodimethylsilane had to be replaced frequently.

On the experimental day, the reference barrel was filled with KCl solution (0.5 mol·L^{-1}) via a MicroFil micropipette (34Gauge/67 mm, World Precision Instruments, Sarasota, FL, USA), while the pH-sensitive barrel was filled with KCl/HEPES-buffer (in mmol·L^{-1}: 500 KCl, 20 HEPES, pH 7.2 adjusted with Tris). Microelectrodes were then trimmed (0.5-30 MΩ) to remove clogging silane residues using a beveller (BV-10, Sutter Instrument, Novato, CA, USA).

Measurements were performed in a continuously perfused bath chamber. Via chlorinated silver wires, the two barrels were connected to an amplifier (F-223 A Dual Electrometer, World Precision Instruments). The bath was grounded to a common

technical earth via a chlorinated silver wire. In addition, the bath was connected to a commercial electrode (Metrohm, Filderstadt, Germany) via a KCl (3 mol·L^{-1}) agar bridge to minimize liquid junction potential effects (ground signal) [2]. All three signals were measured versus the technical earth and recorded using LabChart 7 software (ADintruments Ltd, Oxford, UK). The potential difference between the two barrels was used to determine the intracellular pH (pH_i), while the potential difference between the reference barrel and the ground signal from the bath corresponded to the membrane potential (U_{mem}).

Electrodes were calibrated before and after each measurement using solution NaCl (pH 7.4) and NaCl-6.4 (pH 6.4). Suitable electrodes showed a stable potential difference of 45 mV or higher measured by the pH-sensitive barrel with effects at the reference electrode < 0.3 mV.

A micromanipulator (Mini 25, Luigs & Neumann, Ratingen, Germany) was used to insert the microelectrode into the oocyte. Impalement was considered to be successful if a sharp drop in the potential across the reference channel to values under -10 mV could be observed.

Analysis of single-channel data

For analysis of single-channel data, an Igor macro (Igor Pro 6.2.2.2; WaveMetrics Inc., Lake Oswego, USA) was used to fit amplitude histograms to a Gaussian distribution with the distance of the maxima giving the unitary current of one channel opening and cross-checked by direct measurements. The unitary currents were then plotted against the clamped pipette potentials (IV-plot), which were corrected for liquid junction potentials throughout. For symmetrical solutions, the slope of the linear regression equals the conductance. For asymmetrical solutions, GHK theory was used to fit the IV-plot, yielding the permeability for two ions (P_A and P_B) as described in detail in [3].

$$(1) \quad I = \frac{U \cdot F^2}{R \cdot T} \cdot \left(\frac{P_A \cdot [A]_i + P_B \cdot [B]_i - (P_A \cdot [A]_o + (P_B \cdot [B]_o) \cdot \exp\left(-U \cdot \frac{F}{R \cdot T}\right)}{1 - \exp\left(-U \cdot \frac{F}{R \cdot T}\right)} \right)$$

The values for P_x resulting from the fit of currents in asymmetrical solutions were used to predict the conductances (G_x) in symmetrical oocyte Ringer solution at 96 mmol·L^{-1} according to:

$$(2) \qquad G_X = \frac{I}{U} = \frac{F^2}{R \cdot T} \cdot P_X \cdot 96\ \mathrm{mmol \cdot L^{-1}}$$

To compare these conductance values with data obtained in a previous study with HEK-293 cells in standard Ringer solutions (145 mmol·L^{-1}) [3], G_x in oocyte solution was multiplied by the concentration ratio yielding:

$$(3)\ G_X\ (145\ \mathrm{mmol \cdot L^{-1}}) = G_X\ (96\ \mathrm{mmol \cdot L^{-1}}) \times \frac{145\ \mathrm{mmol \cdot L^{-1}}}{96\ \mathrm{mmol \cdot L^{-1}}}$$

Supplemental Figure

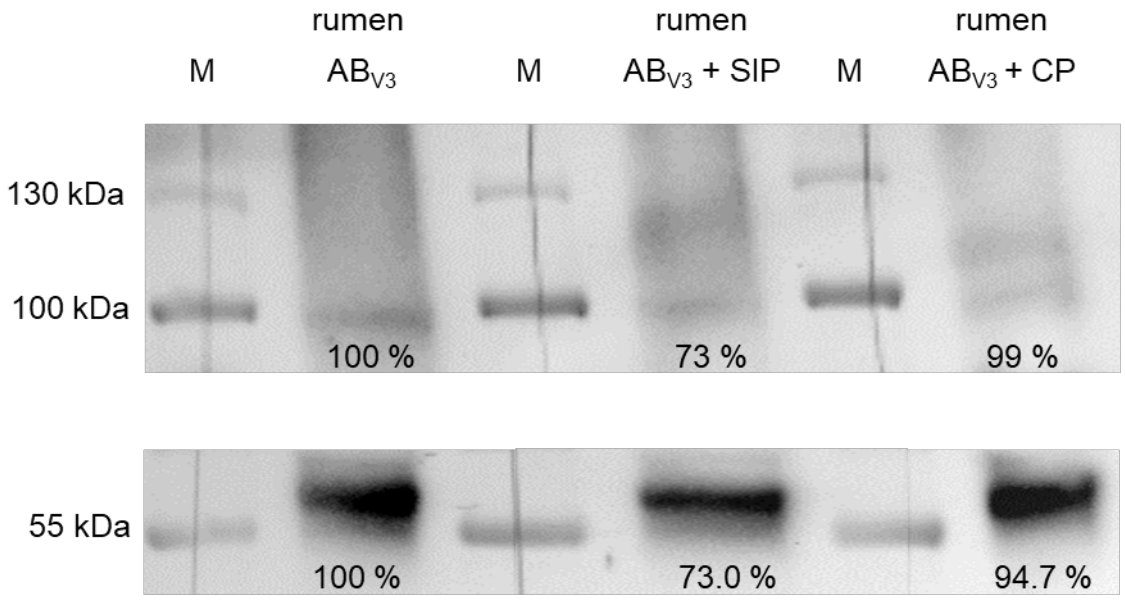

Immunoblot of protein from one animal with a weak band at 90 kDa. Each lane contains 50 µg of ruminal protein (rumen) and is preceded by a marker lane (M). After blotting, the membrane was cut for separate treatment with the TRPV3 antibody (AB$_{V3}$), antibody and specific immunizing peptide (AB$_{V3}$ + SIP), or antibody and control peptide (AB$_{V3}$ + CP). To optimize the exposure time for both of the two bands, all three membrane slices were cut at 72 kDa. The percentages under the lanes represent the relative quantities determinded using ImageLab software (BioRad).

References

1. Abdoun K, Stumpff F, Rabbani I, Martens H (2010) Modulation of urea transport across sheep rumen epithelium in vitro by SCFA and CO2. American journal of physiology Gastrointestinal and liver physiology 298:G190-202. doi:10.1152/ajpgi.00216.2009

2. Barry PH, Lynch JW (1991) Liquid junction potentials and small cell effects in patch-clamp analysis. J Membr Biol 121:101-117. doi:10.1007/BF01870526

3. Schrapers KT, Sponder G, Liebe F, Liebe H, Stumpff F (2018) The bovine TRPV3 as a pathway for the uptake of Na+, Ca2+, and NH4+. PLoS One 13:e0193519. doi:10.1371/journal.pone.0193519

5

Discussion

5. Discussion

Summarized, this study investigated the permeability of human TRPV3 (hTRPV3) and bovine TRPV3 (bTRPV3) to NH_4^+ using *X*. oocytes and HEK-293 cells as expression systems. Expression and trafficking were verified using immunoblotting and immunostaining, while the permeability was determined using single-channel patch clamp experiments. Whole-cell experiments investigated the effect of menthol enantiomers on NH_4^+ influx in HEK-293 cells expressing hTRPV3. Furthermore, the internal pH of hTRPV3 and bTRPV3 expressing *X*. oocytes was measured using pH-sensitive microelectrodes, demonstrating acidification after exposure to NH_4Cl. Trafficking, cell viability, and supplementation of ruthenium red (RR) was investigated in HEK-293 cells expressing wild-type hTRPV3 ($hTRPV3_{wt}$) or the OS mutant G573S. The study shows that hTRPV3 was expressed by keratinocytes in a model of human skin, while bTRPV3 was expressed by keratinocytes in the bovine rumen, with little staining of subepithelial layers.

In conjunction, this thesis clearly shows that both the hTRPV3 and the bTRPV3 channel conduct NH_4^+. It might be argued that this is hardly surprising considering the promiscuous behavior of TRPV3 towards cations [191], but a conductance of TRPV3 to NH_4^+ has to be shown rigorously before any further deliberations are possible. Parts of this study were performed in a manner to allow direct comparison between the human and bovine TRPV3, but the findings of this thesis do not support a significant functional difference between the two homologues. We conclude that while TRPV3 is definitely important for Ca^{2+} signaling as previously described in the literature [43,172], it might also mediate relevant exchanges of monovalent cations such as NH_4^+ both between organelles and the cytoplasm and between the cytoplasm and the extracellular space with possible consequences for nitrogen exchange and protein metabolism. Our immunostainings of native human skin showing hTRPV3 trafficked to the cellular membrane (see Liebe *et al.* 2021 [139] **Figure 4**) as well as signs of an expression in intracellular organelles supports this hypothesis.

It may be argued that the uncharged NH_3 simply defuses through the lipid membranes like other gases and no transport protein is required as classically assumed [125,184] and sometimes even hypothesized in recent studies [33]. Using the Henderson-Hasselbalch equation, 98% of the ammonia is found as positively charged NH_4^+ at physiological pH due to the alkaline character of NH_3 (pk_a of 9.25 at 25 °C for the reaction $NH_3 + H_2O \Leftrightarrow NH_4OH \Leftrightarrow NH_4^+ + OH^-$ [102]) although the proportion of un-ionized ammonia increases with increasing temperature and pH while decreases with increasing salinity. This argument of low NH_3 concentrations might be discouraged with the le Chatelier´s principle (also known as

equilibrium law [14]), meaning that even low concentrations of NH_3 would suffice because those would be transported and thereby removed from the reaction shifting the equilibrium towards NH_3. But according to the VSEPR theory [87] (reviewed in **Figure 13**), the structure of NH_3 is distorted tetrahedral and NH_3 has a permanent electric dipole ($4.90 \cdot 10^{-30}$ Cm [102]) which makes it far more likely to require a transport protein the same way that the transport of water is facilitated by aquaporins [10,40,74,149].

The traditional model that NH_3 can permeate through the lipid bilayer surrounding cells is seemingly supported by the observation that many types of cells show strong alkalinization when exposed to NH_4Cl. However, in recent years, it has emerged that the high permeability of biological membranes to NH_3 usually reflects the expression of AQP´s [31] or Rhesus-like glycoproteins [98], which are now known to pass deprotonated NH_4^+ into the cell [170]. Furthermore, other preparations, such as the *Xenopus laevis* oocytes used in this study, are not alkalinized, but acidified by NH_4Cl, confirming that the lipid bilayer surrounding these cells is more permeable to the protonated form (NH_4^+) than to the unprotonated form. It thus appears that the lipid composition of many or possibly most biological membranes limits the unregulated passage of ammonia, allowing influx to be regulated by suitable transport proteins. Our publications demonstrate that TRPV3 is one of them [137,139,220].

Nowadays, it is widely accepted that the traditional dogma that all gasses primarily cross cellular membranes via diffusion has to be retired [31] and NH_3 is a strong candidate to be one of these exceptions [10,74,215,274].

Detection of the protein

The expression of hTRPV3 and bTRPV3 in *X.* oocytes and HEK-293 cells was confirmed using immunoblots and immunostainings utilizing an included Strep-tag in the sequence as well as a murine TRPV3 antibody. In immunoblots, the predicted band for full-length TRPV3 (~95 kDa) could be observed in both expression systems for hTRPV3 (Liebe *et al.* 2021 [139] **Figure 1**) and bTRPV3 (Liebe *et al.* 2020 [137] **Figure 1**) for both antibodies but not in controls. For the anti-TRPV3 antibody (epitope AA 458-474), an additional band (~60 kDa) could be observed in hTRPV3 and G573S HEK-293 cells, in native bovine rumen, and in native human keratinocytes but not in controls. This suggests a specific effect. Due to the known fact in particular in immunohistochemical staining that antibodies may occasionally bind by their constant domains rather than via the high affinity binding domains for the target epitope [37], native bovine rumen was incubated exemplary with anti-TRPV3 antibody in presence with the peptide used to produce the antibody and we observed the predicted quenching of staining as seen in 4.1, strengthening the reliability of the experiment. The anti-Strep antibody could not

detect the 60 kDa band in both expression systems despite using long exposition times but since the Strep-tag is N-terminally placed, cleavage due to splicing at any position would explain this observation. This band was also published in an unrelated study of cultured keratinocytes [245] and in various parts of the porcine intestine, porcine skin, and murine skin [154]. While this band might reflect a breakdown product, the sequence for a ~60 kDa splice variant of TRPV3 are available for the bovine species (AAI46079.1) and for mice (XP_006533411.1) which suggests that in these variants, the protein is truncated after amino acid 527 (mouse) or 526 (bovine). The alignment was published in the supplementary material of Manneck *et al* [154]. This is in the middle of the third transmembrane domain (S3) which can be seen in **Figure 2** so that the pore region (S5 and S6, >aa580) would be missing [266]. Due to the lack of these vital domains, it appears unlikely that this shorter variant acts as an ion channel but it might exhibit unknown regulatory properties that require further research.
In immunofluorescence staining, bTRPV3 was clearly targeted to the cell membrane in overexpressing HEK-293 cells and *X*. oocytes (Liebe *et al.* 2020 [137] **Figure 2 and 3**) and coincided with the expression of cytosolic GFP in HEK-293 cells while controls showed no staining. The same observation was made for hTRPV3 in overexpressing *X*. oocytes and HEK-293 cells (Liebe *et al.* 2021 [139] **Figure 2 and 3**). The functionality of hTRPV3 in overexpressing HEK-293 cells was cross-checked using whole-cell experiments demonstrating currents sensitive to the known TRPV3 agonists menthol, thymol, and 2-APB (**Figure 16**) that were not observable in controls.

Whole-cell experiments using HEK-293 cells

Our group has performed whole-cell experiments with HEK-293 cells overexpressing bTRPV3 [220] and hTRPV3 [139] in comparison to controls using the known TRPV3 agonists menthol, thymol, and 2-APB to confirm stimulated conductance showing functional expression of the channels. As expected, the measured currents significantly rose after incubation with the agonists including significant washout in overexpressing cells but not in controls. In hTRPV3 overexpressing HEK-293 cells, we additionally investigated the permeability to NH_4^+ and calculated the relative permeability ratios for $p(NH_4^+)/p(Na^+)$ using the reversal potentials. Both hTRPV3 HEK-293 cells and controls expressed channels permeable to NH_4^+ with significant increase in influx (-120 mV pipette potential), outward current (+100 mV), and a higher reversal potential (as seen in 3. [139] Table 3). We hypothesize this observation reflects influx of Cl^-, efflux of Na^+, or superposition of both due to swelling or changes of pH_i. Hille *et al.* have also reported an increase in current when the concentration of a permeant ion rises [105]. Application of D-menthol led to a significant increase in reversal potential as well as both inward and outward currents due to influx of NH_4^+ (at -120 mV) and efflux of Na^+ (at +100 mV) with no significant change in controls. Overexpressing cells showed distinctive current

amplitudes as well different current kinetics in comparison to controls. We hypothesize the depolarization repelled divalent cations like Ca^{2+} and Mg^{2+} from the hTRPV3 channel pore (reported as voltage-dependent block [137,185,191]) resulting in the observed time-dependent increase in current at positive potentials. We observed inverse behavior at negative potentials including decreased influx of NH_4^+ due to the attraction of divalent cations into the channel. Additionally, we observed strong tail currents that followed the depolarizing pulses that arguably reflect a diminishing NH_4^+ influx due to the return of divalent cations to the channel mouth.

L-menthol is known to have effects on TRPV3 [150] but we were not aware of studies using D-menthol which is why we performed whole-cell experiments where both enantiomers were consecutively applied with alternating orders between experiments. This series showed no difference between the two enantiomers but we observed that the effect of the second application of the agonist was always significantly larger independently of the chirality despite washout. This effect of pre-activation or sensitizing of the channel has also been reported by Macpherson *et al.* [150] and Moqrich *et al* [165].

Microelectrodes

X. oocytes transfected with hTRPV3 and bTRPV3 vectors as well as controls were used in alternation to investigate the acidification of oocytes and their NH_4^+ permeability utilizing double-barreled microelectrodes to measure pH_i and U_{mem} simultaneously. In accordance with preliminary experiments with hTRPV3 oocytes (see supplementary **Figure S1** in 3.1), all three groups showed depolarization and acidification of the cytosol after incubation with NH_4^+ as well as a slow-going moderate recovery of pH_i after washout (**Figure S2** in 3.1). Albeit slower, peculiarly, the controls behaved in a similar manner as overexpressing cells arguing for amply expressed endogenous pathways of the oocytes for the uptake of NH_4^+ in accordance with reports of other laboratories [39,123,166].

As mentioned, in many cellular systems, incubation with NH_4Cl leads to alkalization due to influx of NH_3 [79,81,108]. Conversely, in other systems, acidification due influx of NH_4^+ with probable subsequent dissociation to protons and NH_3 [38] has been reported – thus, in the ruminal epithelium [147,209] or in astrocytes [168]. In 1992, the German work group around Burckhardt and Frömter [38] first investigated in depth the response of *X*. oocytes to the application of NH_4Cl using pH-sensitive microelectrodes. At the time, the acidification that they observed was completely contrary to expectations of an influx of NH_3 with subsequent protonation and alkalinization. They interpreted their finding as relating to the expression of endogenously expressed non-selective cation channels, without clearly demonstrating these. Given that X. oocytes are an established and widely used overexpression system, there were surprisingly few follow-up studies. The current study now directly confirms Bödeker and

Frömter's hypothesis using the single-channel-configuration of the patch-clamp-technique to study membrane patches of native *X.* oocytes.

In this context it is somewhat surprising to note that *X.* oocytes are frequently used as a system to study NH_3 and NH_4^+ transport by various proteins [42,86]. A high endogenous transport capacity for ammonia will tend to obscure the effects of an overexpression of ammonia transporters. Failure to recognize this problem might explain part of the surrounding controversy about preferred substrates utilized by members of the AMT/Rh transporter family as reported by Neuhäuser *et al.* [170], who noted that the lack of a robust expression system for functional analysis of ammonia transport has impeded this area of research considerably.

For this series of experiments on *X.* oocytes, we kept the stabilizing network of protein fibers called vitelline membrane [117] intact so as to not jeopardize the stability of the oocytes due to impalement with the microelectrodes. This practice has also been utilized by Musa-Aziz *et al.* [166] who arguably reported the most in depth study of this research topic.

In the current study (see **Table S2** in 3.1), the initial values of pH_i and U_{mem} were comparable for hTRPV3 (7.56 ± 0.04, -30.6 ± 2.2 mV, respectively), bTRPV3 (7.52 ± 0.07, -39.2 ± 2.6 mV, respectively), and controls (7.56 ± 0.04, -27.2 ± 1.8 mV, respectively) but the U_{mem} (-40 to -60 mV) of previous studies [38,123,166] were comparatively lower than our experiments which arguably reflects the incubation of our oocytes in NMDGCl solution after injection. We purposefully adopted this approach to circumvent immoderate influx of Na^+ in the overexpressing oocytes which might have caused impeded update of K^+ by the Na^+/K^+-ATPase. As stated previously, all oocytes acidified after application of NH_4^+ with varying rapidity. Overexpressing cells were significantly faster than controls, reflecting the swift influx due to the expressed TRPV3 channels. Strikingly, hTRPV3 cells acidified significantly faster than bTRPV3 cells and after 20 min, the pH_i difference already reached a staggering 0.27 as seen in **Figure S2** in 3.1. We suggest that the expression of hTRPV3 was more efficient than the expression of bTRPV3 which will be explained in more detail in conjunction with the data of our single channel experiments down below. At the end of the NH_4Cl incubation, hTRPV3 cells showed a slight recovery of pH_i which suggests that the equilibrium distribution had been reached [207]. This might also explain why the addition of EDTA to remove divalent cations opening many non-selective cation channels [45,48,282] had no effect on pH_i on this group while it accelerated the acidification of bTRPV3 cells and controls. However, while both hTRPV3 and bTRPV3 oocytes depolarized after EDTA incubation as expected with this hypothesis, conversely, control cells hyperpolarized. This possibly reflects the endogenous expression of chloride channels that can be inactivated by Ca^{2+} [201,272]. Of course, such channels should also be expressed by the overexpressing oocytes, but we suggest that the superposition with a large quantity of TRPV3 openings (leading to a depolarization) obscured the hyperpolarizing effect of an opening of these chloride channels.

Regarding the relative permeability to the $NMDG^+$-ion, we could clearly show that overexpressing cells had a higher permeability for Na^+ than controls and that the permeability for NH_4^+ was higher than that for Na^+. Intriguingly, we could only observe a higher relative permeability for NH_4^+ in bTRPV3 cells in comparison to controls while it was identical for hTRPV3 and controls. The expected difference between these two groups became observable only after the removal of divalent cations by incubation with EDTA which had contrary effects on these groups. Currently, this phenomenon eludes a comprehensive explanation within the confines of this study and the underlying pattern has been proven to be challenging to decipher conclusively highlighting to investigate the nuances in more detail.

Single-channel

Inside-out experiments required the removal of the vitelline membrane before measurements to expose the lipid membrane (known as oolemma) where the channels are expressed. This process rendered the oocytes fragile, causing swelling and eventual breakage, necessitating careful handling. As shown in **Figure S3** of section 3.1, the experiments demonstrated the expression of non-selective cation channels with permeability to NH_4^+ in both controls and overexpressing *X.* oocytes. We observed variable conductance levels, likely attributed to the formation of heteromers with endogenous channels [233]. Interestingly, two distinct populations emerged: small channels with a NH_4^+ conductance below 100 pS and large channels exceeding 100 pS. Native oocytes exclusively displayed conductances below the 100 pS threshold, while overexpressing cells exhibited patches with conductances ranging up to 303 pS. The same pattern was recognizable for Na^+ experiments whereas the threshold was determined to be 60 pS. As shown in **Figure S4** in Section 3.1, the distribution of small and large conductances in single-channel patch-clamp experiments revealed a pattern. We propose that the expression of hTRPV3 or bTRPV3 significantly increased the single-channel conductance while simultaneously suppressing the expression of endogenous channels, mitigating negative effects due to overexpression. This effect was more pronounced for bTRPV3, with the percentage of cells exhibiting small channels decreasing from 67% in controls to 33%. Oocytes overexpressing hTRPV3 exhibited a higher number of channels in individual patches, with a larger percentage (63%) of large channels compared to bTRPV3 overexpressing oocytes (52%). This suggests that the expression of hTRPV3 was more efficient than that of bTRPV3. This hypothesis is supported by the observation that hTRPV3 overexpressing oocytes acidified significantly faster in microelectrode experiments in response to NH_4Cl compared to bTRPV3 oocytes and controls (Section 3.1, part H).

Using the independence principle described in 3.1 equation 4 in part F, our experimental series provided conductance values (G) in standard Ringer solution (145 $mmol \cdot L^{-1}$) in asymmetrical configuration (NaCl bath and NH_4Cl pipette). For hTRPV3, we observed

$G_H(Na^+)$ = 137 ± 42 pS and G_H (NH_4^+) = 287 ± 80 pS. For bTRPV3, the values were $G_B(Na^+)$ = 148 ± 16 pS and $G_B(NH_4^+)$ = 275 ± 19 pS while controls exhibited $G_C(Na^+)$ = 50 ± 16 pS and $G_C(NH_4^+)$ = 65 ± 14 pS. This conversion allowed statistical comparison with data obtained in our previous study of bTRPV3 expressed in HEK-293 cells [220], showing a slight trend ($p = 0.08$) for lower NH_4^+ conductances in oocytes and no difference ($p = 0.8$) in symmetrical NH_4Cl solution as well as no difference ($p = 0.9$) for Na^+ conductance (data shown in Liebe *et al.*[137]).

Logically, we conducted single-channel patch clamp experiments with HEK-293 cells overexpressing hTRPV3 to draw comparisons with our previous findings. Using the same setup employed for measuring hTRPV3 and bTRPV3 overexpressing cells, we successfully established a “gigaohm seal” (also known as gigaseal [11]) on the patch and measured currents in a NaCl bath solution. However, despite our efforts, these seals consistently broke upon changing the solution to NH_4Cl. This issue was replicated independently by four colleagues, and regrettably, no evaluable measurements could be recorded. Exploring further alternative approaches to obtain the required data would have surpassed the defined scope of this study. Notably, when compared to controls and bTRPV3 experiments, the currents in the NaCl solution appeared to be larger for hTRPV3 experiments. We hypothesize that, akin to the observations in oocyte experiments, the expression of hTRPV3 in HEK-293 cells appears to be more efficient, resulting in unstable seals unsuitable for single-channel experiments. To address this limitation in future investigations, we recommend exploring strategies to reduce the effectiveness transfection, trafficking, or functionality of the hTRPV3 channel. This could involve the use of blockers, although it's acknowledged that such interventions may introduce distortions in the results. Alternatively, modifying the transfection protocol to express fewer TRPV3 channels in the membrane could be explored.

G573S trafficking and cell death

Using a vector with a fusion to GFP, we expressed the known OS mutation G573S in HEK-293 cells and confirmed trafficking to the membrane in individual cells (Liebe *et al.* 2021 **Figure 14a**). Arguably, the number of cells showing staining was extremely low and many of these exhibited marked staining within cytosol and severely impaired structural morphology. Intriguingly, no G573S overexpressing HEK-293 cell showed visible GFP staining in marked contrast to $hTRPV3_{wt}$ and bTRPV3 experiments. We hypothesize that the expression of the mutant induced cell death after insertion of the channel protein in the membrane and before sufficient expression of GFP could occur.

Also, we investigated the cell viability of $hTRPV3_{wt}$, G573S, and controls, supplemented with the established antagonist [140] RR to observe its effect (**Figure 14b** in section 3). As expected, controls exhibited the highest cell viability while the addition of RR decreased the

cell count due to its known toxic properties [257]. For $hTRPV3_{wt}$, the cells behaved the similarly, with no significant difference and only a slight trend towards higher death rate in overexpressing cells. In contrast, the cell viability for G573S was significantly lower than controls or $hTRPV3_{wt}$ with a rejuvenating effect of RR increasing the cell viability significantly. This problem of significantly increased cell death rate has been described by Lin *et al.* [140] as reviewed in **Figure 4** and it was postulated to reflect apoptosis or necrosis due to increased Ca^{2+} influx [205]. This might give an explanation to why we were unable to obtain a sufficient number of cells successfully co-expressing GFP to identify mutant cells for patch-clamp experiments although extensive attempts have been tried out as discussed in part G of section 3.1. We hypothesize this predicament might have been avoided using a vector with a fusion of GFP to the channel as used by Lin *et al.* [140] but we purposely avoided this approach as we feared that the fusion of the large marker GFP might alter the properties of the channel like the open probability or conductance and it is possible to speculate that a decrease in conductance enhanced cell viability. Additionally, we hypothesized that the fusion might have been one of the reasons why the mutant channel was not correctly trafficked to the membrane in the study of Yadav *et al.* [286] which was described in **Figure 5** to **Figure 7**. As a reminder, Yadav *et al.* [286] expressed OS-mutants in HaCaT cells and reported impaired vesicular trafficking that resulted in reduced surface localization of known membrane proteins and TRPV3 mutants suggesting that OS might be primarily a lysosomal disorder which is in contradiction to studies reporting successful membrane expression of G573S [140] and other OS associated mutants [299].

In conclusion, our study confirms that expression of the OS mutant G573S severely impairs cell survival and observed partial rescue by the large cation RR, which is most likely blocking the extracellular mouth of the channel. We support the hypothesis that the expression of G573S in the extracellular membrane is essential to lead to cell death under *in vitro* conditions.

Staining of native tissue

Staining analysis of a human fibroblast and keratinocyte-based skin equivalent distinctly revealed the predominant expression of hTRPV3 in keratinocytes, particularly within the apical membrane of the uppermost cell layer (shown in **Figure 4** in section 3). Skin equivalents derived from cultured human keratinocytes have gained prominence as human-centric test systems for foundational and preclinical investigations [145]. Notably, these skin equivalents lack neuronal-origin cells and allow the production of exceptionally thin preparations, ensuring optimal optical properties for confocal laser microscopy. The continuous coverage of the construct with cell culture medium prevented the formation of the stratum corneum, presenting a potential advantage for subsequent transport studies. Within the keratinocyte layer's central region, robust cytosolic staining was observed, likely indicative of hTRPV3 expression by the

endoplasmic reticulum. This phenomenon aligns not only with previous reports on hTRPV3 (as seen in **Figure 5** [286]) but also with various other TRP channels [101]. In contrast, cells in the upper layer displayed a conspicuously hTRPV3-free cytosol, with hTRPV3 staining predominantly localized in the apical membrane, suggesting a role in the apical ion uptake. Overall, the hTRPV3 expression pattern in the skin equivalent closely mirrored that observed in native human skin [188] or our own observations for bTRPV3 in rumen [137]. Here as well, we observed a strong immunohistochemical staining of bTRPV3 within the epithelium, a moderate staining in the cytosol, and a weak subepithelial staining as shown in **Figure 4** in section 4.

According to literature, the colonic epithelium, characterized by a single layer of cells, TRPV3 staining was reportedly primarily concentrated within the apical membrane [154,251] as well, with minimal cytosolic staining. Intriguingly, both colonic and ruminal epithelia demonstrate functional expression of a divalent-sensitive NH_4^+ conductance, responsive to TRPV3 agonists [154,209].

Hypothesis concerning the role of TRPV3

What functional role might a highly versatile channel, demonstrating notably low selectivity to various cations including Ca^{2+}, play in the apical membrane of an epithelium? Undoubtedly, the uptake of Ca^{2+} is pivotal for diverse processes, *inter alia*, to uptake nutrients in the rumen, to activate the transglutaminase in human skin, and potentially for signaling in the colon or caecum. Intriguingly, all three epithelia also release substantial amounts of urea which is degraded by microbiota into ammonia as described in detail in **Figure 15**. In the skin, though further research is warranted, we speculate that sweat-secreted urea, degraded by the dermal microbiome [216,259], releases NH_4^+ and, through small lesions in the stratum corneum, signals the need for localized corneocyte replacement. This initiates a cascade: TRPV3-mediated NH_4^+ influx stimulates glutamine formation, facilitating the synthesis of proteins vital for cornification [35,54,131,176]. Concurrently, TRPV3-mediated Ca^{2+} influx activates transglutaminases, leading to the formation of the corneocyte envelope [43,67]. The TRPV3 signaling complex, activated by EGF present in eccrine sweat [210], completes this intricate process. The significance of cytosolic glutamine production from NH_4^+ is underscored by neonates with glutamine synthetase deficiency, resulting in skin defects [93].

While the precise role of excessive NH_4^+ influx via TRPV3 in OS remains uncertain, its clinical manifestation is predominantly observed in humans, particularly in the palms and soles (as illustrated in **Figure 1**) [63]. Interestingly, humans lead the animal kingdom in eccrine sweat production [129], crucial for thermoregulation [80], with the highest secretion occurring in the palms and soles (palmoplantar skin). Conversely, mice due not share this trait, which might explain why TRPV3 mutant mice fail to display palmoplantar hyperkeratosis.

In the case of the colon, the function of TRPV3 is more evident (more details can be found in **Figure 15a** in section 3). Within the colonic lumen, microbes utilize nitrogen derived from amino acids and urea for protein synthesis, releasing ammonia subsequently absorbed into the portal blood [142,239,265]. Evolutionarily, absorbing nitrogen in the form of ammonia from the gut is advantageous, especially in situations of low protein intake, where it can be repurposed for the synthesis of urea and non-essential amino acids [239]. NH_3 might certainly play a part in this scenario (for example via the ammonia transporter RhCG [98,170]). But, NH_4^+ uptake via TRPV3 has also been reported [154] and should contributes to the pH homeostasis of the colonic lumen, challenged by acids produced during the fermentation process [23]. However, challenges arise when the liver fails to detoxify ammonia in hepatic disease [2,22,239]. Hence, identifying proteins mediating ammonia transport stands as a crucial initial step for potential interventions, in this context and others.

6

Conclusion

6. Conclusion

This comprehensive study investigated the NH_4^+ permeability of human TRPV3 (hTRPV3) and bovine TRPV3 (bTRPV3) using *X*. oocytes and HEK-293 cells, confirming expression and trafficking through immunoblotting and immunostaining. Single-channel patch clamp experiments, whole-cell experiments with menthol enantiomers, and pH-sensitive microelectrode measurements in hTRPV3 and bTRPV3 expressing cells were conducted. Cell viability and trafficking were explored in HEK-293 cells expressing wild-type hTRPV3 or the OS mutant G573S, and localization was observed in human skin for hTRPV3 and bovine rumen for bTRPV3. The immunostainings of hTRPV3 in human skin further support the hypothesis of TRPV3 involvement in relevant cation exchanges.

This study demonstrates the role of cation channels in NH_4^+ transport, with TRPV3 being a candidate. Our data represents a further example challenging established concepts regarding gas diffusion through membranes [31]. The classical hypothesis that NH_3 diffusion through lipid membranes might suffice is countered by the fact that exposing *X*. oocytes to an NH_4Cl solution did not lead to the expected alkalinization, but to an acidification in each one of the cells studied in conjunction with a depolarization of the membrane potential. This response was caused by NH_4^+ conducting cation channels, which were directly observed in patch-clamp experiments. Most likely, any diffusion of NH_3 through the lipid bilayer was severely limited by the electric dipole of NH_3. Evidence of NH_4^+ transport via TRPV3 provides a further example for the involvement of transporters in the uptake of substrates previously thought to permeate membranes via “lipid diffusion”, challenging traditional assumptions.

The expression of hTRPV3 and bTRPV3 in *X*. oocytes and HEK-293 cells was robustly confirmed through immunoblots and immunostainings utilizing Strep-tag and a murine TRPV3 antibody. Immunoblots revealed the presence of the predicted full-length TRPV3 bands in both systems, with an additional band (~60 kDa) observed in overexpressing HEK-293 cells and native tissue, suggesting a potential breakdown product or splice variant. The reliability of the anti-TRPV3 antibody was validated through quenching experiments. Immunofluorescence staining demonstrated clear targeting of bTRPV3 and hTRPV3 to the cell membrane in overexpressing cells and oocytes, coinciding with the expression of cytosolic GFP. While a truncated ~60 kDa splice variant was identified, lacking critical ion channel domains, its potential regulatory properties warrant further exploration. Overall, our protein detection methods provide robust evidence for the expression and subcellular localization of TRPV3 channels in the studied systems.

Our whole-cell experiments with HEK-293 cells overexpressing bTRPV3 and hTRPV3, alongside controls, validated functional expression of the channels using known TRPV3 agonists menthol, thymol, and 2-APB. The expected rise in currents upon agonist incubation, with a significant washout in overexpressing cells, confirmed stimulated conductance. Further investigation in hTRPV3 overexpressing cells revealed permeability to NH_4^+, indicating Cl^- influx, Na^+ efflux, or a combination, possibly influenced by cellular changes. The application of D-menthol led to distinctive current amplitudes and kinetics, suggesting a complex interplay of ion movements, voltage-dependent block, and the influence of divalent cations. Notably, our exploration of both L- and D-menthol revealed no significant difference between enantiomers, but consistent enhanced effects upon the second application, consistent with reported pre-activation or channel sensitizing effects observed by other researchers [135,150]. These findings contribute to the understanding of TRPV3 behavior in response to different agonists.

Our investigation utilizing *X*. oocytes transfected with hTRPV3 and bTRPV3 vectors, along with controls, provided insights into NH_4^+ permeability and acidification dynamics. Despite the initial depolarization and acidification observed in all groups upon NH_4^+ incubation, controls exhibited behavior similar to overexpressing cells, suggesting amply expressed endogenous pathways for NH_4^+ uptake. Notably, our strategic use of $NMDG^+$ solution after injection influenced membrane potential values, but the results underscored the rapid acidification in overexpressing cells, particularly hTRPV3. The faster acidification in hTRPV3 cells, compared to bTRPV3, hints at the efficiency of hTRPV3 expression, a theme explored further in our single-channel experiments. The observed recovery of pH_i in hTRPV3 cells after NH_4Cl incubation and the differential effects of EDTA on pH_i in different groups contribute to our understanding of ion channel behavior. The investigation into relative permeability revealed higher permeability for Na^+ and NH_4^+ in overexpressing cells compared to controls, with nuanced differences between hTRPV3 and bTRPV3. The impact of EDTA on permeability, coupled with the complex interplay of divalent cations, adds depth to our findings. Despite certain complexities awaiting further exploration, our study contributes valuable data to the understanding of ion transport dynamics in *X.* oocytes and the behavior of TRPV3 channels.

Single-channel patch-clamp experiments revealed the expression of non-selective cation channels in both control and overexpressing *X*. oocytes. We observed variable conductance levels, likely influenced by heteromer formation with endogenous channels. Two distinct populations of small and large channels emerged, with overexpressing cells exhibiting a wide range of conductances. The experiments demonstrated that hTRPV3 and bTRPV3 expression significantly increased single-channel conductance while suppressing endogenous channel expression. This effect was more pronounced for bTRPV3. The logical extension of our study

involved single-channel patch clamp experiments with HEK-293 cells overexpressing hTRPV3, revealing challenges in achieving stable seals for NH_4^+ experiments. Future strategies could involve reducing the effectiveness of hTRPV3 channel functionality through blockers or modifications to the transfection protocol. For G573S trafficking and cell viability experiments, our expression of the OS mutation G573S in HEK-293 cells revealed trafficking to the membrane, albeit with a remarkably low number of cells exhibiting staining and impaired morphology. The absence of visible GFP staining in G573S-overexpressing cells, in contrast to wild-type hTRPV3, suggests potential induction of cell death before sufficient GFP expression. Cell viability experiments, supplemented with ruthenium red (RR), indicated significantly lower viability for G573S, with RR partially rescuing cell survival. The observed increased cell death aligns with literature associating OS mutations with apoptosis or necrosis due to heightened Ca^{2+} influx. Despite challenges in obtaining co-expressed GFP cells for patch-clamp experiments, our findings underscore the severe impact of G573S on cell survival. We propose future investigations explore alternative strategies, such as GFP fusion, cautiously considering potential alterations to channel properties, to gain deeper insights into the complex dynamics of G573S expression and its effects on cell viability.

Our staining analysis revealed pronounced hTRPV3 expression in the apical membrane of keratinocytes in the uppermost layer of a human fibroblast and keratinocyte-based skin equivalent. Skin equivalents from cultured human keratinocytes are valued for preclinical studies, offering thin preparations for optimal confocal microscopy. The absence of neuronal cells and prevention of stratum corneum formation present advantages for future transport studies. Within the central region of the keratinocyte layer, robust cytosolic staining was observed, indicative of hTRPV3 expression by the endoplasmic reticulum, consistent with previous reports on hTRPV3 and various other TRP channels [101,286]. Conversely, cells in the upper layer exhibited a pronounced absence of hTRPV3 in the cytosol, with predominant localization in the apical membrane, suggesting a role in apical ion uptake. The observed hTRPV3 expression pattern aligns with previous reports of native human skin. Mirroring the results for hTRPV3, rumen demonstrated strong immunohistochemical staining within the epithelium, moderate staining in the cytosol, and weak subepithelial staining.

We propose that TRPV3, a promiscuous cation selective channel with low Ca^{2+} selectivity and high versatility, plays crucial roles in various epithelial tissues. In the skin, it might be implicated in the signaling cascade for corneocyte replacement, involving NH_4^+ influx, glutamine formation, and transglutaminase activation. As the clinical manifestation of OS is observed in palmoplantar skin in humans which coincides to produce most of eccrine sweat, we also hypothesize that TRPV3 and its mutations linked to OS might potentially be connected to

eccrine sweat production. In the colon, TRPV3 is implicated in pH homeostasis by facilitating NH_4^+ uptake, contributing to microbial nitrogen utilization and aiding in situations of low protein intake. We recommend to keep identifying proteins like TRPV3 involved in ammonia transport for potential interventions, particularly in hepatic diseases where detoxification may be compromised.

In synthesis, the findings demonstrate that both hTRPV3 and bTRPV3 channels conduct NH_4^+. This suggests a role in monovalent cation exchange within organelles, the cytoplasm, and the extracellular space. These findings contribute to our understanding of TRPV3's role, not only in Ca^{2+} signaling as extensively described in the literature, but also in mediating exchanges of monovalent cations, such as NH_4^+.

7

Bibliography

7. Bibliography

1. Abdoun K, Stumpff F, Martens H (2006) Ammonia and urea transport across the rumen epithelium: a review. Animal Health Research Reviews 7:43-59. doi:10.1017/S1466252307001156
2. Adeva MM, Souto G, Blanco N, Donapetry C (2012) Ammonium metabolism in humans. Metabolism 61:1495-1511. doi:10.1016/j.metabol.2012.07.007
3. Agarwal S, Krishnamurthy K (2023) Histology, Skin. In: StatPearls. StatPearls Publishing © 2023, StatPearls Publishing LLC., Treasure Island (FL), PDMI: 30726010
4. Agency E-USEP (2024) Overview of Greenhouse Gases https://www.epa.gov/ghgemissions/overview-greenhouse-gases#CO2-references. Accessed 20240331 2024
5. Al-Mutairi N, Sharma AK, Nour-Eldin O, Al-Adawy E (2005) Olmsted syndrome: report of a new case with unusual features. Clin Exp Dermatol 30:640-642. doi:10.1111/j.1365-2230.2005.01871.x
6. Alotaibi AK, Alotaibi MK, Alsaeed S, Alyahya A, Shuler CF (2015) Olmsted syndrome with oral involvement, including premature teeth loss. Odontology 103:241-245. doi:10.1007/s10266-014-0148-3
7. Aouizerat B, Dunn L, Cooper B, Paul S, West C, Miaskowski C (2011) Association between of temperature-sensitive transient receptor potential cation channel, subfamily V, member 3 (TRPV3) with preoperative pain in women with breast cancer. The Journal of Pain 12:P25. doi:10.1016/j.jpain.2011.02.102
8. Arwert EN, Hoste E, Watt FM (2012) Epithelial stem cells, wound healing and cancer. Nature Reviews Cancer 12:170-180. doi:10.1038/nrc3217
9. Atherton DJ, Sutton C, Jones BM (1990) Mutilating palmoplantar keratoderma with periorificial keratotic plaques (Olmsted's syndrome). Br J Dermatol 122:245-252. doi:10.1111/j.1365-2133.1990.tb08271.x
10. Azad AK, Raihan T, Ahmed J, Hakim A, Emon TH, Chowdhury PA (2021) Human Aquaporins: Functional Diversity and Potential Roles in Infectious and Non-infectious Diseases. Frontiers in Genetics 12. doi:10.3389/fgene.2021.654865
11. B Sakmann a, Neher E (1984) Patch Clamp Techniques for Studying Ionic Channels in Excitable Membranes. Annu Rev Physiol 46:455-472. doi:10.1146/annurev.ph.46.030184.002323
12. Bakija-Konsuo A, Zitinski M, Fatovic-Ferencic S (2019) Mal de Meleda: A great imitator. Clin Dermatol 37:175-181. doi:10.1016/j.clindermatol.2019.01.003
13. Bakthavatchalam R, Kimball SD (2010) Chapter 3 - Modulators of Transient Receptor Potential Ion Channels. In: Macor JE (ed) Annual Reports in Medicinal Chemistry, vol 45. Academic Press, pp 37-53. doi:10.1016/S0065-7743(10)45003-4
14. Ball DW, Key JA (2014) Introductory Chemistry – 1st Canadian Edition. In. BCcampus Victoria, B.C p591PDMI:
15. Bang S, Yoo S, Yang TJ, Cho H, Hwang SW (2010) Farnesyl pyrophosphate is a novel pain-producing molecule via specific activation of TRPV3. J Biol Chem 285:19362-19371. doi:10.1074/jbc.M109.087742
16. Barnett JH, Estes SA (1985) Multiple epitheliomata cuniculata occurring in a mutilating keratoderma. Cutis 35:345-347PDMI: 3996038
17. Batra P, Shah N (2004) Olmsted syndrome--a rare syndrome with oral manifestations. Oral Surg Oral Med Oral Pathol Oral Radiol Endod 97:599-602. doi:10.1016/s1079210403006619
18. Becker A (2017) Influence of photobiomodulation with blue light on the metabolism, proliferation and gene expression of human keratinocytes. Ruprecht-Karls-Universität, Heidelberg
19. Bédard MS, Powell J, Laberge L, Allard-Dansereau C, Bortoluzzi P, Marcoux D (2008) Palmoplantar keratoderma and skin grafting: postsurgical long-term follow-up of two

cases with Olmsted syndrome. Pediatr Dermatol 25:223-229. doi:10.1111/j.1525-1470.2008.00639.x
20. Behre J, Voigt R, Althoefer I, Schuster S (2012) On the evolutionary significance of the size and planarity of the proline ring. Die Naturwissenschaften 99:789-799. doi:10.1007/s00114-012-0960-y
21. Berends H, van den Borne JJGC, Røjen BA, van Baal J, Gerrits WJJ (2014) Urea Recycling Contributes to Nitrogen Retention in Calves Fed Milk Replacer and Low-Protein Solid Feed. The Journal of Nutrition 144:1043-1049. doi:10.3945/jn.114.191353
22. Bergen WG, Wu G (2009) Intestinal nitrogen recycling and utilization in health and disease. J Nutr 139:821-825. doi:jn.109.104497 [pii]; 10.3945/jn.109.104497
23. Bergman EN (1990) Energy contributions of volatile fatty acids from the gastrointestinal tract in various species. Physiol Rev 70:567-590. doi:10.1152/physrev.1990.70.2.567
24. Bergonse FN, Rabello SM, Barreto RL, Romiti R, Nico MM, Aoki V, Reis VM, Rivitti EA (2003) Olmsted syndrome: the clinical spectrum of mutilating palmoplantar keratoderma. Pediatr Dermatol 20:323-326. doi:10.1046/j.1525-1470.2003.20410.x
25. Bertin S, Aoki-Nonaka Y, Lee J, de Jong PR, Kim P, Han T, Yu T, To K, Takahashi N, Boland BS, Chang JT, Ho SB, Herdman S, Corr M, Franco A, Sharma S, Dong H, Akopian AN, Raz E (2017) The TRPA1 ion channel is expressed in CD4+ T cells and restrains T-cell-mediated colitis through inhibition of TRPV1. Gut 66:1584-1596. doi:10.1136/gutjnl-2015-310710
26. Black AS, Sherlock RR, Cameron KC, Smith NP, Goh KM (1985) Comparison of three field methods for measuring ammonia volatilization from urea granules broadcast on to pasture. Journal of Soil Science 36:271-280. doi:10.1111/j.1365-2389.1985.tb00331.x
27. Black AS, Sherlock RR, Smith NP, Cameron KC, Goh KM (1985) Effects of form of nitrogen, season, and urea application rate on ammonia volatilisation from pastures. New Zealand Journal of Agricultural Research 28:469-474. doi:10.1080/00288233.1985.10417992
28. Blaustein MP (1985) Intracellular Calcium as a Second Messenger. In: Rubin RP, Weiss GB, Putney JW (eds) Calcium in Biological Systems. Springer US, Boston, MA, pp 23-33. doi:10.1007/978-1-4613-2377-8_3
29. Bödeker D, Kemkowski J (1996) Participation of NH4+ in total ammonia absorption across the rumen epithelium of sheep (Ovis aries). Comp Biochem Physiol A Physiol 114:305-310. doi:10.1016/0300-9629(96)00012-6
30. Borbíró I, Lisztes E, Tóth BI, Czifra G, Oláh A, Szöllősi AG, Szentandrássy N, Nánási PP, Péter Z, Paus R, Kovács L, Bíró T (2011) Activation of Transient Receptor Potential Vanilloid-3 Inhibits Human Hair Growth. Journal of Investigative Dermatology 131:1605-1614. doi:10.1038/jid.2011.122
31. Boron WF (2010) Sharpey-Schafer lecture: gas channels. Experimental Physiology 95:1107-1130. doi:10.1113/expphysiol.2010.055244
32. Botchkarev VA, Gdula MR, Mardaryev AN, Sharov AA, Fessing MY (2012) Epigenetic regulation of gene expression in keratinocytes. J Invest Dermatol 132:2505-2521. doi:10.1038/jid.2012.182
33. Brazier BW (2016) Membrane Transport of Ammonia. American Journal of Food and Nutrition 4:135-137. doi:10.12691/ajfn-4-5-4
34. Breitkreutz D, Mirancea N, Nischt R (2009) Basement membranes in skin: unique matrix structures with diverse functions? Histochemistry and Cell Biology 132:1-10. doi:10.1007/s00418-009-0586-0
35. Brown SJ, Irwin McLean WH (2012) One Remarkable Molecule: Filaggrin. Journal of Investigative Dermatology 132:751-762. doi:10.1038/jid.2011.393
36. Brown TM, Krishnamurthy K (2023) Histology, Dermis. In: StatPearls. StatPearls Publishing © 2023, StatPearls Publishing LLC., Treasure Island (FL), PDMI: 30570967

37. Brownjohn PW, Ashton JC (2014) What can be Concluded From Blocking Peptide Controls? Applied Immunohistochemistry & Molecular Morphology 22:634. doi:10.1097/PAI.0b013e3182a77fe5
38. Burckhardt BC, Fromter E (1992) Pathways of NH3/NH4+ permeation across Xenopus laevis oocyte cell membrane. Pflugers Arch 420:83-86. doi:10.1007/BF00378645
39. Burckhardt BC, Kroll B, Fromter E (1992) Proton transport mechanism in the cell membrane of Xenopus laevis oocytes. Pflugers Arch 420:78-82. doi:10.1007/BF00378644
40. Calamita G (2023) Advances in Aquaporins. Cells 12. doi:10.3390/cells12020303
41. Candi E, Schmidt R, Melino G (2005) The cornified envelope: a model of cell death in the skin. Nature Reviews Molecular Cell Biology 6:328-340. doi:10.1038/nrm1619
42. Caner T, Abdulnour-Nakhoul S, Brown K, Islam MT, Hamm LL, Nakhoul NL (2015) Mechanisms of ammonia and ammonium transport by rhesus-associated glycoproteins. Am J Physiol Cell Physiol 309:C747-C758. doi:10.1152/ajpcell.00085.2015
43. Cheng X, Jin J, Hu L, Shen D, Dong XP, Samie MA, Knoff J, Eisinger B, Liu ML, Huang SM, Caterina MJ, Dempsey P, Michael LE, Dlugosz AA, Andrews NC, Clapham DE, Xu H (2010) TRP channel regulates EGFR signaling in hair morphogenesis and skin barrier formation. Cell 141:331-343. doi:10.1016/j.cell.2010.03.013
44. Chiu FP-C, Salas-Alanis JC, Amaya-Guerra M, Cepeda-Valdes R, McGrath JA, Hsu C-K (2020) Novel p.Ala675Thr missense mutation in TRPV3 in Olmsted syndrome. Clinical and Experimental Dermatology 45:796-798. doi:10.1111/ced.14228
45. Choe H, Sackin H, Palmer L (1998) Permeation and Gating of an Inwardly Rectifying Potassium Channel. The Journal of general physiology 112:433-446. doi:10.1085/jgp.112.4.433
46. Chong JA, Fanger C, Larsen GR, Lumma WC, Moran MM, Ripka A, Underwood DJ, Weigele M, Zhen X (2005) Compounds for Modulating trpv3 Function. .
47. Chung M-K, Lee H, Mizuno A, Suzuki M, Caterina MJ (2004) 2-Aminoethoxydiphenyl Borate Activates and Sensitizes the Heat-Gated Ion Channel TRPV3. The Journal of Neuroscience 24:5177-5182. doi:10.1523/jneurosci.0934-04.2004
48. Chung MK, Güler AD, Caterina MJ (2005) Biphasic currents evoked by chemical or thermal activation of the heat-gated ion channel, TRPV3. J Biol Chem 280:15928-15941. doi:10.1074/jbc.M500596200
49. Clapham DE (2003) TRP channels as cellular sensors. Nature 426:517-524. doi:10.1038/nature02196
50. Colton CK, Zhu MX (2007) 2-Aminoethoxydiphenyl Borate as a Common Activator of TRPV1, TRPV2, and TRPV3 Channels. In: Flockerzi V, Nilius B (eds) Transient Receptor Potential (TRP) Channels. Springer Berlin Heidelberg, Berlin, Heidelberg, pp 173-187. doi:10.1007/978-3-540-34891-7_10
51. Cosens DJ, Manning A (1969) Abnormal Electroretinogram from a Drosophila Mutant. Nature 224:285-287. doi:10.1038/224285a0
52. Crutzen PJ (1970) The influence of nitrogen oxides on the atmospheric ozone content. Quarterly Journal of the Royal Meteorological Society 96:320-325. doi:https://doi.org/10.1002/qj.49709640815
53. Dai S, Sun Z, Lee M, Wang H, Yang Y, Lin Z (2020) Olmsted syndrome with alopecia universalis caused by heterozygous mutation in PERP. Br J Dermatol 182:242-244. doi:10.1111/bjd.18311
54. Danielyan L, Zellmer S, Sickinger S, Tolstonog GV, Salvetter J, Lourhmati A, Reissig DD, Gleiter CH, Gebhardt R, Buniatian GH (2009) Keratinocytes as depository of ammonium-inducible glutamine synthetase: age- and anatomy-dependent distribution in human and rat skin. PLoS One 4:e4416. doi:10.1371/journal.pone.0004416
55. Danso-Abeam D, Zhang J, Dooley J, Staats KA, Van Eyck L, Van Brussel T, Zaman S, Hauben E, Van de Velde M, Morren MA, Renard M, Van Geet C, Schaballie H, Lambrechts D, Tao J, Franckaert D, Humblet-Baron S, Meyts I, Liston A (2013)

Olmsted syndrome: exploration of the immunological phenotype. Orphanet J Rare Dis 8:79. doi:10.1186/1750-1172-8-79
56. De Datta SK, Trevitt ACF, Freney JR, Obcemea WN, Real JG, Simpson JR (1989) Measuring Nitrogen Losses from Lowland Rice Using Bulk Aerodynamic and Nitrogen-15 Balance Methods. Soil Science Society of America Journal 53:1275-1281. doi:10.2136/sssaj1989.03615995005300040047x
57. Dessureault J, Poulin Y, Bourcier M, Gagne E (2003) Olmsted syndrome-palmoplantar and periorificial keratodermas: association with malignant melanoma. J Cutan Med Surg 7:236-242. doi:10.1007/s10227-002-0107-4
58. Di Meglio P, Duarte JH, Ahlfors H, Owens ND, Li Y, Villanova F, Tosi I, Hirota K, Nestle FO, Mrowietz U, Gilchrist MJ, Stockinger B (2014) Activation of the aryl hydrocarbon receptor dampens the severity of inflammatory skin conditions. Immunity 40:989-1001. doi:10.1016/j.immuni.2014.04.019
59. Di Meglio P, Perera Gayathri K, Nestle Frank O (2011) The Multitasking Organ: Recent Insights into Skin Immune Function. Immunity 35:857-869. doi:10.1016/j.immuni.2011.12.003
60. Dogra D, Ravindraprasad JS, Khanna N, Pandhi RK (1997) Olmsted syndrome with hypotrichosis. Indian J Dermatol Venereol Leprol 63:120-122PDMI: 20944293
61. Duchatelet S, Boyden LM, Ishida-Yamamoto A, Zhou J, Guibbal L, Hu R, Lim YH, Bole-Feysot C, Nitschké P, Santos-Simarro F, de Lucas R, Milstone LM, Gildenstern V, Helfrich YR, Attardi LD, Lifton RP, Choate KA, Hovnanian A (2019) Mutations in PERP Cause Dominant and Recessive Keratoderma. J Invest Dermatol 139:380-390. doi:10.1016/j.jid.2018.08.026
62. Duchatelet S, Guibbal L, de Veer S, Fraitag S, Nitschké P, Zarhrate M, Bodemer C, Hovnanian A (2014) Olmsted syndrome with erythromelalgia caused by recessive transient receptor potential vanilloid 3 mutations. Br J Dermatol 171:675-678. doi:10.1111/bjd.12951
63. Duchatelet S, Hovnanian A (2015) Olmsted syndrome: clinical, molecular and therapeutic aspects. Orphanet Journal of Rare Diseases 10:33. doi:10.1186/s13023-015-0246-5
64. Duchatelet S, Pruvost S, de Veer S, Fraitag S, Nitschké P, Bole-Feysot C, Bodemer C, Hovnanian A (2014) A New TRPV3 Missense Mutation in a Patient With Olmsted Syndrome and Erythromelalgia. JAMA Dermatology 150:303-306. doi:10.1001/jamadermatol.2013.8709
65. Earley S, Gonzales AL, Garcia ZI (2010) A dietary agonist of transient receptor potential cation channel V3 elicits endothelium-dependent vasodilation. Mol Pharmacol 77:612-620. doi:10.1124/mol.109.060715
66. Eckard RJ, Grainger C, de Klein CAM (2010) Options for the abatement of methane and nitrous oxide from ruminant production: A review. Livestock Science 130:47-56. doi:10.1016/j.livsci.2010.02.010
67. Eckhart L, Lippens S, Tschachler E, Declercq W (2013) Cell death by cornification. Biochim Biophys Acta 1833:3471-3480. doi:10.1016/j.bbamcr.2013.06.010
68. Eisenberg D, Gill HS, Pfluegl GM, Rotstein SH (2000) Structure-function relationships of glutamine synthetases. Biochim Biophys Acta 1477:122-145. doi:10.1016/s0167-4838(99)00270-8
69. Elise Tonoli R, De Villa D, Hübner Frainer R, Pizzarro Meneghello L, Ricachnevsky N, de Quadros M (2012) Olmsted syndrome. Case Rep Dermatol Med 2012:927305. doi:10.1155/2012/927305
70. Ermak G (2015) Emerging Medical Technologies. Emerging Medical Technologies. WSPC. doi:10.1142/9591
71. Eytan O, Fuchs-Telem D, Mevorach B, Indelman M, Bergman R, Sarig O, Goldberg I, Adir N, Sprecher E (2014) Olmsted Syndrome Caused by a Homozygous Recessive Mutation in TRPV3. Journal of Investigative Dermatology 134:1752-1754. doi:10.1038/jid.2014.37

72. Fenn LB, Hossner LR (1985) Ammonia Volatilization from Ammonium or Ammonium-Forming Nitrogen Fertilizers. In: Stewart BA (ed) Advances in Soil Science. Springer New York, New York, NY, pp 123-169. doi:10.1007/978-1-4612-5046-3_4
73. Ferone G, Mollo MR, Thomason HA, Antonini D, Zhou H, Ambrosio R, De Rosa L, Salvatore D, Getsios S, van Bokhoven H, Dixon J, Missero C (2013) p63 control of desmosome gene expression and adhesion is compromised in AEC syndrome. Hum Mol Genet 22:531-543. doi:10.1093/hmg/dds464
74. Finn RN, Cerdà J (2015) Evolution and functional diversity of aquaporins. Biol Bull 229:6-23. doi:10.1086/BBLv229n1p6
75. Fonseca E, Peña C, Del Pozo J, Almagro M, Yebra MT, Cuevas J, Contreras F (2001) Olmsted syndrome. J Cutan Pathol 28:271-275. doi:10.1034/j.1600-0560.2001.028005271.x
76. Freney JR, Leuning R, Simpson JR, Denmead OT, Muirhead WA (1985) Estimating Ammonia Volatilization From Flooded Rice Fields by Simplified Techniques. Soil Science Society of America Journal 49:1049-1054. doi:10.2136/sssaj1985.03615995004900040051x
77. Froghi S, Grant CR, Tandon R, Quaglia A, Davidson B, Fuller B (2021) New Insights on the Role of TRP Channels in Calcium Signalling and Immunomodulation: Review of Pathways and Implications for Clinical Practice. Clinical Reviews in Allergy & Immunology 60:271-292. doi:10.1007/s12016-020-08824-3
78. Fuchs E, Raghavan S (2002) Getting under the skin of epidermal morphogenesis. Nat Rev Genet 3:199-209. doi:10.1038/nrg758
79. Fujita F, Uchida K, Moriyama T, Shima A, Shibasaki K, Inada H, Sokabe T, Tominaga M (2008) Intracellular alkalization causes pain sensation through activation of TRPA1 in mice. The Journal of Clinical Investigation 118:4049-4057. doi:10.1172/JCI35957
80. Gagnon D, Crandall CG (2018) Sweating as a heat loss thermoeffector. Handb Clin Neurol 156:211-232. doi:10.1016/b978-0-444-63912-7.00013-8
81. Garcia-Soto J, de la Torre Ld, Darszon A (1985) Increasing intracellular pH of sea urchin sperm with NH4Cl induces Ca2+ uptake and acrosome reaction in the absence of egg jelly. FEBS Letters 190:33-36. doi:10.1016/0014-5793(85)80421-X
82. Gatault S, Kirby B, Danso-Abeam D (2020) Comment on "Olmsted Syndrome". Case Rep Dermatol Med 2020:8024981. doi:10.1155/2020/8024981
83. Gaudet R (2008) TRP channels entering the structural era. The Journal of Physiology 586:3565-3575. doi:10.1113/jphysiol.2008.155812
84. Gees M, Colsoul B, Nilius B (2010) The role of transient receptor potential cation channels in Ca2+ signaling. Cold Spring Harb Perspect Biol 2:a003962. doi:10.1101/cshperspect.a003962
85. Georgii A, Przybilla B, Schmoeckel C (1989) [Olmstedt syndrome--associated with primary sclerosing cholangitis and immune deficiency of uncertain origin]. Hautarzt 40:708-712PDMI: 2532630
86. Geyer RR, Parker MD, Toye AM, Boron WF, Musa-Aziz R (2013) Relative CO(2)/NH(3) permeabilities of human RhAG, RhBG and RhCG. J Membr Biol 246:915-926. doi:10.1007/s00232-013-9593-0
87. Gillespie RJ (2008) Fifty years of the VSEPR model. Coordination Chemistry Reviews 252:1315-1327. doi:10.1016/j.ccr.2007.07.007
88. Gioacchini P, Nastri A, Marzadori C, Giovannini C, Vittori Antisari L, Gessa C (2002) Influence of urease and nitrification inhibitors on N losses from soils fertilized with urea. Biology and Fertility of Soils 36:129-135. doi:10.1007/s00374-002-0521-1
89. Gopinath P, Wan E, Holdcroft A, Facer P, Davis JB, Smith GD, Bountra C, Anand P (2005) Increased capsaicin receptor TRPV1 in skin nerve fibres and related vanilloid receptors TRPV3 and TRPV4 in keratinocytes in human breast pain. BMC Women's Health 5:2. doi:10.1186/1472-6874-5-2
90. Grafton G, Thwaite L (2001) Calcium channels in lymphocytes. Immunology 104:119-126. doi:10.1046/j.0019-2805.2001.01321.x

91. Greco C, Leclerc-Mercier S, Chaumon S, Doz F, Hadj-Rabia S, Molina T, Boucheix C, Bodemer C (2020) Use of Epidermal Growth Factor Receptor Inhibitor Erlotinib to Treat Palmoplantar Keratoderma in Patients With Olmsted Syndrome Caused by TRPV3 Mutations. JAMA Dermatol 156:191-195. doi:10.1001/jamadermatol.2019.4126
92. Greither A (1959) [Keratosis palmaris et plantaris with periodontopathy (Papilloni-Lefevre)]. Dermatologica 119:248-263PDMI: 13851749
93. Haberle J, Gorg B, Toutain A, Rutsch F, Benoist JF, Gelot A, Suc AL, Koch HG, Schliess F, Haussinger D (2006) Inborn error of amino acid synthesis: human glutamine synthetase deficiency. J Inherit Metab Dis 29:352-358. doi:10.1007/s10545-006-0256-5
94. Haghighi A, Scott CA, Poon DS, Yaghoobi R, Saleh-Gohari N, Plagnol V, Kelsell DP (2013) A Missense Mutation in the MBTPS2 Gene Underlies the X-Linked Form of Olmsted Syndrome. Journal of Investigative Dermatology 133:571-573. doi:10.1038/jid.2012.289
95. Hamamoto T, Takumida M, Hirakawa K, Takeno S, Tatsukawa T (2008) Localization of transient receptor potential channel vanilloid subfamilies in the mouse larynx. Acta Oto-Laryngologica 128:685-693. doi:10.1080/00016480701669489
96. Han KH, Lee HW, Handlogten ME, Whitehill F, Osis G, Croker BP, Clapp WL, Verlander JW, Weiner ID (2013) Expression of the ammonia transporter family member, Rh B Glycoprotein, in the human kidney. Am J Physiol Renal Physiol 304:F972-981. doi:10.1152/ajprenal.00550.2012
97. Han Y, Luo A, Kamau PM, Takomthong P, Hu J, Boonyarat C, Luo L, Lai R (2021) A plant-derived TRPV3 inhibitor suppresses pain and itch. Br J Pharmacol 178:1669-1683. doi:10.1111/bph.15390
98. Handlogten ME, Hong SP, Zhang L, Vander AW, Steinbaum ML, Campbell-Thompson M, Weiner ID (2005) Expression of the ammonia transporter proteins Rh B glycoprotein and Rh C glycoprotein in the intestinal tract. American journal of physiology Gastrointestinal and liver physiology 288:G1036-1047. doi:10.1152/ajpgi.00418.2004
99. Hartinger T, Gresner N, Südekum K-H (2018) Does intra-ruminal nitrogen recycling waste valuable resources? A review of major players and their manipulation. Journal of Animal Science and Biotechnology 9:33. doi:10.1186/s40104-018-0249-x
100. Hausser I, Frantzmann Y, Anton-Lamprecht I, Estes S, Frosch PJ (1993) [Olmsted syndrome. Successful therapy by treatment with etretinate]. Hautarzt 44:394-400PDMI: 8335464
101. Haustrate A, Prevarskaya N, Lehen'kyi V (2020) Role of the TRPV Channels in the Endoplasmic Reticulum Calcium Homeostasis. Cells 9. doi:10.3390/cells9020317
102. Haynes WM (2014) CRC Handbook of Chemistry and Physics. CRC Press, Boca RatonPDMI:
103. He Y, Zeng K, Zhang X, Chen Q, Wu J, Li H, Zhou Y, Glusman G, Roach J, Etheridge A, Qing S, Tian Q, Lee I, Tian X, Wang X, Wu Z, Hood L, Ding Y, Wang K (2015) A gain-of-function mutation in TRPV3 causes focal palmoplantar keratoderma in a Chinese family. J Invest Dermatol 135:907-909. doi:10.1038/jid.2014.429
104. Henry J, Toulza E, Hsu C-Y, Pellerin L, Balica S, Mazereeuw-Hautier J, Paul C, Serre G, Jonca N, Simon M (2012) Update on the epidermal differentiation complex. FBL 17:1517-1532. doi:10.2741/4001
105. Hille B, Schwarz W (1978) Potassium channels as multi-ion single-file pores. J Gen Physiol 72:409-442. doi:10.1085/jgp.72.4.409
106. Höller H, Breves G, Gerdes H, Kocabatmaz M (1988) Flux of calcium across the sheep rumen wall in vivo and in vitro. Quarterly Journal of Experimental Physiology 73:609-618. doi:10.1113/expphysiol.1988.sp003180
107. Hoober JK, Eggink LL (2022) The Discovery and Function of Filaggrin. Int J Mol Sci 23. doi:10.3390/ijms23031455

108. Horie S, Yano S, Watanabe K (1995) Intracellular alkalinization by nh4cl increases cytosolic Ca2+ level and tension in the rat aortic smooth muscle. Life Sciences 56:1835-1843. doi:10.1016/0024-3205(95)00155-Y
109. Hristov AN, Bannink A, Crompton LA, Huhtanen P, Kreuzer M, McGee M, Nozière P, Reynolds CK, Bayat AR, Yáñez-Ruiz DR, Dijkstra J, Kebreab E, Schwarm A, Shingfield KJ, Yu Z (2019) Invited review: Nitrogen in ruminant nutrition: A review of measurement techniques. Journal of Dairy Science 102:5811-5852. doi:10.3168/jds.2018-15829
110. Hu H-Z, Gu Q, Wang C, Colton CK, Tang J, Kinoshita-Kawada M, Lee L-Y, Wood JD, Zhu MX (2004) 2-Aminoethoxydiphenyl Borate Is a Common Activator of TRPV1, TRPV2, and TRPV3 *. Journal of Biological Chemistry 279:35741-35748. doi:10.1074/jbc.M404164200
111. Huang L, Ng NM, Chen M, Lin X, Tang T, Cheng H, Yang C, Jiang S (2014) Inhibition of TRPM7 channels reduces degranulation and release of cytokines in rat bone marrow-derived mast cells. Int J Mol Sci 15:11817-11831. doi:10.3390/ijms150711817
112. Huang SM, Lee H, Chung M-K, Park U, Yu YY, Bradshaw HB, Coulombe PA, Walker JM, Caterina MJ (2008) Overexpressed Transient Receptor Potential Vanilloid 3 Ion Channels in Skin Keratinocytes Modulate Pain Sensitivity via Prostaglandin E2. The Journal of Neuroscience 28:13727-13737. doi:10.1523/jneurosci.5741-07.2008
113. Huang SM, Li X, Yu Y, Wang J, Caterina MJ (2011) TRPV3 and TRPV4 ion channels are not major contributors to mouse heat sensation. Mol Pain 7:37. doi:10.1186/1744-8069-7-37
114. Inamadar AC, Palit A, Athanikar SB, Sampagavi VV, Deshmukh NS (2004) What syndrome is this? Olmsted syndrome. Pediatr Dermatol 21:603-605. doi:10.1111/j.0736-8046.2004.21517.x
115. Iozzo RV (2005) Basement membrane proteoglycans: from cellar to ceiling. Nature Reviews Molecular Cell Biology 6:646-656. doi:10.1038/nrm1702
116. Ishibashi T, Takumida M, Akagi N, Hirakawa K, Anniko M (2008) Expression of transient receptor potential vanilloid (TRPV) 1, 2, 3, and 4 in mouse inner ear. Acta Otolaryngol 128:1286-1293. doi:10.1080/00016480801938958
117. Ivorra I, Alberola-Die A, Cobo R, González-Ros JM, Morales A (2022) Xenopus Oocytes as a Powerful Cellular Model to Study Foreign Fully-Processed Membrane Proteins. Membranes 12:986. doi:10.3390/ membranes12100986
118. Jagadeesan S, Kaliyadan F (2021) Acrodermatitis Enteropathica. In: StatPearls. StatPearls Publishing © 2021, StatPearls Publishing LLC., Treasure Island (FL), PDMI: 28722865
119. Jiang Y, Jin H, Zeng Y (2019) A novel mutation in MBTPS2 causes ichthyosis follicularis, alopecia, and photophobia syndrome. Mol Genet Genomic Med 7:e812. doi:10.1002/mgg3.812
120. Johnston H (1971) Reduction of Stratospheric Ozone by Nitrogen Oxide Catalysts from Supersonic Transport Exhaust. Science 173:517-522. doi:doi:10.1126/science.173.3996.517
121. Judge MR, Misch K, Wright P, Harper JI (1991) Palmoplantar and perioroficial keratoderma with corneal epithelial dysplasia: a new syndrome. Br J Dermatol 125:186-188. doi:10.1111/j.1365-2133.1991.tb06070.x
122. Kariminejad A, Barzegar M, Abdollahimajd F, Pramanik R, McGrath JA (2014) Olmsted syndrome in an Iranian boy with a new de novo mutation in TRPV3. Clin Exp Dermatol 39:492-495. doi:10.1111/ced.12318
123. Keicher E, Meech R (1994) Endogenous Na(+)-K+ (or NH4+)-2Cl- cotransport in Rana oocytes; anomalous effect of external NH4+ on pHi. J Physiol 475:45-57. doi:10.1113/jphysiol.1994.sp020048
124. Keir M (1967) Keratodermia palmaris et plantaris. Br J Dermatol 79:419-421. doi:10.1111/j.1365-2133.1967.tb11523.x
125. Kikeri D, Sun A, Zeidel ML, Hebert SC (1989) Cell membranes impermeable to NH3. Nature 339:478-480. doi:10.1038/339478a0

126. Kim JY, Dao H (2023) Physiology, Integument. In: StatPearls. StatPearls Publishing © 2023, StatPearls Publishing LLC., Treasure Island (FL), PDMI: 32119273
127. Koster MI, Roop DR (2007) Mechanisms Regulating Epithelial Stratification. Annual Review of Cell and Developmental Biology 23:93-113. doi:10.1146/annurev.cellbio.23.090506.123357
128. Kress DW, Seraly MP, Falo L, Kim B, Jegasothy BV, Cohen B (1996) Olmsted syndrome. Case report and identification of a keratin abnormality. Arch Dermatol 132:797-800. doi:10.1001/archderm.132.7.797
129. Kuht J, Farmery AD (2014) Body temperature and its regulation. Anaesthesia & Intensive Care Medicine 15:273-278. doi:10.1016/j.mpaic.2014.03.013
130. Kumar P, Sharma PK, Kar HK (2008) Olmsted syndrome. Indian J Dermatol 53:93-95. doi:10.4103/0019-5154.41657
131. Kypriotou M, Huber M, Hohl D (2012) The human epidermal differentiation complex: cornified envelope precursors, S100 proteins and the 'fused genes' family. Experimental Dermatology 21:643-649. doi:10.1111/j.1600-0625.2012.01472.x
132. Lai-Cheong JE, Sethuraman G, Ramam M, Stone K, Simpson MA, McGrath JA (2012) Recurrent heterozygous missense mutation, p.Gly573Ser, in the TRPV3 gene in an Indian boy with sporadic Olmsted syndrome. British Journal of Dermatology 167:440-442. doi:10.1111/j.1365-2133.2012.11115.x
133. Larrègue M, Callot V, Kanitakis J, Suau AM, Foret M (2000) Olmsted syndrome: report of two new cases and literature review. J Dermatol 27:557-568. doi:10.1111/j.1346-8138.2000.tb02229.x
134. Ledford H (2020) CRISPR treatment inserted directly into the body for first time. Nature 579:185. doi:10.1038/d41586-020-00655-8
135. Lezama-García K, Mota-Rojas D, Pereira AMF, Martínez-Burnes J, Ghezzi M, Domínguez A, Gómez J, de Mira Geraldo A, Lendez P, Hernández-Ávalos I, Falcón I, Olmos-Hernández A, Wang D (2022) Transient Receptor Potential (TRP) and Thermoregulation in Animals: Structural Biology and Neurophysiological Aspects. Animals (Basel) 12. doi:10.3390/ani12010106
136. Li X, Zhang Q, Fan K, Li B, Li H, Qi H, Guo J, Cao Y, Sun H (2016) Overexpression of TRPV3 Correlates with Tumor Progression in Non-Small Cell Lung Cancer. International Journal of Molecular Sciences 17:437. doi:10.3390/ijms17040437
137. Liebe F, Liebe H, Kaessmeyer S, Sponder G, Stumpff F (2020) The TRPV3 channel of the bovine rumen: localization and functional characterization of a protein relevant for ruminal ammonia transport. Pflügers Archiv - European Journal of Physiology 472:693-710. doi:10.1007/s00424-020-02393-2
138. Liebe F, Liebe H, Sponder G, Mergler S, Stumpff F (2022) Effects of butyrate− on ruminal Ca2+ transport: evidence for the involvement of apically expressed TRPV3 and TRPV4 channels. Pflügers Archiv - European Journal of Physiology 474. doi:10.1007/s00424-021-02647-7
139. Liebe H, Liebe F, Sponder G, Hedtrich S, Stumpff F (2021) Beyond Ca2+ signalling: the role of TRPV3 in the transport of NH4+. Pflügers Archiv - European Journal of Physiology 473. doi:10.1007/s00424-021-02616-0
140. Lin Z, Chen Q, Lee M, Cao X, Zhang J, Ma D, Chen L, Hu X, Wang H, Wang X, Zhang P, Liu X, Guan L, Tang Y, Yang H, Tu P, Bu D, Zhu X, Wang K, Li R, Yang Y (2012) Exome Sequencing Reveals Mutations in TRPV3 as a Cause of Olmsted Syndrome. American Journal of Human Genetics 90:558-564. doi:10.1016/j.ajhg.2012.02.006
141. Litman T, Søgaard R, Zeuthen T (2009) Ammonia and Urea Permeability of Mammalian Aquaporins. In: Beitz E (ed) Aquaporins. Springer Berlin Heidelberg, Berlin, Heidelberg, pp 327-358. doi:10.1007/978-3-540-79885-9_17
142. Liu J, Lkhagva E, Chung HJ, Kim HJ, Hong ST (2018) The Pharmabiotic Approach to Treat Hyperammonemia. Nutrients 10. doi:10.3390/nu10020140
143. Liu Q, Wang J, Wei X, Hu J, Ping C, Gao Y, Xie C, Wang P, Cao P, Cao Z, Yu Y, Li D, Yao J (2021) Therapeutic inhibition of keratinocyte TRPV3 sensory channel by local anesthetic dyclonine. Elife 10. doi:10.7554/eLife.68128

144. Liu Y, Qi H, E M, Shi P, Zhang Q, Li S, Wang Y, Cao Y, Chen Y, Ba L, Gao J, Huang W, Sun H (2018) Transient receptor potential vanilloid-3 (TRPV3) activation plays a central role in cardiac fibrosis induced by pressure overload in rats via TGF-β(1) pathway. Naunyn Schmiedebergs Arch Pharmacol 391:131-143. doi:10.1007/s00210-017-1443-7
145. Löwa A, Vogt A, Kaessmeyer S, Hedtrich S (2018) Generation of full-thickness skin equivalents using hair follicle-derived primary human keratinocytes and fibroblasts. J Tissue Eng Regen Med 12:e2134-e2146. doi:10.1002/term.2646
146. Lu J, Hu R, Liu L, Ding H (2021) [Analysis of clinical feature and genetic basis of a rare case with Olmsted syndrome]. Zhonghua Yi Xue Yi Chuan Xue Za Zhi 38:674-677. doi:10.3760/cma.j.cn511374-20200811-00597
147. Lu Z, Stumpff F, Deiner C, Rosendahl J, Braun H, Abdoun K, Aschenbach JR, Martens H (2014) Modulation of sheep ruminal urea transport by ammonia and pH. American Journal of Physiology-Regulatory, Integrative and Comparative Physiology 307:R558-R570. doi:10.1152/ajpregu.00107.2014
148. Lucker GPH, Steijlen PM (1994) The Olmsted syndrome: Mutilating palmoplanar and periorificial keratoderma. Journal of the American Academy of Dermatology 31:508-509. doi:10.1016/S0190-9622(09)80015-7
149. Maclaren OJ, Sneyd J, Crampin EJ (2013) What do aquaporin knockout studies tell us about fluid transport in epithelia? J Membr Biol 246:297-305. doi:10.1007/s00232-013-9530-2
150. Macpherson LJ, Hwang SW, Miyamoto T, Dubin AE, Patapoutian A, Story GM (2006) More than cool: Promiscuous relationships of menthol and other sensory compounds. Molecular and Cellular Neuroscience 32:335-343. doi:10.1016/j.mcn.2006.05.005
151. Macsai MS, Schwartz TL, Hinkle D, Hummel MB, Mulhern MG, Rootman D (2001) Tyrosinemia type II: nine cases of ocular signs and symptoms. Am J Ophthalmol 132:522-527. doi:10.1016/s0002-9394(01)01160-6
152. Madhero88, M.Komorniczak (2012) Skin layers, of both hairy and hairless skin. Wikipedia. doi: Madhero88 and M.Komorniczak (https://commons.wikimedia.org/wiki/File:Skin_layers.svg), „Skin layers“, https://creativecommons.org/licenses/by-sa/3.0/legalcode
153. Mandadi S, Sokabe T, Shibasaki K, Katanosaka K, Mizuno A, Moqrich A, Patapoutian A, Fukumi-Tominaga T, Mizumura K, Tominaga M (2009) TRPV3 in keratinocytes transmits temperature information to sensory neurons via ATP. Pflugers Arch 458:1093-1102. doi:10.1007/s00424-009-0703-x
154. Manneck D, Braun HS, Schrapers KT, Stumpff F (2021) TRPV3 and TRPV4 as candidate proteins for intestinal ammonium absorption. Acta Physiol (Oxf):e13694. doi:10.1111/apha.13694
155. Masamoto Y, Kawabata F, Fushiki T (2009) Intragastric Administration of TRPV1, TRPV3, TRPM8, and TRPA1 Agonists Modulates Autonomic Thermoregulation in Different Manners in Mice. Bioscience, Biotechnology, and Biochemistry 73:1021-1027. doi:10.1271/bbb.80796
156. Matoori S, Leroux J-C (2015) Recent advances in the treatment of hyperammonemia. Advanced Drug Delivery Reviews 90:55-68. doi:10.1016/j.addr.2015.04.009
157. McKemy DD (2007) Frontiers in Neuroscience. In: Liedtke WB, Heller S (eds) TRP Ion Channel Function in Sensory Transduction and Cellular Signaling Cascades. CRC Press/Taylor & Francis © 2007, Taylor & Francis Group, LLC., Boca Raton (FL), PDMI: 21204486
158. Mégarbané H, Zablit C, Waked N, Lefranc G, Tomb R, Mégarbané A (2004) Ichthyosis follicularis, alopecia, and photophobia (IFAP) syndrome: Report of a new family with additional features and review. American Journal of Medical Genetics Part A 124A:323-327. doi:10.1002/ajmg.a.20352
159. Mellerio J, Greenblatt D (1993) Hidrotic Ectodermal Dysplasia 2. In: Adam MP, Ardinger HH, Pagon RA et al. (eds) GeneReviews(®). University of Washington, Seattle

Copyright © 1993-2021, University of Washington, Seattle. , Seattle (WA), PDMI: 20301379
160. Mergler S, Valtink M, Coulson-Thomas VJ, Lindemann D, Reinach PS, Engelmann K, Pleyer U (2010) TRPV channels mediate temperature-sensing in human corneal endothelial cells. Experimental Eye Research 90:758-770. doi:10.1016/j.exer.2010.03.010
161. Mevorah B, Goldberg I, Sprecher E, Bergman R, Metzker A, Luria R, Gat A, Brenner S (2005) Olmsted syndrome: mutilating palmoplantar keratoderma with periorificial keratotic plaques. J Am Acad Dermatol 53:S266-272. doi:10.1016/j.jaad.2005.03.036
162. Mickle AD, Shepherd AJ, Mohapatra DP (2015) Sensory TRP channels: the key transducers of nociception and pain. Prog Mol Biol Transl Sci 131:73-118. doi:10.1016/bs.pmbts.2015.01.002
163. Minke B, Cook B (2002) TRP Channel Proteins and Signal Transduction. Physiological Reviews 82:429-472. doi:10.1152/physrev.00001.2002
164. Moiseenkova-Bell VY, Stanciu LA, Serysheva, II, Tobe BJ, Wensel TG (2008) Structure of TRPV1 channel revealed by electron cryomicroscopy. Proc Natl Acad Sci U S A 105:7451-7455. doi:10.1073/pnas.0711835105
165. Moqrich A, Hwang SW, Earley TJ, Petrus MJ, Murray AN, Spencer KS, Andahazy M, Story GM, Patapoutian A (2005) Impaired thermosensation in mice lacking TRPV3, a heat and camphor sensor in the skin. Science 307:1468-1472. doi:10.1126/science.1108609
166. Musa-Aziz R, Jiang L, Chen LM, Behar KL, Boron WF (2009) Concentration-dependent effects on intracellular and surface pH of exposing Xenopus oocytes to solutions containing NH3/NH4(+). J Membr Biol 228:15-31. doi:10.1007/s00232-009-9155-7
167. Nadezhdin KD, Neuberger A, Trofimov YA, Krylov NA, Sinica V, Kupko N, Vlachova V, Zakharian E, Efremov RG, Sobolevsky AI (2021) Structural mechanism of heat-induced opening of a temperature-sensitive TRP channel. Nature Structural & Molecular Biology 28:564-572. doi:10.1038/s41594-021-00615-4
168. Nagaraja TN, Brookes N (1998) Intracellular acidification induced by passive and active transport of ammonium ions in astrocytes. Am J Physiol 274:C883-891. doi:10.1152/ajpcell.1998.274.4.C883
169. Nemer G, Safi R, Kreidieh F, Usta J, Bergqvist C, Ballout F, Btadini W, Hamzeh N, Abbas O, Kibbi AG, Shimomura Y, Kurban M (2017) Understanding the phenotypic similarities between IFAP and Olmsted syndrome from a molecular perspective: the interaction of MBTPS2 and TRPV3. Arch Dermatol Res 309:637-643. doi:10.1007/s00403-017-1762-z
170. Neuhauser B, Dynowski M, Ludewig U (2014) Switching substrate specificity of AMT/MEP/ Rh proteins. Channels (Austin) 8:496-502. doi:10.4161/19336950.2014.967618
171. Nicolas V, Le Van Kim C, Gane P, Birkenmeier C, Cartron J-P, Colin Y, Mouro-Chanteloup I (2003) Rh-RhAG/Ankyrin-R, a New Interaction Site between the Membrane Bilayer and the Red Cell Skeleton, Is Impaired by Rh_{null}-associated Mutation *. Journal of Biological Chemistry 278:25526-25533. doi:10.1074/jbc.M302816200
172. Nilius B, Biro T (2013) TRPV3: a 'more than skinny' channel. Exp Dermatol 22:447-452. doi:10.1111/exd.12163
173. Nilius B, Biro T, Owsianik G (2014) TRPV3: time to decipher a poorly understood family member! J Physiol 592:295-304. doi:10.1113/jphysiol.2013.255968
174. Nilius B, Owsianik G (2011) The transient receptor potential family of ion channels. Genome Biology 12:218. doi:10.1186/gb-2011-12-3-218
175. Nilius B, Owsianik G, Voets T, Peters JA (2007) Transient Receptor Potential Cation Channels in Disease. Physiological Reviews 87:165-217. doi:10.1152/physrev.00021.2006
176. Nithya S, Radhika T, Jeddy N (2015) Loricrin - an overview. J Oral Maxillofac Pathol 19:64-68. doi:10.4103/0973-029x.157204

177. Nobel A (2021) 2021 Nobel Prize in Physiology or Medicine. https://www.nobelprize.org/prizes/medicine/2021/press-release/, Nobelprize.orgPDMI:
178. Nofal A, Assaf M, Nassar A, Nofal E, Shehab M, El-Kabany M (2010) Nonmutilating palmoplantar and periorificial kertoderma: a variant of Olmsted syndrome or a distinct entity? Int J Dermatol 49:658-665. doi:10.1111/j.1365-4632.2009.04429.x
179. Norlén L, Al-Amoudi A (2004) Stratum Corneum Keratin Structure, Function, and Formation: The Cubic Rod-Packing and Membrane Templating Model. Journal of Investigative Dermatology 123:715-732. doi:10.1111/j.0022-202X.2004.23213.x
180. Ogawa F, Udono M, Murota H, Shimizu K, Takahashi H, Ishida-Yamamoto A, Iizuka H, Katayama I (2003) Olmsted syndrome with squamous cell carcinoma of extremities and adenocarcinoma of the lung: failure to detect loricrin gene mutation. Eur J Dermatol 13:524-528PDMI: 14721769
181. Ogino S, Gulley ML, den Dunnen JT, Wilson RB (2007) Standard mutation nomenclature in molecular diagnostics: practical and educational challenges. J Mol Diagn 9:1-6. doi:10.2353/jmoldx.2007.060081
182. OLMSTED HC, Olmsted HC (1927) Keratodermia palmaris et plantaris congenitalis: report of a case showing associated lesions of unusual location. American Journal of Diseases of Children 33:757-764. doi:10.1001/archpedi.1927.04130170055008
183. Ortar G, Morera L, Schiano Moriello A, Morera E, Nalli M, Di Marzo V, De Petrocellis L (2012) Modulation of thermo-transient receptor potential (thermo-TRP) channels by thymol-based compounds. Bioorganic & Medicinal Chemistry Letters 22:3535-3539. doi:10.1016/j.bmcl.2012.03.055
184. Overton E (1902) Beiträge zur allgemeinen Muskel-und Nervenphysiologie. Archiv für die gesamte Physiologie des Menschen und der Tiere 92:115-280PDMI:
185. Owsianik G, D'Hoedt D, Voets T, Nilius B (2006) Structure-function relationship of the TRP channel superfamily. Rev Physiol Biochem Pharmacol 156:61-90PDMI: 16634147
186. Owsianik G, Talavera K, Voets T, Nilius B (2006) Permeation and selectivity of TRP channels. Annu Rev Physiol 68:685-717. doi:10.1146/annurev.physiol.68.040204.101406
187. Pahwa P, Lamba AK, Faraz F, Tandon S (2010) Haim-Munk syndrome. J Indian Soc Periodontol 14:201-203. doi:10.4103/0972-124x.75919
188. Park CW, Kim HJ, Choi YW, Chung BY, Woo SY, Song DK, Kim HO (2017) TRPV3 Channel in Keratinocytes in Scars with Post-Burn Pruritus. Int J Mol Sci 18. doi:10.3390/ijms18112425
189. Patapoutian A, Tate S, Woolf CJ (2009) Transient receptor potential channels: targeting pain at the source. Nat Rev Drug Discov 8:55-68. doi:10.1038/nrd2757
190. Peier AM, Moqrich A, Hergarden AC, Reeve AJ, Andersson DA, Story GM, Earley TJ, Dragoni I, McIntyre P, Bevan S, Patapoutian A (2002) A TRP channel that senses cold stimuli and menthol. Cell 108:705-715. doi:10.1016/s0092-8674(02)00652-9
191. Peier AM, Reeve AJ, Andersson DA, Moqrich A, Earley TJ, Hergarden AC, Story GM, Colley S, Hogenesch JB, McIntyre P, Bevan S, Patapoutian A (2002) A heat-sensitive TRP channel expressed in keratinocytes. Science 296:2046-2049. doi:10.1126/science.1073140
192. Peng JB, Suzuki Y, Gyimesi G, Hediger MA (2018) TRPV5 and TRPV6 Calcium-Selective Channels. In: Kozak JA, Putney JW, Jr. (eds) Calcium Entry Channels in Non-Excitable Cells. CRC Press/Taylor & Francis © 2017 by Taylor & Francis Group, LLC., Boca Raton (FL), pp 241-274. doi:10.1201/9781315152592-13
193. Perry HO, Su WP (1995) Olmsted syndrome. Semin Dermatol 14:145-151. doi:10.1016/s1085-5629(05)80011-2
194. Phelps CB, Wang RR, Choo SS, Gaudet R (2010) Differential regulation of TRPV1, TRPV3, and TRPV4 sensitivity through a conserved binding site on the ankyrin repeat domain. J Biol Chem 285:731-740. doi:10.1074/jbc.M109.052548

195. Poulin Y, Perry HO, Muller SA (1984) Olmsted syndrome--congenital palmoplantar and periorificial keratoderma. J Am Acad Dermatol 10:600-610. doi:10.1016/s0190-9622(84)80264-9
196. Qamar S, Vadivelu M, Sandford R (2007) TRP channels and kidney disease: lessons from polycystic kidney disease. Biochemical Society Transactions 35:124-128. doi:10.1042/bst0350124
197. Qi H, Shi Y, Wu H, Niu C, Sun X, Wang K (2022) Inhibition of temperature-sensitive TRPV3 channel by two natural isochlorogenic acid isomers for alleviation of dermatitis and chronic pruritus. Acta Pharmaceutica Sinica B 12:723-734. doi:10.1016/j.apsb.2021.08.002
198. Rabbani I, Braun HS, Akhtar T, Liebe F, Rosendahl J, Grunau M, Tietjen U, Masood S, Kaessmeyer S, Gunzel D, Rehman H, Stumpff F (2018) A comparative study of ammonia transport across ruminal epithelia from Bos indicus crossbreds versus Bos taurus. Anim Sci J 89:1692-1700. doi:10.1111/asj.13107
199. Raskin CA, Tu JH (1997) Keratin expression in Olmsted syndrome. Arch Dermatol 133:389. doi:10.1001/archderm.1997.03890390133024
200. Ravishankara AR, Daniel JS, Portmann RW (2009) Nitrous Oxide (N2O): The Dominant Ozone-Depleting Substance Emitted in the 21st Century. Science 326:123-125. doi:10.1126/science.1176985
201. Reifarth FW, Amasheh S, Clauss W, Weber W (1997) The Ca2+-inactivated Cl- channel at work: selectivity, blocker kinetics and transport visualization. J Membr Biol 155:95-104. doi:10.1007/s002329900161
202. Requena L, Manzarbeitia F, Moreno C, Izquierdo M, Pastor-Nieto M, Carrasco L, Fariña C, Martin L (2002) Olmsted syndrome: Report of a case with study of the cellular proliferation in keratoderma. The American Journal of dermatopathology 23:514-520PDMI:
203. Requena L, Manzarbeitia F, Moreno C, Izquierdo MJ, Pastor MA, Carrasco L, Fariña MC, Martín L (2001) Olmsted syndrome: report of a case with study of the cellular proliferation in keratoderma. Am J Dermatopathol 23:514-520. doi:10.1097/00000372-200112000-00003
204. Rivers JK, Duke EE, Justus DW (1985) Etretinate: management of keratoma hereditaria mutilans in four family members. J Am Acad Dermatol 13:43-49. doi:10.1016/s0190-9622(85)70141-7
205. Rizzuto R, Pinton P, Ferrari D, Chami M, Szabadkai G, Magalhães PJ, Virgilio FD, Pozzan T (2003) Calcium and apoptosis: facts and hypotheses. Oncogene 22:8619-8627. doi:10.1038/sj.onc.1207105
206. Røjen BA, Poulsen SB, Theil PK, Fenton RA, Kristensen NB (2011) Short communication: Effects of dietary nitrogen concentration on messenger RNA expression and protein abundance of urea transporter-B and aquaporins in ruminal papillae from lactating Holstein cows. Journal of Dairy Science 94:2587-2591. doi:10.3168/jds.2010-4073
207. Roos A, Boron WF (1981) Intracellular pH. Physiol Rev 61:296-434. doi:10.1152/physrev.1981.61.2.296
208. Rosenbaum T, Morales-Lázaro SL, Islas LD (2022) TRP channels: a journey towards a molecular understanding of pain. Nature Reviews Neuroscience 23:596-610. doi:10.1038/s41583-022-00611-7
209. Rosendahl J, Braun HS, Schrapers KT, Martens H, Stumpff F (2016) Evidence for the functional involvement of members of the TRP channel family in the uptake of Na(+) and NH4 (+) by the ruminal epithelium. Pflugers Arch 468:1333-1352. doi:10.1007/s00424-016-1835-4
210. Saga K, Jimbow K (2001) Immunohistochemical localization of activated EGF receptor in human eccrine and apocrine sweat glands. J Histochem Cytochem 49:597-602. doi:10.1177/002215540104900506
211. Saito S, Fukuta N, Shingai R, Tominaga M (2011) Evolution of Vertebrate Transient Receptor Potential Vanilloid 3 Channels: Opposite Temperature Sensitivity between

Mammals and Western Clawed Frogs. PLOS Genetics 7:e1002041. doi:10.1371/journal.pgen.1002041
212. Saleh D, Tanner LS (2021) Vohwinkel Syndrome. In: StatPearls. StatPearls Publishing © 2021, StatPearls Publishing LLC., Treasure Island (FL), PDMI: 30335335
213. Sandilands A, Sutherland C, Irvine AD, McLean WHI (2009) Filaggrin in the frontline: role in skin barrier function and disease. Journal of Cell Science 122:1285-1294. doi:10.1242/jcs.033969
214. Santos OL, Amorim JH, Voloch K, Gomes M, Ramos-e-Silva M, Pereira Júnior AC (1997) The Olmsted syndrome. Int J Dermatol 36:359-360. doi:10.1111/j.1365-4362.1997.tb03097.x
215. Saparov SM, Liu K, Agre P, Pohl P (2007) Fast and selective ammonia transport by aquaporin-8. J Biol Chem 282:5296-5301. doi:10.1074/jbc.M609343200
216. Scharschmidt TC, Fischbach MA (2013) What Lives On Our Skin: Ecology, Genomics and Therapeutic Opportunities Of the Skin Microbiome. Drug Discov Today Dis Mech 10. doi:10.1016/j.ddmec.2012.12.003
217. Schlingmann KP, Sassen MC, Weber S, Pechmann U, Kusch K, Pelken L, Lotan D, Syrrou M, Prebble JJ, Cole DE, Metzger DL, Rahman S, Tajima T, Shu SG, Waldegger S, Seyberth HW, Konrad M (2005) Novel TRPM6 mutations in 21 families with primary hypomagnesemia and secondary hypocalcemia. J Am Soc Nephrol 16:3061-3069. doi:10.1681/asn.2004110989
218. Schlingmann KP, Waldegger S, Konrad M, Chubanov V, Gudermann T (2007) TRPM6 and TRPM7—Gatekeepers of human magnesium metabolism. Biochimica et Biophysica Acta (BBA) - Molecular Basis of Disease 1772:813-821. doi:10.1016/j.bbadis.2007.03.009
219. Schneider MR, Werner S, Paus R, Wolf E (2008) Beyond wavy hairs: the epidermal growth factor receptor and its ligands in skin biology and pathology. Am J Pathol 173:14-24. doi:10.2353/ajpath.2008.070942
220. Schrapers KT, Sponder G, Liebe F, Liebe H, Stumpff F (2018) The bovine TRPV3 as a pathway for the uptake of Na+, Ca2+, and NH4+. PLoS One 13:e0193519. doi:10.1371/journal.pone.0193519
221. Schröder J-M (2010) The role of keratinocytes in defense against infection. Current Opinion in Infectious Diseases 23:106-110. doi:10.1097/QCO.0b013e328335b004
222. Scott VE, Patel H, Wetter J, Edlmayer R, Neelands T, Miller L, Huang S, Gauld S, Todorovic V, Gomtsian A, Dart M, Honore P, Kym P (2016) 534 - Defining a mechanistic link between TRPV3 activity and psoriasis through IL-1alpha and EGFR signaling pathways. Journal of Investigative Dermatology 136:S94. doi:10.1016/j.jid.2016.02.572
223. Seok Yang Y, Ick Cho S, Gyu Choi M, Hee Choi Y, Suk Kwak I, Wook Park C, One Kim H (2014) Increased Expression of Three Types of Transient Receptor Potential Channels (TRPA1, TRPV4 and TRPV3) in Burn Scars with Post-burn Pruritus. Acta Dermato-Venereologica 95:20-24. doi:10.2340/00015555-1858
224. Sherkheli MA, Vogt-Eisele AK, Weber K, Hatt H (2013) Camphor modulates TRPV3 cation channels activity by interacting with critical pore-region cysteine residues. Pak J Pharm Sci 26:431-438PDMI: 23625413
225. Shilov VN, Sergienko VI (2000) Oxidative stress in keratinocytes as an etiopathogenetic factor of psoriasis. Bulletin of Experimental Biology and Medicine 129:309-313. doi:10.1007/BF02439252
226. Shirakata Y (2010) Regulation of epidermal keratinocytes by growth factors. Journal of Dermatological Science 59:73-80. doi:10.1016/j.jdermsci.2010.05.002
227. Sigurdarson JJ, Svane S, Karring H (2018) The molecular processes of urea hydrolysis in relation to ammonia emissions from agriculture. Reviews in Environmental Science and Bio/Technology 17:241-258. doi:10.1007/s11157-018-9466-1
228. Simon M, Green H (1988) The glutamine residues reactive in transglutaminase-catalyzed cross-linking of involucrin. J Biol Chem 263:18093-18098PDMI: 2461365

229. Singh J, Kunhikrishnan A, Bolan NS, Saggar S (2013) Impact of urease inhibitor on ammonia and nitrous oxide emissions from temperate pasture soil cores receiving urea fertilizer and cattle urine. Science of The Total Environment 465:56-63. doi:10.1016/j.scitotenv.2013.02.018
230. Slominski AT, Zmijewski MA, Semak I, Zbytek B, Pisarchik A, Li W, Zjawiony J, Tuckey RC (2014) Cytochromes p450 and skin cancer: role of local endocrine pathways. Anticancer Agents Med Chem 14:77-96. doi:10.2174/18715206113139990308
231. Slominski AT, Zmijewski MA, Skobowiat C, Zbytek B, Slominski RM, Steketee JD (2012) Sensing the environment: regulation of local and global homeostasis by the skin's neuroendocrine system. Adv Anat Embryol Cell Biol 212:v, vii, 1-115. doi:10.1007/978-3-642-19683-6_1
232. Smith FJD, Hansen CD, Hull PR, Kaspar RL, McLean WHI, O'Toole E, Sprecher E (1993) Pachyonychia Congenita. In: Adam MP, Ardinger HH, Pagon RA et al. (eds) GeneReviews(®). University of Washington, Seattle, Seattle (WA), PDMI: 20301457
233. Smith GD, Gunthorpe MJ, Kelsell RE, Hayes PD, Reilly P, Facer P, Wright JE, Jerman JC, Walhin JP, Ooi L, Egerton J, Charles KJ, Smart D, Randall AD, Anand P, Davis JB (2002) TRPV3 is a temperature-sensitive vanilloid receptor-like protein. Nature 418:186-190. doi:10.1038/nature00894
234. Smith K (2010) Nitrous Oxide and Climate Change. 1st edn. Taylor & Francis, London. doi:10.4324/9781849775113
235. Smith MM, Melrose J (2015) Proteoglycans in Normal and Healing Skin. Advances in Wound Care 4:152-173. doi:10.1089/wound.2013.0464
236. Song D, Ran X, Chen Y, Li Z, Li F, Lan Y, Wang S (2021) Recurrent c.459 C>A mutation of the PERP gene results in severe Olmsted syndrome with congenital hypotrichosis, atopic dermatitis, and growth retardation. J Dermatol 48:E508-e509. doi:10.1111/1346-8138.16060
237. Song Z, Chen X, Zhao Q, Stanic V, Lin Z, Yang S, Chen T, Chen J, Yang Y (2021) Hair Loss Caused by Gain-of-Function Mutant TRPV3 Is Associated with Premature Differentiation of Follicular Keratinocytes. J Invest Dermatol 141:1964-1974. doi:10.1016/j.jid.2020.11.036
238. Sozucan Y, Kalender ME, Sari I, Suner A, Oztuzcu S, Arman K, Yumrutas O, Bozgeyik I, Cengiz B, Igci YZ, Balakan O, Camci C (2015) TRP genes family expression in colorectal cancer. Exp Oncol 37:208-212PDMI: 26422106
239. Stewart GS, Smith CP (2005) Urea nitrogen salvage mechanisms and their relevance to ruminants, non-ruminants and man. Nutr Res Rev 18:49-62. doi:10.1079/NRR200498
240. Su W, Qiao X, Wang W, He S, Liang K, Hong X (2023) TRPV3: Structure, Diseases and Modulators. Molecules 28:774. doi:10.3390/molecules28020774
241. Sulk M, Seeliger S, Aubert J, Schwab VD, Cevikbas F, Rivier M, Nowak P, Voegel JJ, Buddenkotte J, Steinhoff M (2012) Distribution and Expression of Non-Neuronal Transient Receptor Potential (TRPV) Ion Channels in Rosacea. Journal of Investigative Dermatology 132:1253-1262. doi:10.1038/jid.2011.424
242. Sulk M, Steinhoff M (2015) Chapter 17 - Role of TRP Channels in Skin Diseases. In: Szallasi A (ed) TRP Channels as Therapeutic Targets. Academic Press, Boston, pp 293-323. doi:10.1016/B978-0-12-420024-1.00017-5
243. Sun X, Qi H, Wu H, Qu Y, Wang K (2020) Anti-pruritic and anti-inflammatory effects of natural verbascoside through selective inhibition of temperature-sensitive Ca2+-permeable TRPV3 channel. Journal of Dermatological Science 97:229-231. doi:10.1016/j.jdermsci.2020.01.004
244. Sun XY, Sun LL, Qi H, Gao Q, Wang GX, Wei NN, Wang K (2018) Antipruritic Effect of Natural Coumarin Osthole through Selective Inhibition of Thermosensitive TRPV3 Channel in the Skin. Mol Pharmacol 94:1164-1173. doi:10.1124/mol.118.112466
245. Szollosi AG, Vasas N, Angyal A, Kistamas K, Nanasi PP, Mihaly J, Beke G, Herczeg-Lisztes E, Szegedi A, Kawada N, Yanagida T, Mori T, Kemeny L, Biro T (2018) Activation of TRPV3 Regulates Inflammatory Actions of Human Epidermal Keratinocytes. J Invest Dermatol 138:365-374. doi:10.1016/j.jid.2017.07.852

246. Tang L, Zhang L, Ding H, Wang X, Wang H (2012) Olmsted syndrome: a new case complicated with easily broken hair and treated with oral retinoid. J Dermatol 39:816-817. doi:10.1111/j.1346-8138.2012.01535.x
247. Tao J, Huang CZ, Yu NW, Wu Y, Liu YQ, Li Y, Tian J, Yang LY, Zhang J, Li JW, Zhou YW, Tu YT (2008) Olmsted syndrome: a case report and review of literature. Int J Dermatol 47:432-437. doi:10.1111/j.1365-4632.2008.03595.x
248. Tharini GK, Hema N, Jayakumar S, Parveen B (2011) Olmsted syndrome: report of two cases. Indian J Dermatol 56:591-593. doi:10.4103/0019-5154.87166
249. Tominaga M (2007) The Role of TRP Channels in Thermosensation. In: Liedtke WB, S H (eds) TRP Ion Channel Function in Sensory Transduction and Cellular Signaling Cascades. CRC Press/Taylor & Francis, Boca Raton (FL), PDMI:
250. Ueda M, Nakagawa K, Hayashi K, Shimizu R, Ichihashi M (1993) Partial improvement of Olmsted syndrome with etretinate. Pediatr Dermatol 10:376-381. doi:10.1111/j.1525-1470.1993.tb00404.x
251. Ueda T, Yamada T, Ugawa S, Ishida Y, Shimada S (2009) TRPV3, a thermosensitive channel is expressed in mouse distal colon epithelium. Biochemical and biophysical research communications 383:130-134. doi:10.1016/j.bbrc.2009.03.143
252. Valdes Rodriguez R, Kaushik SB, Yosipovitch G (2013) Transient Receptor Potential Channels and Dermatological Disorders. Current topics in medicinal chemistry 13. doi:10.2174/15680266112129990090
253. van Goor MKC, Hoenderop JGJ, van der Wijst J (2017) TRP channels in calcium homeostasis: from hormonal control to structure-function relationship of TRPV5 and TRPV6. Biochimica et Biophysica Acta (BBA) - Molecular Cell Research 1864:883-893. doi:10.1016/j.bbamcr.2016.11.027
254. Van Kim CL, Colin Y, Cartron JP (2006) Rh proteins: key structural and functional components of the red cell membrane. Blood Rev 20:93-110. doi:10.1016/j.blre.2005.04.002
255. Vasas N, Pénzes Z, Kistamás K, Nánási PP, Molnár S, Szegedi A, Szöllősi AG, Bíró T (2022) Transient receptor potential vanilloid 3 expression is increased in non-lesional skin of atopic dermatitis patients. Experimental Dermatology 31:807-813. doi:10.1111/exd.14530
256. Vazquez G, Wedel BJ, Aziz O, Trebak M, Putney JW (2004) The mammalian TRPC cation channels. Biochimica et Biophysica Acta (BBA) - Molecular Cell Research 1742:21-36. doi:10.1016/j.bbamcr.2004.08.015
257. Velasco I, Morán J, Tapia R (1995) Selective neurotoxicity of ruthenium red in primary cultures. Neurochem Res 20:599-604. doi:10.1007/bf01694542
258. Vennekens R, Owsianik G, Nilius B (2008) Vanilloid transient receptor potential cation channels: an overview. Curr Pharm Des 14:18-31. doi:10.2174/138161208783330763
259. Verhulst NO, Andriessen R, Groenhagen U, Bukovinszkine Kiss G, Schulz S, Takken W, van Loon JJ, Schraa G, Smallegange RC (2010) Differential attraction of malaria mosquitoes to volatile blends produced by human skin bacteria. PLoS One 5:e15829. doi:10.1371/journal.pone.0015829
260. Voets T (2012) Quantifying and modeling the temperature-dependent gating of TRP channels. Rev Physiol Biochem Pharmacol 162:91-119. doi:10.1007/112_2011_5
261. Vogt-Eisele AK, Weber K, Sherkheli MA, Vielhaber G, Panten J, Gisselmann G, Hatt H (2007) Monoterpenoid agonists of TRPV3. Br J Pharmacol 151:530-540. doi:10.1038/sj.bjp.0707245
262. Vriens J, Appendino G, Nilius B (2009) Pharmacology of vanilloid transient receptor potential cation channels. Mol Pharmacol 75:1262-1279. doi:10.1124/mol.109.055624
263. Vriens J, Nilius B, Vennekens R (2008) Herbal compounds and toxins modulating TRP channels. Curr Neuropharmacol 6:79-96. doi:10.2174/157015908783769644
264. Wakabayashi K, Gustafson AM, Sidransky E, Goldin E (2011) Mucolipidosis type IV: an update. Mol Genet Metab 104:206-213. doi:10.1016/j.ymgme.2011.06.006

265. Walker V (2014) Ammonia metabolism and hyperammonemic disorders. Adv Clin Chem 67:73-150. doi:10.1016/bs.acc.2014.09.002
266. Wang G, Wang K (2017) The Ca^{2+}-Permeable Cation Transient Receptor Potential TRPV3 Channel: An Emerging Pivotal Target for Itch and Skin Diseases. Molecular Pharmacology 92:193-200. doi:10.1124/mol.116.107946
267. Wang H, Siemens J (2015) TRP ion channels in thermosensation, thermoregulation and metabolism. Temperature 2:178-187. doi:10.1080/23328940.2015.1040604
268. Wang HJ, Tang ZL, Lin ZM, Dai LL, Chen Q, Yang Y (2014) Recurrent splice-site mutation in MBTPS2 underlying IFAP syndrome with Olmsted syndrome-like features in a Chinese patient. Clin Exp Dermatol 39:158-161. doi:10.1111/ced.12248
269. Wang J, Chen X, Huang W (2021) MicroRNA-369 attenuates hypoxia-induced cardiomyocyte apoptosis and inflammation via targeting TRPV3. Braz J Med Biol Res 54:e10550. doi:10.1590/1414-431x202010550
270. Wang JX, Fukunaga-Kalabis M, Herlyn M (2016) Crosstalk in skin: melanocytes, keratinocytes, stem cells, and melanoma. J Cell Commun Signal 10:191-196. doi:10.1007/s12079-016-0349-3
271. Wang Y, Li X, Yang J, Tian Z, Sun Q, Xue W, Dong H (2018) Mitigating Greenhouse Gas and Ammonia Emissions from Beef Cattle Feedlot Production: A System Meta-Analysis. Environmental Science & Technology 52:11232-11242. doi:10.1021/acs.est.8b02475
272. Weber W (1999) Ion currents of Xenopus laevis oocytes: state of the art. Biochim Biophys Acta 1421:213-233. doi:10.1016/s0005-2736(99)00135-2
273. Weiner ID, Mitch WE, Sands JM (2015) Urea and Ammonia Metabolism and the Control of Renal Nitrogen Excretion. Clin J Am Soc Nephrol 10:1444-1458. doi:10.2215/CJN.10311013
274. Weiner ID, Verlander JW (2011) Role of NH3 and NH4+ transporters in renal acid-base transport. American Journal of Physiology-Renal Physiology 300:F11-F23. doi:10.1152/ajprenal.00554.2010
275. Weiner ID, Verlander JW (2014) Ammonia transport in the kidney by Rhesus glycoproteins. American Journal of Physiology-Renal Physiology 306:F1107-F1120. doi:10.1152/ajprenal.00013.2014
276. Weiner ID, Verlander JW (2019) Emerging Features of Ammonia Metabolism and Transport in Acid-Base Balance. Semin Nephrol 39:394-405. doi:10.1016/j.semnephrol.2019.04.008
277. Wilkens MR, Mrochen N, Breves G, Schröder B (2011) Gastrointestinal calcium absorption in sheep is mostly insensitive to an alimentary induced challenge of calcium homeostasis. Comparative Biochemistry and Physiology Part B: Biochemistry and Molecular Biology 158:199-207. doi:10.1016/j.cbpb.2010.11.008
278. Wilkens MR, Nelson CD, Hernandez LL, McArt JAA (2020) Symposium review: Transition cow calcium homeostasis - Health effects of hypocalcemia and strategies for prevention. Journal of Dairy Science 103:2909-2927. doi:10.3168/jds.2019-17268
279. Wilkens MR, Praechter C, Breves G, Schröder B (2016) Stimulating effects of a diet negative in dietary cation–anion difference on calcium absorption from the rumen in sheep. Journal of Animal Physiology and Animal Nutrition 100:156-166. doi:10.1111/jpn.12296
280. Wilson NJ, Cole C, Milstone LM, Kiszewski AE, Hansen CD, O'Toole EA, Schwartz ME, Irwin McLean WH, Smith FJD (2015) Expanding the Phenotypic Spectrum of Olmsted Syndrome. The Journal of investigative dermatology 135:2879-2883. doi:10.1038/jid.2015.217
281. Wu SW, Lindberg JE, Peters JH (2016) Genetic and pharmacological evidence for low-abundance TRPV3 expression in primary vagal afferent neurons. Am J Physiol Regul Integr Comp Physiol 310:R794-805. doi:10.1152/ajpregu.00366.2015
282. Xiao R, Tang J, Wang C, Colton CK, Tian J, Zhu MX (2008) Calcium plays a central role in the sensitization of TRPV3 channel to repetitive stimulations. J Biol Chem 283:6162-6174. doi:10.1074/jbc.M706535200

283. Xiao R, Xu XZS (2021) Temperature Sensation: From Molecular Thermosensors to Neural Circuits and Coding Principles. Annu Rev Physiol 83:205-230. doi:10.1146/annurev-physiol-031220-095215
284. Xu H, Delling M, Jun JC, Clapham DE (2006) Oregano, thyme and clove-derived flavors and skin sensitizers activate specific TRP channels. Nature Neuroscience 9:628-635. doi:10.1038/nn1692
285. Xu H, Ramsey IS, Kotecha SA, Moran MM, Chong JA, Lawson D, Ge P, Lilly J, Silos-Santiago I, Xie Y, DiStefano PS, Curtis R, Clapham DE (2002) TRPV3 is a calcium-permeable temperature-sensitive cation channel. Nature 418:181-186. doi:10.1038/nature00882
286. Yadav M, Goswami C (2017) TRPV3 mutants causing Olmsted Syndrome induce impaired cell adhesion and nonfunctional lysosomes. Channels (Austin) 11:196-208. doi:10.1080/19336950.2016.1249076
287. Yaghoobi R, Omidian M, Sina N, Abtahian SA, Panahi-Bazaz MR (2007) Olmsted syndrome in an Iranian family: report of two new cases. Arch Iran Med 10:246-249PDMI: 17367233
288. Yamamoto-Kasai E, Imura K, Yasui K, Shichijou M, Oshima I, Hirasawa T, Sakata T, Yoshioka T (2012) TRPV3 as a Therapeutic Target for Itch. Journal of Investigative Dermatology 132:2109-2112. doi:10.1038/jid.2012.97
289. Yamamoto-Kasai E, Yasui K, Shichijo M, Sakata T, Yoshioka T (2013) Impact of TRPV3 on the development of allergic dermatitis as a dendritic cell modulator. Experimental Dermatology 22:820-824. doi:10.1111/exd.12273
290. Yan K, Sun X, Wang G, Liu Y, Wang K (2019) Pharmacological Activation of Thermo-Transient Receptor Potential Vanilloid 3 Channels Inhibits Hair Growth by Inducing Cell Death of Hair Follicle Outer Root Sheath. J Pharmacol Exp Ther 370:299-307. doi:10.1124/jpet.119.258087
291. Yoshioka T, Imura K, Asakawa M, Suzuki M, Oshima I, Hirasawa T, Sakata T, Horikawa T, Arimura A (2009) Impact of the Gly573Ser Substitution in TRPV3 on the Development of Allergic and Pruritic Dermatitis in Mice. Journal of Investigative Dermatology 129:714-722. doi:10.1038/jid.2008.245
292. Yoshizaki Y, Kanki H, Ueda T, Ichihashi M, Ueda M (2001) A further case of plantar squamous cell carcinoma arising in Olmsted syndrome. Br J Dermatol 145:685-686. doi:10.1046/j.1365-2133.2001.04453.x
293. Yuan JP, Kiselyov K, Shin DM, Chen J, Shcheynikov N, Kang SH, Dehoff MH, Schwarz MK, Seeburg PH, Muallem S, Worley PF (2003) Homer Binds TRPC Family Channels and Is Required for Gating of TRPC1 by IP3 Receptors. Cell 114:777-789. doi:10.1016/S0092-8674(03)00716-5
294. Zhang A, Duchatelet S, Lakdawala N, Tower RL, Diamond C, Marathe K, Hill I, Richard G, Diab Y, Kirkorian AY, Watanabe F, Siegel DH, Hovnanian A (2020) Targeted Inhibition of the Epidermal Growth Factor Receptor and Mammalian Target of Rapamycin Signaling Pathways in Olmsted Syndrome. JAMA Dermatol 156:196-200. doi:10.1001/jamadermatol.2019.4141
295. Zhang M, Ma Y, Ye X, Zhang N, Pan L, Wang B (2023) TRP (transient receptor potential) ion channel family: structures, biological functions and therapeutic interventions for diseases. Signal Transduction and Targeted Therapy 8:261. doi:10.1038/s41392-023-01464-x
296. Zhang Q, Qi H, Cao Y, Shi P, Song C, Ba L, Chen Y, Gao J, Li S, Li B, Sun H (2018) Activation of transient receptor potential vanilloid 3 channel (TRPV3) aggravated pathological cardiac hypertrophy via calcineurin/NFATc3 pathway in rats. Journal of Cellular and Molecular Medicine 22:6055-6067. doi:10.1111/jcmm.13880
297. Zhang X, Li L, McNaughton PA (2008) Proinflammatory mediators modulate the heat-activated ion channel TRPV1 via the scaffolding protein AKAP79/150. Neuron 59:450-461. doi:10.1016/j.neuron.2008.05.015
298. Zhong C, Farrell A, Stewart GS (2020) Localization of aquaporin-3 proteins in the bovine rumen. Journal of Dairy Science 103:2814-2820. doi:10.3168/jds.2019-17735

299. Zhong W, Hu L, Cao X, Zhao J, Zhang X, Lee M, Wang H, Zhang J, Chen Q, Feng C, Duo L, Wang X, Tang L, Lin Z, Yang Y (2020) GenotypePhenotype Correlation of TRPV3-Related Olmsted Syndrome. J Invest Dermatol. doi:10.1016/j.jid.2020.06.035

8

Appendices

8. Appendices

Peer-reviewed publications

Liebe H, Liebe F, Sponder G, Hedtrich S, Stumpff F (2021): **Beyond Ca^{2+} signalling: the role of TRPV3 in the transport of NH_4^+**. Pflügers Archiv - European Journal of Physiology 473. doi:10.1007/s00424-021-02616-0
https://doi.org/10.1007/s00424-021-02616-0
Reproduced with permission from Springer Nature.

Liebe, F.; Liebe, H.; Kaessmeyer, S.; Sponder, G.; Stumpff, F. (2020): **The TRPV3 channel of the bovine rumen: localization and functional characterization of a protein relevant for ruminal ammonia transport.** Pflügers Archiv: European journal of physiology; **472**(6), S. 693-710, doi: 10.1007/s00424-020-02393-2
https://doi.org/10.1007/s00424-020-02393-2
Reproduced with permission from Springer Nature

Liebe F, Liebe H, Sponder G, Mergler S, Stumpff F (2022): **Effects of $butyrate^-$ on ruminal Ca^{2+} transport: evidence for the involvement of apically expressed TRPV3 and TRPV4 channels**. Pflügers Archiv - European Journal of Physiology 474. doi:10.1007/s00424-021-02647-7

Schrapers, K. T.; Sponder, G.; Liebe, F.; Liebe, H.; Stumpff, F. (2018): **The bovine TRPV3 as a pathway for the uptake of Na^+, Ca^{2+}, and NH_4^+.** PLoS one; **13**(3), S. e0193519, doi: 10.1371/journal.pone.0193519

Congress participations and Posters

Liebe, F.; Liebe, H.; Mergler, S.; Sponder, G.; Stumpff, F. (2021): **Stimulatory effects of butyrate on TRPV3 and TRPV4 with implications for Ca^{2+} uptake in ruminants.** Deutsche Physiologische Gesellschaft

Liebe H.; Liebe F.; Manz G.; Sponder G.; Stumpff F. (2021): **A truly promiscuous channel: D-menthol, L-menthol and the conductance of TRPV3 to NH_4^+.** Deutsche Physiologische Gesellschaft

Liebe, F.; Liebe, H.; Mergler, S.; Sponder, G.; Stumpff, F. (2021): **The effect of butyrate on transport of Ca^{2+} and Na^+ through the bovine TRPV3 channel.** 75. Jahrestagung der Gesellschaft für Ernährungsphysiologie (GfE) Göttingen - 16.-18.03.2021. In: Proceedings of the Society of Nutrition Physiology - Gesellschaft für Ernährungsphysiologie (Hrsg.), Frankfurt am Main: DLG -Verlag; 30, S. 105, ISBN: 978-3-7690-4114-9

Liebe, H.; Liebe, F.; Sponder, G.; Stumpff, F. (2019): **TRPV3 mutation Gly573Ser and its wild type are functionally expressed in the membrane of overexpressing HEK-293 cells.** 98th meeting of the German Physiological Society, Ulm - 30.09.-02.10.2019. In: Acta physiologica Scandinavica; **227**(S719), S. 192

Stumpff, F.; Liebe, F.; Liebe, H.; Sponder, G. (2019): **The TRPV3 channel: a pathway for the uptake of Ca^{2+} from the rumen.** XIIIth International Symposium on Ruminant Physiology, Leipzig - 03.09.-06.09.2019. In: Advances in Animal Biosciences; **10**(3), S. 399

Liebe, H.; Liebe, F.; Vitzthum, C.; Sponder, G.; Stumpff, F. (2018): **A comparative study of the NH_4^+ conductance of human and bovine TRPV3 channels as expressed in Xenopus Oocytes.** Europhysiology, London - 13.09.-16.09.2018. In: Proceedings of the Physiological Society, S. 171P

Liebe, F.; Liebe, H.; Vitzthum, C.; Kaessmeyer, S.; Sponder, G.; Stumpff, F. (2018): **Establishing an antibody to verify expression of the bovine TRPV3 channel by the rumen of cattle.** Europhysiology, London - 13.09.-16.09.2018. In: Proceedings of the Physiological Society, S. 357P

Liebe, F.; Liebe, H.; Käßmeyer, S.; Vitzthum, C.; Sponder, G.; Stumpff, F. (2018): **Characterization of the bovine TRPV3 channel in Xenopus oocytes.** 72nd Conference of the Society of Nutrition Physiology, Göttingen - 13.03.-15.03.2018. In: Proceedings of the Society of Nutrition Physiology - Gesellschaft für Ernährungsphysiologie (Hrsg.), Frankfurt am Main: DLG -Verlag; S. 84, ISBN: 978-3-7690-4111-8

Liebe, F.; Liebe, H.; Vitzthum, C.; Käßmeyer, S.; Sponder, G.; Stumpff, F. (2018): **The bovine rumen expresses bTRPV3 channels as a pathway for the uptake of NH_4^+.** 23. Tagung der DVG-Fachgruppe Physiologie und Biochemie der Deutschen Veterinärmedizinischen Gesellschaft, Wien - 21.02.-23.02.2018. In: 23. Tagung der Fachgruppe Physiologie und Biochemie der Deutschen Veterinärmedizinischen Gesellschaft: PROGRAMM & ABSTRACTS - Veterinärmedizinische Universität Wien (Hrsg.), S. 51, ISBN: 978-3-86345-307-7

Liebe, H.; Liebe, F.; Vitzthum, C.; Sponder, G.; Stumpff, F. (2018): **Investigation of the NH_4^+ conductance of the human analogue of TRPV3**. 23. Tagung der DVG-Fachgruppe Physiologie und Biochemie der Deutschen Veterinärmedizinischen Gesellschaft, Wien - 21.02.-23.02.2018. In: 23. Tagung der Fachgruppe Physiologie und Biochemie der Deutschen Veterinärmedizinischen Gesellschaft: PROGRAMM & ABSTRACTS - Veterinärmedizinische Universität Wien (Hrsg.), Wien, S. 35, ISBN: 978-3-86345-307-7

Liebe, H.; Liebe, F.; Vitzthum, C.; Sponder, G.; Stumpff, F. (2017): **Establishing Xenopus oocytes as a model system for studying the NH_4^+ conductance of human TRPV3 via pH-sensitive microelectrodes.** 6th Symposium of the young physiologists, Jena - 28.09.-29.09.2017. In: 6th symposium of the young physiologists, Jena 2017, S. 54

Liebe, F.; Liebe, H.; Vitzthum, C.; Sponder, G.; Stumpff, F. (2017): **Characterizing the bovine TRPV3 using two classical expression systems.** 6th Symposium of the young physiologists, Jena - 28.09.-29.09.2017. In: 6th symposium of the young physiologists, Jena 2017, S. 40–41

Liebe, F.; Liebe, H.; Schrapers, K. T.; Sponder, G.; Stumpff, F. (2017**): A patch clamp and fura-2 study of the bovine TRPV3 channel.** Deutsche Physiologische Gesellschaft, Greifswald - 16.03.-18.03.2017. In: Acta physiologica Scandinavica; **219**(S711), S. B05–B08

Liebe, F.; Liebe, H.; Schrapers, K. T.; Sponder, G.; Stumpff, F. (2017): **A study of the bovine TRPV3 channel as a pathway for the uptake of Ca^{2+}.** 71st Conference of the Society of Nutrition Physiology, Göttingen - 14.03.-16.03.2017. In: Proceedings of the Society of Nutrition Physiology - Gesellschaft für Ernährungsphysiologie (Hrsg.), Frankfurt am Main: DLG-Verlag; **26**, S. 40, ISBN: 978-3-7690-4110-1